

Dissertation zur Erlangung des Doktorgrades
Fakultät für Chemie und Pharmazie
der Ludwig-Maximilians Universität München

The critical role of microglia and the expression of
BIN1 in Alzheimer's Disease pathogenesis



von

Katharina Ochs

aus

Friedrichshafen, Deutschland

2022

Erklärung und eidesstattliche Versicherung

Erklärung

Diese Dissertation wurde im Sinne von § 7 der Promotionsordnung vom 28. November 2011 von Herrn Prof. Dr. Jochen Herms betreut und von Herrn Prof. Dr. Stylianos Michalakis von der Fakultät für Chemie und Pharmazie vertreten.

Eidesstattliche Versicherung

Diese Dissertation wurde eigenständig und ohne unerlaubte Hilfe erarbeitet.

München, 30.05.22

.....

Katharina Ochs

Dissertation eingereicht am: 30.05.2022

1. Gutachter: Prof. Dr. Stylianos Michalakis
2. Gutachter: Prof. Dr. Jochen Herms

Mündliche Prüfung am: 19.07.2022

Abstract

Alzheimer's Disease (AD) is a fatal form of dementia that affects memory, thinking and behavior. It is a progressive neurodegenerative disease characterized by the extracellular accumulation of A β plaques, intracellular tau tangles and neuroinflammation. Despite tremendous efforts focusing on the treatment of patients, to this day, there is no cure. Microglia, as resident immune cells, are the brain's first line of defense against invading pathogens and contribute to A β plaque clearance but also neuroinflammation. In recent years, they have become the focus of attention as numerous alterations in the microglial genome were identified to confer risk for the development of late-onset AD, the most common form of AD. It has become clearer that those changes mainly relate to microglial defects in the elimination of A β plaques and cellular debris. Thus, the in-depth characterization of microglia aimed at the identification of deregulated pathways and new therapeutic targets has substantially gained importance.

In this study, I investigated the consistency between the transcriptomic and proteomic profile of microglia from a commonly used AD mouse model (APP^{NL-G-F}) and further analyzed the unknown homeostatic functions of the novel high-impact risk gene *BIN1* in microglia. During the first part of my thesis, I validated the downregulation of homeostatic and upregulation of inflammatory pathways in the transcriptome of aged AD microglia. Correlation with a matching proteomic data set pointed towards an inflammatory but also regenerative phenotype, and strengthened the previously identified deficits of the phagocytic machinery. This condition was supported through the distinct enrichment of synaptic debris within the proteome of AD microglia. Interestingly, despite a significant enrichment in AD lysosomes, I found disease-associated cells to be less efficient compared to age-matched controls, further emphasizing the phagocytic and lysosomal dysfunction of AD microglia. To investigate the presumed link between the prominent *BIN1* downregulation in AD microglia and its influence on phagocytosis, I performed functional and AAV-mediated overexpression experiments in the second part of my thesis. Here, I was able to provide meaningful evidence for the direct involvement of *BIN1* in microglial phagocytic processes *in vitro*. I further aimed for *in vivo* transduction experiments as a proof of concept study and to gain valuable insights into the network-dependent impact of *BIN1* overexpression.

Although I could successfully overexpress BIN1 in microglia, which positively correlated with an increase of the lysosomal compartment, cell specificity of the viral construct has to be further improved. Overall, these results signify the importance of the preservation of key microglia functions in the context of AD and that pathogenic downregulation of BIN1 could exacerbate the observed continuous decline. Thus, making microglia phagocytosis and BIN1 itself promising targets for further investigation in the pathogenesis of AD.

Zusammenfassung

Morbus Alzheimer ist eine tödliche Form der Demenz, die das Gedächtnis, Denkvermögen und Verhalten der betroffenen Patienten stark beeinträchtigt. Es handelt sich um eine fortschreitende, neurodegenerative Erkrankung, die sich durch die extrazelluläre Ansammlung von A β -Plaques, intrazellulären Tau-Tangles und ausgeprägte Entzündungsreaktionen im zentralen Nervengewebe charakterisieren lässt. Trotz der enormen Bemühungen um die Behandlung von Patienten, gibt es bis heute keine ursächliche Behandlungsstrategie und nur wenige symptomatische Ansätze. Mikroglia wurden vielfach als aktive Immunantwort des Gehirns beschrieben, die allgemein gegen eindringende Krankheitserreger und im Speziellen auch gegen toxische A β -Plaques vorgeht, jedoch auch zu der fortschreitenden, lokalen Entzündungsreaktion des umliegenden Gewebes beiträgt. In den letzten Jahren sind Mikroglia vermehrt in den Mittelpunkt des Interesses gerückt, da gezeigt wurde, dass zahlreiche Veränderungen in ihrem Genom das Risiko für die Entwicklung von sporadischem M. Alzheimer signifikant erhöhen. In jüngster Zeit ist deutlich geworden, dass diese Veränderungen hauptsächlich die Funktionen von Mikroglia negativ beeinflussen, die mit der Beseitigung von A β -Plaques und Zelltrümmern zusammenhängen. Die gezielte Identifizierung der molekularen Zusammenhänge und damit neuer therapeutischer Angriffspunkte hat damit substanziell an Bedeutung gewonnen.

In dieser Studie habe ich die Übereinstimmung zwischen transkriptomischem und proteomischem Profil von Mikroglia eines gängigen Alzheimer-Mausmodells (APP^{NL-G-F}) untersucht und darüber hinaus den Einfluss des Hochrisiko-Gens *BIN1* auf die physiologische Mikrogliafunktion analysiert. Im ersten Teil meiner Dissertation konnte ich die bereits beschriebene Runterregulierung homöostatischer, sowie die Hochregulierung entzündlicher Signalwege im Transkriptom gealterter M. Alzheimer-Mikroglia bestätigen. Die Korrelation mit einem entsprechenden Proteom-Datensatz ergab, dass sowohl entzündliche als auch regenerative Prozesse in Gang gesetzt wurden. In Übereinstimmung mit der vorherigen Analyse wurden deutliche Defizite auf Seiten der phagozytischen Aktivität festgestellt, was mutmaßlich ursächlich war für die signifikanten Änderungen synaptischen Materials im Proteom erkrankter Mikroglia. Interessanterweise ergab sich trotz gesteigerter Mengen synaptischen Materials im Lysosom ein Defizit in der relativen Aufnahmefähigkeit

erkrankter Mikroglia, was ebenfalls auf einen funktionellen Defekt hindeutet. Aktuelle Studien vermuten einen Zusammenhang zwischen der Runterregulierung von BIN1 und der beobachteten Abnahme der Aufnahmefähigkeit von M. Alzheimer-Mikroglia, welchen ich im zweiten Teil meiner Dissertation mittels funktioneller und viraler Überexpressionsversuche untersucht habe. *In vitro* konnte ich aussagekräftige Ergebnisse gewinnen, die auf ein direktes Mitwirken von BIN1 an phagozytischen Prozessen hindeuten. Darüber hinaus führte ich *in vivo* Transduktionsexperimente durch, um Erkenntnisse über die netzwerkabhängigen Auswirkungen einer *BIN1*-Überexpression zu erlangen. Obwohl *BIN1* erfolgreich in Mikroglia überexprimiert werden konnte und positiv mit der Zunahme lysosomaler Strukturen korrelierte, muss die Spezifität des viralen Konstrukts weiter verbessert werden. Insgesamt zeigen diese Ergebnisse jedoch, wie wichtig der Erhalt der Schlüsselfunktionen von Mikroglia im Zusammenhang mit M. Alzheimer ist und dass eine krankheitsbedingte Runterregulierung von *BIN1* den kontinuierlichen Abbau dieser verstärken könnte. Dies macht den grundlegenden Prozess der Phagozytose und BIN1 selbst zu einem vielversprechenden Ziel für weitere Untersuchungen in der mikrogliabedingten Pathogenese von M. Alzheimer.

Contents

Erklärung und eidesstattliche Versicherung	i
Abstract	iii
Zusammenfassung	v
Contents	vii
Abbreviations	xiv
List of Figures	xx
List of Tables	xxii
1 Introduction	1
1.1 Alzheimer's Disease	1
1.1.1 History and Pathophysiology of Alzheimer's Disease	1
1.1.1.1 Abeta pathology	2
1.1.1.1.1 Abeta peptide processing	2
1.1.1.1.2 Physiological and pathogenic roles of the Abeta peptide	4
1.1.1.1.3 Abeta amyloid pathology	5
1.1.1.2 Neurofibrillary tangles and dystrophic neurites	7
1.1.1.3 Neuroinflammation	8
1.1.2 The amyloid cascade hypothesis	13
1.1.3 Etiology	13
1.1.4 New risk factors and GWAS studies	15
1.2 Microglia in health and disease	16
1.2.1 Ontogeny	17
1.2.2 The physiological role of microglia in the CNS	18
1.2.2.1 Characterization of homeostatic microglia	19
1.2.3 Microglia in Alzheimer's Disease: a double-edged sword	21
1.2.3.1 Mechanisms of abeta clearance in the CNS	22
1.2.3.2 Deficiency of microglial clearance in Alzheimer's Disease	24

1.2.3.3	Transcriptomic characterization of microglia in Alzheimer's Disease	25
1.2.3.3.1	Profiling of murine microglia in Alzheimer's Disease models	26
1.2.3.3.2	Profiling of human microglia in Alzheimer's Disease	27
1.3	Microglia-associated risk factors	28
1.3.1	TREM2 and other rare Alzheimer's Disease risk variants	30
1.3.2	BIN1 as a common Alzheimer's Disease risk variant	31
1.3.2.1	BIN1 physiology	32
1.3.2.1.1	BIN1 isoforms and cellular distribution	32
1.3.2.1.2	BIN1 function	34
1.3.2.2	Pathological implications for Bin1	36
2	Aims of the study	39
3	Materials and Methods	41
3.1	Materials	41
3.1.1	Laboratory equipment and general consumables	41
3.1.2	Cell culture equipment and consumables	42
3.1.3	Surgical instruments	42
3.1.4	Microscopy equipment	43
3.1.5	RNA Sequencing equipment	43
3.1.6	Animals	43
3.1.6.1	Mouse husbandry	43
3.1.6.2	Mouse lines	43
3.1.7	Reagents, solutions and consumables for different applications	44
3.1.7.1	Genotyping of transgenic mouse lines	44
3.1.7.1.1	Primers (Sigma-Aldrich)	44
3.1.7.1.2	Reagents and key consumables	44
3.1.7.2	Primary mouse microglia <i>in vitro</i> applications	45
3.1.7.2.1	Reagents and key consumables for microglia isolation and culture experiments	45

3.1.7.2.2	Solutions for microglia isolation and culture experiments	46
3.1.7.2.3	Reagents and key consumables for RNA sequencing	47
3.1.7.3	Mouse procedures: <i>in vivo</i> treatments and histology	47
3.1.7.3.1	Reagents and key consumables	47
3.1.7.3.2	Primary antibodies	47
3.1.7.3.3	Secondary antibodies	49
3.1.7.3.4	Solutions	50
3.1.7.4	Biochemistry: Western Blotting	51
3.1.7.4.1	Reagents and key consumables	51
3.1.7.4.2	Solutions	51
3.1.8	Software	52
3.2	Methods	53
3.2.1	Genotyping of transgenic mouse lines	53
3.2.1.1	PCR program for APP-KI x GFP-M genotyping	53
3.2.2	Microglia isolation for <i>in vitro</i> applications	54
3.2.2.1	Microglia isolation using MACS technology	54
3.2.2.1.1	Microglia isolation using GentleMACS and Neural Tissue Dissociation Kit (P) for RNAseq and Western blotting	55
3.2.2.1.2	Microglia isolation using manual dissociation and self-made Papain solution for cell culture	55
3.2.3	Biochemistry: Western Blotting of primary microglia	56
3.2.3.1	Protein extraction and quantification	56
3.2.3.2	Western Blotting	57
3.2.4	Culture of primary microglia	57
3.2.4.1	Prior arrangements	57
3.2.4.2	Culture and handling	58
3.2.4.3	Phagocytosis assay with pHrodo Green <i>E.coli</i> particles	58

3.2.4.4	AAV-facilitated mBin1 overexpression in cultured primary microglia	59
3.2.4.4.1	AAV vector design	59
3.2.4.4.2	microglia transduction <i>in vitro</i>	59
3.2.5	RNAseq of primary microglia using the MG400 panel	60
3.2.5.1	RNA isolation and quantification	60
3.2.5.2	RNA quality control	61
3.2.5.3	Bulk RNAseq using Illumina TruSeq Targeted RNA Expression	61
3.2.5.4	Data analysis	62
3.2.6	Mouse procedures	62
3.2.6.1	AAV-facilitated microglial overexpression of mBin1 <i>in vivo</i>	62
3.2.6.1.1	Stereotactic virus injection	62
3.2.6.2	Transcardial perfusion	63
3.2.7	Histology	64
3.2.7.1	Mouse brain sectioning	64
3.2.7.2	Immunofluorescent stainings of mouse brain sections	65
3.2.7.3	Immunofluorescent stainings of primary microglia	65
3.2.8	Immunofluorescence analysis: image acquisition and quantification	66
3.2.8.1	Primary microglia culture: phagocytosis assay validation	66
3.2.8.2	Primary microglia culture: analysis of Bin1 overexpression, activation status, endolysosomal machinery and phagocytosis assays	67
3.2.8.3	Mouse brain sections: analysis of Bin1 downregulation in Alzheimer Disease microglia	67
3.2.8.4	AAV <i>in vivo</i> : analysis of Bin1 overexpression and activation status in microglia and neuronal side-effects	68
3.2.8.5	Mouse brain sections: analysis of synaptic proteins within Alzheimer Disease microglia	68
3.2.9	Statistical analysis	69

4	Results	71
4.1	Characterization of microglial dynamics during Alzheimer’s Disease	71
4.1.1	Transcriptomic profiling of Alzheimer’s Disease mouse microglia	71
4.1.1.1	MG400 chip panel design	72
4.1.1.2	MACS microglial isolation allows for transcriptomic analysis	73
4.1.1.3	RIN score analysis and post-sequencing quality controls	74
4.1.1.4	Genes of aged APP-KI microglia are substantially different compared to age-matched controls	75
4.1.1.5	Transcriptomic comparison with MGnD microglia	77
4.1.1.6	Gene ontology analysis of APP-KI microglia RNA transcripts	78
4.1.2	Overlap between APP-KI microglia transcriptomic and proteomic signatures	81
4.1.2.1	Gene ontology analysis of similarly changed RNA transcripts and proteins in APP-KI microglia	82
4.1.2.2	AD risk factors are significantly changed on the RNA and protein level of APP-KI microglia	84
4.1.3	Synaptic proteins within AD microglia	84
4.1.3.1	Synaptic proteins can be found within microglia proteomic data sets and increase as AD progresses	84
4.1.3.2	Validation of candidate synaptic proteins in free-floating sections	85
4.2	Homeostatic functions of <i>BIN1</i> in microglia	89
4.2.1	<i>BIN1</i> downregulation in the context of AD is recapitulated in free-floating sections of APP-KI mice	89
4.2.2	AAV vector design targeting BIN1 overexpression	90
4.2.3	<i>BIN1</i> overexpression <i>in vitro</i>	91
4.2.3.1	Establishing primary mouse microglia culture	92
4.2.3.2	BIN1 localizes with proteins of the endolysosomal machinery	93
4.2.3.3	AAV-treatment is innocuous and leads to broad mCherry expression	95

4.2.3.4	<i>BIN1</i> overexpression enhances phagocytosis-associated markers and leads to morphological changes	96
4.2.3.5	Bin1 signal increases during phagocytosis	98
4.2.3.6	<i>BIN1</i> overexpression enhances microglia phagocytosis . . .	99
4.2.3.7	Control construct experiments	100
4.2.3.7.1	AAV _{ctr} -treatment is innocuous and leads to broad mCherry expression	100
4.2.3.7.2	AAV _{ctr} -treatment does not enhance phagocytosis associated markers and does not change morphology	101
4.2.3.7.3	AAV _{ctr} -treatment does not increase microglial phagocytic potential	103
4.2.4	<i>BIN1</i> overexpression <i>in vivo</i>	103
4.2.4.1	<i>in vivo</i> distribution and cell specificity of AAV-Bin1	104
4.2.4.2	Microglia-specific increase of BIN1 and lysosomal marker after AAV-Bin1 inoculation	105
4.2.4.3	Correlation of BIN1 with CD68	107
5	Discussion	109
5.1	Primary mouse microglia isolated with MACS-based technology are of high purity and viability	110
5.2	Characterization of microglial dynamics during Alzheimer's Disease	111
5.2.1	Transcriptomic profiling of Alzheimer's Disease mouse microglia . .	111
5.2.1.1	Reduction of homeostatic signature genes	111
5.2.1.2	Increased proliferation and inflammatory phenotype	113
5.2.1.3	Decay of cellular motility and phagocytosis	114
5.2.2	Comparison with MGnD reveals similarities but also differences . .	115
5.2.3	Overlap between transcriptomic and proteomic signatures	116
5.2.3.1	Matching upregulated transcripts and proteins imply shift towards a more regenerative phenotype	117
5.2.3.2	Matching downregulated transcripts and proteins strengthen previously observed phagocytic dysfunction	118

5.2.4	Synaptic proteins are enriched within AD microglia lysosomes and correlate with phagocytic dysfunction	120
5.3	Homeostatic functions of BIN1 in microglia	121
5.3.1	<i>In vitro</i> primary mouse microglia culture	121
5.3.1.1	AAV/TM6 serotype as an excellent tool for <i>in vitro</i> microglia manipulation	122
5.3.1.2	<i>In vitro</i> , BIN1 localizes with proteins of the endolysosomal machinery and is upregulated during phagocytosis	122
5.3.1.3	BIN1 function in cultured microglia is linked to phagocytosis	123
5.3.2	<i>In vivo</i> overexpression of <i>BIN1</i>	124
5.3.2.1	Viral distribution is limited to targeted injection site but not limited to microglia	124
5.3.2.2	<i>BIN1</i> overexpression is specific for microglia and correlates with lysosomal marker CD68	126
5.4	Conclusions	127
	References	129
	Acknowledgements	169

Abbreviations

°C	Degree Celsius
µg	Microgram
µl	Microliter
1st	First
2nd	Second
3rd	Third
AACS	Acetoacetyl-CoA synthetase
AAV	Adeno-associated virus
Aβ	Amyloid-beta peptide
AD	Alzheimer's Disease
ADAD	Autosomal dominant Alzheimer's Disease
ADP	Adenosine diphosphate
AICD	Amyloid precursor protein intracellular domain
APC	Antigen presenting cell
APOD	Apolipoprotein D
APOE	Apolipoprotein E
APP	Amyloid precursor protein
ATP	Adenosine triphosphate
AU	Arbitrary units
β-actin	Beta-actin
BACE1	β-site APP-cleaving enzyme
BBB	Blood brain barrier
BCA	Bicinchoninic acid
BDNF	Brain-derived neurotrophic factor
Bin1	Bridging integrator 1
BrdU	5-Bromo-2'-deoxyuridine

BSA	Bovine serum albumin
CAA	Cerebral Amyloid Angiopathy
CA1	Subfield of hippocampal brain region
CCL	C-C motif chemokine ligand
CD11b	Cluster of differentiation molecule 11b
CD2AP	Cluster of differentiation molecule 2-associated protein
CD68	Cluster of differentiation molecule 68
cDNA	Complementary DNA
cKO	Conditional knock-out
CLAP	Clathrin and AP2 binding domain
CNS	Central nervous system
CSF	Cerebrospinal fluid
CSF1/M-CSF1	Colony stimulating factor 1/Macrophage colony stimulating factor 1
CSF1R	Colony stimulating factor 1 receptor
CX3CL1	C-X3-C motif chemokine ligand 1
CX3CR1	C-X3-C motif chemokine receptor 1
CXCL1	C-X-C motif chemokine ligand 1
CytoD	Cytochalasin D
DAM	Disease-associated microglia
DAMPs	Damage-associated molecular patterns
DAPI	4',6-diamidino-2-phenylindole
DIV	Days <i>in vitro</i>
DMEM/F-12	Dulbecco's Modified Eagle Medium/Nutrient Mixture F-12
DMSO	Dimethylsulfoxide
DNA	Deoxyribonucleic acid
DPBS	Dulbecco's phosphate buffered saline
EEA1	Early endosome antigen 1
E. coli	<i>Escherichia coli</i>

EDTA	Ethylenediaminetetraacetic acid
<i>e.g.</i>	lat. <i>exempli gratia</i> (for example)
EOAD	Early-onset Alzheimer's Disease
<i>et.al.</i>	lat. <i>et alia</i> (and others)
F4/80	Transmembrane G-protein coupled receptor in monocytes/macrophages
FAD	Familial Alzheimer's Disease
FBS	Fetal bovine serum
FcR	Fc receptor
FCS	Fetal calf serum
FDR	False discovery rate
g	Gram
GAPDH	Glyceraldehyde 3-phosphate dehydrogenase
GFAP	Glial fibrillary acidic protein
GM-CSF	Granulocyte macrophage-colony stimulating factor
GM-CSFα/β	Granulocyte macrophage-colony stimulating factor receptor α/β
GO	Gene ontology
GOF	Gain-of-function
GPM6A	Glycoprotein M6A
GWAS	Genome-wide association studies
h	Hour
hBIN1	human BIN1
HBSS	Hank's buffered salt solution
HEPES	Zwitterionic organic chemical buffering agent
HRP	Horseradish peroxidase
Iba1	Ionized calcium-binding adapter molecule
<i>i.e.</i>	lat. <i>id est</i> (that is)
IFN	Interferon
IL-1α/β	Interleukin 1 α/β

KD	Knock-down
kDa	Kilodalton
KI	Knock-in
KO	Knock-out
Lamp1	Lysosomal-associated membrane protein 1
LOAD	Late-onset Alzheimer's Disease
LOF	Loss-of-function
LSM	Laser scanning microscope
MACS	Magnetic-activated cell sorting
MAP	Microtubule-associated protein
MAPT	Microtubule-associated protein tau
MBD	Myc-binding domain
mBIN1	murine BIN1
mCherry	Basic monomeric red-fluorescent protein
mg	Milligram
MGnD	Microglial neurodegenerative phenotype
MHC	Major histocompatibility complex
MHC-II	Major histocompatibility complex class II
ml	Milliliter
mo	Months old
MOI	Multiplicity of infection
MS	Multiple Sclerosis
MW	Molecular weight
MYO5A	Unconventional myosin 5A
N	Number
NA	Numerical aperture
n.a.	Not applicable
NaCl	Sodium chloride

NADPH	Nicotinamide adenine dinucleotide phosphate
NDS	Normal donkey serum
NFT	Neurofibrillary tangles
NGS	Normal goat serum
NO	Nitric oxide
n.s.	Not significant
p	P-value
P2YR12	Purinergic receptor 12
LOAD	Late-onset Alzheimer's Disease
P4	Postnatal day 4
P5	Postnatal day 5
P6	Postnatal day 6
PAMPs	Pathogen-associated molecular patterns
PBS	Phosphate buffered saline
PCR	Polymerase chain reaction
PFA	Paraformaldehyde
pH	Potential hydrogen
PHF	Paired helical filament
PI	Phosphoinositide binding motif
PSD95	Postsynaptic density protein 95
PS-1/2	Presenilin-1/2 protein
PSEN1/2	Presenilin-1/2 gene
Rab5	Ras-related protein 5
RIN	RNA integrity number
RNA	Ribonucleic acid
RNAseq	RNA sequencing
ROI	Region of interest
ROS	Reactive oxygen species

RT	Room temperature
SAD	Sporadic Alzheimer's Disease
s.c.	Subcutaneous
scRNAseq	single-cell RNA sequencing
SD	Standard deviation
SH3	Src homology domain
SIGLECH	Sialic acid binding Ig-like lectin H
SMR	summary data-based Mendelian randomization
SNP	Single nucleotide polymorphism
snRNAseq	single nucleus RNA sequencing
SORL1	Sortilin-related receptor 1
STAT1/2	Signal transducer and activator of transcription 1/2
SIM	Structured super-resolution illumination technology
Syngn3	Synaptogyrin 3
t	Time
tg	transgene
TGF-β	Transforming growth factor β
TLR	Toll-like receptor
TMEM119	Transmembrane protein 119
TNFα	Tumor necrosis factor- α
TREM2	Triggering receptor expressed on myeloid cells 2
t-test	Student's t-test
U	Units
vg	Vector genome
vs.	lat. <i>versus</i> (against)
VGLUT1	Vesicular glutamate transporter 1
WB	Western Blot
WT	Wildtype

List of Figures

1	Alzheimer's Disease brain pathophysiology.	2
2	APP processing and amyloid plaque formation.	4
3	Main types of extracellular amyloid deposits in human Alzheimer's Disease brains.	6
4	Neurofibrillary tangle and dystrophic neurite pathology in Alzheimer's Disease.	8
5	Activated Microglia and Astrocytes cluster around amyloid plaques.	9
6	Microglia and Astrocytes during physiological and pathological conditions.	12
7	Microglia show a ramified morphology in the healthy, adult mouse brain.	19
8	Entrance pathways into the microglial cell.	23
9	Endolysosomal processing in microglia and links to candidate AD risk genes.	25
10	Candidate causal genes nominated through Hi-C and SMR approaches in 20 loci.	30
11	BIN1 isoforms and cellular distribution in humans and mice.	34
12	MG400 panel used for bulk RNAseq.	73
13	Microglia isolated with MACS are of high quality and purity.	74
14	RNA and post-sequencing quality control.	75
15	Transcriptomic signature of aged APP ^{NL-G-F} microglia is substantially dif- ferent compared to age-matched WT controls.	77
16	Overlap between MGnD and 12 mo APP ^{NL-G-F} microglia transcriptomics.	78
17	Gene ontology enrichment analysis for 12 mo APP ^{NL-G-F} microglia tran- scripts.	80
18	Comparison of significantly changed transcriptomic signature and proteom changes in APP ^{NL-G-F} microglia.	81
19	Gene ontology enrichment analysis for similarly regulated RNA transcripts and proteins in 12 mo APP ^{NL-G-F} microglia.	83
20	Synaptic proteins are significantly enriched in lysosomes of 6 and 12 mo APP ^{NL-G-F} microglia.	87
21	Lysosomal area increases in APP ^{NL-G-F} microglia but is less densely occupied.	88

22	BIN1 is downregulated in microglia from 12 mo APP ^{NL-G-F} mice.	90
23	BIN1 overexpression AAV construct.	91
24	Primary microglia cell culture.	92
25	Potential ligands and interaction partners of BIN1.	94
26	mCherry is abundantly expressed in transfected primary microglia.	96
27	Bin1 overexpression leads to changes in endolysosomal-associated markers and morphology.	97
28	CytoD efficiently decreases phagocytic activity.	98
29	BIN1 expression increases during phagocytic activity.	99
30	BIN1 overexpression enhances microglia phagocytosis.	100
31	mcherry is abundantly expressed in AAV _{ctr} transfected microglia.	101
32	AAV _{ctr} treatment does not lead to changes in endolysosomal-associated markers and morphology.	102
33	AAVctr treatment does not enhance microglia phagocytosis.	103
34	<i>In vivo</i> distribution and expression of AAV _{Bin1} after 30 dpi.	104
35	<i>In vivo</i> AAV _{Bin1} treatment leads to significant increases of BIN1 and CD68 in microglia.	106
36	<i>In vivo</i> AAV _{Bin1} treatment does not lead to significant increases of BIN1 in pyramidal neurons.	107
37	BIN1 and CD68 level from single microglia correlate with each other. . . .	108

List of Tables

3.1	List of Laboratory equipment and consumables used in this study	41
3.2	List of cell culture equipment and consumables used in this study	42
3.3	List of surgical equipment used in this study	42
3.4	List of microscopy equipment used in this study	43
3.5	List of RNAseq equipment used in this study	43
3.6	List of mouse lines used in this study	44
3.7	Primers used for genotyping of transgenic mouse lines	44
3.8	Reagents used for genotyping of transgenic mouse lines	44
3.9	Reagents and key consumables used for microglia isolations and culture . .	45
3.10	Solutions for microglia isolations and culture experiments	46
3.11	Reagents and key consumables for RNA sequencing	47
3.12	Reagents and key consumables used for mouse procedures	47
3.14	List of primary antibodies used for Immunofluorescence and Western Blotting	49
3.15	Solutions utilized for mouse procedures including histology	50
3.16	Reagents and key consumables used for Western blotting	51
3.17	Solutions used for Western blotting	52
3.18	Software tools used in this study	52
3.19	PCR master mix recipe	53
3.20	PCR program used to genotype for APP ^{NL-G-F}	54
3.21	PCR program used to genotype for GFP-M	54
4.1	List of 40 genes with the highest FC (up- and downregulated) in 12 mo microglia from APP ^{NL-G-F} mice compared to age-matched WT controls. . .	76
4.2	AD risk genes are significantly ($p_{adj} < 0.05$) changed on the RNA and protein level of 12 mo APP ^{NL-G-F} mice compared to age-matched controls.	84
4.3	List of synaptic proteins enriched in microglia from APP ^{NL-G-F} mice.	85
4.4	Protein fold-change of candidate synaptic proteins within APP ^{NL-G-F} mi- croglia.	86

1 Introduction

1.1 Alzheimer's Disease

lat. *dementia* /de:'men.ti.a/, [de:'mentiä] - "out of mind/madness/insanity"

Worldwide, over 55 million people live with dementia. This number is expected to double by 2030 and more than triple by 2050 (WHO.int/news). Treating and caring for people with dementia currently costs the world more than US\$ 1.3 trillion per year (alzint.org), making it a global concern with an enormous socioeconomic impact. To date, Alzheimer's Disease (AD) is the most prevalent cause of dementia in elderly patients, accounting for 60 - 70 % of all cases (2021 Alzheimer's Disease facts and figures). This progressive, neurodegenerative disease affects language, memory, reasoning and movement, interferes with the patients' daily life and ultimately leads to death. Moreover, disease onset is currently thought to occur 20 years before the manifestation of noticeable symptoms [1]. Despite tremendous efforts to understand the disease, there are currently no effective treatments to stop or delay AD progression. As a result, the World Health Organization (WHO) has acknowledged Alzheimer's Disease as a public health priority [2].

1.1.1 History and Pathophysiology of Alzheimer's Disease

In 1906, the German psychiatrist and neuropathologist Alois Alzheimer was the first to clinically describe an until then unknown form of dementia. His 51 year old patient Auguste Deter suffered from spatial and temporal disorientation, massive memory deficits as well as delusions. She was therefore hospitalized into a mental institution in Frankfurt am Main (Germany) where she died a few years later at the age of 55. The post-mortem neuropathological examination carried out by Alzheimer revealed a severe atrophy of the brain, an arteriosclerotic vasculature, strongly stained neurofibrils and abundant cortical deposits he described to be of an "unknown substance" (Fig. 1) [3, 4]. This unknown substance was later identified as Amyloid- β peptide (A β), the major component of amyloid deposits in the brain parenchyma and vasculature of AD patients [5, 6]. Although Alzheimer's Disease has now been extensively studied for more than 100 years and ma-

For progress has been made, especially on the molecular level, Alois Alzheimer's initial characterization of the main pathological features remains the standard for post-mortem diagnosis of the disease. Extracellular A β plaques (amyloid plaques) together with intracellular neurofibrillary tangles are to date the two hallmarks required for the most accurate neuropathological diagnosis (Fig. 1 C-E) [7].

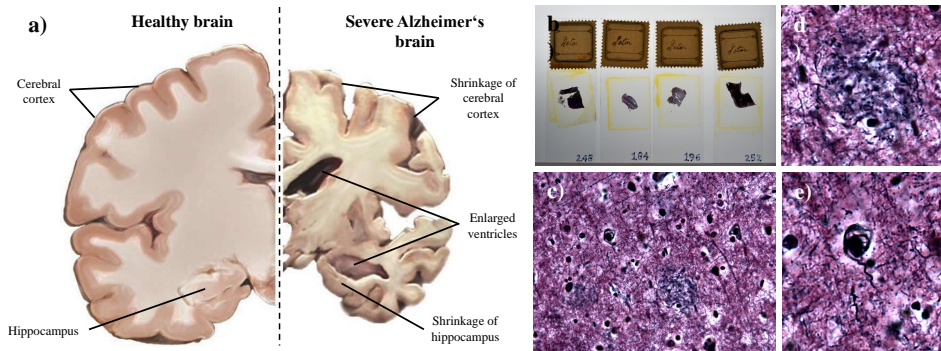


Figure 1: Alzheimer's Disease brain pathophysiology.

(A) A representative brain slice from an advanced-stage Alzheimer's Disease patient showing different signs of brain atrophy, such as enlarged ventricles and substantial shrinkage of cortex and hippocampus. Modified from <https://neurosciencenews.com> (B) Histological brain slice preparations of Auguste Deter by courtesy of Prof. Dr. Dr.h.c. Hans Kretzschmar from the Institute for Neuropathology of the Ludwig-Maximilians-University Munich. (C)-(E) Microscopic images of Auguste Deters brain slices taken and thankfully provided by Dr. Dr. Mario Dorostkar. (C) Overview of Bielschowsky silver staining for the illustration of AD histopathological hallmarks. Closeup images of an A β plaque (D) and neurofibrillary tangle (E).

1.1.1.1 Abeta pathology

1.1.1.1.1 Abeta peptide processing

The amyloid precursor protein (APP) is a type I single-pass transmembrane protein which, in humans, is expressed in three different splicing isoforms. While APP₆₉₅ is primarily expressed by neurons, APP₇₅₁ and APP₇₇₀ can be mainly found in peripheral tissues [8]. Although APP's physiological functions have not yet been fully elucidated, its role in the CNS has been attributed to neuronal and synaptotrophic properties, synaptogenesis, axonal growth and guidance as well as learning and memory functions [8, 9, 10].

The non-pathogenic mechanism of APP processing is known as the non-amyloidogenic or alternative pathway [11] (Fig. 2, left side). By means of APP cleavage with α -secretase, the otherwise pathogenic A β amino acid sequence is ruptured, generating a soluble APP

fragment (APP α) and a C-terminal fragment (CTF α or C83) [12, 13]. The CTF α can be further cleaved by the tetrameric γ -secretase complex (APH1, PEN2, nicastrin and presenilin-PS1 or -PS2), generating a 3 kDa peptide (p3) and a membrane-anchored APP intracellular domain (AICD) [14, 15].

Amyloid plaques are defined as extracellular aggregates of A β peptide that aberrantly accumulate in the brain parenchyma [16]. Generation of the 4 kDa A β occurs through sequential, proteolytic cleavage of APP by β - and γ -secretases (Fig. 2, right side) [14, 17]. The mechanism of APP processing leading to pathogenic A β formation is known as the amyloidogenic pathway and begins with cleavage of the extracellular region by the β -secretase BACE1 (β -site APP cleaving enzyme 1), generating a soluble APP fragment (APP β) and a membrane-bound C-terminal fragment (CTF β or C99) (Fig. 2, right side). Subsequently, the CTF β fragment is cleaved by the γ -secretase complex. Depending on the exact location of the cleavage site, A β -species of different lengths are generated (37 - 43 amino acids or longer) while a short intracellular domain (AICD) remains [14, 17, 18, 19, 20]. The most abundant A β -species are A β 40 (80-90 %) and A β 42 (5-10 %) [21]. Due to their higher hydrophobicity and propensity for aggregation, A β 42 species have been found to be the major constituent of extracellular amyloid plaques [19, 21, 22], making them the main contributor of the amyloidogenic pathway. In addition, N-terminally truncated A β -species, such as Pyroglutamate (pE3-A β) have also been found in amyloid plaques [23]. These modified species were similarly shown to have a high tendency for aggregation in combination with a higher neurotoxicity. Moreover, they seem to appear early in human AD cases and at more advanced pathological stages in AD mouse models [24].

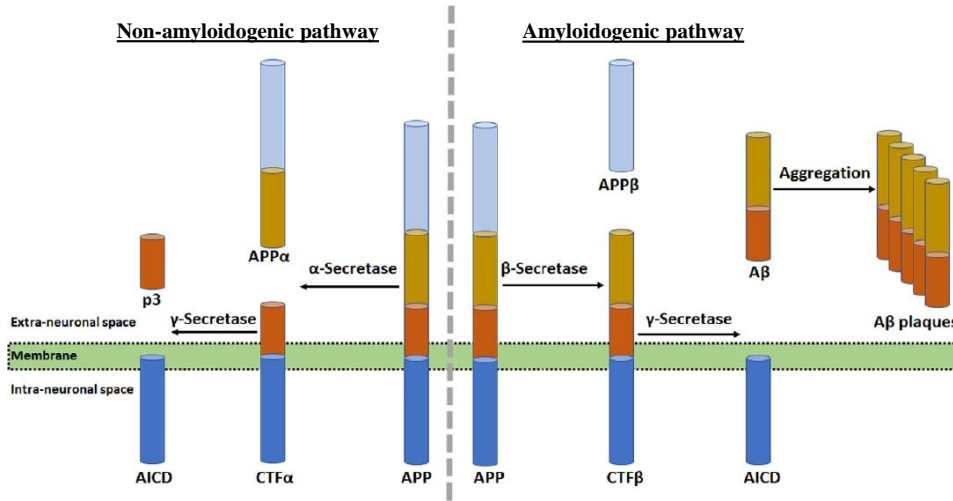


Figure 2: APP processing and amyloid plaque formation.

Graphic scheme showing the two alternative pathways of APP processing. The non-amyloidogenic pathway (left side) involves cleavage by an α -secretase, generating a soluble APP α and a membrane-bound CTF α fragment. Subsequent cleavage of the CTF α is carried out by the γ -secretase complex, leading to the formation of an AICD and a soluble peptide termed p3. During the amyloidogenic pathway (right side) the APP protein is first cleaved by a γ -secretase, generating a soluble APP β and a membrane-bound CTF β fragment. A second cleavage step by the γ -secretase complex results in the formation of an AICD and the pathogenic A β peptide, which, after aggregation, leads to the formation of amyloid plaques. Figure modified from Das *et al.* 2019.

1.1.1.1.2 Physiological and pathogenic roles of the Abeta peptide

Despite its negative connotation owing to its association with AD, A β peptide is also synthesized in healthy individuals under physiological conditions. Throughout the lifespan of an individual it can be readily detected in the cerebrospinal fluid (CSF) and plasma [16, 25, 26, 27]. The physiological functions of A β are currently believed to entail protection against infection, modulation of synaptic activity, neuronal survival and mechanisms required for memory improvement [27, 28, 29]. However, it has also been found that those beneficial functions are strictly linked to low levels of A β , whereas high levels induce deleterious effects [30, 31]. It is commonly believed that an unfavorable imbalance between A β production and clearance mechanisms constitutes one of the main causes of A β accumulation and amyloid pathology [32, 33].

In disease conditions it has been shown that soluble, monomeric A β peptides self-assemble into oligomers, which in turn are capable of aggregating into proto-fibrils and later on mature fibrils which display a typical β -sheet structure [34, 35]. Both A β 40 and A β 42

are capable of forming aggregates [36], however, A β 42 has shown to have a higher predisposition for oligomerization and aggregation than A β 40 [37]. Which A β conformation is primarily liable for the observed neurotoxicity has been fiercely debated for many years. Some studies could associate fibrillary A β formations with progressive neuronal toxicity [38, 39] while others proposed soluble oligomers as the main culprits and linked them to synaptic dysfunction and cognitive decline [40, 41, 42, 43]. Moreover, in AD patients and mouse models, levels of A β oligomers have been shown to correlate much better with AD symptoms and synapse loss than fibrillary amyloid deposits [34, 44, 45, 46]. In addition, initial AD symptoms even occur before plaques accumulate [47, 48, 49]. Perhaps the most persistent argument against the amyloid hypothesis is that many apparently healthy older individuals have substantial amounts of amyloid in their limbic and association cortices upon post-mortem examination [50]. Nevertheless, insoluble plaques in AD patients are typically surrounded by dystrophic neurites and might also act as a reservoir for oligomeric species, creating a continuous detrimental exchange [51, 52]. Notwithstanding, the observed pathogenicity associated with A β oligomers led to the formulation of the "A β oligomer hypothesis", which postulates A β oligomers as the main contributors of AD pathogenesis, especially during very early stages [52, 53]. In general, increasing evidence accumulates that age-related and/or genetic changes are causative for the observed increase in A β generation as well as impaired degradation and clearance pathways, leading to accumulation of A β in amyloid plaques [19, 54].

1.1.1.1.3 Abeta amyloid pathology

There are two main types of A β aggregates in the brain interstitial space of AD patients, which are morphologically distinct from each other [7, 16]. Dense core plaques incorporate a very condensed, fibrillar amyloid core which can be easily stained with β -sheet binding dyes such as Thioflavine S, Congo Red and Thiazine Red. The core is usually enclosed by a halo of less compact A β , where many oligomeric species can be found (FIG 3b and c) [7, 17, 55, 56]. Dense-core plaques are commonly surrounded by large numbers of reactive glial cells (microglia and astrocytes) and are typically associated with dystrophic neurites and synapse loss [7, 17]. On the other hand, diffuse amyloid plaques are made up solely of uncompact, non-fibrillar A β that forms amorphous structures and binds poorly to

amyloid-specific dyes (FIG 3a). In contrast to dense plaques, they seem to trigger a much weaker glial response [7, 16, 17, 56] and have been suggested to represent an early, immature stage of amyloid plaques that can also be found within otherwise healthy individuals during normal aging [7, 17]. Yet another type of extracellular plaque can be found within small to medium cerebral blood vessel walls. This pathological feature termed Cerebral Amyloid Angiopathy (CAA) is present in 85 - 95 % of all AD cases to varying degrees [7, 57] and was found to be the main cause of lobar intracerebral hemorrhages [58]. Similar to dense-core plaques, those deposits can be stained with amyloid-binding dyes (Fig. 3d). However, in contrast to the above described dense and diffuse plaques, they are mainly composed of A β 40 [59, 60].

Although very individual causes may lead to the development of Alzheimer's Disease, the gradual distribution and extension of A β pathology throughout the brain is relatively comparable between patients and has therefore been classified in different amyloid stages or phases. Initially, the Braak system defined three different stages of amyloid pathology: during stage A the basal frontal and temporal lobes are affected, followed by the neocortices and hippocampus in stage B. During the final stage C, amyloid pathology infiltrates the cortices, subcortical nuclei and the cerebellum [61]. A more detailed staging system was proposed shortly afterwards by Dietmar Thal, who described five phases of amyloid pathology: the neocortex is affected first in Thal phase 1, from where it extends into the allocortex in phase 2, then to the diencephalon and the basal ganglia in phase 3, the brainstem and midbrain in phase 4 and finally the cerebellum in phase 5 [62].

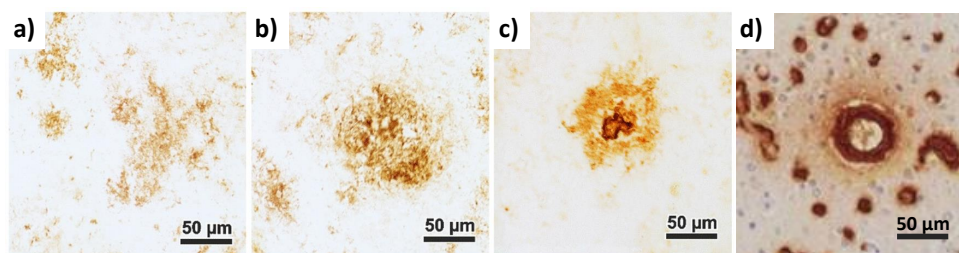


Figure 3: Main types of extracellular amyloid deposits in human Alzheimer's Disease brains. Visualization of different types of A β plaques from human AD patients via immunohistological staining against N-terminal A β . Depicted are diffuse plaques (A), dense plaques (B), dense-core plaques (C) and CAA deposits (D). Scale bars represent 50 μ m. Figures A - C modified from Röhr *et al.* 2020; D modified from Hondius *et al.* 2018.

1.1.1.2 Neurofibrillary tangles and dystrophic neurites

Microtubule-associated protein (MAP) tau, MAP1 and MAP2 are the three major microtubule-associated proteins of mature neurons [63]. There, they seemingly perform redundant functions, *i.e.* promoting the assembly and stability of microtubules. This apparent similarity may be due to the critical requirement of microtubules to maintain the axoplasmic flow, which, in turn, is essential to neuronal function [63]. The biological activity of tau is regulated by its degree of phosphorylation. For optimal activity the protein requires 2-3 mol phosphate/mol tau [64]. In Alzheimer's Disease, tau is abnormally hyperphosphorylated (p-tau), repressing its microtubule assembly and binding activity, leading to a breakdown of microtubules (Fig. 4a) [65, 66]. p-tau accumulates intracellularly as intraneuronal tangles of paired helical filaments (PHF), twisted ribbons and to a lesser extent straight filaments [63, 67, 68]. Those filaments give rise to neurofibrillary tangles (NFT) (Fig 4b), which were found to correlate directly with progressive dementia in AD [69, 70]. Although strictly intraneuronal, extracellular NFTs can be found in the brain parenchyma after neurons have died and are therefore known as ghost tangles (Fig. 4b) [68, 71]. Remarkably, neurofibrillary changes appear earlier and with a higher density in poorly myelinated areas than in myelin-rich regions [72].

In addition to their amyloid staging, H. and E. Braak defined six different stages (I - VI) for the classification of neurofibrillary tangle pathology [61]. Specific projection cells in the temporal lobe are the first cortical neurons to show changes (stage I). The lesions then extend into the entorhinal region (stage II), thus far mostly in the absence of amyloid deposits. The pathological process then extends into the hippocampus and the temporal proneocortex (stage III), followed by infiltration of the adjoining neocortex (stage IV). From here, the NFTs spread superolaterally (stage V) and finally propagate throughout the primary areas of the neocortex (stage VI).

Hyperphosphorylated tau filaments can also be found in dystrophic neurites that occur at amyloid plaques and in the neuropil (neuropil threads) [68]. Dystrophic neurites are abnormal neuronal processes (mainly axons) characterized microscopically by their bulbous swelling, aberrant sprouting and accumulation of various cellular organelles and proteins (*e.g.* degenerating mitochondria, APP, tau, synaptic and neurofilament proteins)

[7]. The observed accumulation of cellular components is presumably due to disrupted transport mechanisms that were previously dependent on functional microtubules [73, 74]. Dystrophic neurites are frequently associated with dense-core senile amyloid plaques and together they form the so-called neuritic plaques (Fig 4c) [7, 75]. Intriguingly, neuritic plaques were shown to correlate well with cognitive decline and neuronal loss observed in AD [7, 71].

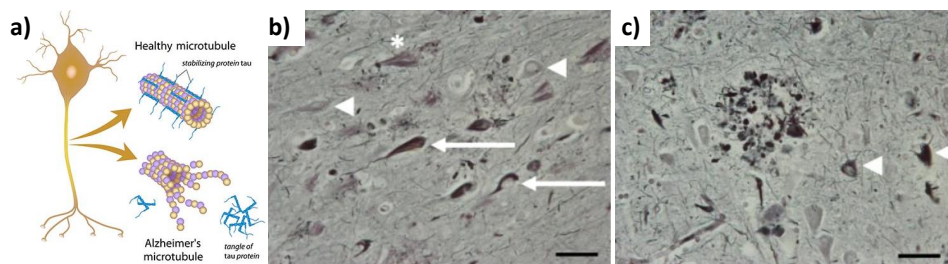


Figure 4: Neurofibrillary tangle and dystrophic neurite pathology in Alzheimer's Disease. (A) Neuronal tau binds to microtubules, helping them to maintain their structure. When tau is hyperphosphorylated and not bound to axonal microtubules, it undergoes conformational changes that lead to its aggregation and tangle formation in the cytoplasm. In this state it no longer stabilizes neuronal structures. Silver stainings showing neurofibrillary tangles (B) and dystrophic neurites from a neuritic plaque (C). In (B), the arrows indicate mature tangles, the arrowheads pre-tangles and the asterisk a ghost tangle. In (C), the arrowheads indicate neurofibrillary tangles. Scale bars represent 40 μm . Figure a) modified from <https://bio-rad-antibodies.com/blog/>; b) and c) modified from DeTure and Dickson 2019.

1.1.1.3 Neuroinflammation

Neuroinflammation generally refers to an inflammatory response of the brain's innate immune system to shield against pathological insults such as infection, trauma, ischemia and toxins [76]. Alois Alzheimer was probably the first to describe signs of neuroinflammation in AD by reporting the presence of fibrous glia (probably astrocytes) and a separate type of glia containing large deposits (probably microglia) in the brain of Auguste Deter [3]. In fact, the presence of reactive microglia and astrocytes adjacent to $\text{A}\beta$ plaques (Fig. 5) and substantially increased levels of pro-inflammatory cytokines and chemokines (*e.g.* IL-1 β , IL-6, IL-18, TNF- α , CCL1, CCL5, CXCL1) as well as small-molecule messengers (including prostaglandins, nitric oxide (NO)) and reactive oxygen species have consistently been observed in both AD patients and mouse models [76, 77, 75, 78, 79, 80, 81]. The most pivotal immune cells involved in this process are microglia and astrocytes, but capillary endothe-

lial cells and infiltrating blood cells also contribute to neuroinflammation, especially when the blood-brain-barrier (BBB) experiences substantial biochemical or mechanical damage [82, 83].

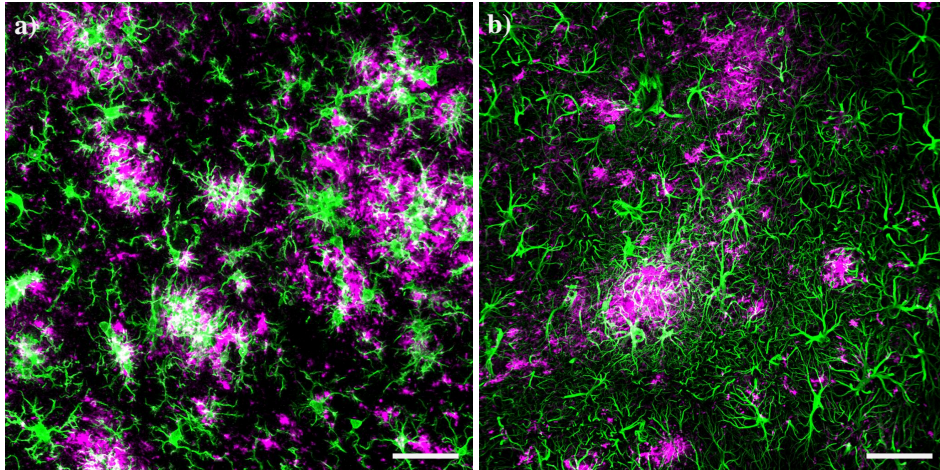


Figure 5: Activated Microglia and Astrocytes cluster around amyloid plaques. Images were acquired in the hippocampal CA1 region of a 12 mo APP^{NL-G-F} mouse. **(A)** Microglia (Iba1, green) are in close contact with the outer and inner regions of diffuse amyloid plaques (NAB228, magenta). **(B)** Astrocytes (GFAP, green) extend their feet towards the plaque (NAB228, magenta), surrounding it. Scale bars represent 50 μm .

The characteristically star-shaped astrocytes (or astroglia) are key players in maintaining brain homeostasis by providing metabolic and trophic support to neurons, regulating cerebral blood flow, maintaining fluid and neurotransmitter homeostasis and inducing synapse formation (Fig. 6a) [84, 85, 86, 87, 88]. Astrocytes also form unique perivascular channels in the CNS, known as the glymphatic system, which eliminates potentially neurotoxic waste products, including amyloid and tau species [89, 90]. In case of pathological insults, astrocytes are known to initiate reactive gliosis (Fig. 6b) [88]. The generic term "reactive astrocyte" has been used in the past to describe astrocytes that, upon pathogenic stimulus, undergo morphological changes towards hypertrophic processes and upregulation of glial fibrillary protein (GFAP). Nowadays it is accepted that there are at least two separate "active" phenotypes, termed A1 and A2 [91]. Inflammatory insults have been proposed to induce the A1 phenotype through the NF- κ B pathway, whereas ischemia induces the A2 phenotype via the signal transducers and activators of transcription 3 (STAT3) pathway [91]. While A2 astrocytes act mainly protective through expression of neurotrophic factors,

A1 astrocytes are characterized by the expression of inflammatory mediators and seem to lose their homeostatic functions, enabling them to induce apoptosis in neurons and oligodendrocytes [92]. In an animal model of AD, those cells were found to release excessive amounts of GABA and glutamate, leading to impaired memory function and synapse loss [93]. Moreover, they contribute to a dysregulated microcirculation and a fractured BBB, which actively promotes the accumulation of A β and disease progression [94, 95]. Also noteworthy is the finding that astrocytes work closely together with microglia and could be mediators of adverse effects in AD [92].

Microglia are innate immune cells of the myeloid lineage and represent the first line of defense in the CNS through active protection against various insults and by promoting tissue repair [96, 97] (the microglial role in the CNS and Alzheimer's Disease is discussed in depth in section 1.2 of the introduction). Ramified microglia continuously survey the CNS microenvironment with their highly motile processes, sense damage signals (such as ATP) and mediate a response towards the injury site (Fig. 6a) [98, 99, 100]. Similar to astrocytes, microglial morphology changes quite drastically upon encountering potential threats and react by releasing a powerful cocktail of inflammatory factors (i.e. cytokines, chemokines and reactive oxygen species) (Fig. 6b). On the other hand, alert microglia consume recognized hazards such as pathogens, cell debris and abnormal proteins (including A β species) [101] and degrade them through various endocytic pathways [102]. Moreover, it has been shown for AD and other neuroinflammatory diseases that they deliberately recruit other immune cells (*e.g.* astrocytes) through release of pro-inflammatory cytokines such as IL-1 α , TNF- α and C1q [92]. This machinery usually ceases once the immune stimulus is eliminated. However, microglia in aged brains have functional impairments and are prone to sustained activation, which might contribute to the pathogenesis of neurodegenerative disorders such as AD. Furthermore, many identified risk genes associated with AD are predominantly expressed in microglia (*e.g.* *TREM2*, *BIN1*, *CR1*, *ABCA7* and *CD33*) [103], suggesting that these factors are involved in pathogenicity through mechanisms involving microglia. However, for most of those factors it is still unclear how they contribute to AD pathology (detrimental or protective) and which functions they cover in homeostatic and disease-associated microglia (DAM).

Assessing the definite role of neuroinflammation in AD is very complex, as both beneficial

and detrimental behavior has been observed for both glia populations. It is also still under debate whether neuroinflammation could be a driving force or is a mere consequence of disease progression [79]. On one hand, microglia and astrocytes confer protection through the clearance of A β and cell debris [104, 105]. On the other hand, once primed and activated, both glia cells are known to release pro-inflammatory cytokines such as IL-1 β , IL-6 or TNF- α that could promote and accelerate a neurotoxic phenotype [105]. Additionally, microglial reactivity probably contributes to both A β and Tau pathology and spreading [106, 107, 108, 109, 110]. The current knowledge implicates that microglia and astrocytes may have a protective role during early disease stages by promoting A β and debris clearance which later on becomes inefficient (decreased clearance) and even detrimental in a vicious cycle of auto-activation and neurotoxicity [105, 111].

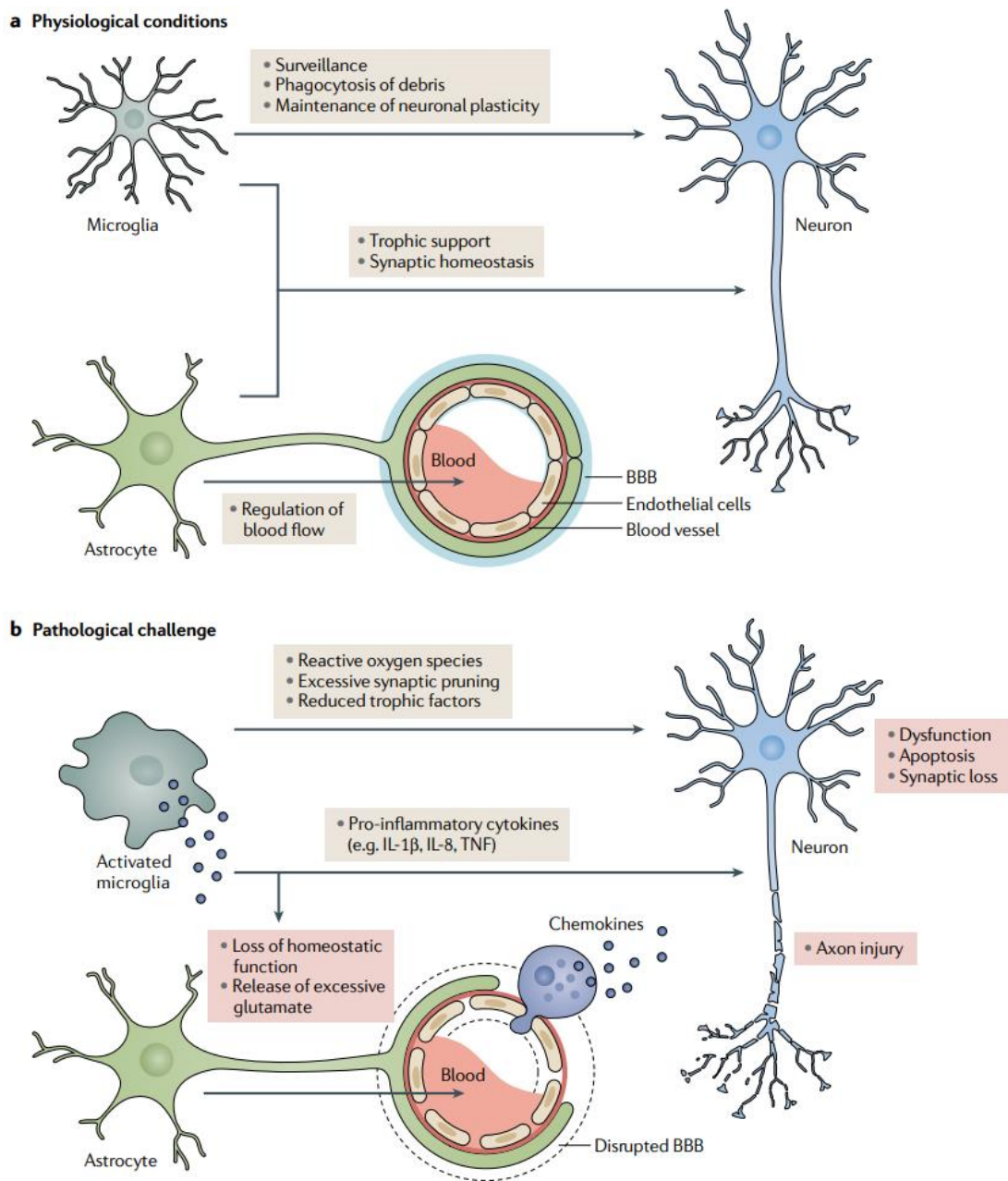


Figure 6: Microglia and Astrocytes during physiological and pathological conditions.

(A) During homeostatic conditions, ramified microglia constantly survey the brain parenchyma with their highly motile processes. They sense damage signals, phagocytose cellular debris and form transient contacts with synapses and axons, thereby maintaining neuronal plasticity. The fine processes of astrocytes tightly envelop blood vessels and synapses. The physiological roles of astrocytes include the regulation of cerebral blood flow, maintenance of synaptic homeostasis and neurotrophic support. (B) During pathological conditions, activated microglia, astrocytes and macrophages migrating through the damaged blood-brain-barrier (BBB) contribute to the development of a neuroinflammatory phenotype. They lose their homeostatic functions, reduce the secretion of neurotrophic factors and instead increase the production of pro-inflammatory factors. The secretion of cytokines and chemokines aids pathogen and toxin clearance but was also shown to lead to neuronal dysfunction and tissue damage. In addition, reactive microglia can directly eliminate synaptic structures. Figure modified from Leng and Edison 2021.

1.1.2 The amyloid cascade hypothesis

The amyloid cascade hypothesis was originally published by Hardy and Higgins in 1992 [112] and later updated based on the knowledge gained in 25 years since its first appearance [113]. The hypothesis proposes that, for Alzheimer's disease, the accumulation and deposition of A β peptides is the main pathogenic event that triggers a vast cascade of pathological insults, such as the formation of NFTs, neuronal cell loss, vasculature damage, neuroinflammation and dementia [112, 113]. The hypothesis was based on the discovery that specific genomic mutations in *APP* or the Presenilin genes (*PSEN1/2*) lead to a shift in A β generation, which causes early-onset AD. In line with those findings, humans with trisomy 21 (triplication of chromosome 21, also known as Down's syndrome) hold three copies of the *APP* gene and invariably develop neuropathological AD, usually at an early age [112, 113]. Yet another piece of evidence supporting this hypothesis is the protective missense mutation "A673T-Icelandic" in the human *APP* gene, which leads to a lifelong reduction of potentially toxic A β species and seems to shield against AD and age-related cognitive decline [114]. Moreover, several AD-related neurotoxic effects could be directly linked to A β [112, 113]. However, the amyloid cascade hypothesis also received some criticism due to the fact that amyloid plaque load (either total amyloid, dense-core plaques or only neuritic plaques) doesn't seem to correlate well with cognitive impairment and neuronal cell loss [115, 116, 117, 118, 119]. In addition, non-demented, elderly individuals frequently show considerable amyloid burden by Positron Emission Tomography (PET) imaging [115]. Although this hypothesis opened up a wide field of possibilities with respect to therapeutic targeting of A β production (through β - and γ -secretase inhibitors) or A β clearance (through active or passive immunization), none of the well-implemented clinical trials succeeded in stopping AD progression [120, 121]. Of note, some trials failed to ameliorate cognitive decline despite achieving substantial clearance of A β plaques from the brain [122, 123, 124]. Therefore, new intervention approaches along with a much more thorough understanding of disease etiology are urgently needed.

1.1.3 Etiology

Both genetic and environmental factors contribute to the manifestation of AD. The greatest risk factor is, however, age. At age 65 the probability of having AD is estimated to be 3 %, rising to over 30 % by age 85 (Alzheimer's Association 2019 AD facts and figures). Alzheimer's Disease is currently classified by age of onset and whether prominent genetic factors are involved or not, which entails two major forms of AD.

Early-onset AD (EOAD), also known as familial AD (FAD) accounts for the minority of all AD cases (1-6 %) and manifests relatively early, usually between age 30 and 65 [1]. FAD cases develop largely due to autosomal dominant mutations in *APP*, *PSEN1* or *PSEN2*. As a result of its considerable inheritance probability, this form was also termed autosomal dominant AD (ADAD) [125]. *APP* was the first gene shown to have far-reaching mutations causing AD, nowadays over 50 are described in the literature. Some of the most studied mutations include the Swedish (KM670/671NL) [126], Arctic (E693G) [127], London (V717I) [128] and Indiana (V717F) [129] mutations, which all cluster around cleavage sites for β - and γ -secretase [130]. Those mutations are described to result in an increased $A\beta$ generation or a shift in the $A\beta$ 40/42 ratio, leading to increased aggregation capability and amyloid accumulation [125].

More commonly for FAD cases are mutations located in *PSEN1* or *PSEN2*, with *PSEN1* mutations alone accounting for 30-50 % of all genetic AD cases [131, 132]. Research shows that *PSEN1* and *PSEN2* mutations alter $A\beta$ generation, similar to those in *APP* [133], but strangely seem to confer a loss of function, raising questions as to how this fits the amyloid hypothesis [134, 135] (More recently discovered risk factors are discussed in the sections below: "New risk factors and GWAS studies" and "Microglia-associated risk factors").

The second and by far most common form of AD, accounting for 94-99 % of all cases, is the so-called sporadic (SAD) or late-onset form of AD (LOAD). It usually manifests beyond the age of 65 and presents no distinct genetic link, although it shares the same clinical and pathological features of EOAD. It is generally believed that LOAD is driven by the interaction between multiple smaller genetic risk variants and environmental factors. The highest scoring genetic risk factor identified for sporadic AD is the $\epsilon 4$ variant of the Apolipoprotein E (*APOE*) gene, while the $\epsilon 2$ variant of the same gene conveys protection

[136]. People carrying one $\epsilon 4$ allele already have a three-fold increased risk of developing AD, while carrying two alleles increases it approx. 12-fold [136]. APOE is a high-density lipoprotein which, although mainly synthesized in the liver, can also be found in the peripheral and central nervous system, where it is mainly produced by astrocytes and to a lesser extent microglia [137, 138]. Additionally, neurons express APOE in response to excitotoxic damage [139]. Although it is not yet clear how APOE affects AD etiology, some studies suggest that binding of APOE and $A\beta$ might influence clearance and aggregation of the latter [140]. Recent genome-wide association studies (GWAS) and sequencing approaches have now detected several interesting risk loci that contribute to sporadic cases of AD [141, 142], however, the search for a unifying cause still goes on.

1.1.4 New risk factors and GWAS studies

Due to the impalpable nature of LOAD, new approaches are undeniably needed to shed more light onto the underlying processes. In-depth human GWAS, along with whole-genome or single-cell sequencing approaches and gene-expression network analysis have concomitantly identified more than 40 novel risk factors, which are mainly involved in lipid metabolism, endocytosis and innate immunity [143, 144, 145, 146, 147, 148, 149, 150, 151]. Importantly, in contrast to sequencing approaches, GWAS identify genome regions (loci) that associate with a trait rather than a specific gene. Some loci may indeed contain a single gene, while others may associate with multiple genes [152]. The challenge is therefore to fine-map these loci to identify specific genes that contain causal functional variants and to understand the pathomechanisms leading to increased or decreased risk for disease. It is also important to note that labeling of those single-nucleotide polymorphisms (SNPs) is based on proximity to the closest gene, which may not necessarily mean that the disease-associated SNP has any functional interaction or relevance for that gene. In fact, the affected gene (if any) could be many kilobases away. Another layer of complexity is added when identified risk loci reside in non-protein-coding or regulatory regions (promoters, enhancers, regulatory RNAs), which make up the vast majority of human DNA ($\sim 90\%$) [153, 154]. Those limitations necessitate careful functional validation, *i.e.* computational fine-mapping approaches that integrate information regarding chromatin state,

DNA methylation, splicing and gene expression. Those should be followed by *in vitro* and *in vivo* studies to further validate the match and seek to determine the effects in an appropriate model [152]. Albeit thorough and complete functional studies are mostly still missing, integrating information from multiple sources can provide meaningful evidence in support of specific genes and pathways (*e.g.* combining GWAS hits with RNAseq and proteomic datasets).

That being said, a considerable number of polymorphisms were found in and near genes that are, in some cases exclusively, expressed in microglia [103]. Among others, coding variants were found in *TREM2*, *BIN1*, *PLCG2*, *AB11*, *ABCA7*, *CD33*, *SPI1*, *CR1*, *MS4A4S* and *INPP5D* [103, 151, 152, 155]. Although it is not yet clear how each polymorphism contributes to AD etiology, it has been recognized that one of the crucial drivers of LOAD could be reduced A β clearance and degradation, leading to the accumulation of oligomeric and eventually fibrillary plaques in the brain, which in turn could amplify the microglial inflammatory phenotype [32, 156]. Moreover, genetic and early functional studies have also implicated microglia as a causal factor in LOAD, as opposed to being solely a biological response [157, 158]. Interestingly, some of the identified risk variants occur in genes that are supposedly involved in the process of microglial phagocytosis and lysosomal degradation, such as *TREM2*, *BIN1*, *CD33*, *CR1* and *ABCA7* [150, 152, 159]. By looking at the role of microglia in AD, we may uncover new therapeutic targets to help treat this disease.

1.2 Microglia in health and disease

Microglia are CNS-resident immune cells that, depending on the region of interest, account for roughly 10 % of the total cell population in humans and mice [160, 161]. A series of influential studies has revealed that they contribute to many aspects of brain development and physiology. In particular, microglia are now known to regulate apoptosis and survival of neurons, neuronal circuit wiring, synaptogenesis, synaptic transmission, pruning of synapses and myelination of axons [162, 163, 164, 165, 166, 167, 168, 169]. Consistent with these functions, microglia are considered either a causal or contributing factor to many brain afflictions, ranging from neurodevelopmental to neurodegenerative disorders [162, 163, 164, 165, 166, 167, 168, 169]. During AD, microglia convey neuroprotective

as well as neuroinflammatory behavior, that - when maintained - can promote neurotoxicity [163, 170]. Despite recent advances in the field, how microglia colonize the brain, whether and how many distinct states of microglia exist, the association between these proposed states and specific functions, and the nature of the lasting impact of microglial dysregulation on the brain remain important and open questions [169].

1.2.1 Ontogeny

Phagocytic microglia were first described by the Spanish researcher Pío del Río-Hortega in 1919 (Río-Hortega, El "Tercer Elemento" de los Centros Nerviosos. I. La Microglia en Estado Normal, 1919). Since the discovery of microglia over 100 years ago, their mesodermal ontogeny was highly debated up until recently, highlighting their complex nature [165, 171, 172]. *In vivo* fate-mapping studies could clearly show that microglia are unique in origin compared to all other brain cell types, which derive from the neuroectoderm [173, 174, 175]. In contrast to other phagocytic cells (*e.g.* peripheral macrophages), microglia develop from early erythro-myeloid progenitors in the yolk sac, starting at embryonic day 7.5 (E7.5) [176, 177]. By E9.5 they begin to migrate into the developing brain, where they rapidly proliferate and colonize the whole brain parenchyma [171, 178]. Following a second wave of yolk sac hematopoiesis, the BBB closes at E13.5, hence restricting the infiltration of other immune cells [179].

The embryonically seeded microglia develop into a population that self-renews throughout life without significant peripheral contributions [164, 180]. Transcription factors that are essential for the regulation of microglia development are primarily RUNX1, PU.1 and IRF8 [181]. During later stages of development CSF1R, IL-34 and TGF- β become additionally involved and are of equal importance [181]. Moreover, the preservation of adult microglia largely depends on the presence and activation of CSF1R. It is known that genetic or chemical inhibition (*e.g.* through PLX5622) of this receptor leads to a dramatic drop in microglia survival, an approach used by scientists for depletion studies [182, 183, 184]. Two well-known ligands for CSF1R are CSF1 and IL-34. Although they are both produced by neurons, CSF1 is additionally released by glial cells [170, 185, 186].

Under physiological conditions, adult human and mouse microglia proliferate in a seemingly

random way but expand clonally when faced with pathological conditions [187]. Interestingly, highly conflicting results have been obtained for the predicted turnover rates in mice, ranging from three months [188] to 15-28 months [189] and even 41 months for a complete turnover in the cortical area [187]. Similarly converse results were obtained when studying the self-renewing capacity of human microglia. One study predicted human microglia to self-renew an estimated 100 times during an average lifespan of 80 years (approx. every 10 months) [188], while another study showed that they renew at a much slower pace with an average turnover rate of 4.2 years (50 months) [190].

1.2.2 The physiological role of microglia in the CNS

Microglia are key players during brain development but also throughout adulthood. They are now characterized to execute different programs with unique molecular signatures [168, 191]. During embryonic and early postnatal development microglia show a less ramified, ameboid morphology (similar to tissue-resident macrophages), which suggests a higher level of activation and phagocytosis [191, 192]. Amid this crucial developmental stage, microglia have been shown to clear excessive or apoptotic neuronal precursor cells [188, 193] but also to promote neuronal precursor proliferation and maturation [194], thereby fundamentally influencing neurogenesis. Furthermore, a very thorough series of publications by Beth Stevens and colleagues could nicely show how microglia in the developing brain are involved in a process called synaptic pruning, a tightly regulated mechanism involved in the removal of excess synapses for the correct establishment of neuronal networks [195, 196, 197, 198]. Besides neurons, microglia have been shown to support the development and function of oligodendrocytes and are additionally involved in the process of postnatal myelination [199, 200]. Studies performed in global CSF1R-deficient mice led to a depletion of microglia and subsequently resulted in manifold brain abnormalities and premature death, further supporting the essential involvement of microglia in the developing brain [201].

In the adult mouse brain, microglia are homogeneously distributed with an average of 6500 cells/mm³ (Fig. 7a) [98], although regional differences are also observed [192]. In contrast to developing microglia, adult cells show a ramified morphology with highly motile second-order branches and filopodia, which allow them to survey the brain parenchyma (Fig. 7b) [100].

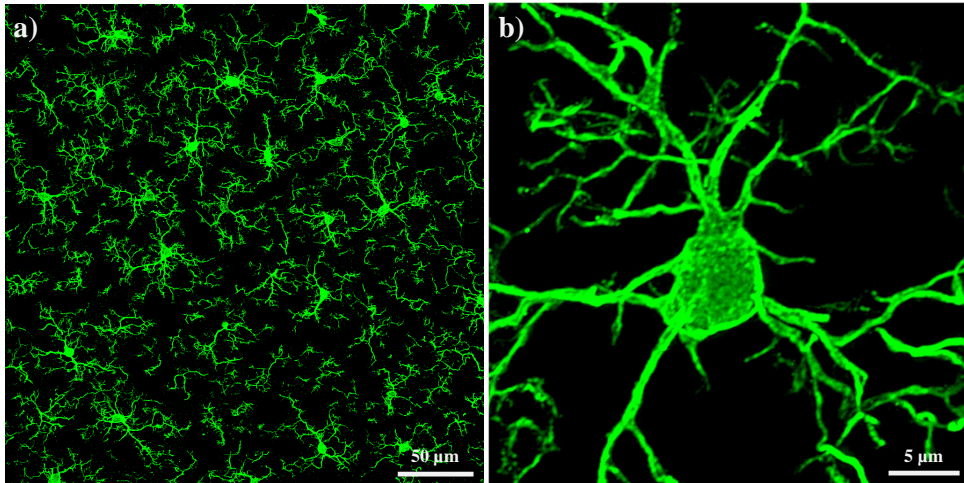


Figure 7: Microglia show a ramified morphology in the healthy adult mouse brain. (A) Microglia labeled with Iba1 (green) show a homogeneous distribution and ramified morphology. (B) Closeup image of a single microglia. Images were acquired in the hippocampal CA1 layer of a healthy, adult C57Bl/6J mouse. Scale bars represent 50 and 5 μm , respectively.

1.2.2.1 Characterization of homeostatic microglia

Microglia, as key regulators of the CNS environment, have been deeply characterized at the molecular level. Despite the detection of region-specific differences [169, 202], common profiles of homeostatic microglia are frequently observed, especially at the transcriptomic level. These so-called homeostatic signatures contain but are not limited to *P2ry12*, *P2ry13*, *Tmem119*, *Cx3cr1*, *HexB*, *Sall1*, *Siglech*, *Csf1r*, *Olfml3* and *Gpr34* [203, 204, 205, 206, 207]. Interestingly, translational studies could identify several homeostatic signature genes in healthy human microglia [208, 209]. In fact, Galato and colleagues could show a substantial overlap between murine and human microglia transcriptomic profiles (*e.g.* *P2ry12* and *Cx3cr1*), although differences were also observed, especially during age-related changes [208]. Of note, in another study aged but otherwise healthy human microglia showed a progression towards an AD-related phenotype with the upregulation of several AD risk-genes such as *Trem2*, *Sorl1*, *CD33* and *MS4A4A* [209].

Sensing subtle changes in the brains microenvironment is one of the major functions of microglia, which is why they express a specific cluster of genes to perform this task, called the sensome. The sensome is mainly composed of receptors which allow the microglia to detect various kinds of threats. To sense pathogen-associated molecular patterns (PAMPs)

and damage-associated molecular patterns (DAMPs), microglia are equipped with pattern-recognition receptors (PRRs), such as scavenger receptors (SRs) (*e.g.* Cd14, Cd36, Cd47), toll-like receptors (*e.g.* Tlr2, Tlr4, Tlr7, Tlr13) and C-type lectin receptors (*e.g.* Clec5a, Clec7a, Clec4a3) [170, 210]. Additionally, the sensome contains purinergic receptors (*e.g.* P2y12, P2y13) to sense extracellular ATP released by dying neurons and cytokine and chemokine receptors (*e.g.* Cx3cr1, Ccr5, Csf1r, Tgfbr1, Tgfbr2) to respond appropriately to cues released from other cells [170, 210]. As the brains resident immune cells, microglia respond to threatening changes in their environment by releasing a powerful cocktail of pro-inflammatory cytokines (*e.g.* IL-1 β , IL-6 and TNF- α) that activates nearby glia, including astrocytes, thereby promoting an inflammatory phenotype [168]. Nevertheless, microglia display exceptional plasticity and are known to vary their response tailored to the type of insult. For example, a bacterial infection results in the production and secretion of pro-inflammatory factors, while the phagocytosis of apoptotic cells and debris is accompanied by the increased production and release of anti-inflammatory factors [211]. Moreover, they are also described to act as antigen-presenting cells (APCs). Similar to macrophages, B-cells and dendritic cells, they express the major histocompatibility complex II (MHCII) together with costimulatory factors required for the presentation of foreign antigens to T-cells [170]. To prevent a state of overactivation in microglia, they are additionally equipped with several checkpoint mechanisms which are mainly triggered through the direct interaction with neurons [211]. Some receptor-ligand interactions known to induce a non-reactive state are described for Cx3cr1 - Cx3cl1 and CD200R - CD200, with the receptors expressed by microglia and the ligands by neurons [211, 212, 213].

Apart from the often described homeostatic markers Tmem119, P2y12 or Cx3cr1, resting but also active microglia are often immunohistochemically visualized with primary antibodies against the ionized calcium-binding adapter molecule 1 (Iba1) (*e.g.* Fig. 5, 7). Cytoplasmic Iba1 has actin-bundling activity and is involved in membrane ruffling and phagocytosis [214, 215, 216]. Another marker for microglia but also macrophages is the cluster of differentiation 11b (CD11b), which is part of complement receptor 3 (CR3) and binds to antigens to facilitate their uptake. Another important microglia marker is the cluster of differentiation 68 (CD68), which, as lysosomal marker, is commonly taken as surrogate for activation, although modest levels are also found in homeostatic cells [216].

Overall, microglia are highly dynamic, powerful cells, that are equipped with a wealth of sensing and reactive mechanisms. Their sensitivity allows them to respond swiftly to changes in the microenvironment and helps to defend it against exo- and endogenous threats but also to maintain brain homeostasis and a healthy neuronal architecture.

1.2.3 Microglia in Alzheimer's Disease: a double-edged sword

The precise role of microglia in AD but also other neurodegenerative diseases is still unclear, due to conflicting studies identifying both beneficial as well as detrimental effects mediated by microglia. As a result, the function of microglia during extreme pathological challenges has been aptly termed a "double-edged sword" [217].

As discussed earlier (section 1.1.1.3), prominent clusters of activated microglia can be found in both murine and human AD tissue surrounding plaques (Fig. 5a) [218]. Earlier *in vivo* two-photon studies reported that microglia react almost immediately to forming amyloid plaques by polarizing their processes and start migrating towards the source [219, 220]. As our brains sentinels, they aim to eliminate toxic insults. To achieve clearance, they express distinct receptors that help to identify and bind A β [163, 221]. To further increase A β removal efficiency, they initiate an inflammatory response which attracts more glia cells [222]. Intriguingly, although the reasons for this are still unknown, it has been shown that the phagocytic capacity of microglia in AD is compromised [223, 224]. As AD progresses and its diverse pathological aspects can not be resolved, inflammation becomes chronic. This inevitably leads to neurotoxic side effects mediated by pro-inflammatory cytokines and uncontrolled pruning of synapses by microglia [163, 222, 225]. Although not intended as a feasible treatment, depletion of the microglia cell population in AD mouse models prevented spine as wells as neuron loss and reduced inflammation, pointing to the detrimental role of microglia during the chronic phase of this disease [226, 227].

In general, microglia seem to have a beneficial effect during the early stages of AD, which later on may become disadvantageous due to impaired or insufficient clearance and degradation of A β deposits. Thus, identifying and analyzing the molecular mechanisms underlying microglial deterioration is fundamental for the identification of novel therapeutic targets that could help increase amyloid clearance and reduce neuroinflammation.

1.2.3.1 Mechanisms of abeta clearance in the CNS

There are two main mechanisms described for the clearance of A β from the brain. One involves its drainage or transport to the peripheral blood and lymphatic system, while the other deals with its on-site degradation within the CNS [228]. The general mechanism of A β clearance from the brain into the peripheral blood stream centers around low-density lipoprotein receptor related protein 1 (LRP1) and receptor for advanced glycation end products (RAGE), which are located within the cerebral endothelium. Binding of A β to LRP1 and RAGE promotes its transcytosis across the BBB, thereby sequestering 70-90 % of plasma A β peptides in healthy individuals [229, 230]. It has been found that the expression of LRP1 is significantly reduced in AD patients, which probably contributes to the accumulation of toxic amyloid species [230, 231]. Furthermore, it has been suggested that APOE might be involved in LRP1-mediated transport of A β across the BBB [231].

Local extracellular clearance of A β takes place through various degrading proteases, such as NEP, IDE, ECE1, ACE, MMP9 and PreP. However, the two metallo-proteases Neprilysin (NEP) and Insulysin (IDE) are considered to be the two major A β degrading enzymes [17, 221]. NEP is a type II integral membrane protease, facing the extracellular space with its active domain. It is primarily expressed by neurons, microglia and astrocytes and is believed to be the most effective amyloid-degrading protease [228]. Interestingly, decreased levels and reduced activity of NEP in the brains of AD patients have been found to inversely correlate with A β accumulation and clinical diagnosis [232]. On the other hand, the zinc metallo-protease IDE is mainly found as a cytosolic protein in microglia but also at the cell surface of neurons [228, 232]. Additionally, it was shown that microglia secrete IDE via an exosome-associated unconventional secretory pathway [233].

Further clearance of A β is achieved through internalization and degradation by microglia and astrocytes, although those processes have been described more thoroughly for microglia [104]. Different mechanisms have been reported for the uptake of amyloid particles, depending on its aggregation state, *e.g.* pinocytosis, receptor-mediated phagocytosis and endocytosis (Fig. 8) [102, 104, 234]. Microglia mediate the clearance of soluble A β (sA β) through a process called fluid-phase macropinocytosis, which is distinct from other endocytic pathways [235]. This process involves the formation of pinosomes and macropinocytic

vesicles through the closure of membrane ruffles and depends on actin-mediated cytoskeletal rearrangements [235]. On the other side, fibrillar A β (fA β) was shown to be cleared by microglia via receptor-mediated phago- and endocytosis [236, 237, 238]. Various kinds of receptors can be included in this process, such as scavenger receptors (SR) (*e.g.* SR-A, SR-B, CD36, CD40, CD47) together with co-receptor CD14, RAGE receptors, Fc-receptors (FcR) (*e.g.* Fc γ RI, Fc γ RII and Fc γ RIII), TREM2 and the complement system (C1q and C3) [104, 234]. Binding of fibrillar A β to one of those receptors triggers an internal signaling cascade that initiates phagocytosis of the bound material [221]. The formation of the phagocytic vesicle (phagosome) requires actin rearrangements, while receptor-mediated endocytosis requires clathrin and dynamin [102]. Engulfed A β passes through early and late endosomes before it reaches the lysosome for degradation. There, internalized materials are enzymatically processed by hydrolytic enzymes such as cathepsins [102, 228].

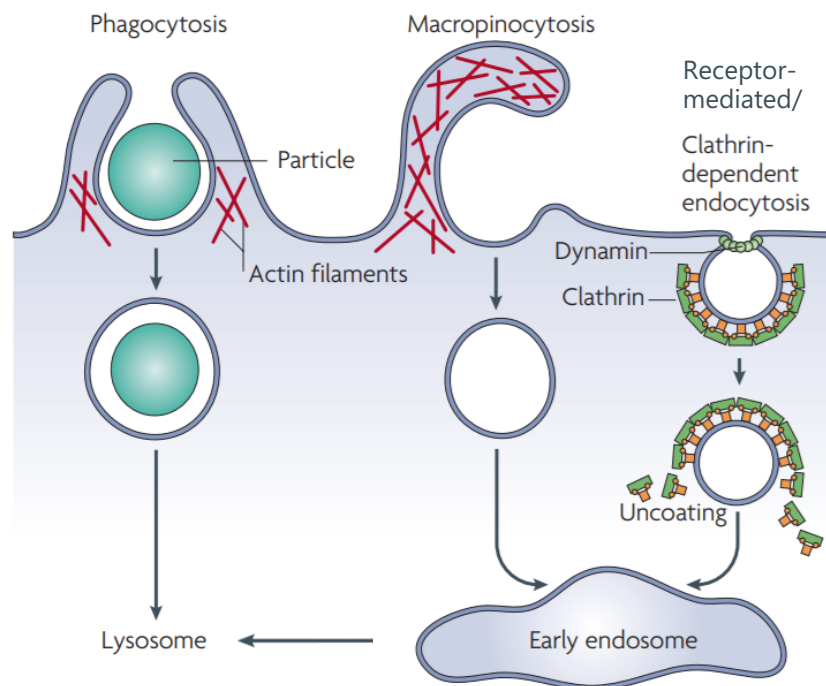


Figure 8: Entrance pathways into the microglial cell.

Larger particles can be taken up by phagocytosis, whereas fluid and soluble particle uptake occurs chiefly by macropinocytosis. Both processes rely on actin-dependent reorganization of the cytoskeleton. Targeted internalization occurs through receptor-mediated endocytosis, which highly depends on the coat protein clathrin and the fission GTPase dynamin. Figure modified from Mayor and Pagano 2007.

1.2.3.2 Deficiency of microglial clearance in Alzheimer's Disease

Genes promoting amyloidogenesis in EOAD (*APP*, *PSEN1*, *PSEN2*) are known to impact the endolysosomal functions of microglia [239]. In particular, early and late endosomes, as the first compartments along the endocytic pathway, display several functional and morphological abnormalities, such as impaired transport mechanisms, enlarged endosomal structures and reduced endocytic/phagocytic function [224, 239]. Moreover, several binding, uptake and degradation mechanisms of A β and cellular debris have been reported to fail in stressed AD microglia. A study conducted by Hickman and colleagues reported a progressive decrease in the levels of CD36, SR-A, NEP, IDE, RAGE and MMP9 in aging AD microglia, while pro-inflammatory cytokines simultaneously increased [218]. They further reported that increasing TNF- α levels triggered the downregulation of *Cd36* and *Sra* gene expression and reduced A β uptake. This suggests that inflammation indirectly compromises A β clearance by inducing the downregulation of essential binding receptors [218]. As outlined in later sections, meta analyses of microglia-specific LOAD risk factors have pointed to failing phagocytic clearance of tissue debris and A β by microglia as a candidate key pathological mechanism [103, 150, 240]. Implemented in this process are genes like *TREM2*, *BIN1*, *RIN3*, *CD2AP*, *CD33*, *SORL1* and *ABCA7*, among many others (Fig. 9) [103, 150].

Deficiencies in the clearance of toxic amyloid species have also been reported in human AD patients compared to healthy controls [32]. Moreover, an insufficient lysosomal acidification could be linked to defective clearance of fibrillar A β by microglia [241] and autophagic as well as lysosomal defects were observed during chronic A β exposure in mouse models and human AD patients [242]. Since aging is still considered the greatest risk factor for the development of AD, it is important to note that aging, "healthy" microglia progressively lose their homeostatic signature and display a pro-inflammatory phenotype, which correlates with observed deficiencies in phagocytosis and immune surveillance [243]. Moreover, it has been shown that microglial phagocytosis of fibrillar A β is reduced during normal aging processes [244].

Taken together, there is considerable evidence supporting a microglial deficiency in the clearance of A β and debris as one of the underlying mechanisms for AD development, es-

pecially LOAD. Thus, a thorough characterization of the molecular and functional changes in AD microglia and the identification of mechanisms that lead to this decline in clearance are necessary to identify novel therapeutic options for AD patients.

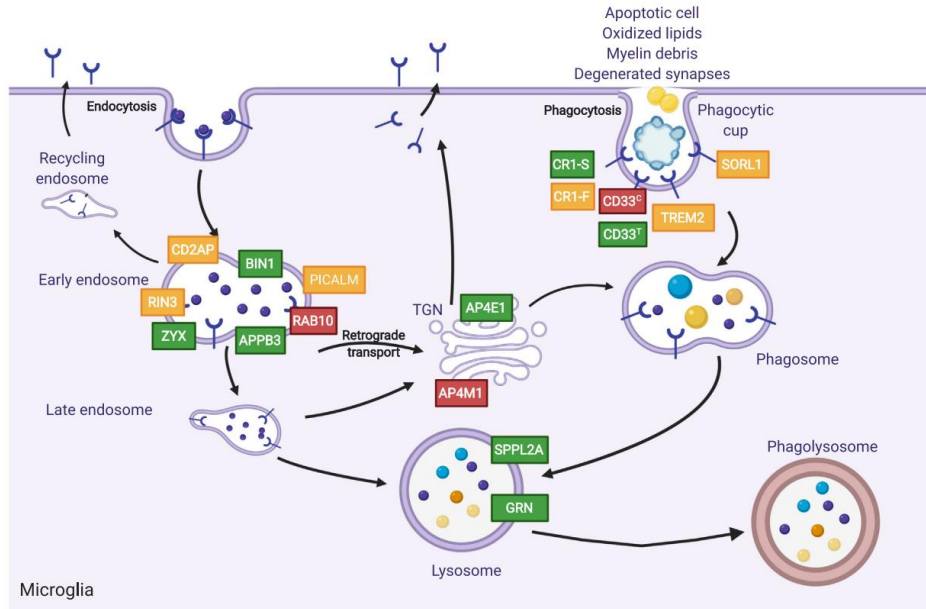


Figure 9: Endolysosomal processing in microglia and links to candidate AD risk genes. Microglia constantly probe membrane fragments by endocytosis (left) and larger particles (*e.g.* cell debris, lipids, degenerated synapses) by phagocytosis (right). Inside the cell, the absorbed material reaches early endosomes or phagosomes, which mature and fuse with acidic lysosomes, forming a phagolysosome. Inside the trans-Golgi network (TGN), proteins are sorted via retrograde transport and recycling endosomes. AD risk genes displayed here are overlaid with the cellular compartment they are known or speculated to regulate. Green indicates AD genes whose decreased expression is associated with increased AD risk; red indicates genes whose increased expression is associated with increased AD risk; yellow indicates an unknown expression effect on AD risk. Figure modified from Podlesny-Drabiniok *et al.* 2020.

1.2.3.3 Transcriptomic characterization of microglia in Alzheimer’s Disease

As previously discussed (sections 1.1.4 and 1.2.3.2), the huge amount of data provided by GWAS and sequencing studies linking microglia-specific genes with an increased risk of developing AD, has put microglia in the spotlight of scientific attention. All the more since microglial phagocytosis emerged as a disease-associated process [150]. Since 2015, the number of publications analyzing microglia in the context of AD has increased almost exponentially (source: pubmed timeline). In particular, transcriptomic studies helped to shape our current understanding of microglial changes in the context of AD.

1.2.3.3.1 Profiling of murine microglia in Alzheimer’s Disease models

Microglia from AD mouse models were extensively studied using bulk and single-cell sequencing approaches. One of the most-cited publications was written by Keren-Shaul and colleagues in 2017, where they performed single-cell RNAseq on microglia isolated from the 5xFAD mouse model. They discovered a distinct disease-associated microglia (DAM) population with a specific transcriptomic signature that implied a reactive but also protective phenotype [245]. They further discovered that the transition into the DAM state requires a two-step activation: the initial TREM2-independent step triggers the upregulation of genes like *ApoE*, *Tyrobp* (Trem2 adaptor), *Ctsb*, *Ctsd* and *B2m* while simultaneously downregulating homeostatic markers such as *P2ry12*, *P2ry13*, *Tmem119*, *Cx3cr1* and *Csf1r*. The second step included the Trem2-dependent upregulation of genes involved in phagocytosis and lipid metabolism such as *Trem2*, *Cst7*, *Clec7a*, *Lpl*, *Cd9* and *Itgax* (CD11c). Interestingly, a similar signature was found in a mouse model for amyotrophic lateral sclerosis (ALS) analyzed in the same study [245]. In yet another influential study, Krasemann and colleagues found a mutual transcriptomic signature in microglia isolated from AD, ALS and multiple sclerosis (MS) mouse models that largely overlapped with the DAM signature [246]. However, they found the microglial changes to be associated with the proximity to neuritic plaques and the phagocytosis of dying neurons and termed this phenotype the microglial neurodegenerative phenotype (MGnD). Moreover, the MGnD phenotype seemed to be more neurotoxic and less homeostatic compared to the DAM phenotype. Despite those dissimilarities, Krasemann and colleagues could also show an upregulation of immune system relevant genes with a concomitant downregulation of homeostatic markers. They found those changes to be regulated via two separate signaling pathways that are TGF β and Trem2-ApoE dependent [246].

Overall, those studies and others [247, 248] could show that murine microglia, upon extensive stimulation and persistent stress, upregulate a specific set of genes which can be associated with increased phagocytic activity, lipid metabolism and inflammation. On the other side, microglia downregulate genes that are commonly associated with homeostatic behavior. However, the conclusions drawn by the authors couldn’t be further apart. While DAM microglia were attributed to convey protection, the MGnD phenotype was connected

to increased neurotoxicity [245, 246]. More functional studies will be needed to identify those specific molecular mechanisms that are essential for a protective performance and those that might be dysfunctional or even detrimental.

1.2.3.3.2 Profiling of human microglia in Alzheimer’s Disease

Microglia isolated from human AD postmortem cases have also been characterized on the transcriptomic level and present a valuable translational resource. A study conducted by Mathys and colleagues sequenced single nuclei (snRNAseq) isolated from frozen prefrontal cortex samples obtained from 24 AD patients and 24 age-matched controls with no or very little amyloid pathology [249]. They found a sub-population of microglia (termed Mic1) that showed a partial overlap with the DAM signature described by Keren-Shaul and colleagues (28 genes out of 229 upregulated in DAM), including *APOE*, *SPP1*, *CD47* and other MHC-II genes [245, 249]. However, they also identified genes that did not show up in the previously analyzed mouse models, such as *C1QB* and *CD14*.

In another snRNAseq study, Zhou and colleagues analyzed samples obtained from the dorsolateral prefrontal cortex of 10 human AD patients carrying the *TREM2* risk variants R47H (common Trem2-variant), R62H or WT *TREM2* and compared those to 11 age-matched control samples [250]. They showed that microglia without *TREM2* mutations had few DAM genes upregulated, such as *APOE*, *TREM2*, *CD68* and MHC-II-related genes. Surprisingly, they also found some classically homeostasis-associated genes to be significantly upregulated like *P2RY12*, *CX3CR1* and *TMEM119*. The authors suggested that the similarly upregulated IRF8 transcription factor could be the main driver for the upregulation of the homeostatic signature, reminiscent of the IRF8-driven reactive phenotype adopted by microglia in peripheral nerve injury cases [250, 251]. Additionally, they could also show that microglia from carriers of *TREM2* variants had a reduced activation profile, which is in line with the previous literature indicating that Trem2 function is indispensable for the acquisition of a reactive phenotype in AD [245, 246, 250, 252].

A different approach was published by Srinivasan and colleagues, who used frozen superior frontal and fusiform gyrus tissue to obtain a FACS-sorted CD11b-enriched myeloid fraction from 15 neuropathologically confirmed AD cases and 15 age-matched, non-demented controls [253]. This study showed a very poor overlap with the murine DAM signature,

with the exception of *APOE*. They concluded that those microglia resembled an enhanced aging profile and termed them "human AD microglia" (HAM). Although the approach is very intriguing, a notable caveat is the low quality of RNA after purification, which might additionally explain the weak overlap between mouse and human AD microglia [253].

Taken together, characterization of human AD microglia has revealed a low overlap with the acquired data from AD mouse models, with the exception of *TREM2* and *APOE*. Although the aforementioned studies reported limitations regarding the integrity or quality of RNA due to the usage of frozen tissue, one should also keep in mind the differences between murine models and human AD patients in terms of pathology. To date, available mouse models recapitulate either amyloid or tau pathology, with the main focus being on the plaque producing amyloid models. Those, at best, would recapitulate an early case of AD, while the analyzed human patient samples were predominantly late-stage cases, which additionally show prominent tau inclusions and nerve cell loss [254]. Thus, it would not be meaningful to aim for a one to one comparison between those current studies. Nevertheless, it highlights the necessity to generate better mouse models and to obtain further insight into the characterization of human AD microglia, especially at earlier time points. That way we can identify clinically relevant AD markers that could help to outline a more accurate disease progression and might also help in developing early-stage biomarkers.

1.3 Microglia-associated risk factors

As discussed earlier (section 1.1.4), sequencing approaches and GWAS have led to the identification of more than 40 genomic loci that were found to be associated with LOAD [148]. Interestingly, pathway analyses could show that the variants mapping within GWAS loci cluster around lipid processing, phagocytosis and functions of the innate immune response, which are biological processes mainly exerted by microglia. Furthermore, several risk variants localize within regulatory regions (enhancers or promoters) that are bound by PU.1, a transcription factor that is crucially involved in the development and function of myeloid cells [255].

Although GWAS enabled major achievements in recognizing the genetic risks of LOAD,

further efforts will be needed to decipher the complex link between AD genetics and pathogenesis. To date, several groups have combined multiple scales of functional data, including gene expression data, epigenetic annotations, network analyses and GWAS to elucidate the biological function of rare (found within coding regions) and common (map within non-coding regions) AD risk variants. Together, these extensive analyses have found that many genes harboring rare variants are highly expressed in microglia [146, 256], and that common AD risk variants are particularly enriched in microglia-specific enhancer regions that affect cell-type specific gene expression, strongly insinuating microglia in disease etiology [147, 255]. By integrating chromatin interactions (promoter-capture Hi-C) and summary data-based Mendelian randomization (SMR), Novikova and colleagues examined the relationship between the active enhancers of myeloid cells containing common AD risk variants, target gene expression regulation and the resulting AD risk modification (Fig 10) [103]. They found that the examined variants that convey AD risk also regulate microglia-specific gene expression. Moreover, they presented candidate causal genes as genome-wide significant loci and identified that several of those genes (*e.g. BIN1, CD33, CD2AP and RIN3*, among others) localize to the endolysosomal network and may therefore regulate endocytic and/or phagocytic processes [103].

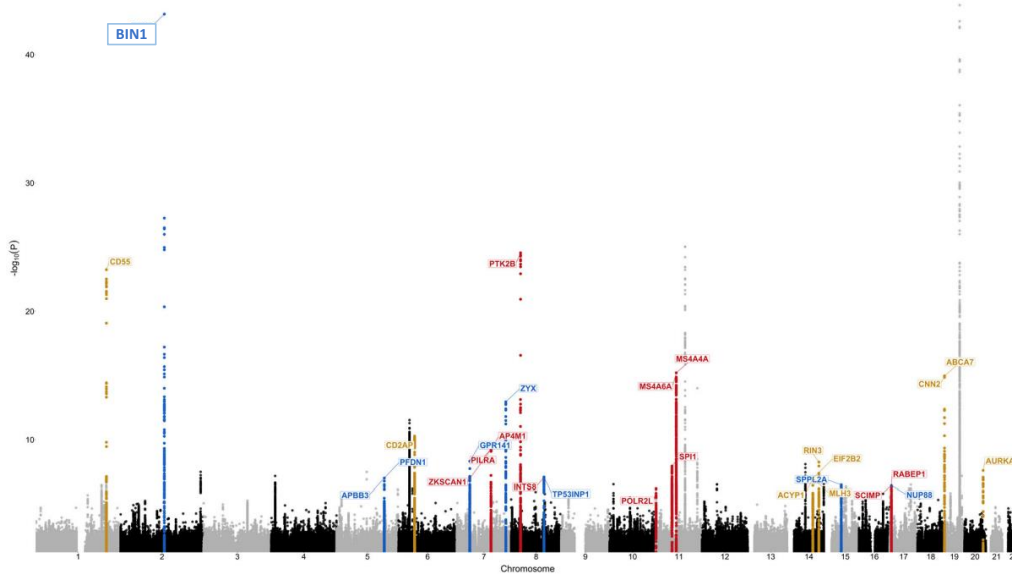


Figure 10: Candidate causal genes nominated through Hi-C and SMR approaches in 20 loci. The Manhattan plot depicts common variants from the International Genomics of Alzheimer’s Project (IGAP) GWAS with the presumed AD risk genes on each chromosome assigned to the respective locus through Hi-C and SMR approaches. Blue indicates that a decreased gene expression is assumed to convey an increased AD susceptibility. Red indicates that an increased gene expression is assumed to convey a decreased AD susceptibility. Yellow indicates that the directionality of gene expression can not be robustly inferred with increased AD susceptibility. The *TREM2* locus is not shown since a well replicated loss-of-function mutation was found. The *PICALM* locus is not shown since the predicted gene from this study is not expressed in microglia. Figure modified from Novikova *et al.* 2021.

1.3.1 TREM2 and other rare Alzheimer’s Disease risk variants

Whole-exome sequencing and microarray studies have discovered rare coding variants located within protein-coding sequences of genes such as *TREM2*, *PLCG2*, *SORL1*, *ABI3* and *ABCA7*, that play important roles in microglia but also myeloid cells of the periphery [114, 146, 257, 258]. A great advantage of those studies is the direct link between functional variants and causal genes, thus providing more imminent clues on how disease risk is modulated.

In *TREM2*, the partial loss-of-function (LOF) missense mutation R47H has been found to increase AD risk approximately 4-fold [114]. As a known A β receptor, *TREM2* LOF impairs A β recognition and phagocytosis, thereby enhancing A β load and disease susceptibility. This notion is supported by multiple studies. For example, *TREM2*-deficient primary microglia were shown to have a decreased phagocytic capacity for amyloid plaques [259].

Moreover, *TREM2*-deficient AD mice displayed a reduced capacity to recruit microglia towards amyloid plaques and had an elevated A β load compared to non-*TREM2*-deficient AD mice [109, 252]. On the other hand, bacterial artificial chromosome (BAC)-mediated overexpression of *TREM2* in AD mice could reprogram microglial responsivity and ameliorated amyloid pathology through increased phagocytic activity [260]. Comparable observations were made by Jiang and colleagues who used a lentiviral carrier for *TREM2* overexpression in primary microglia and an AD mouse model. Here, the reduced A β deposition was accompanied by a diminished neuroinflammatory phenotype and synapse loss, together with improved spatial cognitive function [261].

Taking this into account, the frequently observed microglial upregulation of *TREM2* in the context of AD seems to serve as a compensatory mechanism and subsequently protects against AD progression by modulating microglia function.

Another candidate gene in which rare genetic variants have been detected is *PLCG2*, a member of the phospholipase C γ family. It colocalizes and shares a common interactome with TREM2 and is likely a downstream signaling effector [262]. The identified P522R polymorphism maps within the *PLCG2* regulatory region and has been associated with a decreased risk of AD development [146]. Importantly, this variant slightly increases PLCG2 enzymatic activity, thus acting as a gain-of-function (GOF) mutation [262]. Similar to TREM2, PLCG2 is highly abundant in microglia and its expression increases further in microglia surrounding amyloid plaques [262].

Rare LOF variants have also been detected in *ABCA7*, a member of the highly conserved superfamily of ATP-binding cassette (ABC) transporters, that could be associated with an increased diseases susceptibility [257]. Similarly, several nonsense mutations lead to a reduced *ABCA7* expression and increased AD risk [263]. Moreover, common variants within the *ABCA7* locus were also shown to be associated with AD [145]. *ABCA7* is abundantly expressed in myeloid cells of the periphery and microglia in the CNS where it is thought to play a role in phagocytosis [264].

1.3.2 BIN1 as a common Alzheimer's Disease risk variant

To date, genetic studies of sporadic AD identified more than 40 common non-coding variants to be associated with AD development [148]. Among those, several genes were implicated to have functions in the regulation, trafficking and maturation of early endosomes, including *BIN1*, *CD2AP*, *SORL1* and *PICALM* [265, 266, 267]. Interestingly, the *BIN1* (bridging integrator 1) locus was identified to be the most significant susceptibility locus in AD after *APOE* [268]. Moreover, recent integrative bioinformatic approaches revealed that the *BIN1* gene is the strongest causal candidate within the *BIN1* locus. Furthermore, the authors could link lower expression of *BIN1* in microglia with increased AD risk [103].

1.3.2.1 BIN1 physiology

1.3.2.1.1 BIN1 isoforms and cellular distribution

BIN1, a member of the *BIN1*/Amphiphysin/*RVS167* family, is widely expressed in the cytosol of various mammalian brain cells and other tissues, such as skeletal muscles [269]. It produces multiple isoforms that differ in their subcellular localization, tissue distribution and protein interactions, highlighting its diverse functional roles (discussed in the section below). It is composed of 20 exons that encode distinct structural elements, including an N-BAR domain, a phosphoinositide (PI) binding motif, a clathrin and AP2 (CLAP) binding domain, a Myc-binding domain (MBD) and a Src homology (SH3) domain (Fig. 11a) [270]. The N-BAR domain is encoded by exons 1-10 and is involved in the modulation of membrane curvature [271]. The PI binding motif is encoded by exon 11 and is only present in few *BIN1* isoforms [270]. Those isoforms are presumably involved in lipid-mediated cell-signaling and membrane trafficking [272]. Exons 13-16 were shown to encode the CLAP domain, which is critically involved in endocytic processes [273]. The MBD, encoded by exons 17 and 18, is engaged in the regulation of the transcription factor c-Myc, which modulates histone acetylations [274]. Finally, the SH3 domain, encoded by exons 19 and 20, was shown to directly interact with proteins that have proline-rich domains, such as dynamin and Tau [275, 276]. The majority of *BIN1* transcripts encodes low molecular weight (65-75 kDa) isoforms.

In humans, alternative splicing of *BIN1* generates 14 RNA transcripts that are trans-

lated into 11 respective protein isoforms (Fig. 11b) [270]. Isoforms with a CLAP domain (isoforms 1-7) were shown to be brain specific, while isoform 8 is found in muscle tissue only [277]. Isoforms 9 and 10 are expressed in both brain and muscle tissue [277]. Using antibodies targeting specific epitopes of BIN1 in human brain tissue as well as mRNA expression data, Taga and colleagues recently identified three isoforms that are expressed in neurons and astrocytes (isoforms 1, 2 and 3) and four isoforms expressed in microglia (isoforms 6, 9, 10 and 12) [270]. However, high expression of BIN1 has also been reported for mature oligodendrocytes (Fig. 11d), especially in the white matter [278]. Due to the limited number of commercially available antibodies targeting exon-selective epitopes of BIN1 and the more recent discovery of multiple isoforms being expressed by a single cell type, some conclusions drawn from earlier publications ought to be revised carefully.

In the murine brain, according to the ensemble database, *BIN1* is expressed in two variants (Fig. 11c). Transcript ENSMUST00000025239 encodes for BIN1 isoform 1 (Uniprot O08539-1), which shows 94.8 % homology with human BIN1 (hBIN1) isoform 1. The second transcript, ENSMUST00000091967, encodes for BIN1 isoform 2 (Uniprot Q6P1B9) and shows 95 % homology with hBIN1 isoform 6. Crotti and colleagues could show that murine BIN1 (mBIN1) isoform 1 is predominantly expressed by neurons, while isoform 2 could be associated with microglia and to a lesser extent myelinating oligodendrocytes [279]. Isoform 2 was additionally found to be specific for microglia among myeloid cells, as it is expressed at insignificant levels by monocytes, bone-marrow derived and peritoneal macrophages [279, 280]. Moreover, they found that microglia express by far the highest levels of BIN1, followed by oligodendrocytes and neurons (Fig. 11e) [279].

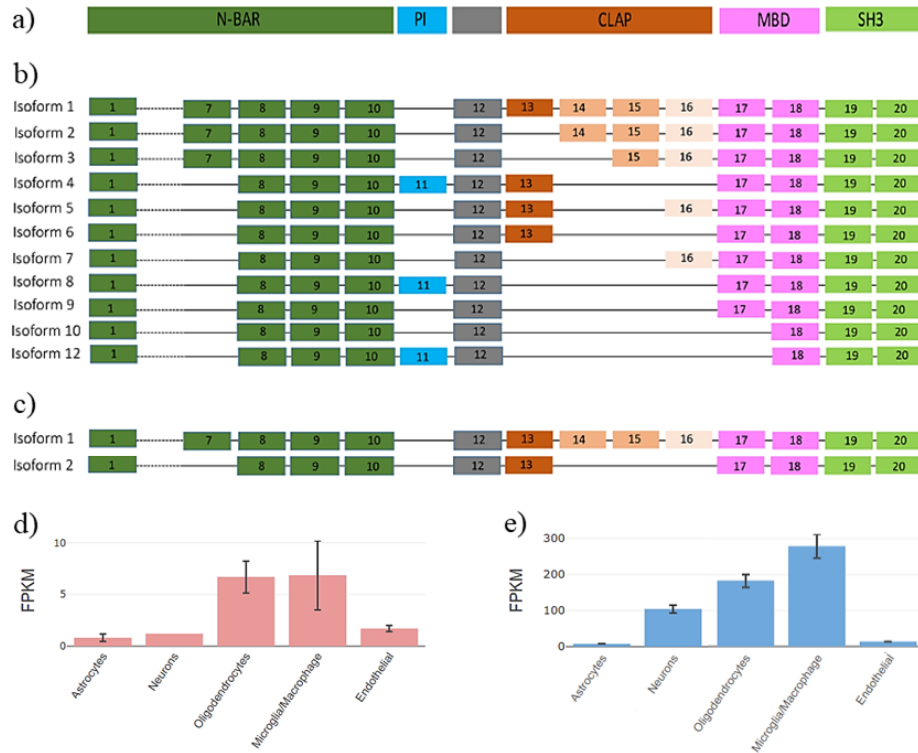


Figure 11: BIN1 isoforms and cellular distribution in humans and mice.

(A) General scheme of motifs and domains included in the BIN1 protein. (B) Diagrams of the 11 human BIN1 isoforms. Exons 2-6 are left out since they're found in all isoforms. (C) Diagrams of the two BIN1 isoforms found in mice. mBIN1 isoform 1 was found to show 94.8 % homology with hBIN1 isoform 1 and is mainly expressed in neurons. mBIN1 isoform 2 shows 95 % homology with hBIN1 isoform 6 and is mainly expressed by microglia. (D) scRNAseq data showing the cellular distribution of BIN1 in the human brain. (E) scRNAseq data showing the cellular distribution of BIN1 in the murine brain. Figure (A)-(C) modified from Taga *et al.* 2020; (D)+(E) modified from brainrnaseq.org, based on Zhang *et al.* 2014 and Zhang *et al.* 2016.

1.3.2.1.2 BIN1 function

While the purpose of BIN1 in neurons has been studied quite extensively, its roles and functions in microglia remain comparably understudied. Nevertheless, those studies represent valuable resources, as they might entail corresponding functions for BIN1 in microglia. So far, BIN1 has been implicated in various cellular mechanisms such as endocytosis, actin dynamics, inflammation, membrane trafficking, DNA repair and apoptosis [281, 282, 283, 284, 285].

Neuronal BIN1: links to axonal and synaptic vesicle trafficking

On the subcellular level, neuronal BIN1 is broadly distributed across endolysosomal struc-

tures, including early and late endosomes, lysosomes and recycling endosomes [286]. Moreover, BIN1 can be found at axonal initial segments, nodes of Ranvier [277] and along axonal tau neurofilaments [278, 287]. Indeed, neuronal BIN1 was found to be involved in the polarized (axonal) endolysosomal transport and also amyloidogenic processing herein. It was shown in primary hippocampal neurons that BIN1 controls the generation of A β through regulation of the endocytic trafficking of APP and BACE1 [288]. Additionally, it is involved in the ubiquitin-dependent and -independent mechanisms of APP- and BACE1-trafficking to lysosomes, respectively [288, 289]. Importantly, those studies showed how a *BIN1* loss-of-function could contribute to the slow accumulation of A β in neurons during LOAD [288, 289]. Technological advances in the field of fluorescent microscopy and the preparation of synaptosomes from whole brain tissue led to the detection of neuronal BIN1 in synaptic terminals [290, 291, 292]. Using structured super-resolution illumination technology (SIM), Schürmann and colleagues could recently show that BIN1 is enriched in postsynaptic compartments, including spines [292]. It was shown that BIN1 colocalizes with major components of the endocytic machinery and small GTPases that are part of the exocytic pathway. Moreover, BIN1 knockdown disrupted postsynaptic trafficking of vesicles and receptors and reduced spine size [292]. In another recent publication using super-resolution and immunoelectron microscopy, De Rossi and colleagues could show that conditional knock-out (cKO) of *BIN1* in neurons resulted in a deficit of presynaptic vesicle release and a slower depletion of neurotransmitter following stimulation [291]. The further observed deficits in synaptic density, spatial learning and memory [291] provide significant insights into AD-relevant functions of BIN1 in synapse physiology.

Microglial BIN1: links to phagocytosis and endolysosomal processing

Although sparse, there are some studies pointing to compelling functions for microglial BIN1. RNAseq of microglia harboring a cKO for *BIN1* revealed that they had significantly reduced mRNA levels of several chaperones known to be involved in proteostasis and clearance (*e.g.* Hspa8, Hsp90aa1, Hsp90ab1, Dnaja1 and Dnajb1) [279, 293], strongly implicating that microglial BIN1 function centers around those processes. Unfortunately, this was not the main focus of the paper and the authors did not follow up on this. Nevertheless, based on studies analyzing BIN1 function in neurons and the high sequence similarity between isoforms, more recent reviews have been speculating about potential roles

of BIN1 in microglia. Probably the most discussed theory is that BIN1 is involved in early endosome function, trafficking and phagocytosis [149, 150, 285]. Moreover, a compelling mechanism was proposed in which BIN1 acts as a downstream effector of TREM2. The authors suggest that activation of the transmembrane TREM2/DAP12 complex through extracellular binding of PAMPs or DAMPs to TREM2 may activate a cytosolic protein complex consisting of SHIP1, CD2AP, RIN3 and BIN1, resulting in the increased uptake and degradation of lipids, debris and A β [294, 295, 296]. However, although tempting and sensible assumptions were made in recent years regarding BIN1 function in microglia, very few have been actively explored. One reason for this could be that microglia are notoriously difficult to transfect, especially *in vivo*, and the generation of microglia-specific cKO or cKI mouse models (*e.g.* $Bin1^{fl/fl}::Cx3Cr1-Cre^+$) is very time-consuming and cost-intensive. Another layer of complexity is added when taking into account that microglia are highly efficient macerators of unknown or unwanted substrates and if in doubt, tend to throw out material via exocytosis [297]. Notwithstanding, given that the microglial *BIN1* locus ranks as the second most prevalent LOAD risk factor after APOE [268], a thorough understanding of the homeostatic processes influenced by BIN1 would help to unravel how this intricate protein participates in the progression of AD.

1.3.2.2 Pathological implications for Bin1

Conflicting results from the available literature suggest that BIN1 may have opposing effects during different stages of AD, or that neuronal and microglial BIN1 have discrete roles during the disease. Moreover, it is still under debate if *BIN1* expression directly influences the development of AD neuropathology. In the following section, the most recent advances in the field will be discussed.

BIN1 and neuropathological hallmarks

Several lines of evidence support the notion that BIN1 is involved in key pathological characteristics of AD. Aberrant accrual of BIN1 near and in amyloid plaques has been observed in multiple transgenic AD mouse models as well as human AD patients [298]. Intriguingly, older individuals without dementia carrying the *BIN1* rs744373 risk allele showed increased tau-PET levels and impaired memory performance but no association with amyloid-PET [299]. Other studies found an inverse correlation between smaller BIN1

isoforms and the amount of neurofibrillary tangles [300]. Nevertheless, the directionality and mechanisms through which *BIN1* confers risk in LOAD remain unclear.

BIN1 expression level changes in the context of AD

Multiple studies have reported a significant decrease of brain-specific BIN1 isoforms concomitant with an increase in ubiquitous BIN1 isoforms [278, 298, 300, 301]. A study from 2012 investigated the potential correlation between clinical features of AD in 73 post-mortem AD tissue samples and their *BIN1* expression level. Interestingly, the results suggested that patients with higher transcript levels of BIN1 were likely to have a later age of disease onset [144]. Another, more recent study investigated the association between BIN1 promoter methylation in peripheral blood samples and preclinical AD symptoms [302]. Their main finding was that hypomethylation of the *BIN1* promoter could be associated with early pathological changes in CSF AD core biomarkers, especially A β -related markers [302]. Mixed results regarding AD-related changes in *BIN1* were described in a comprehensive study performed by Zhu and colleagues. Using peripheral blood eQTL data they identified the genome-wide significant SNP rs11682128 to be linked with *BIN1* gene expression and increased AD risk [303]. Albeit their SMR results suggest that SNP rs11682128 could upregulate *BIN1* expression in blood, they found that BIN1 mRNA levels were significantly downregulated in the hippocampus from AD patients [303]. Although important, the apparent difficulties of human studies highlight the need to address those questions in a more specialized cell type-based approach.

Neuronal and microglial BIN1

At present, identifying relevant variants of LOAD pathogenesis and determining tissue and cell type-specific effects persist as major issues. Despite being challenging to dissect, the affiliation between *BIN1* and AD is evident and urges for more in-depth analysis of separate cell populations. Loss of *BIN1* expression in cultured primary neurons was shown to elevate A β production and could be linked to reduced endolysosomal trafficking and degradation of BACE1 [289], which is in line with other reports [288]. In addition, the well-described interaction between BIN1 and tau [276, 278, 287] leads to the assumption that changes in BIN1 protein levels might influence tau pathology. Knockdown of *BIN1* in cultured neurons promoted tau propagation by modulating its endocytic flux, while *BIN1* overexpression inhibited the process [290]. Intriguing results were also obtained

when analyzing the link between *BIN1* and microglia in the context of AD. In contrast to the previous study, P301S mice harboring a cKO for *BIN1* in microglia were shown to have reduced tau protein secretion [279]. An important study was conducted by Nott *et.al.* who deleted a putative microglia-specific enhancer region harboring several SNPs (*e.g.* known AD risk variant rs6733839) which resulted in ablation of *BIN1* expression in microglia, but not neurons or astrocytes [147]. These findings were of particular importance, since they showed for the first time that SNPs located within the *BIN1* locus are indeed linked to *BIN1* expression, and identified microglia as key risk carriers. Shortly afterwards, Novikova *et.al.* convincingly related lower expression of *BIN1* in microglia with an increased risk to develop AD [103]. Those studies further promote microglia as important contributors to LOAD and give meaningful insights into the risk directionality of *BIN1*.

The current literature suggests that neuronal and microglial *BIN1* could be substantially involved in the exacerbation of AD pathology, albeit probably through different mechanisms. Several studies imply that dysregulation of neuronal *BIN1* could lead to changes in A β generation and processing and tau propagation [288, 290]. However, *in vivo* validation data as well as neuron-specific analysis of *BIN1* levels in the context of AD are still missing. Although functionally not well defined, microglial *BIN1* was found to harbor AD-relevant SNPs within its enhancer region [147] and its downregulation was recognized to have adverse effects on AD development [103]. Interestingly, the hypomethylation of the *BIN1* promoter identified in preclinical AD patients [302] could imply a biphasic behavior of *BIN1*. The early upregulation of *BIN1* would fit the latest observations that initially, microglial activity is beneficial and later on becomes detrimental as the disease progresses and cells are overwhelmed with increasing amounts of amyloid and cellular debris (section 1.2.3). As discussed earlier, microglial phagocytosis and lysosomal processing are impaired in mouse models as well as human AD patients [32, 224, 304] (section 1.2.3.2). Given that microglial *BIN1* is implicated to be involved in those processes (section 1.3.2.1.2), it seems feasible to assume that in the context of AD, downregulation of *BIN1* contributes to the phagocytic impairment of microglia. On a broader scale, the proposed multifactorial dysregulation of microglia phagocytic function (through risk factors like *BIN1*, *TREM2*, *CD33*, *CD2AP* and *RIN3*) could substantially contribute to the sustained deterioration of microglia and their environment observed in LOAD.

2 Aims of the study

In recent years, as the brains resident immune cells, microglia have become the focus of attention in the field of neurodegenerative research. To date, an overabundance of genetic risk variants and SNPs contributing to LOAD have been discovered in microglial genes and regulatory elements. This, along with functional studies points to a deterioration of microglia performance in the context of AD. Although many studies have characterized microglia at the transcriptome level, a comparison with matching proteomic data is often missing. Thus, the first aim of my PhD project focused on sequencing microglia obtained from aged WT and APP^{NL-G-F} mice and subsequently comparing the results to a matching proteomic data set. With this study I intended to elucidate the underlying mechanisms of microglia dysfunction in AD through a more integrative approach.

Nevertheless, deciphering the molecular mechanisms through which common risk factors contribute to disease etiology remains challenging. Based on the findings from the previous analysis, the second main goal of my thesis centered around the characterization of the homeostatic function of common LOAD risk factor *BIN1*. For that purpose I designed an AAV-vector to facilitate microglia-specific overexpression of *BIN1*. I further established the culture of isolated primary mouse microglia in our laboratory and subsequently analyzed the effects of *BIN1* overexpression *in vitro* and performed stereotactic injections *in vivo*. With this I anticipated to gain a deeper understanding of the homeostatic processes influenced by *BIN1*. In turn, this could help unravel how this elaborate protein and risk factor contributes to the progression of AD.

3 Materials and Methods

3.1 Materials

3.1.1 Laboratory equipment and general consumables

Instrument	Company
Analytical balance (0.0001 - 200 g)	Sartorius
Balance (0.01 - 2000 g)	Kern
Capillary puller (PC-10)	Narishige
ChemiDoc MP Imaging System	BioRad
DNA electrophoresis gel system	Bio-Rad
Electrophoresis chambers	PeqLab
Electrophoresis power supply	Hartenstein
Electrophoresis system Mini-Protean	Bio-Rad
Falcons (15 and 50 ml)	Falcon
GentleMACS Dissociator	Miltenyi Biotec
Heating and stirring plate	Hartenstein
Impulse Sealer PFS200	Hanchen
Mastercycler Pro (vapo protect)	Eppendorf
MilliQ plus filtration system	Merck Millipore
Mini Rocker-Shaker	A. Hartenstein
PCR tubes	Neolab
pH meter	Mettler Toledo
Pipette controller Accu-Jet Pro	Brandtech
Pipette set	Eppendorf
Pipette tips (2, 10, 100, 200, 1000 μ l)	Sarstedt
Protein electrophoresis and transfer system	Bio-Rad
Serological pipettes (2, 5, 10 and 25 ml)	Sarstedt
Tabletop centrifuge	Eppendorf
Tubes (0.5, 1.5 and 2.0 ml)	Eppendorf
Ultrasonic waterbath	Brandelin
Vibratome VT1200S	Leica
Vortex mixer	Hartenstein

Table 3.1: List of Laboratory equipment and consumables used in this study

3.1.2 Cell culture equipment and consumables

Instrument	Company
Cell culture treated dishes (Nunc)(3.5 and 6 ml)	Thermo Scientific
Cell culture treated flask with filter cap (Nunc)	Thermo Scientific
Cell culture treated well plates (Nunc)(24 wells)	Thermo Scientific
Centrifuge (5810R)	Thermo Scientific
CO ₂ -incubator (humidified)(Heracell 150i)	Thermo Scientific
Dissecting Forceps (tooth)	Thomas Scientific
Glass Pasteur pipettes	VWR
Laminar flow hood	Thermo Scientific
Minisart single-use filter unit (PES 0.22 μ m)	Sartorius
Oven (UF 30)	Memmert
Porcelain cover glass staining rack	Thomas Scientific
Round glass coverslips (\varnothing 13 and 15 mm)	Marienfeld
Staining trough (glass)	Carl Roth
Stericup filter bottle (500 ml, 0.22 μ m pore size)	Corning
Syringes (20 ml)	Terumo
Thermal beads water bath	GFL

Table 3.2: List of cell culture equipment and consumables used in this study

3.1.3 Surgical instruments

Instrument	Company
Bepanthen eye ointment	Bayer
Bone wax	Ethicon
Disposable scalpels	VWR
Drill and Microinjection Robot	Neurostar
Dumont No.2, Laminectomy Forceps	Fine Science Tools
Dumont No.5, Laminectomy Forceps	Fine Science Tools
Glass capillaries (\varnothing 1.14 mm)	WPI
Hardened fine scissors, straight	Fine Science Tools
Heating pad	Fine Science Tools
Hot Bead Sterilizer	Fine Science Tools
Large spatula, double-ended, one round end	Heathrow scientific
Peristaltic pump (MiniPump variable flow)	Fisherbrand
Thin spatula, double-ended, one round end	Heathrow scientific
Vicryl absorbable suture	Ethicon

Table 3.3: List of surgical equipment used in this study

3.1.4 Microscopy equipment

Instrument	Company
Confocal microscope (LSM900)	Zeiss
Dissection microscope (SZ61)	Olympus
Epifluorescence microscope (AxioImager A2)	Zeiss

Table 3.4: List of microscopy equipment used in this study

3.1.5 RNA Sequencing equipment

Instrument	Company
Bioanalyzer	Agilent
MiniSeq Sequencing System	Illumina
QIAcube	Qiagen
Qubit Fluorometer	Invitrogen

Table 3.5: List of RNAseq equipment used in this study

3.1.6 Animals

3.1.6.1 Mouse husbandry

Mice were bred and kept in the animal housing facility of the Center for Stroke and Dementia Research (CSD) of the Ludwig Maximilians University Munich. Up to six individual animals were grouped together in standard GreenLine cages (30 x 15 x 20 cm, Tecniplast) with bedding and nesting material under pathogen-free conditions. Mice were kept under a standard 12/12 h light/dark cycle and accommodated with food pellets (Ssniff) and water *ad libitum*. All animal studies were conducted according to the German Animal Welfare law and approved by the government of Upper Bavaria. Male and female mice were equally used for this study.

3.1.6.2 Mouse lines

Mice from the APP^{NL-G-F} x GFP-M line used in this study were chosen based on the absence of the heterozygous GFP-M transgene. The Tg(Thy1-EGFP) transgene (MGI:4941461) allows for fluorescent labeling of a subset of principal neurons in the hippocampal and cortical area of the brain, which, in this case, was unnecessary for the study.

Line	Genetic modifications	Reference	Identifier	Additional information
C57Bl/6J	No genetic modifications, wildtype mice	The Jackson Laboratory	RRID:MGI:5313568	Line was used for cross-breeding and generation of P4-P6 pups
APP ^{NL-G-F} x GFP-M	APP KM670/671NL (Swedish), APP E693G (Arctic), APP I716F (Iberian); crossed in-house with the GFP-M mouse line	Saito et al. 2014	RRID:MGI:6160916	Homozygous humanized ki/ki, heterozygous for GFP-M, with pure C57Bl/6J background

Table 3.6: List of mouse lines used in this study

3.1.7 Reagents, solutions and consumables for different applications

3.1.7.1 Genotyping of transgenic mouse lines

3.1.7.1.1 Primers (Sigma-Aldrich)

Mouse line	Primer	Sequence (5' → 3')
APP ^{NL-G-F} (APP KI)	forward	CTCCTTGTGGCTGGCGGTCACAC
	reverse	CTATCGTGGACCGAGAATGGTCATG
GFP-M	forward	AAGTTCATCTGCACCACCG
	reverse	TCCTTGAAGAAGATGGTGCG

Table 3.7: Primers used for genotyping of transgenic mouse lines

3.1.7.1.2 Reagents and key consumables

Instrument	Company
Agarose	Sigma
DNA Ladder (1 kb Plus)	Invitrogen
DNA Polymerase (GoTaq G2)	Promega
Extracta DNA Prep for PCR tissue	QuantaBio
GelRed nucleic acid stain	Merck
GelTrack PCR Supermix (2x)	QuantaBio
OneTaq HS Quick-Load (2x)	New England Biolabs
TAE buffer (10x)	Roth
Tris Base	AppliChem

Table 3.8: Reagents used for genotyping of transgenic mouse lines

3.1.7.2 Primary mouse microglia *in vitro* applications

3.1.7.2.1 Reagents and key consumables for microglia isolation and culture experiments

Reagent	Company
AAV/TM6-F4/80-mBIN1-2A-mCherry	Vector Biolabs
AAV/TM6-F4/80-mCherry	Vector Biolabs
Ammonium chloride	Sigma
Bovine serum albumine, protease-free (BSA)	Sigma
C-Chips (disposable hemocytometer)	NanoEntek
CD11b microbeads (mouse and human)	Miltenyi Biotec
C-tubes (for GentleMACS Dissociator)	Miltenyi Biotec
Cytochalasin D (CytoD)	Sigma
Dimethylsulfoxide (DMSO)	Roth
Dulbecco's Modified Eagle Medium +HEPES (DMEM/F12)(No.31330038)	Thermo Fisher
Dulbecco's Modified Eagle Medium high glucose +pyruvate (DMEM GlutaMax)(No.31966021)	Thermo Fisher
Fetal calf serum (FCS)	Sigma
GM-CSF, recombinant mouse (No.415-ML-010)	R&D systems
Hank's buffered salt solution (HBSS: Calcium, Magnesium, no phenol red)(No.14025100)	Thermo Fisher
HEPES (1M)	Gibco
Horse serum (heat inactivated)	Sigma
L-Cysteine hydrochloride monohydrate	Sigma
LS columns	Miltenyi Biotec
MACS Smart strainers (70 μ m)	Miltenyi Biotec
Neural tissue dissociation kit (P) (No.130-092-628)	Miltenyi Biotec
Papain from <i>papaya latex</i> (buffered aqueous suspension)(No.P3125-250MG)	Sigma
Penicillin-Streptomycin (Pen-Strep, 100x)	Invitrogen
Phosphate buffered saline pH 7.4 (No.10010015)	Thermo Fisher
pHrodo Tm Green <i>E.coli</i> BioParticles Tm (No.P35366)	Invitrogen
QuadroMACS Separator	Miltenyi Biotec
Trypan Blue	Gibco

Table 3.9: Reagents and key consumables used for microglia isolations and culture

3.1.7.2.2 Solutions for microglia isolation and culture experiments

Solution	Composition
4 % Sucrose in 4 % PFA	4 % Sucrose in 4 % PFA; sterile filtered
10x PBS (pH 6.8) (amount specified for 1 l)	137 mM NaCl (80 g) 2.7 mM KCl (2 g) 10 mM Na ₂ HPO ₄ x H ₂ O (18.055 g) 1.8 mM KH ₂ PO ₄ (2.4 g) in ddH ₂ O
1x PBS (pH 7.4)	10 % 10x PBS in ddH ₂ O
Ammonium chloride solution	50 mM NH ₄ Cl in 1x PBS
Blocking solution (manual isolation with Papain)	10 % FBS in DMEM GlutaMax
Blocking solution (primary cell culture stainings)	2 % FCS 2 % BSA in 1x PBS
BSA solution for coating glass Pasteur pipettes	4 % BSA in ddH ₂ O; sterile filtered
CytoD stock solution	10 mM CytoD in DMSO
Digestion medium (manual isolation with Papain)	300 µl Papain 0.01 g L-Cystein 30 µl 1 M NaOH in 9.7 ml DMEM GlutaMax
HBSS+ buffer	7 mM HEPES in 1x HBSS
MACS buffer	0.5 % BSA 2 mM EDTA in 1x PBS; sterile filtered
microglia culture medium	10 % FCS (heat inactivated) 1 % Pen-Strep 10 ng/ml rmGM-CSF added freshly (for adult microglia only) in DMEM/F12 medium; sterile filtered
pHrodo Tm Green <i>E.coli</i> BioParticles Tm working solution	resuspend to 1 mg/ml in 1x PBS (sterile) dilute 1:10 in culture
rmGM-CSF stock solution	10 µg/ml rmGM-CSF in 0.1 % BSA-PBS

Table 3.10: Solutions for microglia isolations and culture experiments

3.1.7.2.3 Reagents and key consumables for RNA sequencing

Reagent	Company
Agilent RNA 6000 Nano Kit	Agilent
MiniSeq mid/high output Reagent Kit (150/300 cycles)	Illumina
RNeasy Plus Micro/Mini Kit	Qiagen
TruSeq RNA Single Indexes set A	Illumina
TruSeq RNA Single Indexes set B	Illumina
TruSeq Stranded Total RNA Kit	Illumina
QiaShredder	Qiagen
Qubit RNA HS Assay Kit	Invitrogen

Table 3.11: Reagents and key consumables for RNA sequencing

3.1.7.3 Mouse procedures: *in vivo* treatments and histology

3.1.7.3.1 Reagents and key consumables

Reagent	Company
4 % PFA	Roth
AAV/TM6-F4/80-mBIN1-2A-mCherry	Vector Biolabs
Cyano fast glue	Hager Werken
Fluorescence mounting medium	Dako
Fluorescence mounting medium with DAPI	Dako
Microscope polysine slides	Thermo Scientific
Normal donkey serum	Sigma
Normal goat serum	Sigma
Precision cover glasses, thickness No.1.5H (24 x 50 mm)	Marienfeld
Sodium azide (NaN ₃)	Roth
Triton X-100	Sigma

Table 3.12: Reagents and key consumables used for mouse procedures

3.1.7.3.2 Primary antibodies

Company	Host	Source	Identifier	Dilution
Amphiphysin II (2F11)	mouse monoclonal	Santa Cruz	sc-23918	1:100
Amphiphysin II (99D)	mouse monoclonal	Santa Cruz	sc-13575	1:100

APP/ β -amyloid (NAB228)	mouse monoclonal	Cell Signaling	2450	1:500
Bin1 (EPR13463-25)	rabbit monoclonal	Abcam	ab185950	1:200
β -Actin (AC-15)	mouse monoclonal	Abcam	ab6276	1:200
β -Actin (13-E5)	rabbit monoclonal	Cell Signaling	5125	1:1000 (Western blot)
CD2AP	rabbit polyclonal	Merck	HPA003326	1:200
CD68 (FA-11)	rat monoclonal	BioRad	MCA1957	1:500
EEA1 (F.43.1)	rabbit monoclonal	Invitrogen	MA5-14794	1:200
F4/80 (BM8.1)	rat monoclonal	Cell Signaling	71299	1:100
F4/80 (CI-A3-1)	rat monoclonal	Abcam	ab6640	1:200
GAPDH (D16H11)	rabbit monoclonal	Cell Signaling	5174	1:1000 (Western blot)
Gephyrin (mAb7a)	mouse monoclonal	Synaptic Systems	147 021	1:500
GFAP	goat monoclonal	Abcam	ab53554	1:500 (Western blot)
Gpm6a (321)	rat monoclonal	Origene	AM26432 AF-N	1:500
Homer1	rabbit polyclonal	Synaptic Systems	160 003	1:500
β -Actin (AC-15)	mouse monoclonal	Abcam	ab6276	1:500

Iba1	rabbit polyclonal	Wako	019-19741	1:500
Iba1	rabbit polyclonal	Wako	016-20001	1:1000 (Western blot)
Iba1	guinea pig polyclonal	Synaptic Systems	234 004	1:500
Lamp1 (EPR21026)	rabbit monoclonal	Abcam	ab208943	1:100
mCherry (16D7)	rat monoclonal	Invitrogen	M11217	1:500
mCherry	rabbit polyclonal	Abcam	ab167453	1:250
NeuN (A60)	mouse monoclonal	Millipore	MAB377	1:500 (Western blot)
PSD95 (108E10)	mouse monoclonal	Synaptic Systems	124 011	1:500
Rab5 (EPR21801)	rabbit monoclonal	Abcam	ab218624	1:500
Synaptogyrin-3 (G-3)	mouse monoclonal	Santa Cruz	sc-514081	1:500
Synaptophysin (7.2)	mouse monoclonal	Synaptic Systems	101 011	1:500

Table 3.14: List of primary antibodies used for Immunofluorescence and Western Blotting

3.1.7.3.3 Secondary antibodies

Fluorescently-labeled (H+L) secondary antibodies Alexa Fluor 405, 488, 594 and 647 were purchased from Invitrogen and used at a concentration of 1:500. Antibodies were raised either in goat or donkey.

3.1.7.3.4 Solutions

Solution	Composition
Anti-freeze solution (for storage of brain slices at -20 °C)	25 % Glycerol 25 % Ethylene glycol in 1x PBS
Blocking solution (brain slices)	10 % goat/donkey serum 3 % BSA in 0.3 % Triton X-100 in 1x PBS
Blocking solution (cell culture)	2 % FCS 2 % BSA in 1x PBS
Carprofen (applied s.c.)	8 % Carprofen in NaCl (final conc. 0.004 mg/g body weight)
DAPI staining (brain slices)	Diluted 1:1000 in 0.3 % Triton X-100 in 1x PBS
Enrofloxacin (Baytril) (applied s.c.)	20 % Enrofloxacin in NaCl (final conc. 0.005 mg/g body weight)
Ketamin/Xylazin anesthetic (applied i.p.)	13 % Ketamin 3.25 % Xylazin in NaCl (final conc. 0.13/0.01 mg/g body weight)
Permeabilization solution (brain slices)	2 % Triton X-100 in 1x PBS
Permeabilization solution (cell culture)	0.3 % Triton X-100 in 1x PBS
Sodium azide solution (short-term storage of perfused brains)	0.05 % NaN ₃ in 1x PBS

Table 3.15: Solutions utilized for mouse procedures including histology

3.1.7.4 Biochemistry: Western Blotting

3.1.7.4.1 Reagents and key consumables

Reagent	Company
Amersham ECL Prime Western Blotting Detection Kit	GE Healthcare
BC assay (protein quantitation kit)	Interchim
Blotting paper	A. Hartenstein
Glycerol	Sigma
Immobilon PVDF membrane (0.45 μm pore size)	Merck
Methanol (99.9 %)	Thermo Fisher
milk powder (blotting grade)	Roth
Mini-PROTEAN TGX Gels (4-20 %)	BioRad
Ponceau S solution	Sigma
Precision Plus Dual Color Standard (protein standard)	BioRad
Precision Plus Dual Xtra Prestained (protein standard)	BioRad
Protease Inhibitor Cocktail	Sigma
Restore PLUS Western Blot Stripping Buffer	Thermo Fisher
Sodium dodecyl sulfate (SDS) for molecular biology	AppliChem
Triton X-100 Lysis Buffer (pH 7.4)	Alfa Aesar
Tris for molecular biology	AppliChem
Tween-20	AppliChem

Table 3.16: Reagents and key consumables used for Western blotting

3.1.7.4.2 Solutions

Antibodies used for Western blotting are listed together with histology antibodies. See above, section "Mouse procedures: primary antibodies".

Solution	Composition
Blocking solution (BSA)	5 % BSA in PBS-Tween
Blocking solution (milk)	5 % non-fat milk in PBS-Tween
PBS-Tween (PBS-T)	0.1 % Tween-20 in 1x PBS
Running buffer (10x)	30.3 g Tris 144 g Glycine 10 g SDS fill up to 1 l with dH ₂ O
Running buffer (1x)	10 % 10x Running buffer 90 % dH ₂ O
Transfer buffer (10x)	30.3 g Tris 144 g Glycine fill up to 1 l with dH ₂ O
Transfer buffer (1x)	10 % 10x Transfer buffer 20 % Methanol 70 % dH ₂ O

Table 3.17: Solutions used for Western blotting

3.1.8 Software

Name	Source
Galaxy	https://usegalaxy.org
GraphPad Prism 7	https://www.graphpad.com/scientific-software/prism/
Igor Pro	WaveMetrics
Image Lab	Bio-Rad
ImageJ FIJI	https://imagej.net/software/fiji/
LaTeX	https://www.latex-project.org/
StereoDrive	Neurostar
STRING	https://string-db.org/
TexStudio	https://www.texstudio.org/
WebGestalt	https://www.webgestalt.org
ZEN2012	Zeiss

Table 3.18: Software tools used in this study

3.2 Methods

3.2.1 Genotyping of transgenic mouse lines

Genomic DNA was extracted from mouse ear or tail biopsies with the AccuStart II Mouse Genotyping Kit. In brief, small tissue pieces were submerged in 100 μ l Extracta DNA Prep for PCR -solution and heated to 95 °C for 30 minutes. After cooling down to room temperature an equal volume of Stabilization Buffer was added to stop the lysis reaction. Supernatants containing extracted DNA were subsequently stored at 4 °C until further processing.

For the Polymerase chain reaction (PCR) a master mix was prepared to ensure equal conditions for all samples. The final volume (20 μ l/sample) was composed as follows:

Reagent	amount/sample	final conc.
AccuStart II GelTrack PCR Supermix (2x)	12.5 μ l	1x
Forward primer	0.5 μ l	10 μ M
Reverse primer	0.5 μ l	10 μ M
Template DNA (added last)	1 μ l	20 μ M
ddH ₂ O	12.5 μ l	n.a.

Table 3.19: PCR master mix recipe

3.2.1.1 PCR program for APP-KI x GFP-M genotyping

To obtain the correct genotype from the APP^{NL-G-F} x GFP-M line two separate PCR programs had to be performed. One for confirming the homozygous knock-in of the humanized a β mutations inside the *APP* gene (between exons 16 and 17) and the second one for identifying those mice that were wt/wt for the otherwise heterozygous GFP-M locus. The following programs were installed on our Thermocycler (Eppendorf) and subsequently performed for APP^{NL-G-F} and GFP-M locus.

Step	Temperature [°C]	Duration	Cycles
Initial Denaturation	94	3 min	1x
Denaturation	98	10 sec	27x
Annealing	60	30 sec	
Extension	68	50 sec	
Final Extension	68	2 min	1x
Holding	4	unlimited	n.a.

Table 3.20: PCR program used to genotype for APP^{NL-G-F}

Step	Temperature [°C]	Duration	Cycles
Initial Denaturation	94	3 min	1x
Denaturation	94	30 sec	27x
Annealing	60	1 min	
Extension	68	20 sec	
Final Extension	68	2 min	1x
Holding	4	unlimited	n.a.

Table 3.21: PCR program used to genotype for GFP-M

PCR products were separated using a 1.5 % agarose gel supplemented with GelRed nucleic acid stain (1:20000) for visualization of DNA bands. Electrophoresis was carried out in 1x TAE buffer at 80 V for approximately 1 h (depending on gel and fragment size). The following amplification products were visualized under UV light:

APP^{NL-G-F} ki/ki: ~ 850 bp (wt/ki: 670 + 850 bp) and GFP-M wt/tg: ~ 173 bp.

3.2.2 Microglia isolation for *in vitro* applications

3.2.2.1 Microglia isolation using MACS technology

Depending on the downstream application, living microglia were isolated with one of two different techniques. For RNAseq and Western Blotting experiments the GentleMACS Dissociator was used in combination with the Neural Tissue Dissociation Kit (P) (both Miltenyi), while P4-6 microglia for cell culture experiments appeared healthier when using a manual dissociation protocol and a self-made enzyme solution. Both techniques allowed for successful positive selection and isolation of CD11b-labeled microglia. Brains were not pooled for any of the downstream applications.

3.2.2.1.1 Microglia isolation using GentleMACS and Neural Tissue Dissociation Kit (P) for RNAseq and Western blotting

12 mo APP^{NL-G-F} and C57Bl/6J mice were euthanized without prior CO₂ or other volatile anesthetic treatment (e.g. Isofluran) to avoid potential adverse effects on microglia activity [REF] and to keep the stress level as low as possible. Instead, rapid cervical dislocation was performed. Afterwards, steps were carried out on ice to preserve the RNA and proteins. Cerebellum, Olfactory Bulbs and Brain Stem were removed and the remaining brain tissue (Cerebrum) manually freed from its meninges and cut into smaller pieces. Enzymes "A" and "P" from the Neural Tissue Dissociation Kit (P) were added for enzymatic digestion of the tissue. Further homogenization was achieved using the GentleMACS Dissociator with a pre-installed mouse neural tissue dissociation program. After filtration, the obtained single-cell suspension was incubated with CD11b-coupled magnetic microbeads and loaded onto LS columns of the QuadroMACS separator. This important step allowed for the collection of a very pure CD11b-enriched microglial fraction while the CD11b-depleted flow-through contained mainly neurons, astrocytes and oligodendrocytes. Both fractions were manually counted with a C-Chip. Microglial yield was highly dependent on the age and genetic background of the mouse, ranging from 5×10^5 (younger controls) to 1.7×10^6 (older APP^{NL-G-F}) microglia. Cells were washed with PBS to remove residual BSA, supplemented with RNase or protease inhibitor, snap frozen in liquid nitrogen and stored at -80 °C until further processing.

3.2.2.1.2 Microglia isolation using manual dissociation and self-made Papain solution for cell culture

Cell culture experiments were performed with microglia obtained from C57Bl/6J postnatal day 4-6 pups (P4-6). According to the Animal Welfare Act pups were rapidly decapitated using scissors. To ensure a high survival rate of the cells, all further steps were continued at room temperature. In contrast to the above procedure, the whole brain was used to compensate for the otherwise low microglial yield from pup brains. Similarly, the brain was manually freed from its meninges and cut into small pieces. After digesting the tissue with a self-made Papain solution (buffered aqueous suspension derived from *papaya latex*, adjusted to 200 U, supplemented with L-cystein) the pieces were carefully homogenized

using a 2 ml serological pipette and two additional BSA-coated glass Pasteur pipettes with flame-polished decreasing diameters. Likewise to the procedure above, the single-cell suspension was loaded onto LS columns and separated into CD11b-enriched and CD11b-depleted fraction. Depending on the age of the pups, microglial yield varied between 8×10^5 and 1.2×10^6 cells. Subsequently, microglia were manually counted and plated for cell culture experiments.

3.2.3 Biochemistry: Western Blotting of primary microglia

To initially assess the purity of isolated microglia, western blots were performed for the microglia-enriched as well as the flow-through fraction of two independent isolations from 12 mo WT mice. Stainings were performed for Iba1, NeuN and GAPDH.

3.2.3.1 Protein extraction and quantification

Snap-frozen cell pellets were resuspended in 100 μ l Triton-X-100 Lysis Buffer supplemented with 1 μ l protease inhibitor. Samples were incubated 30 min on ice and subsequently centrifuged for 15 min with full speed at 4 °C. Supernatants were transferred to a new eppi. For protein quantification, a standard BC assay was performed. First, eight standards were prepared from 2 mg/ml BSA standard solution, ranging from 1000 μ g/ml to 15.625 μ g/ml plus an additional "empty" tube with 0 μ g/ml. To be able to subtract plate background, the 96-well plate used for subsequent measurements was inserted empty into the plate reader and measured at 562 nm wavelength. Then, Interchim BC assay reagents A and B were mixed 50:1 (200 μ l/well) and 20 μ l standard and diluted samples (10x - 30x in lysis buffer) added to the 96-well plate. After adding the Interchim mixture to all wells, the plate was covered with tin foil and incubated for 30 min at 37 °C. Lastly, the microplate was measured at 562 nm wavelength. Background was subtracted from standard and sample data and a standard curve plotted containing the respective equation and R²-value. Using the displayed equation, sample concentrations could be measured and were adjusted to 5 μ g/ μ l with loading buffer. After additional 1:3 dilution in loading buffer, samples were stored at - 20 °C until further processing.

3.2.3.2 Western Blotting

For Western Blotting, 10 μg sample and 10 μl marker were loaded in precast MiniProtean TGX gels submerged in 1x running buffer inside the BioRad MiniProtean electrophoresis system. Stacking of proteins was carried out at 80 V and subsequent separation at 110 V. Later on, proteins were transferred onto a methanol-activated PVDF membrane using a sandwich system in 1x transfer buffer for 1.5 h at a constant current of 300 mA. Afterwards, membranes were briefly washed in PBS-Tween to remove residual methanol. Blocking was carried out for 1.5 h with either 5 % non-fat milk or 5 % BSA in PBS-Tween, depending on the primary antibody requirements. Primary antibodies were diluted in blocking solution according to the respective data sheet and the membranes covered with solution sealed inside small plastic bags to reduce the amount of required antibodies. Incubation was carried out overnight at 4 °C on a slightly rocking shaker. The following day, membranes were washed three times in PBS-Tween for 10 min each. Secondary antibody solutions were similarly prepared either in 5 % non-fat milk or BSA in PBS-Tween, ranging from 1:2000 - 1:3000. Incubation was carried out in small, sealed plastic bags for 1 h at room temperature on a gentle rocking device. Afterwards, membranes were washed three times with PBS-Tween for 10 min each. Chemiluminescence was detected with Amersham ECL Western Blotting Detection Reagents and the ChemiDoc MP Imaging System. Further stainings were carried out after stripping the membranes from its bound antibodies. Blots were briefly washed twice with PBS-Tween and subsequently incubated for 10 min with Restore PLUS Western Blot Stripping Buffer on a gentle rocking device. Then, blots were washed twice with PBS-Tween, incubated for 1 h with the appropriate blocking solution and subsequently primary and secondary antibodies. Stripping and re-staining of blots could be performed up to three consecutive times.

3.2.4 Culture of primary microglia

3.2.4.1 Prior arrangements

Round coverslips (13 or 15 mm \varnothing) needed for culture experiments were mounted onto porcelain staining racks and submerged in 65 % Nitric acid for an overnight treatment on a shaker. The following day the acid was carefully removed and the coverslips washed six

times at least 20 min with autoclaved ddH₂O. Following, the staining racks were put (with closed lids) into the oven for 1 h at 100 °C and an additional 6 h at 220 °C. Fully sterile coverslips were placed with forceps into 6 cm petri dishes without overlapping each other. Additionally, freshly-prepared culture medium was placed inside the CO₂ incubator the night before to allow for proper gas and pH adjustments. Already adjusted medium could be used for two weeks while freshly prepared medium could be stored in the fridge for a month.

3.2.4.2 Culture and handling

Cells obtained from pups were seeded either in 24-well plates at a density of 2×10^5 cells/well onto a single coverslip or into 6 cm petri dishes at a density of at least 1×10^6 cells with multiple glass coverslips. Plates were cultured in a humidified incubator at 37 °C and 5 % CO₂. The following day medium was carefully aspirated and replaced with fresh one to remove dead or not fully attached cells. Treatments (AAV or phagocytosis assays) were started on day 3-4 in culture to ensure that cells had time to recover.

3.2.4.3 Phagocytosis assay with pHrodo Green *E.coli* particles

Microglial phagocytosis assay was performed as previously described [224, 305]. Briefly, microglia isolated from P4-6 C57Bl/6J pups were seeded in 24-well plates at a density of 2×10^5 cells/well, creating at least four biological replicates from one animal. After 3-4 days in culture, microglia were visually inspected to confirm an appropriate level of ramification and even distribution within and across wells. Cells were subsequently incubated with 50 μ l of pHrodo Green *E.coli* BioParticles (Invitrogen) for 1 h (or 30 min for the shortened phagocytosis assay). As negative control and phagocytosis inhibitor CytoD (10 μ M) was applied 30 min prior to the application of pH-sensitive particles. Afterwards, cells were carefully washed 3x with pre-warmed 1x PBS to remove remaining *E.coli* particles. Fixation and fluorescent staining of cells was performed immediately afterwards. Due to the sensitive nature of the pHrodo Green BioParticles image acquisition was carried out within the following day, latest 48 h after application. At least two biological replicates were used in each experiment per condition and compared to biological replicates from the same animal (e.g. treated vs. untreated). Experiments were performed as triplicates.

pHrodo Green *E. coli* suspension was prepared according to the manufacturers instructions. Lyophilized particles were resuspended in autoclaved 1x PBS to a final concentration of 1 mg/ml and stored at 4 °C (protected from light). To assist homogenization of the suspension it was first vigorously vortexed and the required amount subsequently sonicated for 5 min in a water bath. Vials containing resuspended bacterial particles could be used within 4 months after reconstitution.

3.2.4.4 AAV-facilitated mBin1 overexpression in cultured primary microglia

3.2.4.4.1 AAV vector design

For microglial overexpression of *BIN1* a custom-made vector was produced by Vector Biolabs [306]. The construct AAV/TM6-F4/80-mBin1-2A-mCherry was designed to specifically overexpress mouse *BIN1* isoform 2 (mBin1). Transgene expression was controlled by the microglia-specific F4/80 promoter. The fluorescent reporter mCherry was added to the construct but not linked to BIN1. The produced batch was delivered with a final titer of 5.2×10^{11} GC/ml and stored at - 80 °C after aliquoting.

For *in vitro* control experiments the construct AAV/TM6-F4/80-mCherry was similarly produced by Vector Biolabs. The manufactured batch was delivered with a final titer of 2.0×10^{12} GC/ml and likewise aliquoted and stored at - 80 °C.

3.2.4.4.2 microglia transduction *in vitro*

Microglia isolated from P4-6 C57Bl/6J pups were seeded in 24-well plates at a density of 2×10^5 cells/well, creating at least four biological replicates from one animal. Cultures were visually inspected under binoculars on day 3-4 after isolation to confirm an appropriate level of ramification and even distribution of cells within and across wells. The Bin1 overexpression construct AAV/TM6-F4/80-mBin1-2A-mCherry (5.2×10^{11} GC/ml original titer) was applied by aspirating 500 μ l medium out of single wells and adding 0.2 μ l virus (equaling a MOI of 2500), leading to a final dilution of 1:5000 after reintroducing the thoroughly-mixed virus-containing medium. Cultures were then incubated for five days at 37 °C and subsequently fixed for immunohistological examination. At least two biological replicates were used in each experiment per condition and compared to biological replicates from the same animal (e.g. treated vs. untreated). Experiments were performed as

triplicates.

For control experiments the construct AAV/TM6-F4/80-mCherry (2.0×10^{12} GC/ml original titer) was used. To facilitate a proper comparison between overexpression and control construct the MOI was calculated similar for both treatments. The higher titer of the control construct required a 1:10 dilution in 5 % Glycerol in PBS after which 0,52 μ l could be added to the cultures in a similar manner as described above. Cultures were then incubated for five days at 37 °C and subsequently fixed for immunohistological examination. At least two biological replicates were used in each experiment per condition and compared to biological replicates from the same animal (e.g. treated vs. untreated). Experiments were performed as triplicates.

3.2.5 RNAseq of primary microglia using the MG400 panel

Bulk RNAseq experiments were designed as targeted expression analysis of 400 microglia-specific homeostatic and inflammation-associated genes and proteins as well as several housekeeping genes for normalization. Conceptual design of the MG400 panel was adapted from Butovsky *et al.* 2014. In this study we isolated and sequenced microglia obtained from 12 mo APP^{NL-G-F} and C57Bl/6J mice with four animals per group.

3.2.5.1 RNA isolation and quantification

Adult microglia isolated with GentleMACS and Neural Tissue Dissociation Kit (P) were washed once with PBS, supplemented with RNase inhibitor and stored at - 80 °C until further processing. Depending on the amount of harvested cells, the RNeasy Plus Micro or Mini Kit from Qiagen was used according to the manufacturers instructions together with the QIAcube. Both methods allowed for specific enrichment of mRNA since most RNAs <200 nucleotides (e.g. 5.8S RNA, 5S RNA and tRNA) were selectively excluded. In brief, cells were lysed and homogenized using a highly denaturing guanidine-isothiocyanate-containing buffer, which immediately inactivated RNases to ensure isolation of intact RNA. Subsequently, the lysate was passed through gDNA eliminator columns to efficiently remove genomic DNA. After several washing steps the sample was applied to an RNeasy MinElute spin column where total RNA could bind the membrane. RNA was then eluted in 20 μ l ultrapure water and immediately afterwards quantified using the Qubit RNA HS (high

sensitivity) Assay and Qubit Fluorometer.

The Qubit RNA HS Assay Kit was used according to the manufacturers instructions. In brief, 2 μ l sample and 10 μ l of both standards were separately diluted in freshly prepared working solution. After thoroughly vortexing samples and standards, all tubes were allowed to incubate at least 2 min at room temperature. To calibrate the Qubit Fluorometer standards were measured first, creating a curve. Samples usually achieved at least 50 ng of RNA. Afterwards, samples were stored at - 20 °C until all specimen were collected.

3.2.5.2 RNA quality control

Here, we used the Agilent 2100 Bioanalyzer and the RNA 6000 Nano Kit for RIN score analysis. Sample analysis was performed according to the manufacturers instructions. In brief, reagents were allowed to equilibrate to room temperature before use while setting up the Chip Priming Station. Using the plunger, gel-dye mix was carefully pipetted into the marked wells on the chip. Afterwards, RNA marker was given into all sample wells and also into the ladder well. Finally, ladder and 1 μ l sample material were added. To ensure even distribution of all reagents within their well, the IKA vortexer was used right before running the chip with the Bioanalyzer. Samples were considered for sequencing if they achieved a RIN score ≥ 7 .

3.2.5.3 Bulk RNAseq using Illumina TruSeq Targeted RNA Expression

For targeted bulk RNAseq experiments a custom-made panel was designed based on Butovsky *et al.* 2014 with Illumina DesignStudio. 400 microglia-specific homeostatic and inflammation-associated genes together with five additional housekeeping genes for normalization were selected. Library preparation for TruSeq Targeted RNA Expression was performed after all samples were acquired and tested for their suitability. No changes were made to the protocol provided by Illumina. All required buffers, solutions and active compounds were supplied in their respective kits. To ensure higher stability of samples, isolated RNA was reverse transcribed into first strand cDNA using reverse transcriptase and random primers. Next, the oligo pool was hybridized to generate upstream and downstream oligos specific to the targeted regions of interest. To remove unbound oligos, samples were washed and additional sequences ligated with DNA polymerase to facilitate amplifi-

cation. Following, the extension-ligation products were amplified and Index Adapters (Kit A) bound to the samples. To purify the PCR products from other reaction components, AMPure XP beads were used. Finally, the separately prepared libraries of all samples were combined, quantified, denatured and diluted in hybridization buffer. Sequencing was carried out using a MiniSeq Mid output kit on the Illumina MiniSeq sequencer.

3.2.5.4 Data analysis

As a first control after sequencing, runs were analyzed for their signal density (over- or underclustering) and Q score value for base call accuracy. For raw data analysis, the open source web-based platform Galaxy was used. There, reads were aligned to the mouse genome (mm10) using RNA STAR and quantified using featureCounts. Differential expression was analyzed using DESeq2 and results with an absolute fold-change ≥ 1.5 and FDR ≤ 0.05 were deemed statistically significant and biologically relevant. Further organization and analysis of the data was performed using Igor Pro, STRING and WebGestalt.

3.2.6 Mouse procedures

3.2.6.1 AAV-facilitated microglial overexpression of mBin1 *in vivo*

3.2.6.1.1 Stereotactic virus injection

In this study we used 3 mo WT animals from the Iba1-GFP line for *in vivo* transduction with AAV_{Bin1}. Four groups were defined containing each three animals. To gain insight into distribution of the construct, the vector was injected either uni- or bilaterally into the hippocampal CA1 region or bilaterally into the lateral ventricles. The fourth group contained native mice for comparison.

Before starting with the virus injection, surgery tools were thoroughly sterilized in a hot bead sterilizer and the heated cage intended for recovery of the animals after surgery turned on. Mice were deeply anesthetized by i.p. injecting a mix of Ketamin/Xylazin (130/10 $\mu\text{g}/\text{g}$ body weight). The depth of anesthesia was determined by pinching the interdigital space with forceps. Additionally, the anti-inflammatory drug Carprofen (4 $\mu\text{g}/\text{g}$ body weight) and the antibiotic drug Enrofloxacin (5 $\mu\text{g}/\text{g}$ body weight) were s.c. administered right before starting the procedure. While the mouse was falling asleep, the prepared injection

glass capillary was fixed to the Neurostar Robot Stereotactic System, filled with mineral oil and the virus carefully absorbed. The head of the mouse was planar fixed between two ear bars of the stereotactic injection setup and the eyes protected from dryness by applying Bepanthen eye ointment (Bayer). During surgery, the body temperature of the mouse was kept at 37 °C with a heating pad. After cleaning the top of the mouse head with 70 % ethanol, the skin was longitudinally cut with a scalpel to expose the cortical skull area. To facilitate straightforward working conditions, all following steps were carried out through binoculars with a cold light source. Skull and edges of the skin were cleaned from loose hair and connective tissue with 70 % ethanol drenched cotton swabs. To properly assess the brain position, Lambda, Bregma as well as the lateral tilt were defined using the StereoDrive software. The injection site was specified using the mouse brain atlas implemented within StereoDrive. For hippocampal injections, the target area was allocated to Bregma - 1.46 mm, between stratum pyramidale and stratum radiatum. When aiming for the lateral ventricles, the injection sites were placed at Bregma - 0.46 mm in the middle of both ventricles. A hole was drilled manually right above the previously determined injection site and the capillary inserted with a defined speed of 10 $\mu\text{m}/\text{sec}$. 1 μl virus was released with a speed of 67 nl/min, accumulating to 15 min of injection. Afterwards, the capillary was kept for 5 min at the injection site before retracting with 0.1 mm/sec. The small holes in the skull were closed with bone wax and the skin sewn with absorbable sutures. Mice were then transferred to the heated cage and examined again 1 h later. If the animal was awake and lively, it was subsequently transferred to its separate cage with easy access to mashed and watered food in a petri dish on the cage floor. All animals were inspected during the three consecutive days. Mice were perfused 30 days post injection and the brains extracted for immunohistological examination.

3.2.6.2 Transcardial perfusion

Mice were deeply anesthetized by i.p. injecting a mixed solution of Ketamin and Xylazine in NaCl. While the mouse was falling asleep the peristaltic pump was set up with cooled 1x PBS and 4 % PFA (fixative) in separate falcons. After roughly 10 min sensory reflexes were checked by pinching the interdigital space with forceps and the mouse was fixed to a polystyrene surface if no further reflexes were observed. Just below the sternum a

small piece of skin was removed to increase the accessibility of the subjacent musculature. Carefully, without damaging internal organs, transversal and longitudinal cuts were made into the thoracic cavity to fully expose the heart. While gently holding the heart with blunt forceps the tip of a butterfly needle (connected to the peristaltic pump) was inserted into the left ventricle where the tissue appeared lighter in color. To prevent the needle from moving it was fixed with two additional needles creating a x-shape. Next, the pump connected to the cold 1x PBS solution was turned on and immediately afterwards a small incision was made just before the right atrium to allow the fluids to extravasate. Flow rate was set to 5 ml/min. After 5 min the pump was briefly stopped and the cold 4 % PFA solution was connected to the pump. Additional 5 min of PFA perfusion later the mouse was rapidly decapitated, the brain very carefully extracted and placed inside a small vial containing 4 % PFA in which it would stay overnight at 4 °C on a slightly rocking shaker. The next day PFA was removed and the tissue washed 3x with 1x PBS. Brains were considered for sectioning and consecutive stainings if their appearance was overall whitish. If the tissues could not be processed immediately they were stored short term in 0.05 % NaN₃ in 1x PBS at 4 °C.

3.2.7 Histology

3.2.7.1 Mouse brain sectioning

PBS and 4 % PFA perfused brains were embedded in melted 1.5 % agarose in 1x PBS to ensure sufficient stability during coronal sectioning with the Leica Vibratome VT1200S. Hardened agarose blocks containing the brain tissue were mounted on the vibratome platform with Cyano fast glue and submerged in 1x PBS. The following settings were applied: Speed: 0.8-1.0 mm/sec; amplitude: 1.60 mm; step size: 50 μ m

Whole brain serial sections were collected with 1x PBS in two 24-well plates with four to six slices in one well (depending on the respective size). For short-term storage sections were stored at 4 °C in 0.05 % NaN₃ in 1x PBS. Long-term storage was achieved by using anti-freeze solution. Slices were kept at 4 °C for 48 h and only afterwards transferred to -20 °C to avoid crystal formation and other artifacts.

3.2.7.2 Immunofluorescent stainings of mouse brain sections

Stainings were carried out using free-floating conditions in 24-well plates with single coronal sections placed in individual wells. To facilitate a homogeneous distribution of reagents and solutions all steps were carried out on a shaker.

50 μm thick slices were washed twice with 1x PBS to remove either NaN_3 or anti-freeze solution (depending on the previous storage condition). Afterwards, sections were permeabilized using 2 % Triton X-100 in 1x PBS for 4 h at room temperature or overnight at 4 °C. To reduce unspecific background, slices were blocked for 4 h at room temperature in blocking solution. Next, primary antibody solution was prepared in blocking solution and applied for 24-48 h at 4 °C (see section 3.1.7.3.2 for dilutions). In general, synaptic stainings had to be incubated for 48 h to achieve the desired intensity and depth, while other stainings were sufficiently prominent after 24 h. When combining antibodies that required different incubation times, the antibody with the shorter incubation time was diluted in 20 μl blocking solution and after 24 h joined with the first primary antibody. Later, slices were washed 3x for 10 min in 1x PBS and incubated with the corresponding secondary antibodies for 1 h. Due to the light sensitive nature of secondary antibodies, all following incubation and washing steps were performed with the plate being covered with tin foil. If DAPI stainings were performed, sections had to be washed twice for 10 min in 1x PBS, then incubated for 10 min with DAPI in 0.3 % Triton X-100 in 1x PBS and washed again 3x for 10 min with 1x PBS. Slices were mounted on glass slides with the help of a small brush. Without touching the slices, residual PBS was carefully removed with lint-free Kim Wipes after which slices were kept in the dark to air dry for several minutes. As soon as most of the fluid was evaporated, slices were covered with mounting medium and a glass coverslip for microscopic analysis. The finished slides were kept at room temperature in the dark for 30-60 min and then stored at 4 °C until microscopic examination.

3.2.7.3 Immunofluorescent stainings of primary microglia

In general, immunofluorescent stainings of primary microglia had to be carried out very carefully to avoid damaging the fine processes and filopodia. Additionally, all steps were carried out at room temperature without shaker.

Fixation was performed using pre-warmed 4 % sucrose in 4 % PFA for 15 min, followed by three washes with 1x PBS. Cells were quenched with 50 mM ammonium chloride for 10 min and afterwards washed 3x with 1x PBS. Permeabilization was achieved using 0.3 % Triton X-100 in 1x PBS for 5 min. Subsequently, cells were washed 3x with 1x PBS and the coverslips transferred into a dark wet chamber where all following steps were carried out. To reduce unspecific background, blocking solution was applied for 1 h. This was followed by another hour of incubation with primary antibody in blocking solution (see section 3.1.7.3.2 for dilutions). Afterwards, cells were washed 3x with 1x PBS and incubated with the required secondary antibodies in blocking solution for 1 h. Following, cells were washed 3x with 1x PBS and the coverslips dipped twice into dH₂O to remove the salts contained in PBS. Lint-free Kim Wipes were used to remove excess water at the edges and the coverslips placed facing downward onto a glass slide prepped with a drop of mounting medium. Finalized slides were kept at room temperature in the dark for 30-60 min and then stored at 4 °C until microscopic examination.

3.2.8 Immunofluorescence analysis: image acquisition and quantification

Immunofluorescent pictures were acquired with the confocal microscope LSM900 (Zeiss) with a Plan Aplanachromat 40x or 63x/NA 1.4 oil immersion objective and the pinhole set to 1 AU, unless specified otherwise. In order to enable a comparative analysis, laser settings were consistent between separate batches which included all respective groups that were up for comparison. Image format was set to 1024 x 1024 pixels. Image analysis was performed with ImageJ.

The more detailed specifications for each representative image are described in the figure legends. All pictures are shown as orthogonal projections from z-stack images.

3.2.8.1 Primary microglia culture: phagocytosis assay validation

For the quantification of phagocytosis assays with and without CytoD in cultured primary microglia five pictures (from one culture dish) were taken per experiment and condition. A total of three independent experiments was performed using the 40x oil immersion objective with no additional zoom. Each image contained 6-13 microglia cells.

Area and %-area covered by the autofluorescent *E.coli* particles were determined using

the "Threshold" and "Analyze Particles" functions from the software ImageJ. The area and %-area of Iba1-positive microglia (No. 234004) was used to normalize stainings. The average of three independent experiments was calculated.

3.2.8.2 Primary microglia culture: analysis of Bin1 overexpression, activation status, endolysosomal machinery and phagocytosis assays

For the quantification of Bin1 ([EPR13463-25] No.ab185950), CD68 ([FA-11] No.MCA1957), Lamp1 ([EPR21026] No.ab208943), β -actin ([AC-15] No.ab6276) and phagocytosis assays in cultured primary microglia ten pictures (from two separate culture dishes) were taken per experimental batch and condition. A total of three independent experiments was performed using the 40x oil immersion objective with no additional zoom. Each image contained 6-13 microglia cells.

Area and %-area covered by the respective stainings were determined using the "Threshold" and "Analyze Particles" functions from the software ImageJ. The area and %-area of Iba1-positive microglia (No. 234004) was used to normalize stainings. The average of three independent experiments was calculated.

3.2.8.3 Mouse brain sections: analysis of Bin1 downregulation in Alzheimer Disease microglia

Images of multiple microglia were obtained in the hippocampal CA1 region of 12 mo APP^{NL-G-F} and C57Bl/6J mice. For the quantification of Bin1 ([2F11] No.sc-23918) in microglia, five images were taken per condition and experiment. A total of three independent experiments was performed using the 40x oil immersion objective with zoom 0.5. Three mice were analyzed per condition.

The area of Iba1-positive microglia (No. 234004) was used to create a thresholded mask within which Bin1 was quantified. Area and %-area were determined using the "Threshold" and "Analyze Particles" functions from the software ImageJ. The average of three independent experiments was calculated.

3.2.8.4 AAV *in vivo*: analysis of Bin1 overexpression and activation status in microglia and neuronal side-effects

Images of single microglia were obtained in the hippocampal CA1 region of 4 mo WT mice 30 days post unilateral AAV/TM6-F4/80-mBin1-2A-mCherry injection and native 4 mo WT mice. For the quantification of Bin1 ([2F11] No.sc-23918) and CD68 ([FA-11] No.MCA1957) in microglia, five images were taken per condition and experiment. A total of three independent experiments was performed using the 40x oil immersion objective with zoom 4. Three mice were analyzed per condition.

The area of Iba1-positive microglia (No. 234004) was used to create a thresholded mask within which other stainings were quantified. Area and %-area covered by Bin1 and CD68 were determined using the "Threshold" and "Analyze Particles" functions from the software ImageJ. The average of three independent experiments was calculated.

Due to obvious mCherry-positive signals emerging from pyramidal layer neurons in AAV-injected animals, Bin1 ([2F11] No.sc-23918) was additionally quantified for those cells. Images of multiple mCherry-positive neuronal cell bodies and 3-4 microglial cells were acquired using the 40x oil immersion objective with zoom 2. Five pictures were taken per condition and experiment and a total of three independent experiments performed. Three mice were analyzed per condition.

The area of Iba1-positive microglia (No. 234004) was used to create a thresholded mask within which the Bin1 signal was removed. The remaining Bin1 area and %-area was determined using the "Threshold" and "Analyze Particles" functions from the software ImageJ. The average of three independent experiments was calculated.

3.2.8.5 Mouse brain sections: analysis of synaptic proteins within Alzheimer Disease microglia

Images of single microglia were obtained in the hippocampal CA1 region of 3, 6 and 12 mo APP^{NL-G-F} and C57Bl/6J mice. For the quantification of Homer1 (No.160 003), Synaptogyrin3 ([G3] No.sc-514081) and Synaptophysin (No.AB9272) in microglia, three images were taken per condition and experiment. A total of three independent experiments was performed using the 40x oil immersion objective with zoom 3. Three mice were

analyzed per condition.

The area of CD68 in Iba1-positive microglia ([FA-11] No.MCA1957) was used to create a thresholded mask within which synaptic proteins were quantified. Area and %-area were determined using the "Threshold" and "Analyze Particles" functions from the software ImageJ. The average of three independent experiments was calculated.

3.2.9 Statistical analysis

Statistical analysis for all described experiments (excluding RNAseq) was performed in GraphPad Prism using the appropriate test according to the experimental design. If not indicated otherwise Welch's t-test was performed to correct for unequal variances in limited populations. Analyzed data from replicates (N) are expressed as the mean \pm standard deviation (SD) from at least three independent experiments. P-values were deemed statistically significant if $p < 0.05$ (* $p < 0.05$, ** $p < 0.01$, *** $p < 0.001$, **** $p < 0.0001$, n.s. $p > 0.05$).

4 Results

4.1 Characterization of microglial dynamics during Alzheimer's Disease

Since its discovery more than 100 years ago, the intricate mechanisms underlying AD have proven to be particularly difficult to dissect and even more challenging to treat in patients. Nevertheless, valuable and meaningful advances were made not only but also on the immunological side of AD. Microglia were identified to be both remedy and perpetrator of this complex disease (section 1.2.3). Still, the precise mechanisms and switches that could also be vital for successful therapeutic approaches are not yet fully disclosed. In recent years, omics studies (genome, transcriptome and proteome) have become increasingly popular as they hold a huge potential in predicting how diseases evolve, uncovering the mechanism of action for certain drugs and discovering new subtypes of cells, among others. Moreover, integrating data from different experimental approaches (*e.g.* RNAseq and proteomics) can give valuable results as it holds the potential to strengthen or weaken certain assumptions drawn from studies utilizing a single method. Therefore, the first aim of my thesis centered around the characterization of aged AD mouse microglia by establishing and utilizing RNAseq and subsequently comparing the results to a previously published matching proteomic dataset [224].

4.1.1 Transcriptomic profiling of Alzheimer's Disease mouse microglia

Although single-cell sequencing (scRNAseq) has now evolved to be faster and cheaper since its introduction to the scientific community, it still requires a considerable amount of sample material and is still more labor- and cost-intensive than bulk RNAseq. Moreover, scRNAseq provides the potential to identify molecular mechanisms that are linked to a specific cell type. To circumvent this clear disadvantage of bulk RNAseq, I isolated primary mouse microglia and sequenced their RNA to gain insight into microglia-specific changes in the context of AD. For my thesis I focused on a data set obtained through isolation of microglia from 12 months old (mo) WT and APP^{NL-G-F} mice using magnetic-activated cell

sorting (MACS) technology. Subsequently, extracted mRNA transcripts were sequenced with the MG400 chip panel originally described by Butovsky and colleagues [307].

4.1.1.1 MG400 chip panel design

The MG400 chip panel was designed by Oleg Butovsky and colleagues and is aimed at the targeted sequencing of 400 genes that are enriched in adult mouse microglia [307]. Gene-array analysis and mass spectrometry quantitative TMT-analysis led to the identification of 245 genes and 100 proteins that were specifically or highly expressed in adult mouse microglia [307]. In addition, it contains 40 inflammation genes that were significantly affected in EAE, APPPS1 and SOD1 mice and five housekeeping genes for data normalization (*Gapdh*, *Cltc*, *Gusb*, *Hprt1* and *Pgk1*) (Fig. 12). The authors describe that this signature can not be observed in other brain cell types, microglial cell lines or in monocytes recruited to the CNS [307]. The sequencing of cells with this panel allows for targeted analysis approaches aimed at the immunomodulatory function of microglia.

1810011010Rik	Bend6	Cntn6	Exoc5	Havcr2	Limk1	Olfml3	Ptprg	Slc24a3	Tlr1
9030625A04Rik	Bhlhe41	Cpne2	Extl3	Hexb	Liph	Olfrl110	Ptprm	Slc2a3	Tlr2
Abca1	Bln1	Crybb1	Eyo4	Hist1h2ac	Lrp12	Olfrl920	Ptprz1	Slc2a5	Tlr3
Abcc3	Blink	Cryl1	F11r	Hmgm1	Lrrc3	Omg	Qdpr	Slc30a4	Tlr4
Abhd12	C1qa	Csf1	Fads1	Hpgds	Lrrc8a	Ophn1	Rab3il1	Slc46a1	Tlr5
Abhd6	C1qb	Csf1r	Fbxo21	Hprt	Ltc4s	P2rx7	Rab6b	Slc4a2	Tlr6
Abi1	C1qc	Csf3r	Fcgr1	Hps4	Ly96	P2ry12	Rap1gds1	Slc6a1	Tlr7
Abi3	C3ar1	Cst3	Fcgrt	Hspa1a	Mafb	P2ry13	Rapgef5	Slc7a8	Tm9sf4
Acp2	C4a	Ctnna2	Fcnb	Hvcn1	Magi3	P2ry6	Rasgef1b	Slco1a4	Tmc7
Acvr1	Cables1	Ctsd	Fcrls	Icam1	Manba	P4ha1	Rasgrp3	Slco2b1	Tmcc3
Adamts1	Cadm1	Ctsf	Fgd2	Igf1	Map2k1	Paki	Rbbp9	Sjfn14	Tmeff1
Adamts16	Camk2n1	Ctsl	Fgfr1	Igf2	Map3k7	Pde3b	Rgl1	Sncalp	Tmem100
Adap2	Cbr1	Ctss	Flot1	Igsf8	Mapk14	Pdgfra	Rgmb	Snn	Tmem119
Adcyap1r1	Cbr3	Cttntp2nl	Flot2	Il10ra	Mecp2	Pdgfra	Rgs1	Srx24	Tmem144
Add1	Ccl12	Cx3cr1	Fos	Il10rb	Mef2a	Pea15a	Rhob	Socs3	Tmem206
Adora3	Ccl2	Cxcl16	Frm4a	Il18	Mef2c	Pgk1	Rilp1	Sparc	Tmem47
Adrb1	Ccl3	Cxcl5	Frm4b	Il1a	Mef2d	Pgrmc1	Ripk2	Spint1	Tmem64
Agmo	Ccl4	Cysltr1	Fscn1	Il1rl2	Mertk	Pik3r4	Rnf180	Spire1	Tmem86a
Agpat3	Ccl5	D18Ert653e	Gab1	Il21r	Milp	Pitnm1	Rock2	Sprb4	Tnfrsf11a
Ahcy1l	Ccl6	D3Bwg0562e	Ganc	Inpp4b	Mmp2	Pla2g15	Rptor	Spry1	Tnfrsf17
Aif1	Ccnd1	Dab2	Gapdh	Itga6	Mir1	Plxdc2	Rtn1	Spsb1	Tppp
Ak1	Ccr5	Dagla	Garni3	Itga9	Mras	Plxna1	Rtn4rl1	St3gal6	Trappc10
Ang	Cd14	Dfna5	Gas6	Itgb5	Myc	Plxna4	Rufy3	Stab1	Trem2
Ank2	Cd34	Dip2a	Gas7	Jam2	Myef2	Pmepa1	Ryk	Strn	Trim47
Ap3d1	Cd83	Dnajb4	Gbas	Jmy	Myo1b	Pmp22	Sall1	Sult1a1	Tspan18
Apbb2	Cd86	Dst	Gbg1	Jun	Naop	Palr2b	Sall3	Sup15h	Tspan3
Appl1	Cfp	Ebf3	Gmfb	Kcnd1	Nav2	Pon3	Sbf2	Sv2a	Tspan4
Apoe	Chl3l1	Egr1	Gnaq	Kcnk13	Ncam1	Ppap2a	Scamp5	Sv2b	Tspan7
App	Chl1	Egr2	Gnas	Kcnma1	Necap1	Ppfa4	Scarb2	Syng1	Ttc28
Arhgap12	Chn2	Eng	Golga3	Kctd12	Nedd1	Ppm1l	Scoc	Synj1	Ttr
Arhgap22	Chst7	Enpp2	Golm1	Khdrbs3	Nefl	Ppp1r15a	Sec22b	Sytl1	Tubb5
Arhgap5	Ckb	Entpd1	Gp9	Kitl	Nfia	Ppp1r9a	Sema6d	Tanc2	Tubgcp5
Asph	Clstn1	Epb4.1l2	Gpm6a	Kl	Nfkb1	Pros1	Serpine2	Tceal1	Unc13a
Atf3	Cltc	Epn2	Gpm6b	Klf12	Nlgn3	Prpf31	Sesn1	Tgfa	Upk1b
Atg4b	Clu	Eps15l1	Gpr34	Klhl38	Npl	Prrt2	Sez6l	Tgfb1	Usp2
Atp8a2	Cmkir1	Erlin2	Gpr37l1	Lag3	Npnt	Prune2	Sgce	Tgfb1	Vot1l
Axl	Cnn3	Errfi1	Gpr56	Lair1	Nr3c1	Psd	Siglech	Tgfb2	Vps11
B4galt4	Cnrip1	Etv1	Grm1	Large	Nrcam	Ptgds	Sirt2	Tgm1	Vta1
Bosp1	Cntn1	Etv5	Gtf2h2	Leprel1	Nrip1	Ptgsfrn	Slc12a2	Timp2	X99384
Bco2	Cntn3	Exoc1	Gusb	Lgmn	Nuak1	Ptms	Slc1a3	Tjp1	Zmynd8

 = Microglia-specific
 = inflammation-associated
 = housekeeping gene

Figure 12: MG400 panel used for bulk RNAseq.

The chip panel was originally designed by Butovsky and colleagues and describes a unique microglia signature that is not found in other cells of the myeloid lineage and cell types of the CNS. Green panels highlight genes and proteins found to be microglia-specific. Red panels highlight genes and proteins found to be associated with inflammation in three different mouse models. Yellow panels highlight housekeeping genes. Green panels with red font highlight genes and proteins that are both microglia-specific and inflammation-associated.

4.1.1.2 MACS microglial isolation allows for transcriptomic analysis

For downstream RNAseq I isolated living microglia from cortices and hippocampus tissue extracted from 12 mo WT and APP^{NL-G-F} mice using magnetic-activated cell sorting (MACS) technology, which allows for a rapid and gentle isolation of whole cells from intact brain tissues. To ensure that microglia obtained with this method were of sufficient quality, I visually inspected a small aliquot from each isolation for general cell morphology, debris and dead cells (Fig. 13 a). Isolations with insufficient quality were not regarded for sequencing. To validate the advertised purity of microglia isolated with CD11b magnetic microbeads, I performed western blots of the microglia-enriched and the microglia-depleted

(flow-through) fraction. Stainings were performed for Iba1 and NeuN (Fig. 13 b). Western blot experiments revealed that the CD11b-enriched microglia fraction was of high purity while the CD11b-depleted fraction was almost devoid of microglia, an important indicator for a good efficiency of the procedure. The results obtained with those control experiment suggested that microglia isolated with MACS technology were of high quality and purity that is needed for RNAseq experiments.

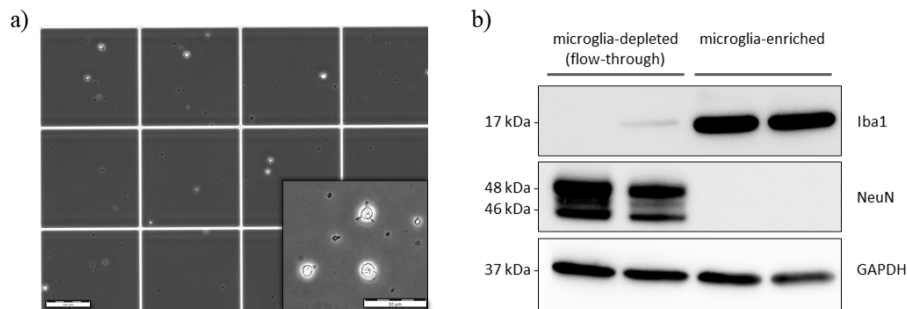


Figure 13: Microglia isolated with MACS are of high quality and purity.

(A) Microglia isolated with CD11b microbeads were 1:1 diluted with trypan blue and visually inspected under the binocular in a C-Chip chamber. Living microglia appear as bright, round spots. Small dark spots label cellular debris. The higher magnification picture captures how shortly after isolation microglia start to extract their processes again. (B) Western Blots of the microglia-depleted and microglia-enriched fraction post isolation. Blots were stained for Iba1 and NeuN.

4.1.1.3 RIN score analysis and post-sequencing quality controls

Measuring RNA quality through RIN score analysis is an important step to determine if the isolated RNA is of adequate integrity for downstream sequencing approaches. For example, cross contamination with DNA could lead to underestimating the amount of RNA used and differential degradation could be interpreted as differential expression. Experiments were performed for three representative isolations on a Bioanalyzer. In line with other publications [308], samples with a RIN score ≥ 7 were considered to be of sufficient quality for sequencing (Fig. 14 a).

Additionally, the post-sequencing quality measurements were analyzed carefully. Especially important were the flow cell chart as an indicator for flow cell load and the Q-score (phred quality score) distribution (Fig. 14 b) as an index for the overall base call accuracy and sample quality. The graphs depicted in Fig. 14 show that RIN score analysis and the sequencing run discussed in this thesis were of high quality, allowing further analysis.

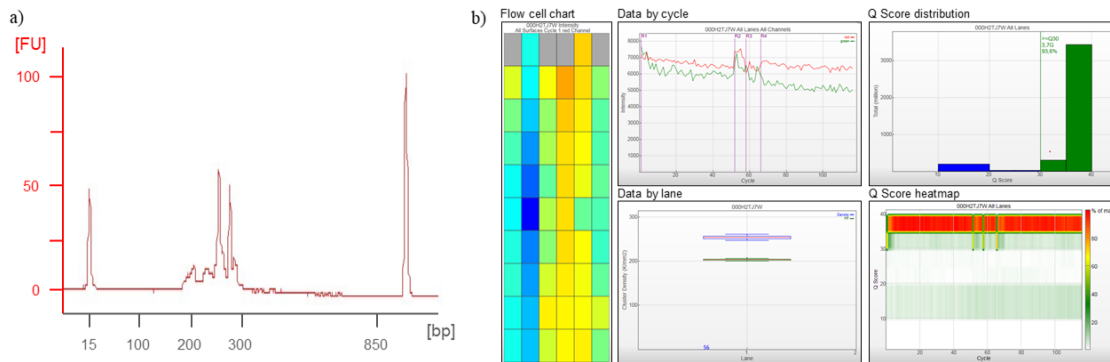


Figure 14: RNA and post-sequencing quality control.

(A) RNA quality control was conducted as RIN score analysis with a Bioanalyzer. RNA quality was deemed sufficient if a RIN score ≥ 7 was achieved. (B) Post-sequencing quality control shows that the flow cell was not overloaded (flow cell chart) and that base call accuracy (Q-score distribution and heatmap) was predominantly above Q30 and Q40 (base call accuracy 99,9 % and 99,99 %, respectively).

4.1.1.4 Genes of aged APP-KI microglia are substantially different compared to age-matched controls

To assess transcriptomic alterations in sequenced microglia, significant changes were defined according to the following criteria: a log₂ fold-change larger than +1 or smaller than -1, with a significant p-value of ≤ 0.05 after FDR correction to avoid the detection of false positive values.

Comparison between 12 mo WT and APP^{NL-G-F} microglia revealed that the transcriptomic signature was significantly different between groups (Fig. 15). Out of 400 genes from the chip panel we found 105 genes significantly upregulated and 112 to be significantly downregulated. The 40 most affected genes are displayed in table 4.1. The highest FC was found for insulin-like growth factor 1 (Igf1), a known modulator of neuroinflammation and microglia phenotypes with neurotrophic properties [309]. The most remarkable downregulation (> 83 %) was detected for crystallin β B1 (Crybb1), a homeostatic microglia gene recently described to be downregulated in microglia associated with A β plaque phagocytosis [310]. Several more genes associated with a homeostatic signature were downregulated, such as *Tmem119*, *Cx3cr1*, *Siglech*, *Hspa1a* and *Gpr34*. On the other side, genes associated with increased activity and inflammatory behavior such as *Trem2*, *Csf1*, *ApoE*, *Ctsd*, *Gas7* and *Axl* were highly upregulated.

gene	description	FC	P _{adj.}
Igf1	insulin-like growth factor 1	60,3348	4,31E-96
Axl	AXL receptor tyrosine kinase	21,1459	1,65E-59
Csf1	colony stimulating factor 1	19,2954	1,08E-19
Gas7	growth arrest specific 7	16,2560	9,88E-51
Olf110	olfactory receptor 110	14,5480	7,39E-15
Olf111	olfactory receptor 111	13,2689	1,62E-56
Ccl6	chemokine (C-C motif) ligand 6	11,0469	1,76E-77
Apoe	apolipoprotein E	7,7118	4,45E-25
Ccl3	chemokine (C-C motif) ligand 3	4,8052	2,99E-28
Serpine2	serine (or cysteine) peptidase inhibitor, 2	4,2709	4,19E-71
Ctsd	cathepsin D	3,9821	3,49E-18
Tlr2	toll-like receptor 2	3,9689	1,18E-36
Gnas	GNAS complex locus	3,9398	3,51E-43
Kcnma1	K/Ca-activated channel subfamily M, α -1	3,8876	3,13E-09
Apbb2	amyloid beta precursor protein-binding, B2	3,7105	9,77E-19
Rgs1	regulator of G-protein signaling 1	3,4937	1,29E-14
Gusb	glucuronidase, beta	3,4925	8,97E-14
Trem2	triggering receptor expressed on myeloid cells 2	3,3654	1,58E-40
Cadm1	cell adhesion molecule 1	3,3395	1,84E-15
Ctsl	cathepsin L	3,0999	3,14E-10
Ccl2	chemokine (C-C motif) ligand 2	0,3740	5,15E-07
Socs3	suppressor of cytokine signaling 3	0,3722	0,0106
Khdrbs3	KH domain, signal transduction associated 3	0,3663	6,27E-05
Tmeff1	TM protein with EGF-like and 2 FST-like domains 1	0,3543	0,0182
Tgm1	transglutaminase 1, K polypeptide	0,3503	0,0349
Cfp	complement factor properdin	0,3143	1,57E-07
Ppp1r15a	protein phosphatase 1, regulatory subunit 15A	0,3078	4,15E-05
Tmem86a	transmembrane protein 86A	0,3016	1,20E-10
Slco1a4	solute carrier organic anion transporter, 1a4	0,2928	0,0001
Camk2n1	Ca/CaM-dependent protein kinase 2 inhibitor 1	0,2924	5,22E-06
Tnfrsf11a	tumor necrosis factor receptor superfamily, 11a	0,2871	2,44E-08
Aif11	allograft inflammatory factor 1-like	0,2735	0,0024
Jun	jun proto-oncogene	0,2715	1,34E-08
Tmem119	transmembrane protein 119	0,2420	1,00E-22
Chst7	carbohydrate sulfotransferase 7	0,2186	3,12E-31
Hspa1a	heat shock protein 1A	0,2125	0,0018
Trim47	tripartite motif-containing 47	0,2103	7,40E-06
C1qa	complement component 1q, α polypeptide	0,2076	6,34E-06
Plxna1	plexin A1	0,1820	2,77E-07
Crybb1	crystallin, beta B1	0,1658	1,35E-18

Table 4.1: List of 40 genes with the highest FC (up- and downregulated) in 12 mo microglia from APP^{NL-G-F} mice compared to age-matched WT controls.

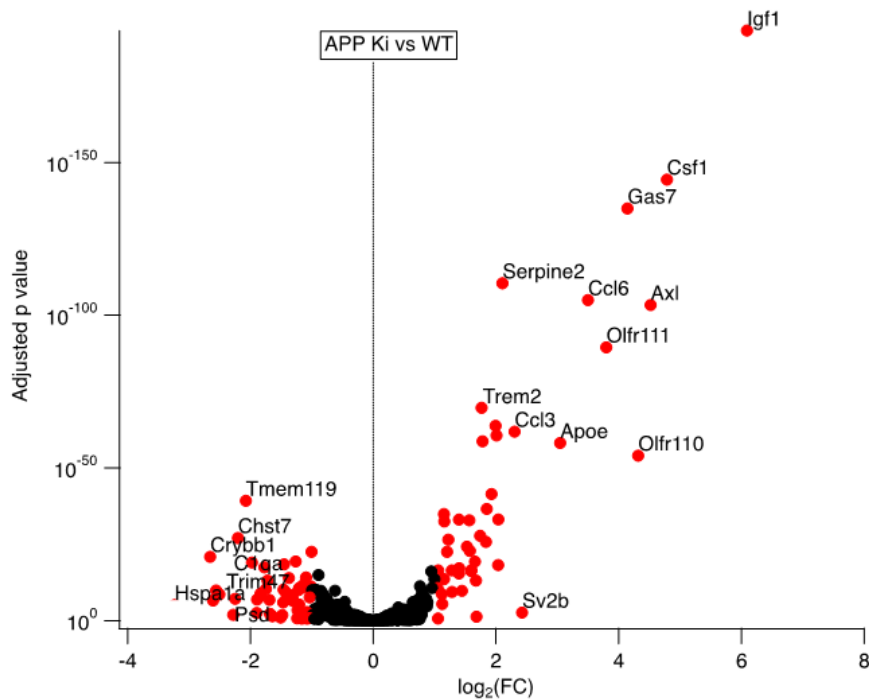


Figure 15: Transcriptomic signature of aged APP^{NL-G-F} microglia is substantially different compared to age-matched WT controls.

Volcano plot depicting the transcriptomic changes observed in 12 mo microglia from APP^{NL-G-F} mice compared to age-matched WT controls. Changes are displayed on the axes with log₂(fold-change) and FDR-corrected p-values (p_{adj}). Significantly changed gene expression is marked in red. Detected genes with non-significant changes are marked in black. A subset of selected genes is labeled with their name.

4.1.1.5 Transcriptomic comparison with MGnD microglia

To examine the overlap of transcriptomic profiles between aged APP^{NL-G-F} microglia and the published literature, I chose the often-cited MGnD microglia phenotype, which describes a microglial signature associated with high activity and neurotoxicity [246]. In their publication, Krasemann and colleagues incorporate the transcriptomic signatures from phenotypically advanced APPPS1, EAE and SOD1 mice through sequencing with the MG550 chip panel and define a novel, common microglia phenotype associated with neurodegeneration, termed MgnD. Comparison between the MG550 and the MG400 chip panel used in this study yielded an overlap of 367 similarly analyzed genes. Accordingly, I re-analyzed both datasets in a manner that would give results only for genes found on both chip panels. This resulted in 9 significantly up- and 67 downregulated genes for MGnD microglia and 87 significantly up- and 106 downregulated genes in 12 mo APP^{NL-G-F}

microglia (Fig. 16). Interestingly, with exception of two genes (*Ccl2* and *Cfp*), the remaining 7 upregulated genes of the MGnD phenotype overlapped completely with those found in APP^{NL-G-F} microglia. Shared downregulated genes were also found (29 genes from 67 significantly downregulated genes in MGnD), albeit with a lower overlap (77,78 % and 43,28 %, shared up vs. shared down, respectively). Shared upregulated genes included *ApoE*, *Csf1*, *Gas7*, *Axl*, *Tlr2*, *Cxcl16* and *Lag3*. Shared downregulated genes contained the characteristic homeostatic genes *Tmem119*, *Bin1*, *Crybb1*, *Cx3cr1*, *Abi3*, *Jun* and *Gpr34*, among others. Moreover, I additionally identified 10 genes which were downregulated in MGnD but upregulated in APP^{NL-G-F} microglia (*Olfml3*, *Tgfb1*, *Tgfb2*, *Arhgap5*, *Hpgds*, *Lair1*, *Pde3b*, *Plxdc2*, *Itga6* and *Rap1gds1*). In general, the overlap between transcriptomic signatures appears significant with pronounced differences on the side of downregulated genes.

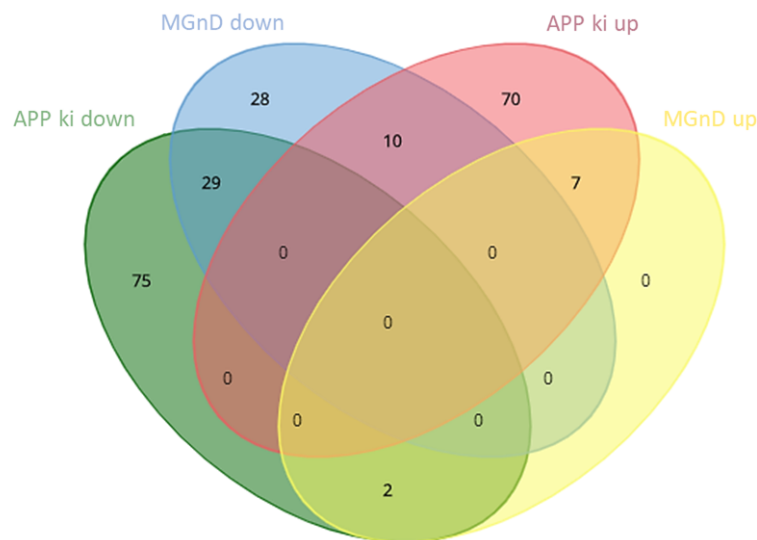


Figure 16: Overlap between MGnD and 12 mo APP^{NL-G-F} microglia transcriptomics.

Venn diagram depicting the overlap between up- and downregulated genes found in MGnD and aged APP^{NL-G-F} microglia. Chip panel comparison resulted in 367 similarly analyzed genes on both panels. Depicted are significantly up- and downregulated genes of MGnD microglia (yellow and blue ellipses, respectively) and significantly up- and downregulated genes of APP^{NL-G-F} microglia (red and green ellipses, respectively). 7 out of 9 upregulated MGnD genes were found in APP^{NL-G-F} microglia and 29 out of 67 significantly downregulated MGnD genes were shared with APP^{NL-G-F} microglia.

4.1.1.6 Gene ontology analysis of APP-KI microglia RNA transcripts

To explore the biological processes and molecular mechanisms that are divergently regulated in 12 mo APP^{NL-G-F} microglia, I performed gene set enrichment analysis (GSEA) with all significantly changed genes (Fig. 17). Results from this analysis revealed that upregulated processes and mechanisms were mainly related to immune system responses and cellular expansion, such as cytokine stimulus responses, peptide secretion, ERK signaling, cellular development and growth, but also neuron death (Fig. 17 a, b). Fitting the mainly external orientation of those mechanisms and processes, upregulated processes could be primarily associated with outward faced compartments of microglia, such as secretory granules and the external side of the plasma membrane but also lytic vacuoles and transport vesicles (Fig. 17 c).

Interestingly, negatively affected processes were found to encompass mechanisms such as actin binding, microtubule-based processes, cytokine binding, protein autophosphorylation and ubiquitin-like protein ligase binding, pointing to a decrease in motility, intracellular transport, chemotaxis and transcription activity (Fig. 17 a, b). In line with the mainly internal orientation of negatively affected mechanisms and processes, they were found to be enriched in inward faced compartments of microglia, such as endosomes, the actin cytoskeleton and the microtubule organizing center (Fig. 17 c).

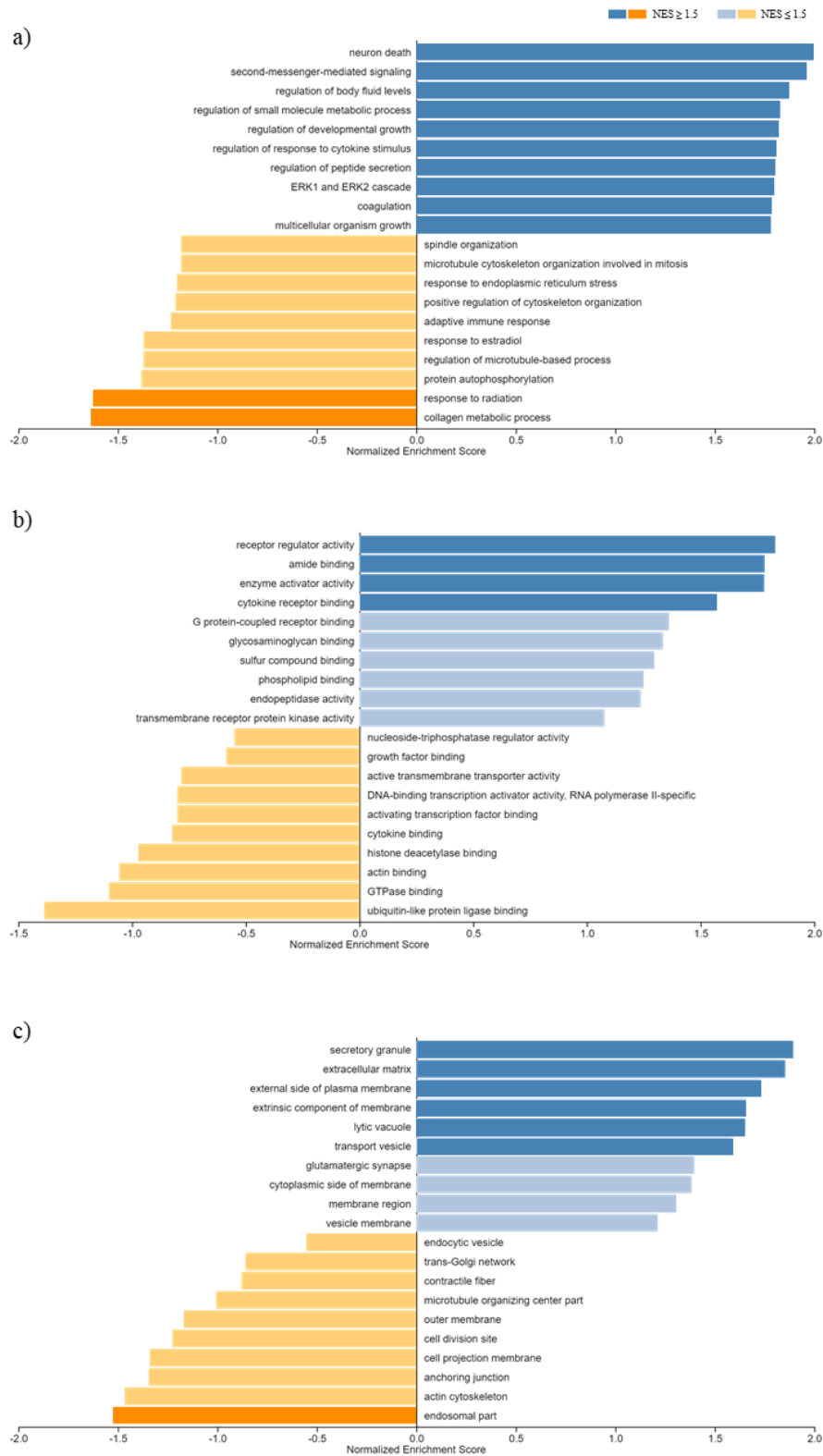


Figure 17: Gene ontology enrichment analysis for 12 mo APP^{NL-G-F} microglia transcripts. Bar plots depict the normalized enrichment for (A) biological processes, (B) molecular mechanisms and (C) cellular compartments in 12 mo APP^{NL-G-F} microglia. Processes with a normalized enrichment score (NES) > 1.5 (depicted in darkened colors) were deemed highly significant.

upregulated while the corresponding RNA transcripts were downregulated (*e.g.* *C1qa*, *Tgm1*, *Gpm6a*). In contrast, 20 % of proteins were significantly downregulated while the corresponding RNA transcripts were upregulated (*e.g.* *Axl*, *Kcnma1*, *Timp2*). Although partially unsatisfactory, the correlation between mRNA and protein expression levels are notoriously poor, typically around 40 % [311, 312]. This discrepancy is usually attributed to differential regulation of transcript and protein product [313] and opens up novel questions regarding gene expression changes in AD. Nevertheless, RNA transcripts and protein products did show a trend towards a positive correlation ($R^2 = 0.285$, $p > 0.05$) with a general overlap of 69,08 %, implicating a biological relevance for the generated data.

4.1.2.1 Gene ontology analysis of similarly changed RNA transcripts and proteins in APP-KI microglia

After identifying 90 similarly regulated RNA transcripts and proteins, I next sought to re-analyze the biological processes and molecular mechanisms previously analyzed for significantly changed RNA transcripts only (Fig. 17).

GSEA for biological processes and molecular mechanisms of shared upregulated transcripts and proteins revealed that cellular growth, inflammatory- and wound healing-related processes were significantly enriched (Fig. 19 a, b). However, transport, cell activity and growth were also simultaneously negatively influenced among the upregulated processes. In contrast to the previous analysis, neuron death was no longer part of the upregulated biological processes. Interestingly, those mechanisms point to a more regenerative phenotype. Processes were mainly associated with the external membrane and lytic vacuoles but to a lesser extent to secretory vesicles compared to the previous analysis (Fig. 19 c).

Negatively affected processes were found to entail mechanisms such as cell adhesion, actin filament organization, cellular transport, carboxylic ester hydrolase and lipase activity (Fig. 19 a, b), pointing to disturbances in motility, phagocytosis and processing. Those processes were found to be highly enriched in endosomes and the actin cytoskeleton (Fig. 19 c). For the downregulated processes, impairments in microglial phagocytosis and processing were further strengthened.

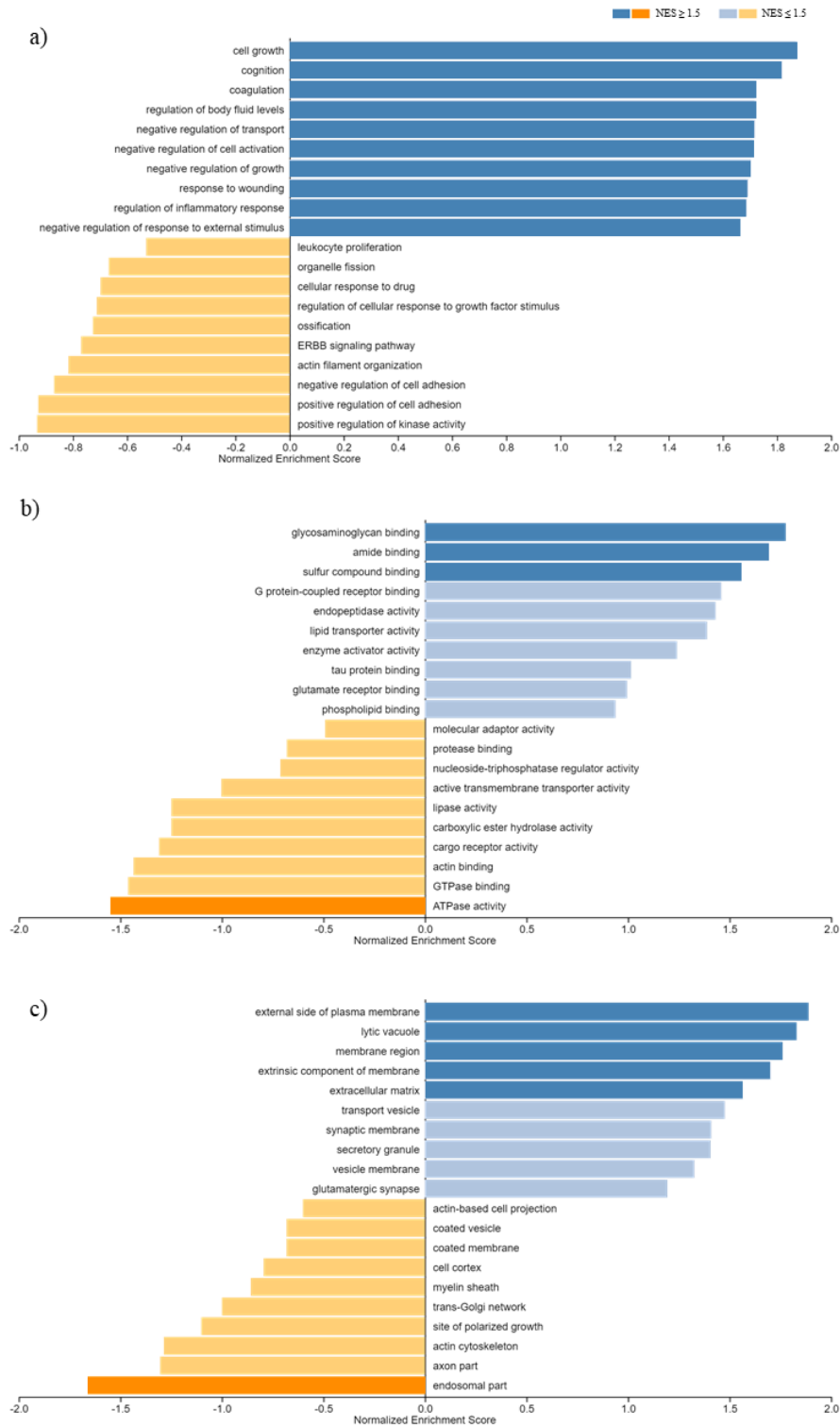


Figure 19: Gene ontology enrichment analysis for similarly regulated RNA transcripts and proteins in 12 mo APPki microglia.

Bar plots depict the normalized enrichment for (A) biological processes, (B) molecular mechanisms and (C) cellular compartments for similarly regulated RNA transcripts and proteins in 12 mo APP^{NL-G-F} microglia. Processes with a normalized enrichment score (NES) > 1.5 (depicted in darkened colors) were deemed highly significant.

4.1.2.2 AD risk factors are significantly changed on the RNA and protein level of APP-KI microglia

I identified several known common LOAD risk factors to be significantly changed ($p_{adj.} < 0.05$) on both RNA and protein level of aged APP^{NL-G-F} microglia (table 4.2). Interestingly, transcripts and corresponding proteins were similarly up- or downregulated. ApoE and especially Trem2 were exceedingly upregulated (385 - 1500 %), while Bin1, Abi3 and Clu were found to be highly downregulated (40 - 60 %).

Fold change 12 mo APP ^{NL-G-F} vs. WT		
Gene/Protein	RNAseq	Proteomics
Abi3	0.62	0.53
ApoE	8.25	15.03
Bin1	0.57	0.59
Clu	0.39	0.72
Trem2	3.40	3.85

Table 4.2: AD risk genes are significantly ($p_{adj.} < 0.05$) changed on the RNA and protein level of 12 mo APP^{NL-G-F} mice compared to age-matched controls.

4.1.3 Synaptic proteins within AD microglia

4.1.3.1 Synaptic proteins can be found within microglia proteomic data sets and increase as AD progresses

Despite not being inherently expressed by microglia, I identified several synaptic proteins within APP^{NL-G-F} microglia. In their publication, Sébastien-Monador and colleagues MACS-isolated primary microglia from the cerebrum of APP^{NL-G-F} and corresponding WT controls and performed mass-spectrometry based proteomics [224]. To recapitulate AD disease progression in this mouse model, microglia were isolated from 1 mo (pre-disposition stage), 3 mo, 6 mo and 12 mo animals (early, middle and advanced stage). Interestingly, synaptic proteins were significantly decreased in early stage AD microglia and became enriched ($p_{adj.} < 0.05$) starting from 6 mo of age [224]. To verify the neuronal origin of the detected proteins, I examined their respective expression profiles through accessible scRNAseq data (table 4.3) [206]. Moreover, the proteomic data set contained synaptic proteins found on both pre- and post-synapses (table 4.3).

Gene	Protein	main cell type	MG
<i>Aldh1b1</i>	Aldehyde dehydrogenase X	N, OPC, olig	very low
<i>Gpm6a</i>	Neuronal membrane glycoprotein M6-a	astro, N, OPC	none
<i>Homer1</i>	Homer protein homolog 1	N, astro, OPC	very low
<i>Hpca</i>	Neuron-specific Ca-binding protein hippocalcin	N	low
<i>Mgst3</i>	Microsomal glutathione S-transferase 3	N, olig, endo	low
<i>Myo5a</i>	Unconventional myosin-Va	N, OPC, olig	very low
<i>Ncan</i>	Neurocan core protein	Astro, N, OPC	none
<i>Nfasc</i>	Neurofascin	olig, N	none
<i>Pacsin1</i>	PKC and casein kinase substrate in neurons 1	N	low
<i>Rap2b</i>	Ras-related protein Rap-2b	astro, N, OPC	low
<i>Scg5</i>	Neuroendocrine protein 7B2	N, OPC	none
<i>Sv2a</i>	Synaptic vesicle glycoprotein 2A	N, olig	very low
<i>Sv2b</i>	Synaptic vesicle glycoprotein 2B	N	none
<i>Syngap1</i>	Ras/Rap GTPase-activating protein SynGAP	N, astro, olig	low
<i>Syng3</i>	Synaptogyrin-3	N, OPC	none
<i>Synpr</i>	Synaptopodin	N	none
<i>Syp</i>	Synaptophysin	N	very low
<i>Syt1</i>	Synaptotagmin-1	N	none
<i>Tmem163</i>	Transmembrane protein 163	N, OPC, olig	none
<i>Vat1</i>	Synaptic vesicle membrane protein VAT-1 homolog	N, olig, endo	low
<i>Xpo5</i>	Exportin-5	astro, N, OPC	low

Table 4.3: List of synaptic proteins enriched in microglia from APP^{NL-G-F} mice.

Listed are proteins that were significantly enriched ($p_{adj.} < 0.05$) in isolated microglia from 6 mo and/or 12 mo APP^{NL-G-F} mice. Proteins highlighted in blue are predominantly pre-synaptic and proteins highlighted in yellow are predominantly post-synaptic. N = neurons, astro = astrocytes, olig = oligodendrocytes, OPC = oligodendrocyte precursor cells.

4.1.3.2 Validation of candidate synaptic proteins in free-floating sections

To further validate the proteomic detection of distinct synaptic proteins within microglia, I performed stainings in free-floating sections of the hippocampal CA1 region of 6 mo and 12 mo APP^{NL-G-F} and C57Bl/6J mice. To this end, I imaged the CD68-positive lysosomal compartment of single microglia (Iba1), and quantified the amount of synaptic proteins within lysosomes (CD68). As surrogate synaptic proteins I chose Homer1, Synaptogyrin 3 (Syng3) and Synaptophysin (Syp) since high protein levels could already be detected in microglia from 6 mo APP^{NL-G-F} animals (table 4.4) [224]. Interestingly, at 3 mo of age, a significant decrease of synaptic proteins could be detected in APP^{NL-G-F} microglia compared to C57Bl/6J (except for Homer1) (table 4.4). Validation of this important early stage AD group is still ongoing.

	protein fold-change		
	3 mo	6 mo	12 mo
Homer1	0.92 _(n.s.)	1.44	3.25
Syngn3	0.36	2.51	2.20
Syp	0.52	1.54	2.39

Table 4.4: Protein fold-change of candidate synaptic proteins within APP^{NL-G-F} microglia.

In accordance with the proteomic data, I detected a significant enrichment of the synaptic proteins Homer1, Synaptogyrin3 and Synaptophysin in single microglia from 6 and 12 mo APP^{NL-G-F} mice, compared to age-matched C57Bl/6J controls (Fig. 20). Importantly, I affirmed their localization to the CD68-positive lysosomal compartment (Fig. 20 a-c). For Homer1, a significant ($p_{adj.} = 0.001$ and 0.038) FC of 1.89 and $2.59 \pm SD$ could be detected for 6 and 12 mo animals, respectively (Fig. 20 a). Similarly, Synaptogyrin3 was found to be significantly changed ($p_{adj.} = 0.016$ and 0.017) with FCs of 2.65 and $3.23 \pm SD$ for 6 and 12 mo animals, respectively (Fig. 20 b). Finally, lysosomal levels of Synaptophysin were detected to be significantly different ($p_{adj.} = 0.032$ and 0.009) with FCs of 2.11 and $2.96 \pm SD$ between 6 and 12 mo tg and WT animals, respectively (Fig. 20 c).

In line with the current literature [314], I detected a significant increase of CD68-positive lysosomes in single APP^{NL-G-F} microglia from 6 mo animals ($p_{adj.} = 0.005$, FC $1.85 \pm SD$) that further increased in 12 mo animals ($p_{adj.} = 0.001$, FC $3.30 \pm SD$) (Fig. 21 a). When performing linear regression analysis for 6 mo and 12 mo animals, I could positively correlate CD68 and the total synaptic area within lysosomes of microglia (6 mo: $R^2 = 0.416$, $p = 0.0001$; 12 mo: $R^2 = 0.68$, $p = 0.0001$) (Fig. 21 c,d). Interestingly, the occupied area in lysosomes did not increase respective to its size when comparing WT and tg animals of both age cohorts (Fig. 21 b). In fact, although not significant, I observed a trend towards a decreased occupancy of lysosomes from 6 and 12 mo APP^{NL-G-F} microglia compared to controls (FC = 0.94 and 0.91 , respectively) (Fig. 21 b). In order to investigate the potential correlation between CD68 of single microglia and its relative occupancy, I performed linear regression analysis. Strikingly, I found a significant negative correlation between both factors in 6 mo animals ($R^2 = 0.025$, $p = 0.045$), which became more distinct in 12 mo animals ($R^2 = 0.093$, $p = 0.0001$) (Fig. 21 c,d).

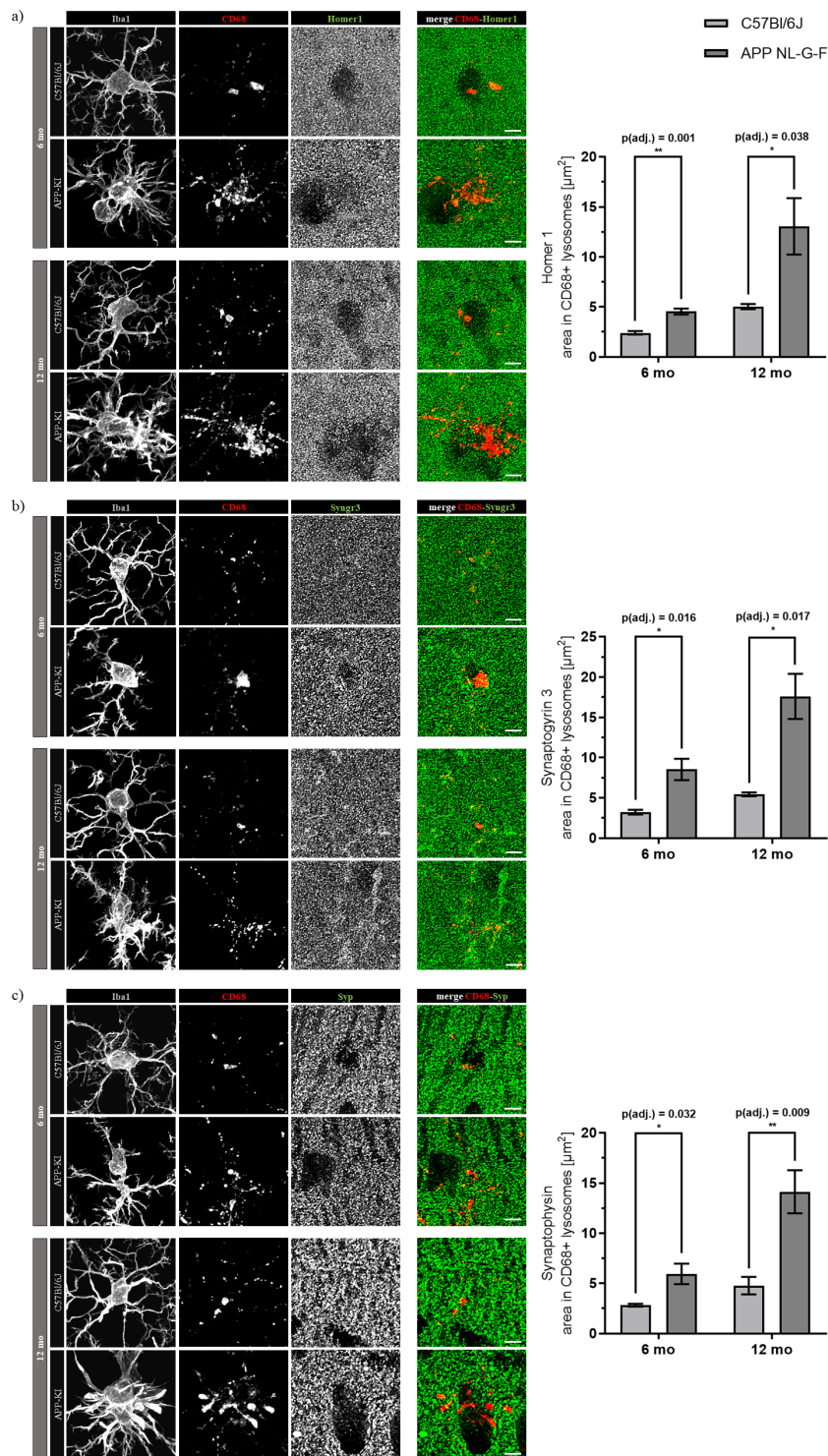


Figure 20: Synaptic proteins are significantly enriched in lysosomes of 6 and 12 mo APP^{NL-G-F} microglia.

Immunohistochemical analysis of single microglia from 6 and 12 mo C57Bl/6J (light grey) and APP^{NL-G-F} (dark grey) microglia in the hippocampal CA1 region. Depicted are representative pictures and quantification from the analysis of Homer1 (A), Synaptogyrin3 (B) and Synaptophysin (C). Synaptic proteins (green) were found to be significantly enriched in CD68-positive lysosomes (CD68, red) from 6 and 12 mo APP^{NL-G-F} microglia (Iba1, grey). Images were acquired with a 63x oil immersion objective (3x digital zoom). Scale bars represent 5 μm . Values were calculated as the mean (\pm SD) from N=3 animals and three independent triplicats (unpaired two-tailed Student's t-test with Welch's correction)

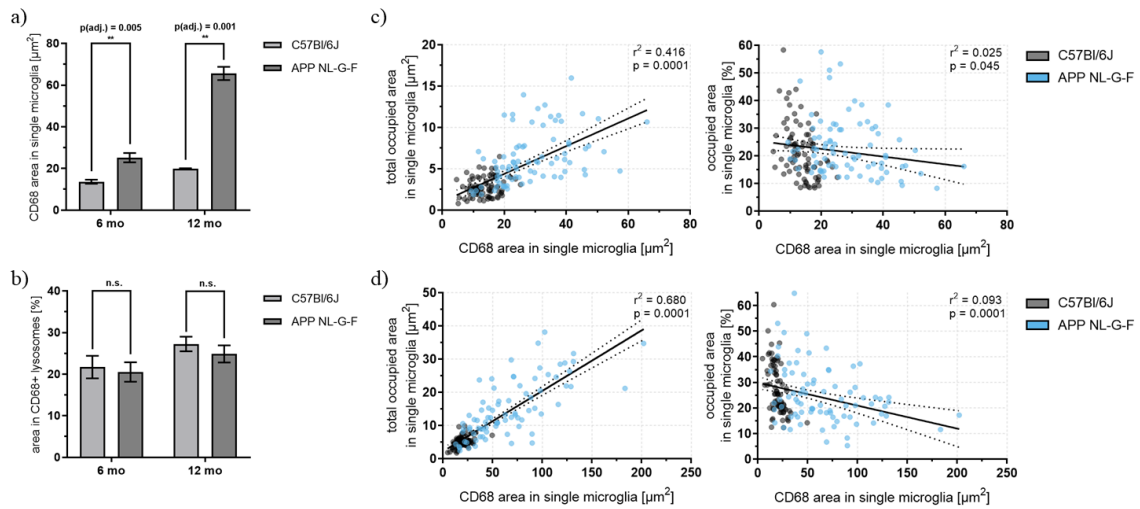


Figure 21: Lysosomal area increases in APP^{NL-G-F} microglia but is less densely occupied. Quantification of CD68-positive lysosomes and their relation to total quantified synaptic proteins and their relative occupancy in single microglia from 6 and 12 mo C57Bl/6J and APP^{NL-G-F} microglia. **(A)** CD68 is significantly increased in single microglia from 6 and 12 mo APP^{NL-G-F} animals. **(B)** No significant changes can be observed when comparing the relative occupancy (in %) of lysosomes within both age cohorts. **(C)** In 6 mo animals, a positive correlation can be observed when performing linear regression analysis for CD68 and its respective protein load. Simultaneously, CD68 and its relative protein load (% occupancy) are negatively correlated. Similar but more pronounced effects can be observed in single microglia from 12 mo animals **(D)**. Values for **(A)** and **(B)** were calculated as the mean (\pm SD) from N=3 animals (unpaired two-tailed Student's t-test with Welch's correction). Data for **(C)** and **(D)** was collected from N=3 animals and three independent triplicates. Black dots represent single microglia from C57Bl/6J while blue dots represent single microglia from APP^{NL-G-F} mice. Dotted lines represent the 95 % confidence interval of the calculated best-fit line.

4.2 Homeostatic functions of *BIN1* in microglia

The second main aim of my thesis centered around the characterization of the homeostatic functions of *BIN1* in microglia. Recently, common *BIN1* risk variants were identified to be functionally linked to *BIN* expression in microglia [103, 147]. Moreover, the downregulation of *BIN1* in microglia during AD was shown to be detrimental for disease progression [103]. Importantly, I found *BIN1* to be downregulated in microglia isolated from APP^{NL-G-F} mice on both RNA and protein level (section 4.1.2.2). Although many compelling functions have been proposed for *BIN1* in microglia (*e.g.* regulation of phagocytosis, lysosomal processing, trafficking) [150, 279], they have not been investigated yet. To address this issue, I designed a novel AAV-construct driving *BIN1* overexpression in microglia and analyzed the effects *in vitro* in primary mouse microglia and *in vivo* after stereotactic injection into WT mice.

4.2.1 *BIN1* downregulation in the context of AD is recapitulated in free-floating sections of APP-KI mice

To further validate the downregulation of *BIN1* in microglia previously observed on RNA- and protein-levels (table 4.2), I analyzed the total and microglia-specific *BIN1* signal in free-floating sections from the hippocampal CA region of 12 mo APP^{NL-G-F} and C57Bl/6J mice. Based on the well-described impairment of the hippocampus in AD [315], its inclusion in both RNAseq and proteome data sets and my earlier analysis of the CA1 region (section 4.1.3.2), I chose hippocampal CA1 as region of interest. Fitting to previous observations, I found the total as well as the microglia-specific *BIN1* to be significantly downregulated ($FC_{total} = 0.34 \pm SD$, $p_{adj.,total} = 0.0015$; $FC_{microglia} = 0.39 \pm SD$, $p_{adj.,microglia} = 0.0072$) (Fig. 22 a-c). In accordance with multiple studies (for review see [316]), I found *Iba1* as microglia marker to be significantly upregulated in this AD mouse model ($FC = 1.21 \pm SD$, $p_{adj.} = 0.011$) (Fig. 22 d).

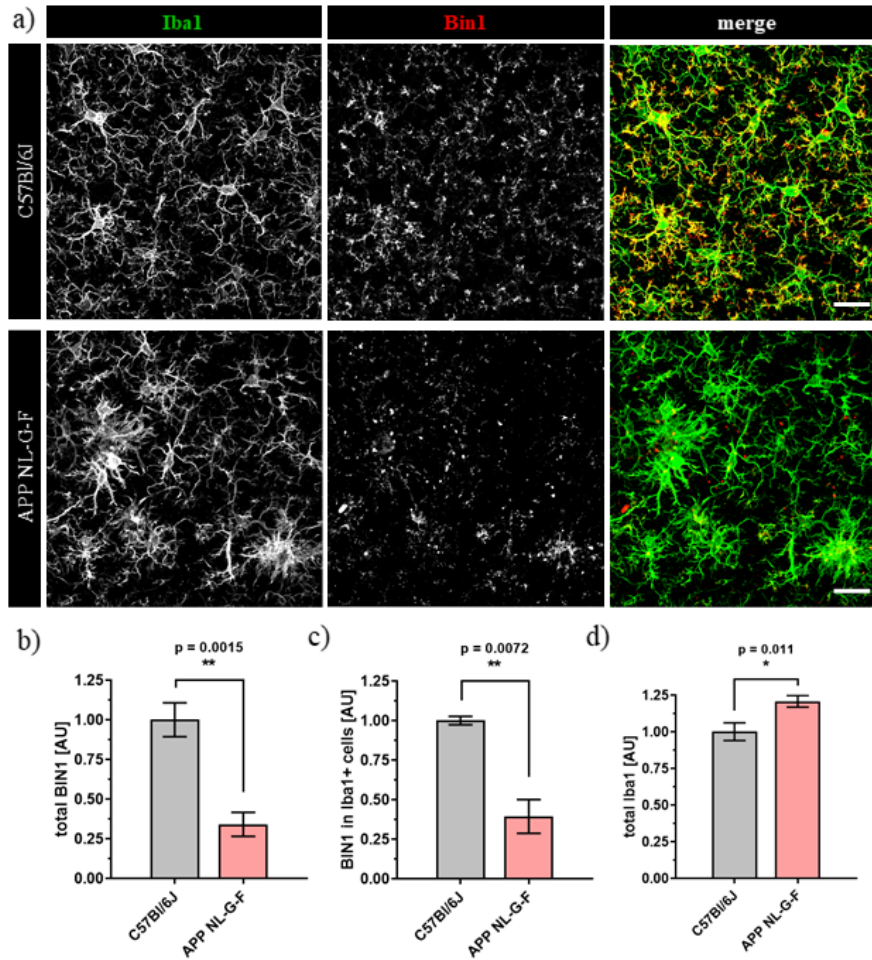


Figure 22: BIN1 is downregulated in microglia from 12 mo APP^{NL-G-F} mice. (A) Representative images of the hippocampal CA1 region of 12 mo APP^{NL-G-F} and C57Bl/6J mice stained for Iba1 (green) and Bin1 (red). Scale bars represent 20 μm. Quantitative analysis of Iba1 (B), total (C) and microglia-specific BIN1 (D). Values represent the normalized covered area calculated as the mean (±SD) from N=3 animals and three independent experiments (unpaired two-tailed Student's t-test with Welch's correction)

4.2.2 AAV vector design targeting BIN1 overexpression

Microglia are known to be notoriously difficult to transduce due to their highly efficient macrophage function (section 1.3.2.1.2). Nevertheless, an increasing number of new papers with promising techniques are being published. For microglial overexpression of *BIN1*, I designed a custom-made vector based on the publication from Rosario and colleagues [306]. The construct AAV/TM6-F4/80-mBin1-2A-mCherry (AAV_{Bin1}) (Fig. 23) was built to specifically overexpress mouse *BIN1* isoform 2 (mBin1), which is the main isoform ex-

pressed by microglia [279]. Sequence accuracy of the transgene was verified using the NCBI FASTA sequence alignment tool. The capsid optimized AAV6 serotype with its triple mutated 5' intron (Y731F/Y705F/T492V) was chosen due to its high tropism for monocytes, which is achieved by increasing the transduction efficiency and simultaneously limiting proteasomal degradation [306]. Transgene expression was controlled by the microglia-specific F4/80 promoter. Microglial specificity of F4/80 was confirmed with on-line scRNAseq tools (*e.g.* brainrnaseq.org). In contrast to other available microglia-specific promoters (*i.e.* CD68), F4/80 expression remains more stable throughout microglia activation processes. To verify transduction accuracy and efficiency in later experiments, the fluorescent reporter mCherry was added to the construct. Transgene and reporter were separated by a 2A self-cleaving peptide, to ensure physiological distribution of BIN1. For control experiments, the construct AAV/TM6-F4/80-mCherry (AAV_{ctr}) was built.

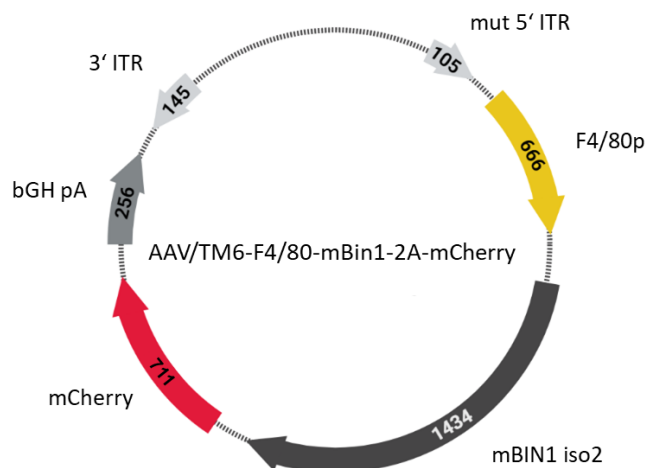


Figure 23: BIN1 overexpression AAV construct.

Schematic representation of the mBIN1 overexpression construct. Displayed are the mutated 5' intron (Y731F/Y705F/T492V), the microglia-specific F4/80 promoter, the gene insert mBIN1_{iso2}, the fluorescent reporter mCherry, the bovine growth hormone poly-A element and the closing 3' intron region. Numbers inside the respective construct element represent base pairs.

4.2.3 *BIN1* overexpression *in vitro*

To ascertain viral transduction efficiency and evaluate the impact of *BIN1* overexpression, I transfected cultured primary microglia isolated from C57Bl/6J pups using MACS technology. In contrast to *in vivo* experiments, this convenient model grants easier accessibility

while simultaneously providing a more genuine microglial behavior compared to immortalized cell lines (*e.g.* BV2) [317]. After establishing a well-functioning primary microglia isolation and culture protocol, cells were transfected for 5 days with AAV_{Bin1} or AAV_{ctr} and subsequently analyzed for stable expression of the construct, changes in endolysosomal markers and their innate phagocytic capacity.

4.2.3.1 Establishing primary mouse microglia culture

Prior to my planned *in vitro* experiments it was necessary to set up a primary microglia isolation and culture protocol. Although well-suited for downstream RNAseq analysis, several adjustments had to be made to the previously established protocol for isolation of primary microglia. Main changes included performing all steps at room temperature in contrast to on ice, using Papain (*papaya latex*, buffered aqueous solution, 200 U) instead of pre-made enzyme kits and performing manual brain tissue dissociation using fire-polished glass pipettes instead of the GentleMACS system (for details see Materials and Methods). Positive selection of microglia was equivalently performed using CD11b microbeads and MACS. While the previous protocol was aimed at preserving RNA integrity and a fast microglia isolation, the culture of primary cells required a more gentle approach. To ensure proper surface attachment and recovery of cells, experiments were started on day 4-5 post isolation (DPI), after verification of ramified morphology (Fig. 24).

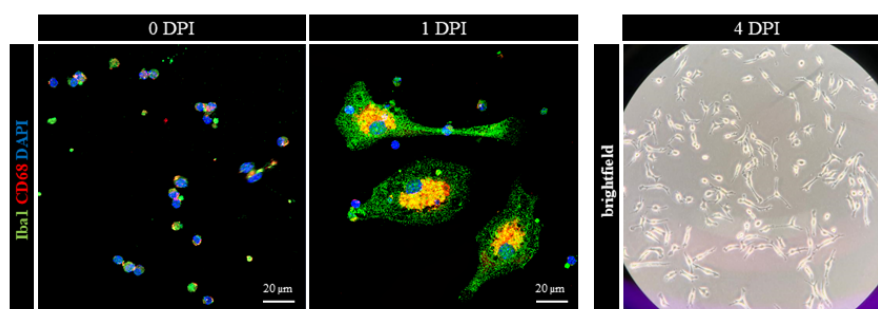


Figure 24: Primary microglia cell culture.

Representative images of cultured, primary microglia isolated with MACS technology. Left and middle panel microglia were stained with Iba1 (green), CD68 (red) and DAPI (blue). Directly after isolation, cells consist mostly of nucleus and cell body (left). At 1 DPI (middle), roughly 50-60 % of all cells are flattened and properly attached to the glass coverslip. At 4 DPI (right), microglia display a mostly ramified morphology, indicative of a homeostatic phenotype. Scale bars represent 20 μm .

4.2.3.2 BIN1 localizes with proteins of the endolysosomal machinery

To initially assess BIN1 distribution and localization in cultured primary microglia, cells were stained with Bin1-antibodies targeting exon 13 of the CLAP-domain or specific amino acid sequences of the N-BAR-domain (see Fig. 11). BIN1 in microglia was found to be expressed in a punctate staining pattern with mostly small dots, irregular larger dots and seldom reticulate appearance around the nucleus, resembling mitochondria. Based on the observed vesicle-like staining pattern in microglia and the experimentally verified involvement of neuronal BIN1 in endocytic trafficking and processing [288, 289, 291, 292], I stained for several microglial proteins known to be involved in these processes. Here, I compared their staining pattern with one of the two microglia-specific Bin1-antibodies mentioned above and looked for a potential overlap that could be indicative of a shared reactive compartment or a direct interaction (Fig. 25).

Reorganization of the actin cytoskeleton is necessary for cellular uptake of fluids and particles during microglial phagocytosis (see Fig. 8), but also cell motility [318]. Interestingly, neuronal BIN1 was shown to directly interact with β -actin through its BAR domain and to participate in its remodeling [291, 292]. Here, I found a noticeable overlap between the two signals, indicative of a comparable BIN1 function in microglia (Fig. 25a). Moreover, BIN1 was found to partially co-localize with CD2AP (Fig. 25b), a scaffolding protein that is involved in actin remodeling and a known AD risk factor [103, 319]. I further stained for early-endosome antigen 1 (EEA1) and Rab5, who both localize primarily to early endosomes [320, 321]. Interestingly, they were previously shown to co-localize with neuronal BIN1 and to react to changes in BIN1 levels [288]. Both stainings yielded a partial overlap with microglial BIN1 (Fig. 25 c,d). Lastly, to assess if microglial BIN1 could also be involved in lysosomal processing, I stained for CD68 and found a prominent overlap between the two signals (Fig. 25e).

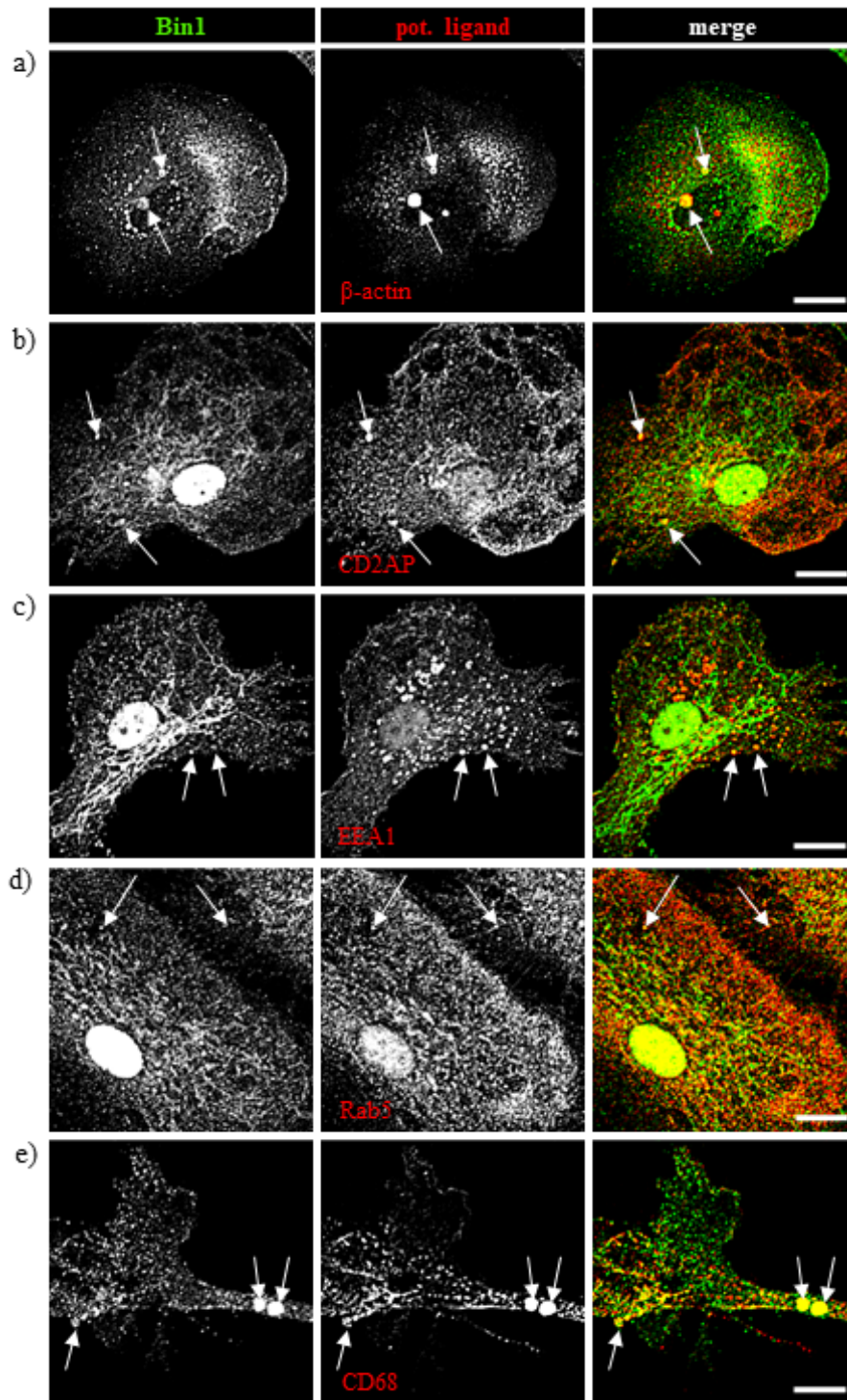


Figure 25: Potential ligands and interaction partners of BIN1.

Representative images of cultured primary microglia stained for BIN1 (green) and potential ligands and interaction partners (red) of BIN1 based on the current literature. Depicted are β -actin (A), CD2AP (B), EEA1 (C), Rab5 (D) and CD68 (E). Due to conflicting host species, different Bin1-antibodies had to be used in this figure. Rows (A),(E) were stained with Bin1-antibody [2F11] and rows (B)-(D) with Bin1-antibody [99D], which additionally stains BIN1 located in the nucleus of microglia cells. Scale bars represent 10 μ m.

4.2.3.3 AAV-treatment is innocuous and leads to broad mCherry expression

To determine the infectious potential of AAV_{Bin1} on cultured primary microglia, I performed dilutions with different multiplicity of infection (MOI). The MOI is the ratio of the amount of viral particles to the number of targeted cells when referring to a given quantity of cells inoculated with viral particles. Establishing an appropriate MOI can be challenging, as it highly depends on the used AAV serotype, construct size and targeted cell type. Typical MOI ranges for AAV constructs are mostly between 2000 - 50.000, sometimes even 500.000 (source: VectorBiolabs). The above mentioned formula can be rearranged to describe the number of needed AAV genome copy (GC) particles from a given titer:

$$AAV\ GC\ particles = MOI \times number\ of\ targeted\ cells$$

However, toxic side effects of higher MOIs have to be assessed carefully to avoid cell death. Based on the current literature I applied AAV_{Bin1} concentrations that translated to MOIs of 1000, 3000, 10.000 and 30.000. Viral transduction was carried out for 5 consecutive days in a humidified incubator based on the publication from Rosario and colleagues, who designed and tested the capsid-optimized AAV/TM6-F4/80 serotype-promoter construct [306]. I observed apparent cell death in a concentration-dependent manner for the MOIs 10.000 and 30.000. Compared to MOI 3000, MOI 1000 did not yield sufficient mCherry signal after 5 days and was therefore discarded. To further refine the MOI, I applied AAV_{Bin1} starting from MOI 2000 to 4000 in steps of 500. The MOIs 2000-3500 gave comparable results regarding viability and mCherry signal intensity. Finally, I settled for an MOI of 2500 for all following experiments (biological replicats from single animals \pm AAV) (Fig. 26). Previous studies aiming at viral microglia transduction often describe a rapid proteasomal degradation of the construct once it escapes the endosomal compartment [306, 322, 323, 324]. To gain insight into localization of the exogenous mCherry after transduction, I performed stainings for CD68, targeting the lysosomal compartment of microglia. After 5 days of AAV_{Bin1} treatment, mCherry was mainly localized to the membrane and cytosol of microglia and only to a neglectable extent in lysosomes (Fig. 26). Thus, indicating a successful transduction after 5 days.

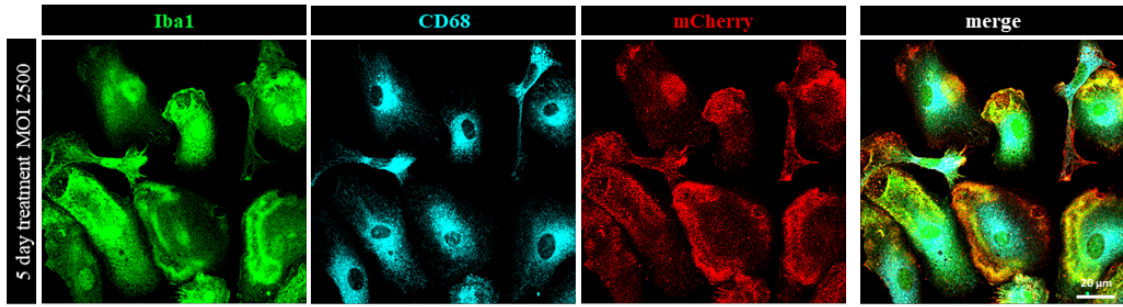


Figure 26: mCherry is abundantly expressed in transfected primary microglia.

Representative images of cultured primary microglia transfected for 5 days with an MOI of 2500. Cells were stained for Iba1 (green), CD68 (cyan) and mCherry (red). After 5 days of treatment with AAV_{Bin1}, mCherry was mostly found at the membrane and in the cytosol but not in the lysosomal compartment of cells. Scale bars represent 20 µm.

4.2.3.4 *BIN1* overexpression enhances phagocytosis-associated markers and leads to morphological changes

To assess BIN1 overexpression magnitude and potential downstream effects, I quantified BIN1 and potential downstream effectors. I found that after 5 days of AAV_{Bin1} treatment, BIN1 was markedly increased approx. 2.2-fold (\pm SD, $p_{adj.} = 0.0341$) compared to untreated controls (*i.e.* biological replicates) from the same animal (Fig. 27 a,b). CD68 increased approx. 1.5-fold (\pm SD, $p_{adj.} = 0.0002$) and β -actin 1.3-fold (\pm SD, $p_{adj.} = 0.0053$) (Fig. 27 a,c,d). I additionally quantified lysosomal-associated membrane protein 1 (Lamp1) in treated vs. untreated cells to exclude that observed changes in the lysosomal compartment (CD68) are due to potential virus-triggered activation of microglia. I found Lamp1 to be increased approx. 1.4-fold (\pm SD, $p_{adj.} = 0.0158$) (Fig. 27 e,f), which is slightly less than the fold-change observed for CD68.

Additionally, I noticed morphological changes in microglia transfected with AAV_{Bin1}. Cells were overall more roundish in appearance and displayed to a lesser extent the distinct polarized shape with filopodia extending from the cell body (Fig. 27 a,f), which could be indicative of a more active phenotype [318]. Interestingly, similar morphological changes were not observed when performing experiments with AAV_{ctr} (section 4.2.3.7).

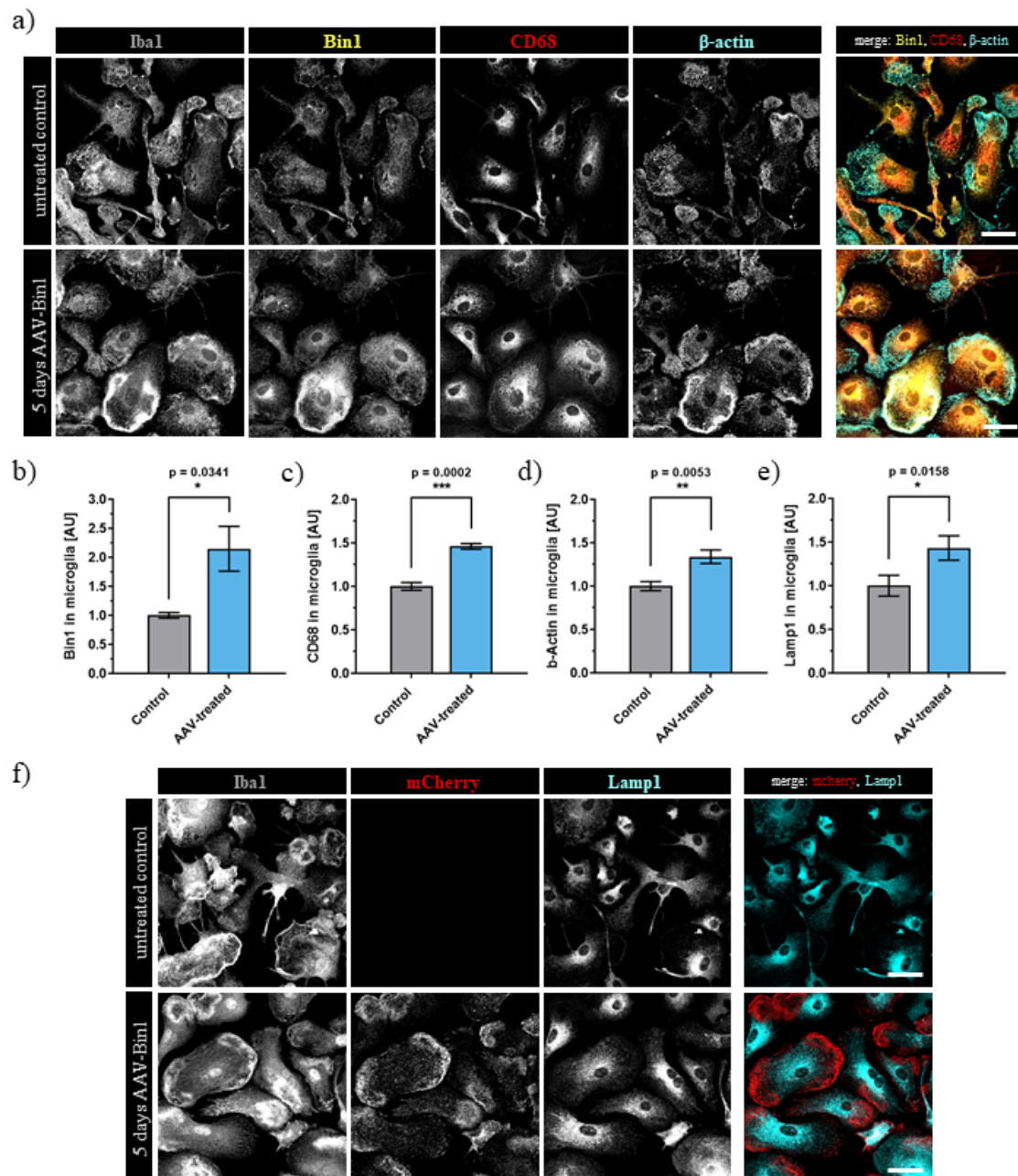


Figure 27: Bin1 overexpression leads to changes in endolysosomal-associated markers and morphology.

Representative images of cultured primary microglia \pm transfected for 5 days with AAV_{Bin1}. (A) Cells were stained for Iba1 (grey), Bin1 (yellow), CD68 (red) and β -actin (cyan). In the bottom panel (F), cells were stained for Iba (grey), mCherry (red) and Lamp1 (cyan). (B)-(E) After 5 days of treatment with AAV_{Bin1}, BIN1, CD68, β -actin and Lamp1 are significantly upregulated. Values represent the Iba1-normalized covered area calculated as the mean (\pm SD) from N=3 experiments and two biological replicates each (unpaired two-tailed Student's t-test with Welch's correction). Scale bars represent 20 μ m.

4.2.3.5 Bin1 signal increases during phagocytosis

Given the previously observed localization of BIN1 with proteins of the endolysosomal machinery (section 4.2.3.2) and the direct influence of *BIN1* overexpression on phagocytosis-associated markers (section 4.2.3.4), I next analyzed whether BIN1 levels are subject to changes during phagocytosis. Prior to those experiments, I examined whether the phagocytic behavior of isolated primary mouse microglia could be classified as "normal". For this, I used the well-established paradigm of phagocytosis inhibition through Cytochalasin D (CytoD), a potent actin-polymerization inhibitor that efficiently blocks microglia movement and the formation of membrane ruffles. CytoD was applied prior to challenging the cells with pHrodo Green *E.coli* Bioparticles. As expected, microglia treated with CytoD phagocytosed significantly less *E.coli* particles compared to untreated controls from the same animal (FC $0.14 \pm \text{SD}$, $p_{\text{adj.}} = 0.0025$) (Fig. 28), which is indicative of a healthy microglia behavior. Importantly, I could observe that the pH-sensitive *E.Coli* Bioparticles were indeed strictly localized to CD68-positive acidic lysosomes (Fig. 28).

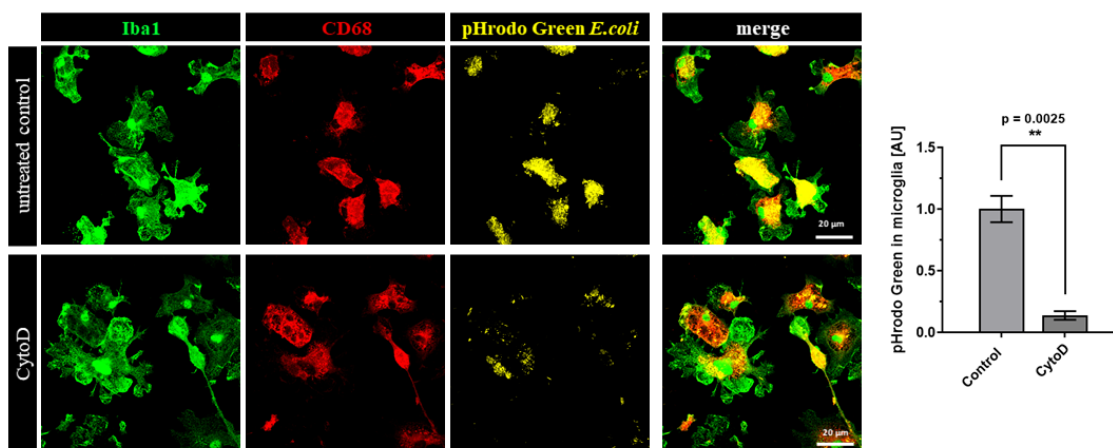


Figure 28: CytoD efficiently decreases phagocytic activity.

Representative images of cultured, primary microglia \pm treated with CytoD prior to performing a phagocytosis assay with pHrodo Green *E.coli* Bioparticles. Cells were stained for Iba1 (green) and CD68 (red). *E.coli* pHrodo Green particles were stimulated with the 488 laser. Scale bars represent 20 μm . Values represent the Iba1-normalized covered area calculated as the mean ($\pm\text{SD}$) from N=3 experiments and two biological replicates each (unpaired two-tailed Student's t-test with Welch's correction)

Subsequently, I explored the possibility of changed BIN1 levels during phagocytosis. To this end, I performed shortened phagocytosis assays (half the time usually required) to

prevent oversaturation of the cells. I found that BIN1 levels were significantly increased when microglia were challenged with *E.coli* particles compared to phagocytic non-active controls from the same animal (FC $1.22 \pm \text{SD}$, $p_{\text{adj.}} = 0.0046$) (Fig. 29), which distinctly implies that microglial BIN1 might take part in phagocytic processes.

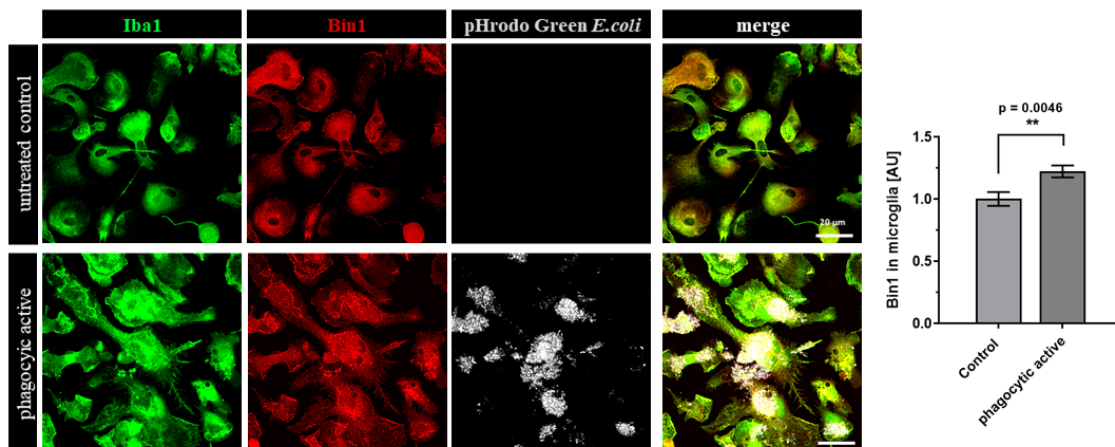


Figure 29: BIN1 expression increases during phagocytic activity.

Representative images of cultured, primary microglia \pm challenged with pHrodo Green *E.coli* Bioparticles. Cells were stained for Iba1 (green) and Bin1 (red). *E.coli* pHrodo Green particles were stimulated with the 488 laser. Scale bars represent 20 μm . Values represent the Iba1-normalized covered area calculated as the mean ($\pm\text{SD}$) from N=3 experiments and two biological replicates each (unpaired two-tailed Student's t-test with Welch's correction)

4.2.3.6 *BIN1* overexpression enhances microglia phagocytosis

Based on the previously observed upregulation of *BIN1* during microglial phagocytosis, I next considered the probability of *BIN1* upregulation leading to an enhanced phagocytic capacity of microglial cells. For this, I transfected primary microglia with AAV_{Bin1} for 5 consecutive days. At the 5th day, I performed phagocytosis assays with pHrodo Green *E.coli* Bioparticles and found that microglia transfected with AAV_{Bin1} phagocytosed significantly more Bioparticles compared to untreated controls from the same animal (FC $1.46 \pm \text{SD}$, $p_{\text{adj.}} = 0.0134$) (Fig. 30), hinting at an improved phagocytic capability due to BIN1 overexpression.

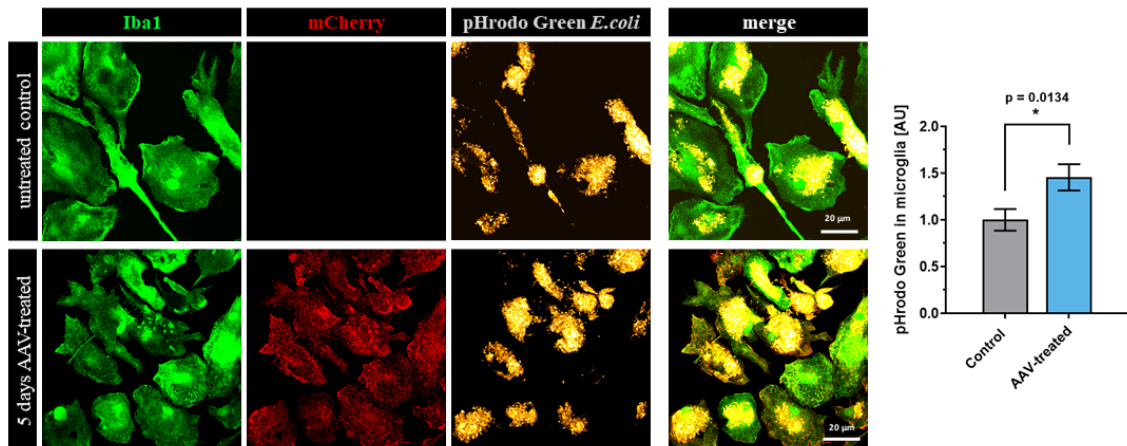


Figure 30: BIN1 overexpression enhances microglia phagocytosis.

Representative images of cultured primary microglia \pm transfected for 5 days with AAV_{Bin1} and after performing a phagocytosis assay with pHrodo Green *E. coli* Bioparticles. Cells were stained for Iba1 (green) and mCherry (red). *E. coli* pHrodo Green particles were stimulated with the 488 laser. Scale bars represent 20 μ m. Values represent the Iba1-normalized covered area calculated as the mean (\pm SD) from N=3 experiments and two biological replicates each (unpaired two-tailed Student's t-test with Welch's correction)

4.2.3.7 Control construct experiments

To exclude the possibility of generating unforeseen immunological side-effects in AAV-transfected microglia, I designed a second vector construct based on the previously described AAV_{Bin1}. The construct AAV/TM6-F4/80-mCherry (AAV_{ctr}) was built to resemble AAV_{Bin1}, with the only genetic difference being that it did not overexpress mBin1 isoform 2.

4.2.3.7.1 AAV_{ctr}-treatment is innocuous and leads to broad mCherry expression

To facilitate a valid comparison between both constructs described in this study, I used the earlier established MOI of 2500 for microglia transductions with AAV_{ctr}. That way, I accounted for the difference in GC/ml concentration between batches. Correspondingly, cells were transfected for 5 consecutive days in a humidified incubator. Likewise to experiments performed with AAV_{Bin1}, transduction of cells with AAV_{ctr} led to an abundant expression of mCherry with the signal being located mostly at the membrane and cytosol of microglia and only to a small extent in the lysosomal compartment (Fig. 31).

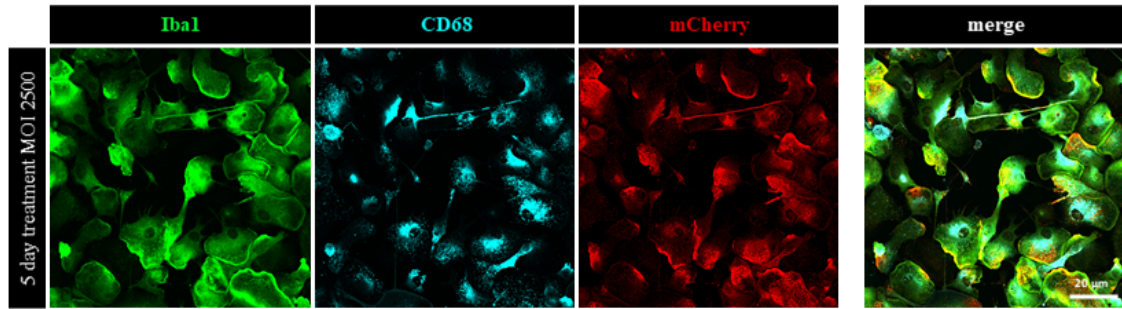


Figure 31: mcherry is abundantly expressed in AAV_{ctr} transfected microglia.

Representative images of cultured primary microglia transfected for 5 days with an MOI of 2500. Cells were stained for Iba1 (green), CD68 (cyan) and mCherry (red). After 5 days of treatment with AAV_{ctr}, mCherry is mostly found at the membrane and in the cytosol but not in the lysosomal compartment of cells. Scale bars represent 20 μm .

4.2.3.7.2 AAV_{ctr}-treatment does not enhance phagocytosis associated markers and does not change morphology

Similar to the experiments performed with AAV_{Bin1}, I quantified BIN1 and potentially associated proteins of the endolysosomal machinery (CD68, β -actin and Lamp1) after 5 day-treatment with AAV_{ctr}. In contrast to earlier experiments performed with AAV_{Bin1} (section 4.2.3.4), I found that microglia transfected with AAV_{ctr} did not upregulate BIN1 or any of the analyzed potential downstream effectors (Fig. 32 a-f).

Moreover, microglia transfected with AAV_{ctr} did not appear to display morphological changes compared to untreated cells from the same animal. The overall polarized appearance of cultured primary microglia was unaltered (Fig. 32 a, f), which is likewise in contrast to the experiments performed with AAV_{Bin1} (section 4.2.3.4).

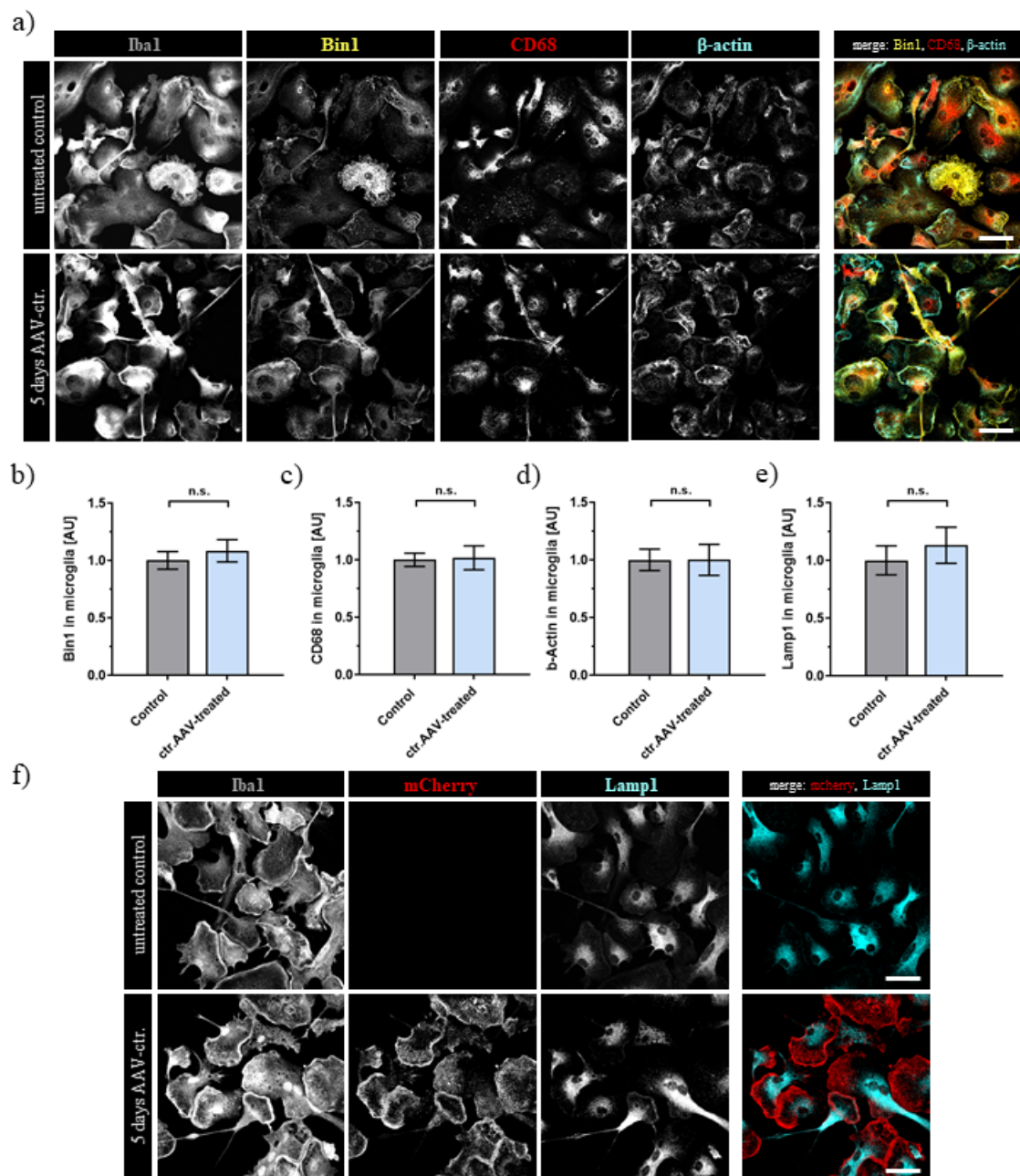


Figure 32: AAV_{ctr} treatment does not lead to changes in endolysosomal-associated markers and morphology.

Representative images of cultured primary microglia \pm transfected for 5 days with AAV_{ctr}. (A) Cells were stained for Iba1 (grey), Bin1 (yellow), CD68 (red) and β -actin (cyan). In the bottom panel (F), cells were stained for Iba (grey), mCherry (red) and Lamp1 (cyan). (B)-(E) After 5 days of treatment with AAV_{ctr}, no changes were observed in the signal intensity of the analyzed stainings. Values represent the Iba1-normalized covered area calculated as the mean (\pm SD) from N=3 experiments and two biological replicates each (unpaired two-tailed Student's t-test with Welch's correction). Scale bars represent 20 μ m.

4.2.3.7.3 AAV_{ctr}-treatment does not increase microglial phagocytic potential

To assess the effect of AAV_{ctr}-transduction on microglial phagocytosis, primary microglia were transfected for 5 consecutive days. At the 5th day, I performed phagocytosis assays with pHrodo Green *E.coli* Bioparticles, similar to experiments performed with AAV_{Bin1} (section 4.2.3.6). However, cells treated with AAV_{ctr} did not appear to phagocytose more Bioparticles compared to untreated controls from the same animal (Fig. 33).

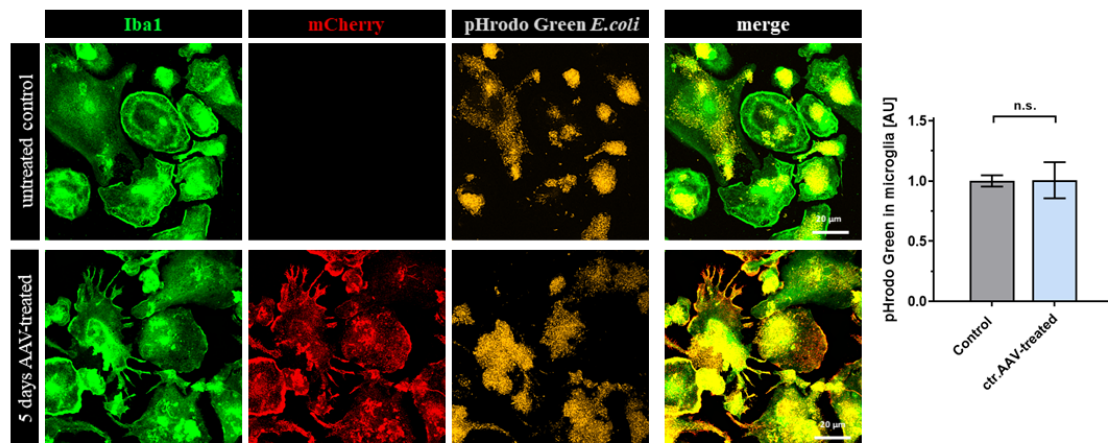


Figure 33: AAV_{ctr} treatment does not enhance microglia phagocytosis.

Representative images of cultured primary microglia \pm transfected for 5 days with AAV_{ctr} and after performing a phagocytosis assay with pHrodo Green *E.coli* Bioparticles. Cells were stained for Iba1 (green) and mCherry (red). *E.coli* pHrodo Green particles were stimulated with the 488 laser. Scale bars represent 20 μ m. Values represent the Iba1-normalized covered area calculated as the mean (\pm SD) from N=3 experiments and two biological replicates each (unpaired two-tailed Student's t-test with Welch's correction)

4.2.4 BIN1 overexpression *in vivo*

Given the promising results from the *in vitro* experiments, I wanted to explore the possibility of targeted microglia *BIN1* overexpression *in vivo*. For that purpose, I injected 3 mo WT animals into the hippocampal CA1 area (Bregma - 1.70 mm) or bilaterally into the lateral ventricles (Bregma - 1.06 mm) with AAV_{Bin1}. Based on the previous literature [306], mice were locally transduced for 30 days with the viral construct and subsequently perfused for further immunohistochemical analysis. Three animals were used per experimental condition and compared to three untreated WT littermates.

I found that mice injected into the lateral ventricles did not present any noticeable mCherry

signal throughout the brain and were therefore discarded from any further analysis (not shown). However, CA1-injected mice displayed consistent phenotypes with respect to virus distribution and localization.

4.2.4.1 *in vivo* distribution and cell specificity of AAV-Bin1

When analyzing CA1-injected mice, I found prominent mCherry signals throughout the CA1 that extended into the CA2 and to a lesser extent the dorsally adjacent somatosensory cortex. Pronounced signal intensity was observed in the oriens and pyramidal cell layer as well as the lacunosum moleculare layer of the hippocampus (Fig. 34 a). When looking at the cellular expression level, it was evident that the strongest mCherry signal derived from a subset of neuronal cell bodies and axons located in the pyramidal cell layer. Importantly, upon closer examination of single cells I could capture mCherry inside microglia (Fig. 34 b), albeit with much lower intensity compared to the mCherry signal captured in neurons and axons.

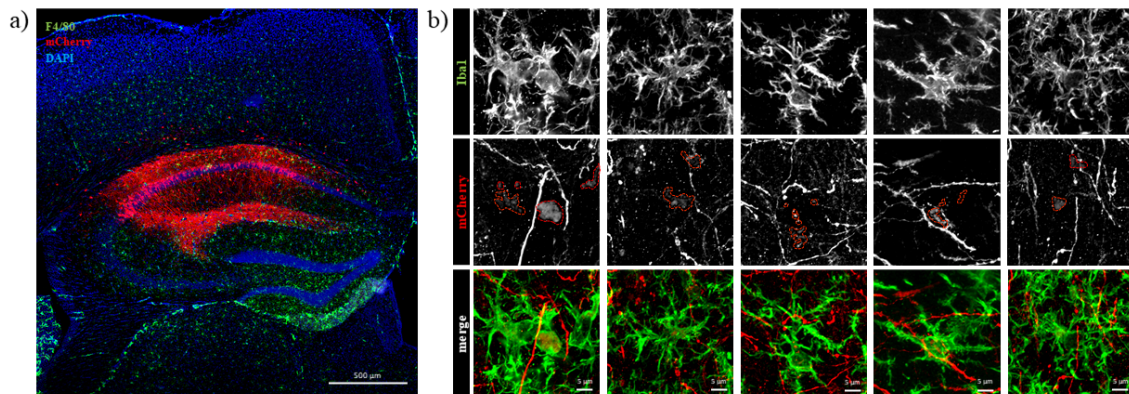


Figure 34: *In vivo* distribution and expression of AAV_{Bin1} after 30 dpi.

(A) Overview image of the cortical and hippocampal area of one hemisphere of a 4 mo WT animal unilaterally injected with AAV_{Bin1}. Animals were sacrificed 30 dpi. Slices were stained for F4/80 (green), mCherry (red) and DAPI (blue). Scale bar represents 500 μm. (B) Closeup images of single microglia in the hippocampal CA1 area of an animal that was injected unilaterally with AAV_{Bin1}. Slices were stained for Iba1 (green), mCherry (red) and DAPI (blue). Scale bars represents 5 μm.

4.2.4.2 Microglia-specific increase of BIN1 and lysosomal marker after AAV-Bin1 inoculation

Interestingly, the majority of mCherry-positive microglia located in the CA1 region exhibited prominent phenotypical changes resembling those of highly activated microglia (*e.g.* in neurodegenerative diseases [7]). Compared to untreated controls, microglia were overall less arborized with shortened but thickened branches extending from the cell body (Fig. 35 a). Comparable results were also obtained *in vitro* (section 4.2.3.4).

Despite the weak mCherry signal observed in microglia from AAV_{Bin1}-transfected animals, I was interested if the observed morphological changes could be due to increases in BIN1 levels. Accordingly, I compared injected mice to untreated WT controls and found that BIN1 was significantly upregulated in those cells (FC 2.42 ± SD, $p_{adj.} = 0.0003$) (Fig. 35 b), which is in line with the previous *in vitro* results (section 4.2.3.4). Moreover, I found that the lysosomal marker CD68 was significantly upregulated in microglia from animals inoculated with AAV_{Bin1} (FC 1.72 ± SD, $p_{adj.} = 0.0025$) (Fig. 35 b). The above described morphological changes were additionally quantified by measuring the Iba1-positive area in single microglia. Matching the observed changes in morphology, the Iba1-positive area was significantly increased in single microglia from AAV-treated animals (FC 1.22 ± SD, $p_{adj.} = 0.0047$) (Fig. 35 b).

Importantly, I noticed that stainings for BIN1 and CD68 overlapped substantially in control and AAV_{Bin1} treated animals (Fig. 35 a), in line with the observation from cultured primary microglia (section 4.2.3.2). Additionally, I could recognize an increase (not quantified) in the amount of small vesicle-like patterns at the distal end of microglia filopodia, which did rarely overlap with CD68 (Fig. 35 a) and might therefore represent an increase in endosomal structures.

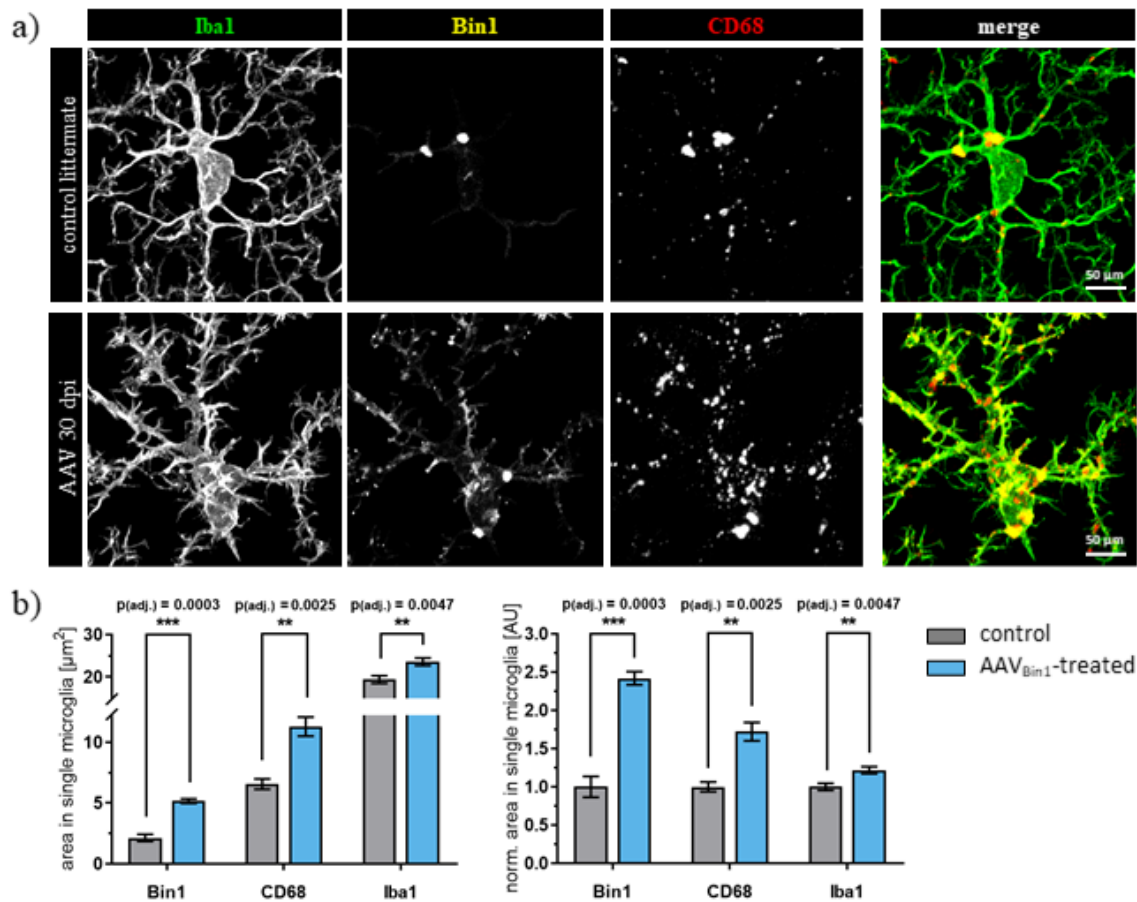


Figure 35: *In vivo* AAV_{Bin1} treatment leads to significant increases of BIN1 and CD68 in microglia.

(A) Representative single microglia images acquired in the hippocampal CA1 region of a 4 mo WT animal ± unilaterally injected with AAV_{Bin1}. Animals were sacrificed 30 dpi. Slices were stained for Iba1 (green), Bin1 (yellow) and CD68 (red). Scale bars represents 50 μm. (B) Quantification for Bin1, CD68 and Iba1 area [μm²] and normalized area [AU] in microglia. AAV_{Bin1} treatment led to significant increases in Bin1, CD68 and Iba1. Values represent the actual and normalized area calculated as the mean (± SD) from N=3 animals and three independent triplicats (unpaired two-tailed Student's t-test with Welch's correction)

Given the prominent mCherry signal in neurons and the well-described expression of a neuron-specific BIN1 isoform (isoform 1) [270], I was interested to see whether BIN1 levels would be changed in pyramidal neurons following AAV_{Bin1} inoculation. Intriguingly, I could not observe significant changes in BIN1 signal intensity in pyramidal cell bodies from mice injected with AAV_{Bin1} (Fig. 36).

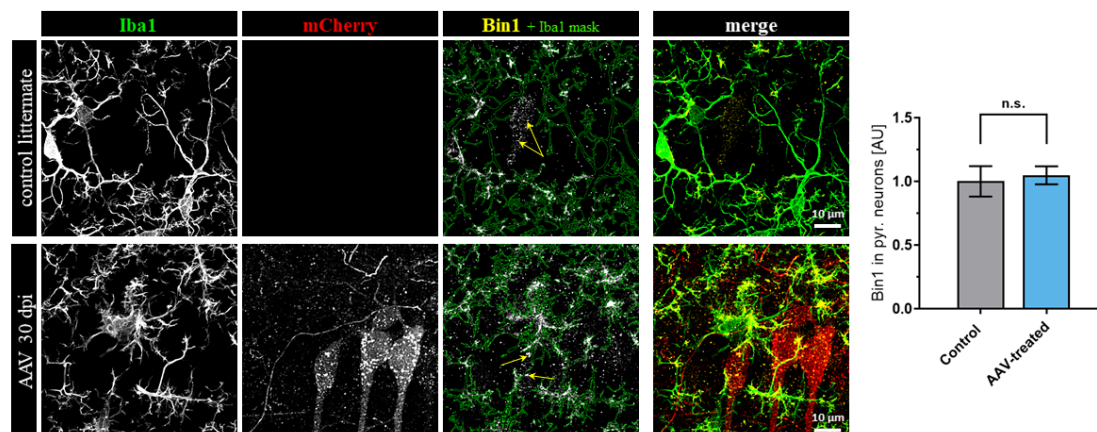


Figure 36: *In vivo* AAV_{Bin1} treatment does not lead to significant increases of BIN1 in pyramidal neurons.

Representative images acquired in the pyramidal cell layer of a 4 mo WT animal \pm unilaterally injected with AAV_{Bin1}. Animals were sacrificed 30 dpi. Slices were stained for Iba1 (green), mCherry (red) and Bin1 (yellow). Scale bars represents 10 μ m. Quantification for Bin1 area in pyramidal neurons. BIN1 localized in microglia was subtracted (see mask overlay) and the remaining signal quantified. AAV_{Bin1} treatment led to no significant increase of BIN1 in pyramidal neurons. Values represent the normalized covered area calculated as the mean (\pm SD) from N=3 animals and three independent triplicats (unpaired two-tailed Student's t-test with Welch's correction)

4.2.4.3 Correlation of BIN1 with CD68

In previous experiments with control and AAV_{Bin1}-treated animals, I could show that BIN1 and CD68 significantly increased in microglia after AAV_{Bin}-treatment and that both stainings overlapped partially in treated but also untreated animals (section 4.2.4.2). To test whether increasing BIN1 and CD68 levels would correlate with each other, I performed a linear regression analysis. For this, I reused images acquired from single microglia in the hippocampal CA1 region from control and AAV_{Bin1}-treated animals. Brain slices were concomitantly stained and analyzed for BIN1 and CD68. That way I could directly assign a matching CD68 value to BIN1 and *vice versa*. I found that both values significantly and positively correlated with each other ($R^2=0.137$, $p=0.0003$) (Fig. 37).

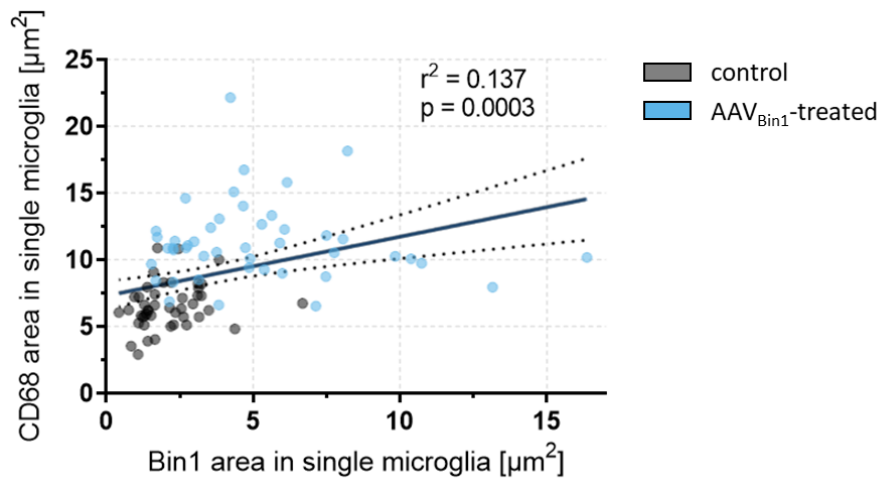


Figure 37: BIN1 and CD68 level from single microglia correlate with each other.

Linear regression analysis of BIN1 and CD68 area concomitantly acquired in single microglia cells from 4 mo WT animals ± unilaterally injected with AAV_{Bin1}. Animals were sacrificed 30 dpi. Images were taken in the hippocampal CA1 area. Goodness of fit is described as $R^2=0.137$ and a significant deviation from zero with $p=0.0003$. Grey colored dots represent values acquired from untreated controls (N=3), blue colored dots represent values acquired from animals inoculated with AAV_{Bin1} (N=3). Dotted lines represent the 95 % confidence interval of the best-fit line.

5 Discussion

During the course of my PhD I was given the opportunity to establish and optimize two different MACS-based primary mouse microglia isolation protocols with the ambition to cover two distinct objectives. Those procedures were the foundation for my analysis of microglia dysfunctionality in an AD mouse model and the, to our knowledge, first study assessing the homeostatic processes affected by BIN1 in microglia, a recently discovered high-impact LOAD risk factor, which is second only to ApoE [103].

I successfully sequenced RNA isolated from an aged AD mouse model and could confirm the previously described changes towards an inflammatory phenotype, which was partially recapitulated upon comparison with the well-known MGnD phenotype. Correlation with a matching proteomic data set pointed towards an inflammatory but also regenerative phenotype and strengthened other aspects, such as dysregulation of the phagocytic machinery. This condition was further backed up through the identification of several distinct synaptic proteins within the proteome of APP^{NL-G-F} microglia. Interestingly, despite being significantly enriched in AD mouse lysosomes, I found those compartments to be less densely occupied by synaptic material compared to age-matched controls, further promoting the phagocytic dysfunctionality of AD microglia.

To investigate the potential link between LOAD risk factor *BIN1* downregulation in AD microglia and its presumed influence on phagocytic function, I overexpressed *BIN1* in microglia through AAV-mediated transduction *in vitro* and *in vivo*. In primary mouse microglia cultures, BIN1 localized with proteins of the endolysosomal system and was upregulated during phagocytosis. Moreover, viral upregulation of *BIN1* expression increased the microglial phagocytic capacity along with enhancing the expression of multiple proteins associated with this process. *In vivo* stereotactic injections led to the off-target detection of mCherry in pyramidal neurons, and to a lesser extent in microglia of the region of interest. Nevertheless, I found BIN1 and CD68 to be specifically upregulated in transduced microglia and not in neurons. Taken together, those studies imply that microglial BIN1 contributes to homeostatic phagocytosis and offer a direct mechanistic link between the previously described phagocytic impairment of AD microglia and *BIN1* downregulation.

5.1 Primary mouse microglia isolated with MACS-based technology are of high purity and viability

In the present study, I established and optimized two different MACS-based microglia isolation procedures for downstream RNAseq and primary cell culture experiments, which were likewise novel to our laboratory. Both isolation procedures generated markedly pure microglia/macrophage-enriched fractions with a minimal amount of microglia remaining in the depleted fraction. Thus, highlighting the efficiency of the applied procedure. Importantly, I could not detect any neuronal contaminants in the microglia-enriched fraction, which are a major source for impurities during primary cell isolation. Other studies reported a significantly decreased isolation yield for different cell types which, among others, could be linked to the use of a Percoll gradient [325, 326]. Similar steps were omitted in this study without detriment to the purity of isolated fractions. The achieved high numbers didn't require pooling of samples, thus, enabling a more precise analysis during RNAseq and allowed for the generation of multiple biological replicates during culture experiments. The more convenient approach with the GentleMACS device and factory-made enzyme kits (Miltenyi Biotec) allowed for a quicker, less labor-intensive isolation procedure. This, in combination with performing all working steps on ice or cooled conditions favored the indispensable preservation of RNA integrity [327]. Importantly, RNA integrity was shown to be largely intact, therefore permitting highly sensitive sequencing of RNA samples. However, this approach proved unfit for the subsequent culture of primary cells. Most likely, the low temperatures and too harsh dissociation conditions caused metabolic perturbations and small membrane breaches from which the cells could not recover during culture. Therefore, I adapted the protocol towards manual dissociation at room temperature and enzymatic digestion with self-made papain enzyme solutions. Papain is a plant-based proteolytic enzyme from the cysteine proteinase family and is generally regarded as mild compared to other frequently used proteases, such as Trypsin [328, 329]. In addition, the manual use of multiple coated glass pipettes with decreasing diameters instead of a remote-controlled blade rendered the procedure more flexible. Increased viability of cells was mainly assessed through greatly lifted success rates during culture, but also through the observation that healthy cells almost immediately after isolation started to extend their processes again.

5.2 Characterization of microglial dynamics during Alzheimer's Disease

In recent years, many intriguing studies have aimed to elucidate the underlying mechanisms of AD pathology through single-cell or bulk RNAseq [245, 246, 247, 248, 307, 330, 331], while only few have attempted to directly compare matching transcriptome and proteome [332]. During the first part of my thesis, I focused on the transcriptomic profiling of an aged AD mouse model, which was re-evaluated after comparison with a recently published matching proteomic data set [224]. Moreover, I identified and quantified several synaptic proteins within AD microglia lysosomes and could link them with the observed phagocytic impairment of microglia that are chronically exposed to increasing amounts of A β .

5.2.1 Transcriptomic profiling of Alzheimer's Disease mouse microglia

Transcriptomic analysis of advanced-stage AD microglia extracted from 12 mo APP^{NL-G-F} mice revealed several patterns described in the previous literature [245, 246, 307]. Matching those observations, I found a prominent decrease in genes associated with the homeostatic signature and a marked increase of inflammation-associated transcripts. Moreover, I could detect enrichments pointing towards a dysregulation of the endolysosomal system.

5.2.1.1 Reduction of homeostatic signature genes

In line with previous reports [245, 246, 307], I observed a partially severe downregulation (≥ 80 %) of homeostatic signature genes, which is a clear indicator for the advanced loss of microglia function due to the increasing accumulation of A β . This was further backed up through GSEA, which revealed a downregulation for processes associated with motility, intracellular transport and transcription activity.

Microglia as the brains principal neuroimmune sentinels continuously sense changes in their environment [98]. In fact, multiple genes belonging to the microglial "sensible" [210] were strongly downregulated in aged APP^{NL-G-F} microglia. These genes included *Tmem119*, *Cx3cr1*, *Crybb1*, *Siglech*, *Hspa1a* and *Gpr34*. Among those, *Cx3cr1* was identified as one of the biologically most relevant downregulated transcripts. *Cx3cr1* is a trans-membrane receptor for its neuronally expressed chemokine ligand fractalkine (Cx3cr1l) and medi-

ates both migratory and adhesive functions in microglia [333]. Interestingly, downregulation of this homeostatic gene might in fact be both beneficial and detrimental during AD. In combination with the APP/PS1 transgene, *Cx3cr1* deficiency reduced A β plaque load [221]. In addition, two-photon microscopic comparison of APP:PS1:taup^{301L}:Thy1-YFP: CX3CR1^{GFP/+} and APP:PS1:taup^{301L}:Thy1-YFP: CX3CR1^{gfp/gfp} mice revealed that *Cx3cr1* deficiency resulted in a decline of microglia-mediated neuronal cell death, as well as mitigated microglial velocity [334]. In contrast, hAPP-J20/CX3CR1^{-/-} mice expressed higher levels of Il-6 and TNF- α levels, leading to an increased neurotoxic phenotype and exacerbated cognitive deficits [335]. Moreover, both ligand and receptor are reportedly downregulated in human AD [335]. In summary, negative regulation of the *Cx3cr1* axis probably entail the beneficial enhanced phagocytosis of debris and plaques, but could also be associated with the detrimental secretion of pro-inflammatory cytokines causing neurotoxicity [336].

In addition, I detected a strong downregulation of Tmem119 (FC 0.24), a homeostatic marker which was similarly altered in other transgenic mice and human AD patients [245, 246, 307]. However, despite being highly microglia-specific, its precise functions, especially in the context of AD, are largely understudied [337].

Trying to increase homeostatic markers to alleviate AD pathology may seem as a valid approach and multiple attempts have been made. An interesting study published by Park and colleagues describes the treatment of two different AD mouse models with DAPPD, a small synthetic molecule composed of a benzene ring and two acetamide groups [338]. In their study, they characterize increased homeostatic and decreased DAM signatures, which could be linked to increased phagocytic activity, reduced A β load and improved cognition [338]. However, constraining microglia in a homeostatic state as has been reported for Trem2^{-/-} mice, seems to be detrimental for AD pathology. Multiple groups demonstrated that Trem2^{-/-} microglia lose their capacity to respond to amyloid deposits and injury conditions [245, 252, 339, 340, 341]. Moreover, in contrast to AD mice, some homeostatic markers (such as P2RY12) were found to be higher expressed in human AD patient microglia [250]. Therefore, the nature and influence of homeostatic signatures is not yet fully understood and demands further investigation.

5.2.1.2 Increased proliferation and inflammatory phenotype

Increased microglial proliferation and inflammatory behavior are among the main hallmarks of various neurodegenerative diseases, including AD (section 1.1.1.3). GSEA of 12 mo APP^{NL-G-F} microglia revealed a significant enrichment for processes associated with cellular expansion, cytokine stimulus responses, peptide secretion and ERK signaling. Similar to homeostatic signatures, delineating beneficial and detrimental factors of this phenotype may be a highly complex venture towards understanding and treating AD.

Cellular expansion

GSEA identified several genes that could be positively associated with cellular expansion in APP^{NL-G-F} microglia, e.g. *Igf1*, *CSF1*, *Gnas*, *Pmp22* and *ApoE*. CSF1R signaling can be activated by its ligand colony-stimulating factor 1 (CSF1), which was noticed to be among those transcripts with the highest upregulation (FC 19.30). Both are essential for microglia proliferation, differentiation and survival during physiological conditions [183, 201]. Interestingly, CSF1 was shown to reduce microglia-mediated neuroinflammatory effects in various brain diseases [342, 343]. AD mice treated with CSF1 showed higher numbers of microglia and a significant plaque-load reduction due to increased microglia phagocytosis [344]. In accordance with this study, cultured human microglia treated with CSF1 displayed enhanced proliferation and phagocytosis of β -amyloid [345]. Moreover, increased levels of CSFR1 and CSF1 were also found in human post-mortem AD brain samples [346, 347, 348]. However, blocking the CSF1R pathway in APP/PS1 mice resulted in an improved cognitive performance and prevented synaptic degeneration correlating with arrested microglia proliferation [348]. Thus, on one hand, CSF1 upregulation is most likely beneficial for microglia proliferation and survival, but might also compensate for the described deficiency of phagocytic function in AD microglia. On the other side, it might also be responsible for a worsening of the degenerative phenotype.

Pro-inflammatory phenotype

Recent advances strongly suggest that ERK signaling could be a major regulator of pro-inflammatory immune responses in AD pathogenesis and might also be involved in the negative regulation of microglial phagocytosis [349, 350]. GSEA of our data revealed several high-FC genes known to be involved in this signaling cascade, such as *Igf1*, *Axl*, *Ccl6*, *ApoE*,

Ccl3, *Tlr2* and *Trem2*. *In vitro* transcriptomic profiling and functional phagocytosis assays could show that ERK is a critical regulator of IFN γ -mediated pro-inflammatory microglia activation and lies upstream of several microglia-specific LOAD risk genes (*Bin1*, *Trem2*, *Cd33* and *Cnn2*) [349].

In line with increased ERK signaling, secretory granules (also called exosomes) were the cellular component with the highest enrichment in 12 mo APP^{NL-G-F} microglia. Several transcripts could be positively linked through GSEA, such as *Igf1*, *Serpine2*, *Ctsl*, *Sv2b*, *Ccl3*, *Tlr2*, *Cadm1* and *Cd34*. Exosomes (with a typical size range of 30 - 100 nm) are a sub-type of extracellular vesicles with endocytic origin that are released into the extracellular space through outward budding of the plasma membrane [351, 352]. Originally assumed to be waste products, they are now believed to play important roles in intercellular communication and the elimination of cellular residues [353]. It has been shown that microglia participate in the extracellular clearance of A β through exosome-mediated release of the amyloid-degrading enzyme IDE [233]. On the other side, high levels of extracellular vesicles loaded with neurotoxic A β and hyper-phosphorylated tau species were detected in the CSF of AD patients and might substantially contribute to neuropathological spreading of amyloid and tau pathology [107, 354]. Exosomes released from microglia typically also contain pro-inflammatory cytokines (*e.g.* TNF α , IL-1b) that lead to the activation of nearby but also distant astrocytes and microglia [355, 356, 357]. The high plasticity of activated microglia and their increased exosomal communication with other brain cells has made them an appealing target for the development of new CSF biomarkers but also to therapeutically limit A β and tau transmission between cells [357, 358].

5.2.1.3 Decay of cellular motility and phagocytosis

One of the most important machineries concerning physiological microglia function is the coordination of the actin cytoskeleton that controls the key processes motility and phagocytosis [318]. Interestingly, I could locate the highest negative GSEA enrichments in endosomes and the actin cytoskeleton of 12 mo APP^{NL-G-F} microglia. GSEA further revealed several downregulated transcripts to be linked to the actin cytoskeleton, such as *Aif1l*, *Myo1b*, *Fscn1*, *Ophn1* and *Fgd2*. Transcripts negatively associated with the endosome entailed *Fgd2*, *Myo1b* and *Rhob*. This observation is in line with previous studies showing

reduced motility and phagocytosis in AD microglia [32, 224, 304]. Although not directly linked to the actin cytoskeleton through GSEA, the observed downregulation of the homeostatic *Cx3cr1* (FC 0.81) likely contributes to this phenotype, as decreased motility and phagocytic behavior were also described for AD mice deficient for *Cx3cr1* [334]. Moreover, I detected a substantial downregulation of *Bin1* (FC 0.57) and *Abi3* (FC 0.62), two LOAD risk factors that are currently assumed to be involved in actin cytoskeleton regulation and endocytosis/phagocytosis as downstream effectors of *Trem2* [150, 359]. Interestingly, a recent study published by Karahan and colleagues could nicely demonstrate how 5xFAD/ABI3^{-/-} mice harbored increased A β accumulation and neuroinflammation, which could be attributed to highly impaired microglia migration behavior [359]. Other studies report a similar downregulation of *BIN1* in APP^{NL-G-F} microglia, such as the scRNAseq data published by Frigerio and colleagues [248], but also in other AD mouse models [224]. Although sparse, there are some compelling studies pointing to functions for BIN1 in microglia related to migration, proteostasis and clearance [149, 150, 279, 285] (see also section 1.3). Therefore, we were intrigued to find out more about the highly understudied contribution of BIN1 towards the sustained deterioration of microglia during AD. In summary, the data so far supports the finding that even though *Trem2* as A β -binding receptor is substantially upregulated (FC 3.37), its downstream signaling might be heavily impaired and could promote the defective clearance function of microglia.

5.2.2 Comparison with MGnD reveals similarities but also differences

I further compared my sequencing results to the available literature, *i.e.* the neurotoxic MGnD phenotype published by Krasemann and colleagues [246]. In their study, models from three different neurodegenerative diseases (ALS, MS and AD) were incorporated and a common ApoE-Trem2 pathway was identified as major regulator for phenotypic changes in microglia. They further postulate that the uptake of neuritic A β plaques triggers this switch in AD microglia. After adjusting the data sets towards those genes that were similarly analyzed on both panels, I could detect a prominent overlap for upregulated (77.78 %) and a low overlap (43.28 %) for downregulated transcripts. Interestingly, transcripts that were similarly upregulated in MGnD and APP^{NL-G-F} microglia, centered around functions related to cellular expansion, the detection of foreign material and the regulation

of response to cytokine stimulus (*e.g.* *ApoE*, *Csf1*, *Axl* and *Tlr2*, among others). In general, genes that are associated with an increased inflammatory behavior. Shared downregulated genes could be linked to a decreased homeostatic signature and also decreases in motility (*e.g.* *Tmem119*, *Cx3cr1*, *Crybb*, *Bin1* and *Abi3*, among others).

Interestingly, I could detect dissimilarities regarding the regulation of two prominent microglia activation and pruning markers. The potent monocyte chemoattractant *Ccl2* [360] and complement factor properdin *Cfp* [361] were found to be highly downregulated in 12 mo APP^{NL-G-F} microglia (FC 0.37 and 0.31, respectively) but upregulated in MGnD [246]. Prominent differences were also apparent on the side of upregulated transcripts from APP^{NL-G-F} microglia that were downregulated in MGnD. Among those transcripts were the homeostatic and anti-inflammatory *Lair1* (FC 1.69) and *Tgfb* (FC 1.23) [362, 363] and the microglia sensome receptor *Itga6* (FC 1.53) [364]. Those dissimilarities might be due to the extraction of microglia from the spinal cord of the ALS and MS model or the inclusion of different neurodegenerative diseases. However, when comparing the transcriptomic profile of the additionally included APP/PS1 AD model with the profile of the APP^{NL-G-F} microglia from this study, I could find that those discrepancies further persisted. Comparison of our transcripts with a study performing scRNAseq on aged APP^{NL-G-F} microglia [248] supported the significant changes observed in our data. Therefore, the recognized opposing regulation of several transcripts might be due to model-specific differences (APP overexpression in APP/PS1 *vs.* increased total A β 42, A β 42/A β 40 ratio and promoted aggregation in APP^{NL-G-F} mice). Overall, this comparison opens up the question whether microglia from APP^{NL-G-F} mice truly fit the aggressive MGnD phenotype or if they more closely relate to the DAM phenotype postulated to restrict neurodegeneration [245]. Based on the original publication from Takashi Saito describing the APP^{NL-G-F} line [365] and a lack of follow-up reports, those mice do not exhibit an overt synaptic or neuronal phenotype, in contrast to the APP/PS1 [366, 367].

5.2.3 Overlap between transcriptomic and proteomic signatures

Differential mRNA expression studies (*e.g.* bulk or scRNAseq) implicitly assume that changes in transcript expression have a direct biological meaning, often thought to be mediated by corresponding protein level changes. However, studies analyzing the correla-

tion between mRNA and protein expression level typically detect a very moderate overlap of 40 % [311, 312], creating concerns regarding the validity of data derived from mRNA expression analysis only. This apparent mismatch is usually attributed to differential regulation through post-transcriptional and -translational modifications, different half-lives of transcripts and proteins, but also experimental error and noise [313]. Interestingly, it has been shown that mRNA and corresponding protein correlate better in systems undergoing constant changes than in steady-state systems [368], supporting the assumption that differential mRNA expression has biological meaning. Fitting those observations, I could detect a decent overlap of almost 70 % between similarly detected mRNA and protein in 12 mo APP^{NL-G-F} microglia. Interestingly, GSEA of transcripts and proteins with matching directionality implied a more regenerative microglia phenotype (compared to RNAseq only) with persisting difficulties on the side of phagocytic and lysosomal function.

5.2.3.1 Matching upregulated transcripts and proteins imply shift towards a more regenerative phenotype

Analysis of biological and molecular mechanisms through GSEA of shared upregulated transcripts and proteins revealed that cellular growth and inflammatory but also wound-healing related processes were among the most substantially changed in 12 mo APP^{NL-G-F} microglia. Those processes were primarily influenced by *ApoE*, *Tlr2*, *Serpine2*, *Apbb2*, *Cadm1*, *Tgfbr2*, *Gnas* and *Cd34*. Moreover, neuron death was no longer listed among the positively influenced biological processes, and cellular growth and activation were simultaneously negatively regulated, indicating an overall less aggressive and more neurotrophic phenotype. Fitting those observations, secretory granules showed a lower normalized enrichment score compared to RNAseq only (1.4 vs. 1.8), implying an active but dampened release of pro-inflammatory cytokines compared to the previous GSEA analysis. Instead, upregulated transcripts and proteins were significantly enriched at the external plasma membrane (*e.g.* *Tgfbr2*, *Tlr2*, *Gusb*, *Cd34* and *Ank2*) and the lytic vacuole (*e.g.* *ApoE*, *Ctsd*, *Ctsl*, *Manba* and *Tlr7*), suggesting an upregulation of transcripts associated with the enhanced detection and degradation of A β [170, 210, 369, 370]. Nevertheless, homeostatic markers crucially involved in the detection and uptake of A β were also simultaneously downregulated (discussed below).

Based on the current analysis it is tempting to conclude that in fact, advanced-stage APP^{NL-G-F} microglia exhibit a less neurotoxic phenotype than previously assumed and try to counteract the advancing deterioration of their environment, *e.g.* through release of BDNF [371]. Several additional points would be in favor for this, given the earlier observation that the herein analyzed APP^{NL-G-F} microglia only partially overlap with the aggressive MGnD phenotype (section 5.2.2) and that the model itself lacks a prominent synaptic or neuronal phenotype [365]. A separate in-depth comparison with the more protective DAM phenotype and longitudinal correlation between APP^{NL-G-F} microglia transcriptome and proteome would improve our understanding of this frequently used mouse model and could clarify the intertwined regulatory mechanisms of the two-faced microglia behavior during AD progression.

5.2.3.2 Matching downregulated transcripts and proteins strengthen previously observed phagocytic dysfunction

In agreement with the more powerful correlation between similarly downregulated transcripts and proteins of 12 mo APP^{NL-G-F} microglia (78.79 % of shared downregulated *vs.* 59.37 % of shared upregulated), I could observe fewer differences between the GSEAs of RNAseq only and matching downregulated transcripts and proteins (sections 4.1.1.6 and 4.1.2). Negatively affected processes still had a distinct enrichment for mechanisms related to cell adhesion, actin filament organization, cellular transport, carboxylic ester hydrolase and lipase activity, supporting the previously observed disturbances in motility, phagocytosis and processing.

Strong similarities were noticed when comparing key homeostatic markers, such as Tmem119, Cx3cr1, Crybb1 and Gpr34. The previously identified transcripts *Siglech* and *Hspa1a* were not detected in the proteome of 12 mo APP^{NL-G-F} microglia. Instead, other influential homeostatic markers such as P2ry12 were significantly downregulated [224]. Among the most influential transcripts and proteins related to decreased motility and processing I identified *Myo1b*, *Fgd2*, *Rhob*, *Fscn1*, *Bin1*, *Ophn1* and *Enpp2*. Actin-based motor proteins such as Myosins (*e.g.* Myo1b) use the energy derived from ATP hydrolysis to relocate actin filaments and produce force [372]. Interestingly, I could detect a significant negative enrichment score for ATPase activity, which is compatible with the reduced

motility and phagocytosis of AD microglia. Lipase and carboxylic ester hydrolase activity have been recognized to play important roles in the active uptake and degradation of lipid debris and other phagocytosed materials [373, 374, 375]. It was further reported that Trem2 senses damage-associated lipid patterns from neuronal membranes that associate with fibrillar A β , thereby triggering the microglia response to amyloid deposits [252]. Moreover, Trem2 binds ApoE and other apolipoproteins (like ApoJ/Clu), which form A β -lipoprotein complexes that are efficiently phagocytosed in a Trem2-dependent manner [376]. Although *Trem2* and *ApoE* were found to be highly upregulated in 12 mo APP^{NL-G-F} microglia (transcript and proteins), the concomitant downregulation of lysophosphatidic acid (LPA)-synthesizing enzyme Autotaxin (*ATX*, *Enpp2*) [377] and other potential effector proteins (*e.g.* *Bin1*, *Abi3*) further strengthens the assumption that clearance is heavily impaired in aged AD microglia (see also 5.2.1.3).

In general, comparing changes on the mRNA and protein level of 12 mo APP^{NL-G-F} microglia could show how including additional data might be beneficial for the ongoing process of understanding highly complex diseases such as AD. To date, studies unifying both methodological approaches are scarce, which might be due to their complex regulatory nature (*i.e.* mechanisms such as post-transcriptional and -translational modifications and different half-lives) but also the financial outlay. With the assistance of a recently published matching proteomic data set I could detect a decent overall correlation of 70 % from the analyzed transcripts included in our panel, signifying a biological relevance of the generated data. Interestingly, our current comprehensive RNAseq/proteomics data indicates that advanced-stage APP^{NL-G-F} microglia are potentially not as neurotoxic as microglia from other neurodegenerative AD models (*e.g.* APP/PS1), which is also reflected in the relative low overlap (approx. 60 %) with MGnD microglia (section 5.2.2). Moreover, similarly downregulated transcripts and proteins correlated better with each other than upregulated ones, supporting our previous identification of processes associated with the continuous decline of microglia phagocytic and degrading function. Importantly, our sequencing panel contained several known microglia-specific LOAD risk factors (*Trem2*, *ApoE*, *Bin1*, *Abi3* and *Clu*) that were identified to be significantly and similarly regulated on both RNA and protein level, promoting the potential influence of human-derived LOAD risk factors in AD mouse models.

5.2.4 Synaptic proteins are enriched within AD microglia lysosomes and correlate with phagocytic dysfunction

Despite not being intrinsically expressed by microglia, I identified several synaptic proteins within the proteomic data set published by Sébastien-Monazor *et al.* 2020. In line with the current literature [378], I could identify proteins primarily located on pre- and post-synapses. Interestingly, synaptic proteins were significantly decreased in early-stage 3 mo APP^{NL-G-F} microglia and became enriched starting from 6 mo of age. Moreover, Sébastien-Monazor and colleagues identified an early upregulation of proteins associated with increased lysosomal function (*e.g.* CD74, CTSD, CTSH, CTSZ, HEXA, GLB1, CD68, NPC2 and CLN3) and fatty acid metabolism (APOE, ACACA and SOAT1), which they term early microglia A β response proteins (MARPs) [224, 379]. For this thesis, I quantified three surrogate synaptic proteins in 6 and 12 mo APP^{NL-G-F} and C57Bl/6J single microglia stainings and could confirm their significant lysosomal enrichment in AD mice. Matching the Mass Spectrometry-based proteomic detection, synaptic proteins were significantly enriched in 6 mo AD mice and further increased in late-stage AD microglia. Although additional quantification for the early-stage age group is still missing, this finding further promotes the conception that early-AD microglia are highly functional with respect to their innate phagocytic and degrading function, which later on becomes dysfunctional as accumulating A β and debris contribute to the sustained neuroinflammatory phenotype.

To further analyze lysosomal function in AD microglia, I quantified the lysosomal area within single cells and could detect a significant increase in middle- and advanced-stage AD animals compared to age-matched controls, which is in line with the previous literature [216, 380]. Total CD68 within single cells positively correlated with the total area of synaptic proteins within single cell lysosomes, matching the quantified enrichment of synaptic proteins in AD microglia lysosomes. Notwithstanding, I detected a trend towards a lower occupancy of CD68-positive lysosomes in 6 and 12 mo APP^{NL-G-F} microglia, despite the previous identification of increased amounts of synaptic material within the same cells. Furthermore, I observed a significant negative correlation between total lysosomal area in single cells and relative occupancy, which became more apparent in advanced-stage AD microglia. Bearing in mind the substantial downregulation of genes and proteins asso-

ciated with actin cytoskeleton regulation and phagocytosis/endocytosis in aged AD mice (section 5.2.3.2), this data endorses a highly dysfunctional microglia phenotype. In spite of accumulating debris and plaques in their periphery, middle- and advanced-stage AD microglia appear overwhelmed with the perpetual deterioration of their environment, which is reflected on the transcriptomic and proteomic levels (this study, [224]) but also in their *in vitro* and *in vivo* behavior [32, 224, 304, 334].

5.3 Homeostatic functions of BIN1 in microglia

For the second main part of my thesis, I intended to analyze the nature and influence of the novel high-impact AD risk factor BIN1 on microglia physiology *in vitro* and *in vivo*. With this, I anticipated to gain novel insights into the mechanisms contributing to AD physiology. Preceding transcriptomic and proteomic analysis revealed a considerable downregulation of BIN1 in microglia from 6 and 12 mo APP^{NL-G-F} mice, which could be recapitulated in free-floating sections. Interestingly, Sébastien-Monason and colleagues further analyzed the proteomic profile of APP/PS1 microglia and found a similar decrease of BIN1 levels in 6 and 12 mo AD animals, arguing against a model-specific effect [224]. Increasing evidence suggests that microglial BIN1, through direct regulation of the actin cytoskeleton, could provide a mechanistic link between its downregulation in the context of AD and the elusive phagocytic impairment of microglia [150, 284, 301]. Here, I provide strong evidence for this hypothesis that could help shape our understanding of the highly complex homeostatic-but also inflammatory-related dysregulation observed in AD microglia.

5.3.1 *In vitro* primary mouse microglia culture

In primary microglia cultures, I observed BIN1 to localize with proteins of the endolysosomal machinery and quantified its upregulation during phagocytosis. Interestingly, AAV-mediated BIN1 overexpression led to the significant upregulation of several deputy endolysosomal-associated proteins. Moreover, I could show that BIN1 overexpression increased the microglial phagocytic capacity, providing distinct evidence that BIN1 contributes to homeostatic phagocytosis in microglia. Importantly, those effects could not be observed upon transduction with a control virus construct.

5.3.1.1 AAV/TM6 serotype as an excellent tool for *in vitro* microglia manipulation

To date, rabies, herpes simplex, lenti-, adeno- and adeno-associated viruses (AAV) have been successfully used to visualize and genetically manipulate neural circuits and specific cell types *in vitro* and *in vivo* [297]. For basic research, lenti-viruses and AAVs are commonly used due to their high transduction efficiency and the lack of an immediate immune response, cytotoxicity and cell lysis [381, 382]. For microglia, numerous attempts have been made with promising techniques but moderate success upon closer examination [322, 323, 324, 383, 384, 385, 386]. To tackle this well-known obstacle, I employed a capsid-optimized AAV6 serotype construct first described by Rosario *et al.* 2016. Site-directed mutagenesis of two tyrosine residues to phenylalanine and a threonine to valine (Y731F/Y705F/T492V) was shown to prevent proteasomal degradation and enhance transduction efficiency in monocyte-derived dendritic cells for the AAV serotypes 2 and 6 [387, 388, 389, 390]. The construct AAV/TM6-F4/80-mBIN1-2A-mCherry was built to overexpress mouse microglial BIN1 isoform 2 under control of the highly microglia-specific F4/80 promoter [206] and demonstrated excellent transduction efficiency with the desired overexpression of BIN1 (FC 2.20) *in vitro*. Of importance, at 5 dpi, expression of the fluorescent marker mCherry could be chiefly localized to the outer membrane regions and cytosol and only marginally to the CD68-positive lysosomal compartment, indicating a well-functioning escape mechanism from proteasomal degradation at this time point. Equivalent observations could be made for the control construct AAV/TM6-F4/80-mCherry without overexpressing BIN1. Out of estimated 1500 imaged cultured microglia, six did not appear to express the fluorescent marker mCherry, resulting in an estimated transduction efficiency of > 99 % (not shown). Moreover, no cytotoxic side effects could be observed. To the best of our knowledge, we are the first to describe the use of a highly efficient AAV-mediated microglia transduction vector *in vitro*.

5.3.1.2 *In vitro*, BIN1 localizes with proteins of the endolysosomal machinery and is upregulated during phagocytosis

Several lines of evidence demonstrate the direct involvement of BIN1 in the reorganization of the actin cytoskeleton and endocytic trafficking, thereby implicating an important

contribution to the homeostatic processes migration and phagocytosis [288, 289, 291, 292]. However, explicit evidence for similar functions of the microglial isoforms of BIN1 are still missing [103, 150]. In primary microglia culture stainings, I noticed that microglial BIN1 localized with β -actin and another scaffolding protein known to modulate the cytoskeleton, CD2AP [319]. Based on the described co-localization and modulatory effect of neuronal BIN1 on the early endosome markers EEA1 and Rab5 [288], I stained for those markers and could detect an overlap in their respective staining patterns with BIN1. Similarly good results were obtained when co-staining for BIN1 and the lysosomal marker CD68. To give tangible biological meaning to those observations, co-localization and quantitative binding assays should be performed. Importantly, I could show that microglial BIN1 was upregulated in primary cells during phagocytosis. Overall, those results argue for an involvement of BIN1 in phagocytic and endolysosomal processes.

5.3.1.3 BIN1 function in cultured microglia is linked to phagocytosis

To promote a more thorough analysis of the potential involvement of microglial BIN1 in migration- and phagocytosis-related processes, I analyzed the influence of AAV-mediated BIN1 overexpression on a subset of phagocytosis and activation markers as well as on the intrinsic phagocytic activity itself. At 5 dpi, I could detect not only a substantial upregulation of BIN1 (FC 2.20), but also a significant increase of normalized β -actin, CD68 and Lamp1, supporting the direct link between microglial BIN1 and the actin-cytoskeleton [284] and pointing towards a higher activation level [318]. This was further supported by the observation that AAV_{Bin1}-treated cells exhibited morphological changes reminiscent of a more active phenotype [318]. In addition, I quantified the phagocytic activity of cells overexpressing *BIN1* compared to untreated controls and noticed a significant increase in the normalized amount of phagocytosed material. Importantly, all of the above described changes could not be observed in cultures treated with AAV_{ctr.}, strongly arguing for the specificity of the quantified effects following *BIN1* overexpression.

Based on the direct link shown for neuronal BIN1 and early endosome markers EEA1 and Rab1 [288] and the above described overlapping localization within primary microglia, it would be very interesting to see whether *BIN1* overexpression would lead to changes in their respective expression levels. Moreover, it would deepen the proposed link between mi-

croglia BIN1 and the endosomal compartment [150]. To increase viability and throughput during primary microglia culture experiments, I chose performing all isolations on P4-P6 pups obtained from C57Bl/6J matings. However, implementing cell culture experiments with primary cells acquired from different adult age cohorts or separate mouse lines would open up more possibilities with respect to analyzing distinct age or AD-related phenotypical effects, *e.g.* through rescue experiments. In summary, the data so far insinuates that in primary mouse microglia cultures BIN1 is intrinsically involved in the homeostatic uptake and endocytosis of foreign material. In turn, this further implies that the ascertained downregulation of microglial *BIN1* in the context of AD in mice but also human patients (this study, [103, 224, 301]) could provide a rationale for the detected phagocytic impairment of disease-associated microglia.

5.3.2 *In vivo* overexpression of *BIN1*

In vivo manipulation of specific cellular subpopulations is still an important prerequisite to decipher functional interactions, *e.g.* between microglia and their neuronal environment but also to assess the effects of a genetic manipulation in a natural setting. To test the efficacy of our new viral construct *in vivo*, I stereotactically injected WT mice with AAV_{Bin1}. At 30 dpi, injection into the hippocampal CA1 region led to a region-confined spread of the viral construct, which, despite being equipped with the highly microglia-specific F4/80 promoter, could also be observed in a subset of pyramidal cell layer neurons. Nevertheless, mCherry could be detected in microglia that further displayed morphological changes towards a more activated phenotype. Importantly, I could quantify a microglia-specific increase of BIN1 and CD68 in transduced microglia, which was not evident in the subset of transduced neurons.

5.3.2.1 Viral distribution is limited to targeted injection site but not limited to microglia

For this study, I evaluated the efficiency of two different routes of viral injection, based on the original paper describing the herein used modified AAV construct [306]. WT animals were either injected into the hippocampal CA1, or the lateral ventricles. Although the authors describe a successful transduction with 80 % microglial specificity after injection

into the ventricles, I could not observe mCherry-positive microglia adjacent or distant from the injection site. In contrast to the original paper, I injected adult instead of neonatal mice, whose neuroepithelium and ependyma might possess different permeability properties [391]. Other studies reported a successful neuronal AAV-mediated transduction after neonatal intraventricular injection that persisted until adulthood [392, 393]. Given the apparent lack of microglia transduction following intraventricular AAV injection, we did not follow up on this approach.

In addition, I injected mice into the hippocampal CA1 region. Rosario *et al.* describe a 70 % specificity for this target region, which was unfortunately not further quantified with respect to efficiency [306]. Here, analysis of three animals each revealed that uni- and bilateral CA1 injections were equal with respect to their viral distribution pattern and yielded a transduction specificity comparable to the original paper [306]. Positive mCherry labeling could be observed throughout the CA1 region, extending into CA2 and the dentate gyrus. Occasional mCherry signal was additionally noted in the adjacent dorsal cortical area. For this thesis, I quantified the effects in unilaterally injected animals, which I compared to age-matched naive littermates.

At 30 dpi, I noticed a strong mCherry-positive signal from a subset of CA1 pyramidal cell layer neurons that was present within cell bodies and extending projections. Upon closer examination of single microglia, I could identify many cells positive for mCherry, albeit with much lower intensity compared to neurons. Given the high microglia-specificity of the selected F4/80 promoter [206], it seems unlikely that the strong mCherry signal in pyramidal layer neurons derives from a faulty promoter. It would be interesting to pursue an injection approach with lower titer and subsequently evaluate the off-target labeling of neurons. However, it was repeatedly shown in recent years that microglia remain notoriously difficult to transfect or transduce [297]. This could be due to their highly skilled macrophage function that allows them to detect, engulf and dismantle pathogens. Given the distinct mCherry-positive labeling of primary cultured microglia 5 days after transduction, it seems feasible to assume that after 30 days *in vivo*, microglia have degraded the exogenous mCherry, making it increasingly difficult to detect. Thus, perfusing animals *e.g.* 10 days after transduction would be beneficial with respect to uncovering the potential degradation of mCherry in microglia. Some viruses, such as HIV-1 have been described to

successfully circumvent monocyte defense mechanisms and are known to specifically infect microglia and macrophages in the brain [394]. The development of viral tools capitalizing on those mechanisms would be of immense value for the whole microglia-oriented scientific community. Another possible explanation for the off-target labeling of pyramidal layer neurons might lie within the increasingly well-described microglia-neuron communication via exosomes or nanotubes [395], which seems of particular importance during disease-related challenges [357, 396]. mCherry could have been exocytosed by microglia and taken up by neurons, which are less well equipped to degrade foreign material.

An alternative strategy for future attempts of microglia transduction could be the use of Cre-expressing mouse lines in combination with viral vectors. In those systems, the transfer vector would include a microglia-specific promoter and a double-floxed inverted orientation (DIO) sequence, which is inverted upon Cre-activation [397]. Specific targeting of microglia would be achieved in combination with the tamoxifen-inducible $Cx3cr1^{CreERT2}$ mouse line [398]. The flexible administration of tamoxifen rapidly induces Cre recombinase activity in microglia and macrophages [399, 400], allowing the targeted induction of Cre in combination with virus application. Nie *et al.* were one of the first to combine the $Cx3cr1^{CreERT2}$ mouse with a DIO-expressing lentiviral approach to target microglia *in vivo* [401]. In their study, they report a high microglia-specificity (90 %), suggesting that this would be a valuable strategy for future transduction experiments in adult microglia.

5.3.2.2 *BIN1* overexpression is specific for microglia and correlates with lysosomal marker CD68

Despite the off-target detection of mCherry in neurons, quantification for BIN1 in pyramidal layer neurons and single microglia revealed a microglia-specific increase for BIN1 (FC 2.42). In turn, this might support the previously discussed degradation or exocytosis of microglial mCherry. Moreover, lysosomal CD68 was significantly upregulated (FC 1.72) and transduced microglia exhibited changes towards a more activated phenotype, which I could also observe in transduced cultured primary microglia (section 5.3.1.3). Although reported to be of low immunogenicity [381, 382], I currently can not exclude the possibility of phenotypical changes due to the presence of viral particles or inflicted tissue damage during injections. Analogous to the observations made in cultured primary microglia, BIN1

in naive and transfected animals was found to distinctly localize with CD68, although not completely. In microglia from transduced animals, many small BIN1-positive vesicle-like formations became apparent that might indicate an increase of endosomal structures, as those were primarily located at the distal end of microglia filopodia and rarely overlapped with CD68. Moreover, I detected a significant positive correlation between BIN1 and CD68, indicating a direct link.

Although promising observations could be made during the *in vivo* experiments, there is room for improvement. Of particular importance would be the enhancement of microglial specificity with subsequent quantification for efficiency (*e.g.* through the combined use of microglia-specific Cx3cr1^{CreERT} mice and DIO-sequence AAV). Moreover, the shortage of control experiments (*e.g.* injection of AAV_{ctr.} or PBS) currently prevents the designation of explicit conclusions. Nevertheless, the microglia-specific upregulation of *BIN1* and the positive correlation with CD68 is encouraging enough to improve and continue our *in vivo* approaches regarding BIN1 function in microglia. If successful, they could prove valuable tools in future endeavors aimed at the rescue of microglia-mediated defects in AD mouse models.

5.4 Conclusions

In this study, I successfully sequenced and correlated mRNA transcripts from an aged AD mouse model with a matching proteomic data set. Thus, providing a more integrative approach compared to studies depending on a single omics methodology. Interestingly, the GSEA assigned highly inflammatory associated processes from isolated transcripts had to be partially mitigated towards a more regenerative phenotype upon comparison with the proteomic data set. However, the correlation also markedly underscored microglial phagocytic dysfunctions. This phenotype was further validated through the enrichment of synaptic proteins within lysosomes of phagocytic less functional disease-associated microglia. Moreover, several LOAD risk genes suspected to contribute to an impaired microglia phenotype were identified to be downregulated in this AD model, such as *BIN1*.

In addition, I could provide substantial evidence for the involvement of microglial BIN1 in phagocytic processes *in vitro* through functional and overexpression experiments in pri-

mary cells. Furthermore, those results insinuate a direct mechanistic link between the described multifactorial phagocytic impairment of AD microglia and *BIN1* downregulation. Although similar to the original paper, the improved design of the herein used AAV/TM6 serotype construct was not sufficient to result in a microglia-specific detection of the fluorescent marker mCherry *in vivo*. Nevertheless, *in vitro* efficiency and efficacy of primary microglia transduction could be convincingly shown. Thus, paving the way for succeeding experiments aimed at the targeted manipulation of primary microglia *in vitro*. Overall, this study signifies the importance of the preservation of microglia function in the context of AD and that *BIN1* downregulation is detrimental for disease progression. Moreover, microglia phagocytosis and BIN1 itself represent promising targets for further studies aimed at the comprehension of AD pathogenesis.

Bibliography

- [1] Masters, C. L, Bateman, R, Blennow, K, et al. (2015) Alzheimer's disease. *Nature Reviews Disease Primers* **1**, 1–18.
- [2] Catania, M, Giaccone, G, Salmona, M, et al. (2019) Dreaming of a New World Where Alzheimer's Is a Treatable Disorder. *Frontiers in Aging Neuroscience* **11**, 1–8.
- [3] Alzheimer, A. (1907) Über eine eigenartige Erkrankung der Hirnrinde. *Allgemeine Zeitschrift für Psychiatrie und Psychisch-gerichtliche Medizin* **Jan**, 146–8.
- [4] Alzheimer, A, Stelzmann, R. A, Norman Schnitzlein, H, & Reed Murtagh, F. (1995) An english translation of Alzheimer's 1907 paper, "Über eine eigenartige Erkankung der Hirnrinde". *Clinical Anatomy* **8**, 429–431.
- [5] Masters, C. L, Simms, G, Weinman, N. A, et al. (1985) Amyloid plaque core protein in Alzheimer disease and Down syndrome. *Proceedings of the National Academy of Sciences of the United States of America* **82**, 4245–4249.
- [6] Glenner, G. G. (1989) The Pathobiology of Alzheimer's Disease. *Annual Review of Neuroscience* **40**, 45–51.
- [7] DeTure, M. A & Dickson, D. W. (2019) The neuropathological diagnosis of Alzheimer's disease. *Molecular Neurodegeneration* **14**, 1–18.
- [8] Müller, U. C, Deller, T, & Korte, M. (2017) Not just amyloid: Physiological functions of the amyloid precursor protein family. *Nature Reviews Neuroscience* **18**, 281–298.
- [9] Müller, U. C & Zheng, H. (2012) Physiological functions of APP family proteins. *Cold Spring Harbor Perspectives in Medicine* **2**, 1–17.
- [10] Dawkins, E & Small, D. H. (2014) Insights into the physiological function of the β -amyloid precursor protein: Beyond Alzheimer's disease. *Journal of Neurochemistry* **129**, 756–769.
- [11] Kojro, E & Fahrenholz, F. (2005) The Non-Amyloidogenic Pathway: Structure and Function of α -Secretases. *Alzheimer's Disease* pp. 105–127.

- [12] Sisodia, S. S, Koo, E. H, Beyreuther, K, et al. (1990) Evidence that amyloid-beta protein in AD is not derived by normal processing. *Science* **248**, 492–495.
- [13] De Strooper, B, Umans, L, Van Leuven, F, & Van Den Berghe, H. (1993) Study of the synthesis and secretion of normal and artificial mutants of murine amyloid precursor protein (APP): Cleavage of APP occurs in a late compartment of the default secretion pathway. *Journal of Cell Biology* **121**, 295–304.
- [14] Haass, C & Selkoe, D. J. (1993) Cellular Processing of P-Amyloid Precursor Protein and the Genesis of Amyloid P-Peptide Minireview. *Cell* **75**, 1039–1042.
- [15] Cao, X & Sudhof, T. C. (2001) A transcriptionally active complex of APP with Fe65 and histone acetyltransferase Tip60. *Science* **293**, 115–120.
- [16] Holtzman, D. M, Morris, J. C, & Goate, A. M. (2011) Alzheimer's Disease: The Challenge of the Second Century. *Science Translational Medicine* **3**, 1–17.
- [17] Selkoe, D. J. (2001) Alzheimer's disease : Genes , proteins , and therapy. *Physiological Reviews* **81**.
- [18] Edbauer, D, Winkler, E, Regula, J. T, et al. (2003) Reconstitution of γ -secretase activity. *Nature Cell Biology* **5**, 486–488.
- [19] Haass, C. (2004) Take five - BACE and the γ -secretase quartet conduct Alzheimer's amyloid β -peptide generation. *EMBO Journal* **23**, 483–488.
- [20] Steiner, H, Fukumori, A, Tagami, S, & Okochi, M. (2018) Making the final cut: Pathogenic amyloid- β peptide generation by γ -secretase. *Cell Stress* **2**, 292–310.
- [21] Murphy, M. P & Levine, H. (2010) Alzheimer's disease and the amyloid- β peptide. *Journal of Alzheimer's Disease* **19**, 311–323.
- [22] Iwatsubo, T, Odaka, A, Suzuki, N, et al. (1994) Visualization of A β 42(43) and A β 40 in senile plaques with end-specific A β monoclonals: Evidence that an initially deposited species is A β 42(43). *Neuron* **13**, 45–53.

- [23] Saido, T. C, Iwatsubo, T, Mann, D. M, et al. (1995) Dominant and differential deposition of distinct β -amyloid peptide species, A β N3(pE), in senile plaques. *Neuron* **14**, 457–466.
- [24] Frost, S, Kanagasingam, Y, Sohrabi, H, et al. (2013) Retinal vascular biomarkers for early detection and monitoring of Alzheimer’s disease. *Translational Psychiatry* **3**.
- [25] Selkoe, D. J & Schenk, D. (2003) Alzheimer’s Disease: Molecular Understanding Predicts Amyloid-Based Therapeutics. *Annual Review of Pharmacology and Toxicology* **43**, 545–584.
- [26] Puig, K. L & Combs, C. K. (2013) Expression and Function of APP and its Metabolites Outside the Central Nervous System. *Experimental Gerontology* **48**, 608–611.
- [27] Brothers, H. M, Gosztyla, M. L, & Robinson, S. R. (2018) The physiological roles of amyloid- β peptide hint at new ways to treat Alzheimer’s disease. *Frontiers in Aging Neuroscience* **10**, 1–16.
- [28] Morley, J, Farr, S, Banks, W, et al. (2010) A Physiological Role for Amyloid Beta Protein: Enhancement of Learning and Memory. *Journal of Alzheimer’s Disease* **19**, 441–9.
- [29] Puzzo, D, Privitera, L, Fa, M, et al. (2011) Endogenous Amyloid- β is Necessary for Hippocampal Synaptic Plasticity and Memory. *Annals of Neurology* **69**, 819–830.
- [30] Morley, J. E & Farr, S. A. (2012) Hormesis and amyloid- β protein: Physiology or pathology? *Journal of Alzheimer’s Disease* **29**, 487–492.
- [31] Morley, J. E, Farr, S. A, Nguyen, A. D, & Xu, F. (2019) What is the Physiological Function of Amyloid-Beta Protein? *Journal of Nutrition, Health and Aging* **23**, 225–226.
- [32] Mawuenyega, K. G, Sigurdson, W, Ovod, V, et al. (2010) Decreased clearance of CNS β -amyloid in Alzheimer’s disease. *Science* **330**, 1774.
- [33] Saido, T & Leissring, M. A. (2012) Proteolytic Degradation of Amyloid b-Protein. *Cold Spring Harbor Perspectives in Medicine* **2**, 1–18.

- [34] Finder, V. H & Glockshuber, R. (2007) Amyloid- β aggregation. *Neurodegenerative Diseases* **4**, 13–27.
- [35] Ahmed, M, Davis, J, Aucoin, D, et al. (2010) Structural conversion of neurotoxic amyloid-B 1-42 oligomers to fibrils. *Nature Structural and Molecular Biology* **17**, 561–567.
- [36] Friedrich, R. P, Tepper, K, Rönicke, R, et al. (2010) Mechanism of amyloid plaque formation suggests an intracellular basis of A β pathogenicity. *Proceedings of the National Academy of Sciences of the United States of America* **107**, 1942–1947.
- [37] Bitan, G, Kirkitadze, M. D, Lomakin, A, et al. (2003) Amyloid-beta protein (A β) assembly : A β 40 and A β 42 oligomerize through distinct pathways. *Proceedings of the National Academy of Sciences of the United States of America* **100**, 330–335.
- [38] Geula, C, Mesulam, M.-M, Saroff, D. M, & Wu, C.-K. (1998) Relationship between Plaques, Tangles and Loss of Cortical Cholinergic Fibers in Alzheimer’s Disease. *Journal of Neuropathology and Experimental Neurology* **57**, 63–75.
- [39] Yankner, B. A & Lu, T. (2009) Amyloid β -protein toxicity and the pathogenesis of Alzheimer disease. *Journal of Biological Chemistry* **284**, 4755–4759.
- [40] O’Hare, E, Weldon, D. T, Mantyh, P. W, et al. (1999) Delayed behavioral effects following intrahippocampal injection of aggregated A β (1-42). *Brain Research* **815**, 1–10.
- [41] Cleary, J. P, Walsh, D. M, Hofmeister, J. J, et al. (2005) Natural oligomers of the amyloid- β protein specifically disrupt cognitive function. *Nature Neuroscience* **8**, 79–84.
- [42] Shankar, G. M, Bloodgood, B. L, Townsend, M, et al. (2007) Natural oligomers of the Alzheimer amyloid- β protein induce reversible synapse loss by modulating an NMDA-type glutamate receptor-dependent signaling pathway. *Journal of Neuroscience* **27**, 2866–2875.

- [43] Selkoe, D. J. (2008) Soluble Oligomers of the Amyloid β -Protein Impair Synaptic Plasticity and Behavior. *Behavioural brain research* **192**, 106–113.
- [44] Terry, R. D, Masliah, E, Salmon, D. P, et al. (1991) Physical Basis of Cognitive Alterations in Alzheimer's Disease: Synapse hss Is the Major Correlate of Cognitive Impairment. *Annals of Neurology* **30**, 572–580.
- [45] Dahlgren, K. N, Manelli, A. M, Blaine Stine, W, et al. (2002) Oligomeric and fibrillar species of amyloid- β peptides differentially affect neuronal viability. *Journal of Biological Chemistry* **277**, 32046–32053.
- [46] Walsh, D. M, Klyubin, I, Fadeeva, J. V, et al. (2002) Naturally secreted oligomers of amyloid β protein potently inhibit hippocampal long-term potentiation in vivo. *Nature* **416**, 535–539.
- [47] Hsia, A. Y, Masliah, E, Mcconlogue, L, et al. (1999) Plaque-independent disruption of neural circuits in Alzheimer's disease mouse models. *Proceedings of the National Academy of Sciences of the United States of America* **96**, 3228–3233.
- [48] Mucke, L, Masliah, E, Yu, G, et al. (2000) High-Level Neuronal Expression of A β 1–42 in Wild-Type Human Amyloid Precursor Transgenic Mice: Synaptotoxicity without Plaque Formation.pdf. *J Neurosci* **20**, 4050–8.
- [49] Westerman, M. A, Cooper-Blacketer, D, Mariash, A, et al. (2002) The relationship between A β and memory in the Tg2576 mouse model of Alzheimer's disease. *Journal of Neuroscience* **22**, 1858–1867.
- [50] Dickson, D. W. (1997) Neuropathological diagnosis of Alzheimer's disease: A perspective from longitudinal clinicopathological studies. *Neurobiology of Aging* **18**.
- [51] Tsai, J, Grutzendler, J, Duff, K, & Gan, W. B. (2004) Fibrillar amyloid deposition leads to local synaptic abnormalities and breakage of neuronal branches. *Nature Neuroscience* **7**, 1181–1183.
- [52] Haass, C & Selkoe, D. J. (2007) Soluble protein oligomers in neurodegeneration: Lessons from the Alzheimer's amyloid β -peptide. *Nature Reviews Molecular Cell Biology* **8**, 101–112.

- [53] Ferreira, S. T & Klein, W. L. (2011) The A β oligomer hypothesis for synapse failure and memory loss in Alzheimer's disease. *Neurobiology of Learning and Memory* **96**, 529–543.
- [54] Pearson, H. A & Peers, C. (2006) Physiological roles for amyloid β peptides. *Journal of Physiology* **575**, 5–10.
- [55] Koffie, R. M, Meyer-Luehmann, M, Hashimoto, T, et al. (2009) Oligomeric amyloid β associates with postsynaptic densities and correlates with excitatory synapse loss near senile plaques. *Proceedings of the National Academy of Sciences of the United States of America* **106**, 4012–4017.
- [56] Van Groen, T, Miettinen, P, & Kadish, I. (2011) Transgenic AD model mice, effects of potential anti-AD treatments on inflammation, and pathology. *Journal of Alzheimer's Disease* **24**, 301–313.
- [57] Greenberg, S. M, Bacskai, B. J, Hernandez-Guillamon, M, et al. (2020) Cerebral amyloid angiopathy and Alzheimer disease — one peptide, two pathways. *Nature Reviews Neurology* **16**, 30–42.
- [58] Charidimou, A, Boulouis, G, Gurol, M. E, et al. (2017) Emerging concepts in sporadic cerebral amyloid angiopathy. *Brain* **140**, 1829–1850.
- [59] Suzuki, N, Cheung, T. T, Cai, X.-D, et al. (1994) Increased percentage AB42 secreted by familial amyloid b protein precursor (bAPP717) mutants. *Science* pp. 15–19.
- [60] Yamada, M. (2015) Cerebral amyloid angiopathy: Emerging concepts. *Journal of Stroke* **17**, 17–30.
- [61] Braak, H & Braak, E. (1997) Frequency of Stages of Alzheimer-Related Lesions in Different Age Categories. *Neurobiology of Aging*.
- [62] Thal, D. R, Rüb, U, Orantes, M, & Braak, H. (2002) Phases of A β -deposition in the human brain and its relevance for the development of AD. *Neurology* **58**, 1791–1800.
- [63] Iqbal, K, Del C. Alonso, A, Chen, S, et al. (2005) Tau pathology in Alzheimer disease

- and other tauopathies. *Biochimica et Biophysica Acta - Molecular Basis of Disease* **1739**, 198–210.
- [64] Kopke, E, Tung, Y. C, Shaikh, S, et al. (1993) Microtubule-associated protein tau. Abnormal phosphorylation of a non- paired helical filament pool in Alzheimer disease. *Journal of Biological Chemistry* **268**, 24374–24384.
- [65] Lindwall, G & Cole, R. D. (1984) Phosphorylation affects the ability of tau protein to promote microtubule assembly. *Journal of Biological Chemistry* **259**, 5301–5305.
- [66] Alonso, A. D. C, Zaidi, T, Grundke-Iqbal, I, & Iqbal, K. (1994) Role of abnormally phosphorylated tau in the breakdown of microtubules in Alzheimer disease. *Proceedings of the National Academy of Sciences of the United States of America* **91**, 5562–5566.
- [67] Wiśniewski, H. M, Narang, H. K, & Terry, R. D. (1976) Neurofibrillary tangles of paired helical filaments. *Journal of the Neurological Sciences* **27**, 173–181.
- [68] Grundke-Iqbal, I, Iqbal, K, Tung, Y. C, et al. (1986) Abnormal phosphorylation of the microtubule-associated protein tau (tau) in Alzheimer cytoskeletal pathology. *Proceedings of the National Academy of Sciences of the United States of America* **83**, 4913–4917.
- [69] Alafuzoff, I, Iqbal, K, Friden, H, et al. (1987) Histopathological criteria for progressive dementia disorders: clinical-pathological correlation and classification by multivariate data analysis. *Acta Neuropathologica* **74**, 209–225.
- [70] Arriagada, P. V, Marzloff, K, & Hyman, B. T. (1992) Distribution of Alzheimer-type pathologic changes in nondemented elderly individuals matches the pattern in Alzheimer's disease. *Neurology*.
- [71] Spires-Jones, T. L & Hyman, B. T. (2014) The Intersection of Amyloid Beta and Tau at Synapses in Alzheimer's Disease. *Neuron* **82**, 756–771.
- [72] Braak, H & Braak, E. (1996) Development of Alzheimer-related neurofibrillary changes in the neocortex inversely recapitulates cortical myelogenesis. *Acta Neuropathologica* **92**, 197–201.

- [73] Woodhouse, A, West, A. K, Chuckowree, J. A, et al. (2005) Does β -amyloid plaque formation cause structural injury to neuronal processes? *Neurotoxicity Research* **7**, 5–15.
- [74] Serrano-Pozo, A, Mielke, M. L, Gómez-Isla, T, et al. (2011) Reactive glia not only associates with plaques but also parallels tangles in Alzheimer’s disease. *American Journal of Pathology* **179**, 1373–1384.
- [75] Benzing, W. C, Wujek, J. R, Ward, E. K, et al. (1999) Evidence for glial-mediated inflammation in aged APP(SW) transgenic mice. *Neurobiology of Aging* **20**, 581–589.
- [76] Leng, F & Edison, P. (2021) Neuroinflammation and microglial activation in Alzheimer disease: where do we go from here?
- [77] McGeer, P. L, Itagaki, S, Tago, H, & McGeer, E. G. (1987) Reactive microglia in patients with senile dementia of the Alzheimer type are positive for the histocompatibility glycoprotein HLA-DR. *Neuroscience Letters* **79**, 195–200.
- [78] Akiyama, H, Barger, S, Barnum, S, et al. (2000) *Inflammation and Alzheimer’s Disease*. Vol. 21, pp. 383–421.
- [79] Wyss-Coray, T. (2006) Inflammation in Alzheimer disease: driving force, bystander or beneficial response? *Nature Medicine* **12**, 1005–1015.
- [80] Motta, M, Imbesi, R, Di Rosa, M, et al. (2007) Altered plasma cytokine levels in Alzheimer’s disease: Correlation with the disease progression. *Immunology Letters* **114**, 46–51.
- [81] Saito, T & Saido, T. C. (2018) Neuroinflammation in mouse models of Alzheimer’s disease.
- [82] Heneka, M. T, Kummer, M. P, & Latz, E. (2014) Innate immune activation in neurodegenerative disease. *Nature Reviews Immunology* **14**, 463–477.
- [83] DiSabato, D. J, Quan, N, & Godbout, J. P. (2016) Neuroinflammation: the devil is in the details. *Journal of Neurochemistry* **139**, 136–153.

- [84] Simard, M & Nedergaard, M. (2004) The neurobiology of glia in the context of water and ion homeostasis. *Neuroscience* **129**, 877–896.
- [85] Rouach, N, Koulakoff, A, Abudara, V, et al. (2008) Astroglial metabolic networks sustain hippocampal synaptic transmission. *Science* **322**, 1551–1555.
- [86] Attwell, D, Buchan, A. M, Charpak, S, et al. (2010) Glial and neuronal control of brain blood flow. *Nature* **468**, 232–243.
- [87] Eroglu, C & Barres, B. A. (2010) Regulation of synaptic connectivity by glia. *Nature* **468**, 223–231.
- [88] Pekny, M & Pekna, M. (2014) Astrocyte reactivity and reactive astrogliosis: Costs and benefits. *Physiological Reviews* **94**, 1077–1098.
- [89] Jessen, N. A, Munk, A. S. F, Lundgaard, I, & Nedergaard, M. (2015) The Glymphatic System: A Beginner’s Guide. *Neurochemical Research* **40**, 2583–2599.
- [90] Tarasoff-Conway, J. M, Carare, R. O, Osorio, R. S, et al. (2015) Clearance systems in the brain - Implications for Alzheimer disease. *Nature Reviews Neurology* **11**, 457–470.
- [91] Liddelow, S. A & Barres, B. A. (2017) Reactive Astrocytes: Production, Function, and Therapeutic Potential. *Immunity* **46**, 957–967.
- [92] Liddelow, S. A, Guttenplan, K. A, Clarke, L. E, et al. (2017) Neurotoxic reactive astrocytes are induced by activated microglia. *Nature* **541**, 481–487.
- [93] Jo, S, Yarishkin, O, Hwang, Y. J, et al. (2014) GABA from reactive astrocytes impairs memory in mouse models of Alzheimer’s disease. *Nature Medicine* **20**, 886–896.
- [94] Winkler, E. A, Nishida, Y, Sagare, A. P, et al. (2015) GLUT1 reductions exacerbate Alzheimer’s disease vasculo-neuronal dysfunction and degeneration. *Nature Neuroscience* **18**, 521–530.

- [95] Kisler, K, Nelson, A. R, Montagne, A, & Zlokovic, B. V. (2017) Cerebral blood flow regulation and neurovascular dysfunction in Alzheimer disease. *Nature Reviews Neuroscience* **18**, 419–434.
- [96] Zhang, H, Wu, L, Pchitskaya, E, et al. (2015) Neuronal store-operated calcium entry and mushroom spine loss in amyloid precursor protein knock-in mouse model of Alzheimer’s disease. *Journal of Neuroscience* **35**, 13275–13286.
- [97] Fakhoury, M. (2018) Microglia and astrocytes in Alzheimer’s disease: implications for therapy. *Current Neuropharmacology* **15**, 508–518.
- [98] Nimmerjahn, A, Kirchhoff, F, & Helmchen, F. (2005) Neuroscience: Resting microglial cells are highly dynamic surveillants of brain parenchyma in vivo. *Science* **308**, 1314–1318.
- [99] Davalos, D, Grutzendler, J, Yang, G, et al. (2005) ATP mediates rapid microglial response to local brain injury in vivo. *Nature Neuroscience* **8**, 752–758.
- [100] Bernier, L. P, Bohlen, C. J, York, E. M, et al. (2019) Nanoscale Surveillance of the Brain by Microglia via cAMP-Regulated Filopodia. *Cell Reports* **27**, 2895–2908.e4.
- [101] Heneka, M. T, Carson, M. J, Khoury, J. E, et al. (2015) Neuroinflammation in Alzheimer’s disease. *The Lancet Neurology* **14**, 388–405.
- [102] Solé-Domenech, S, Cruz, D, Capetillo-Zarate, E, & Maxfield, F. R. (2016) The Endocytic Pathway in Microglia During Health, Aging and Alzheimer’s Disease. *Ageing Res Rev.* **32**, 89–103.
- [103] Novikova, G, Kapoor, M, Tcw, J, et al. (2021) Integration of Alzheimer’s disease genetics and myeloid genomics identifies disease risk regulatory elements and genes. *Nature Communications* **12**.
- [104] Ries, M & Sastre, M. (2016) Mechanisms of A β clearance and degradation by glial cells. *Frontiers in Aging Neuroscience* **8**, 1–9.
- [105] Kaur, D, Sharma, V, & Deshmukh, R. (2019) Activation of microglia and astrocytes: a roadway to neuroinflammation and Alzheimer’s disease.

- [106] Metcalfe, M. J & Figueiredo-Pereira, M. E. (2010) Relationship Between Tau Pathology and Neuroinflammation in Alzheimer's Disease. *Mount Sinai Journal of Medicine* **77**, 50–58.
- [107] Asai, H, Ikezu, S, Tsunoda, S, et al. (2015) Depletion of microglia and inhibition of exosome synthesis halt tau propagation. *Nature Neuroscience* **18**, 1584–1593.
- [108] Maphis, N, Xu, G, Kokiko-Cochran, O. N, et al. (2015) Reactive microglia drive tau pathology and contribute to the spreading of pathological tau in the brain. *Brain* **138**, 1738–1755.
- [109] Parhizkar, S, Arzberger, T, Brendel, M, et al. (2019) Loss of TREM2 function increases amyloid seeding but reduces plaque-associated ApoE. *Nature Neuroscience* **22**, 191–204.
- [110] Spangenberg, E, Severson, P. L, Hohsfield, L. A, et al. (2019) Sustained microglial depletion with CSF1R inhibitor impairs parenchymal plaque development in an Alzheimer's disease model. *Nature Communications* **10**, 1–21.
- [111] Du, L, Zhang, Y, Chen, Y, et al. (2017) Role of Microglia in Neurological Disorders and Their Potentials as a Therapeutic Target. *Molecular Neurobiology* **54**, 7567–7584.
- [112] Hardy, J. A & Higgins, G. A. (1992) Alzheimer ' s Disease : The Amyloid Cascade Hypothesis Published by : American Association for the Advancement of Science Alzheimer ' s Disease : The Amyloid Cascade Hypothesis. *Science* **256**, 184–185.
- [113] Selkoe, D. J & Hardy, J. (2016) The amyloid hypothesis of Alzheimer's disease at 25 years. *EMBO Molecular Medicine* **8**, 595–608.
- [114] Thorlakur Jonsson, Ph.D., Hreinn Stefansson, Ph.D., Stacy Steinberg, Ph.D., Ingileif Jonsdottir, Ph.D., Palmi V. Jonsson, M.D., Jon Snaedal, M.D., Sigurbjorn Bjornsson, M.D., Johanna Huttenlocher, B.S., Allan I. Levey, M.D., Ph.D., James J. Lah, M.D., Ph., P & From. (2013) Variant of TREM2 associated with the risk of Alzheimer's Disease. *New England Journal of Medicine* **368**, 107–116.

- [115] Arriagada, P. V, Marzloff, K, & Hyman, B. T. (1992) Distribution of Alzheimer-type pathologic changes in nondemented elderly individuals matches the pattern in Alzheimer's disease. *Neurology* **42**, 1681–1688.
- [116] Hyman, B. T, Marzloff, K, & Arriagada, P. V. (1993) The lack of accumulation of senile plaques or amyloid burden in Alzheimer's Disease suggests a dynamic balance between amyloid deposition and resolution. *Journal of Neuropathology and Experimental Neurology* **52**, 594–600.
- [117] Bierer, L. M, Haroutunian, V, Gabriel, S, et al. (1995) Neurochemical Correlates of Dementia Severity in Alzheimer's Disease: Relative Importance of the Cholinergic Deficits. *Journal of Neurochemistry* **64**, 749–760.
- [118] Gomez-Isla, T. (1997) Neuron Loss Correlates with but Exceeds Neurofibrillary Tangles in Alzheimer's Disease. *Annals of Neurology* **41**, 17–24.
- [119] Ingelsson, M, Fukumoto, H, Newell, K. L, et al. (2004) Early A β accumulation and progressive synaptic loss, gliosis, and tangle formation in AD brain. *Neurology* **62**, 925–931.
- [120] Ricciarelli, R & Fedele, E. (2017) The Amyloid Cascade Hypothesis in Alzheimer's Disease: It's Time to Change Our Mind. *Current Neuropharmacology* **15**, 926–935.
- [121] Makin, S. (2018) The amyloid hypothesis on trial. *Nature* **559**, 4–7.
- [122] S. Gilman, M. Koller, R.S. Black, L. Jenkins, S.G. Griffith, N.C. Fox, L. Eisner, L. Kirby, M. Boada Rovira, F. Forette, J. O. (2005) Clinical Effect of AB immunization (AN1792) in patients with AD in an interrupted trial. *Neurology* **64**, 1553–1562.
- [123] Farlow, M, Arnold, S. E, Van Dyck, C. H, et al. (2012) Safety and biomarker effects of solanezumab in patients with Alzheimer's disease. *Alzheimer's and Dementia* **8**, 261–271.
- [124] Ostrowitzki, S, Deptula, D, Thurfjell, L, et al. (2012) Mechanism of amyloid removal in patients with Alzheimer disease treated with gantenerumab. *Archives of Neurology* **69**, 198–207.

- [125] Bateman, R. J, Xiong, C, Benzinger, T. L, et al. (2012) Clinical and Biomarker Changes in Dominantly Inherited Alzheimer's Disease. *New England Journal of Medicine* **367**, 795–804.
- [126] Mullan, M, Crawford, F, Axelman, K, et al. (1992) Mullan, M., Crawford, F., Axelman, K., Houlden, H., Lilius, L., Winblad, B. & Lannfelt, L. (1992) A pathogenic mutation for probable Alzheimer's disease in the APP gene at the N-terminus of beta-amyloid, *Nat Genet.* 1, 345-7. *Nature* **I**, 345–347.
- [127] Nilsberth, C, Westlind-Danielsson, A, Eckman, C. B, et al. (2001) The 'Arctic' APP mutation (E693G) causes Alzheimer's disease by enhanced A β protofibril formation. *Nature Neuroscience* **4**, 887–893.
- [128] Eckman, C. B, Mehta, N. D, Crook, R, et al. (1997) A new pathogenic mutation in the APP gene (1716V) increases the relative proportion of A β 42(43). *Human Molecular Genetics* **6**, 2087–2089.
- [129] Murrell, J, Farlow, M, Ghetti, B, & Benson, M. D. (1991) A Mutation in the Amyloid Precursor Protein Associated with Hereditary Alzheimer 's Disease. *Science* **254**, 97–99.
- [130] De Jonghe, C. (2001) Pathogenic APP mutations near the gamma-secretase cleavage site differentially affect Abeta secretion and APP C-terminal fragment stability. *Human Molecular Genetics* **10**, 1665–1671.
- [131] Cruts, M, Van Duijn, C. M, Backhovens, H, et al. (1998) Estimation of the genetic contribution of presenilin-1 and -2 mutations in a population-based study of presenile Alzheimer disease. *Human Molecular Genetics* **7**, 43–51.
- [132] Singleton, A. B, Hall, R, Ballard, C. G, et al. (2000) Pathology of early-onset Alzheimer's disease cases bearing the Thr113-114ins presenilin-1 mutation. *Brain* **123**, 2467–2474.
- [133] Borchelt, D. R & Thinakaran, G. (1996) Familial Alzheimer's Disease-Linked Presenilin 1 Variants Elevate A1-42/1-40 Ratio In Vitro and In Vivo. *Neuron* **17**, 1005–1013.

- [134] De Strooper, B. (2007) Loss-of-function presenilin mutations in Alzheimer disease. Talking Point on the role of presenilin mutations in Alzheimer disease. *EMBO Reports* **8**, 141–146.
- [135] Xia, D, Watanabe, H, Wu, B, et al. (2015) Presenilin-1 knockin mice reveal loss-of-function mechanism for familial alzheimer’s disease. *Neuron* **85**, 967–981.
- [136] Slooter, A. J, Cruts, M, Kalmijn, S, et al. (1998) Risk estimates of dementia by apolipoprotein E genotypes from a population-based incidence study: The Rotterdam study. *Archives of Neurology* **55**, 964–968.
- [137] Parasuraman, R, Greenwood, P. M, & Sunderland, T. (2002) The apolipoprotein E gene, attention, and brain function. *Neuropsychology* **16**, 254–274.
- [138] Liao, F, Yoon, H, & Kim, J. (2017) Apolipoprotein e metabolism and functions in brain and its role in Alzheimer’s disease. *Current Opinion in Lipidology* **28**, 60–67.
- [139] Huang, Y & Mahley, R. W. (2014) Apolipoprotein E: Structure and Function in Lipid Metabolism, Neurobiology, and Alzheimer’s Disease. *Neurobiology of Disease* **72**, 3–12.
- [140] Kim, J, Basak, J. M, & Holtzman, D. M. (2009) The Role of Apolipoprotein E in Alzheimer’s Disease. *Neuron* **63**, 287–303.
- [141] Cuyvers, E & Sleegers, K. (2016) Genetic variations underlying Alzheimer’s disease: Evidence from genome-wide association studies and beyond. *The Lancet Neurology* **15**, 857–868.
- [142] de Rojas, I, Moreno-Grau, S, Tesi, N, et al. (2021) Common variants in Alzheimer’s disease and risk stratification by polygenic risk scores. *Nature Communications* **12**.
- [143] Bertram, L, Lange, C, Mullin, K, et al. (2008) Genome-wide Association Analysis Reveals Putative Alzheimer’s Disease Susceptibility Loci in Addition to APOE. *American Journal of Human Genetics* **83**, 623–632.
- [144] Karch, C. M, Jeng, A. T, Nowotny, P, et al. (2012) Expression of Novel Alzheimer’s Disease Risk Genes in Control and Alzheimer’s Disease Brains. *PLoS ONE* **7**.

- [145] Lambert, J. C, Ibrahim-Verbaas, C. A, Harold, D, et al. (2013) Meta-analysis of 74,046 individuals identifies 11 new susceptibility loci for Alzheimer’s disease. *Nature Genetics* **45**, 1452–1458.
- [146] Sims, R, Van Der Lee, S. J, Naj, A. C, et al. (2017) Rare coding variants in PLCG2, ABI3, and TREM2 implicate microglial-mediated innate immunity in Alzheimer’s disease. *Nature Genetics* **49**, 1373–1384.
- [147] Nott, A, Holtman, I. R, Coufal, N. G, et al. (2019) Brain cell type-specific enhancer–promoter interactome maps and disease-risk association. *Science* **366**, 1134–1139.
- [148] Andrews, S. J, Fulton-Howard, B, O’Reilly, P, et al. (2020) Causal Associations Between Modifiable Risk Factors and the Alzheimer’s Phenome. *Annals of Neurology*.
- [149] Lee, J. Y, Marian, O. C, & Don, A. S. (2021) Defective Lysosomal Lipid Catabolism as a Common Pathogenic Mechanism for Dementia.
- [150] Podleśny-Drabiniok, A, Marcora, E, & Goate, A. M. (2020) Microglial Phagocytosis: A Disease-Associated Process Emerging from Alzheimer’s Disease Genetics.
- [151] Bellenguez, C, Küçükali, F, Jansen, I. E, et al. (2022) New insights into the genetic etiology of Alzheimer’s disease and related dementias. *Nature Genetics* **54**, 412–436.
- [152] Efstathiou, A. G & Goate, A. M. (2017) Late onset Alzheimer’s disease genetics implicates microglial pathways in disease risk.
- [153] Piovesan, A, Antonaros, F, Vitale, L, et al. (2019) Human protein-coding genes and gene feature statistics in 2019. *BMC Research Notes* **12**.
- [154] Palazzo, A. F & Koonin, E. V. (2020) Functional Long Non-coding RNAs Evolve from Junk Transcripts. *Cell* **183**, 1151–1161.
- [155] McQuade, A & Blurton-Jones, M. (2019) Microglia in Alzheimer’s Disease: Exploring How Genetics and Phenotype Influence Risk. *Journal of Molecular Biology* **431**, 1805–1817.

- [156] Daria, A, Colombo, A, Llovera, G, et al. (2017) Young microglia restore amyloid plaque clearance of aged microglia. *The EMBO Journal* **36**, 583–603.
- [157] Mosher, K & Wyss-Coray, T. (2014) Microglial Dysfunction in Brain Aging and Alzheimer’s Disease. *Biochemical Pharmacology* **88**, 594–604.
- [158] Mhatre, S. D, Tsai, C. A, Rubin, A. J, et al. (2015) Microglial Malfunction: The Third Rail in the Development of Alzheimer’s Disease. *Trends in Neurosciences* **38**, 621–636.
- [159] Crehan, H, Hardy, J, & Pocock, J. (2013) Blockage of CR1 prevents activation of rodent microglia. *Neurobiology of Disease* **54**, 139–149.
- [160] Lawson, L. J, Perry, V. H, & Gordon, S. (1992) Turnover of resident microglia in the normal adult mouse brain. *Neuroscience* **48**, 405–415.
- [161] Mittelbronn, M, Dietz, K, Schluesener, H. J, & Meyermann, R. (2001) Local distribution of microglia in the normal adult human central nervous system differs by up to one order of magnitude. *Acta Neuropathologica* **101**, 249–255.
- [162] Mosser, C. A, Baptista, S, Arnoux, I, & Audinat, E. (2017) Microglia in CNS development: Shaping the brain for the future. *Progress in Neurobiology* **149-150**, 1–20.
- [163] Hansen, D. V, Hanson, J. E, & Sheng, M. (2017) Microglia in Alzheimer ’ s disease
Microglia in Alzheimer ’ s disease. *Journal of Cell Biology* **217**, 459–472.
- [164] Li, Q & Barres, B. A. (2018) Microglia and macrophages in brain homeostasis and disease. *Nature Reviews Immunology* **18**, 225–242.
- [165] Hoeffel, G & Ginhoux, F. (2018) Fetal monocytes and the origins of tissue-resident macrophages. *Cellular Immunology* **330**, 5–15.
- [166] Thion, M. S, Ginhoux, F, & Garel, S. (2018) Microglia and early brain development: An intimate journey. *Science*.
- [167] Sierra, A, Paolicelli, R. C, & Kettenmann, H. (2019) Cien Años de Microglía: Milestones in a Century of Microglial Research.

- [168] Prinz, M, Jung, S, & Priller, J. (2019) Microglia Biology: One Century of Evolving Concepts. *Cell* **179**, 292–311.
- [169] Thion, M. S & Garel, S. (2020) Microglial ontogeny, diversity and neurodevelopmental functions.
- [170] Colonna, M & Butovsky, O. (2017) Microglia Function in the Central Nervous System During Health and Neurodegeneration. *Annu. Rev. Immunol.*
- [171] Stremmel, C, Schuchert, R, Wagner, F, et al. (2018) Yolk sac macrophage progenitors traffic to the embryo during defined stages of development. *Nature Communications* **9**.
- [172] Liu, Y, Cheng, A, Li, Y. J, et al. (2019) SIRT3 mediates hippocampal synaptic adaptations to intermittent fasting and ameliorates deficits in APP mutant mice. *Nature Communications* **10**.
- [173] Sidman, R. L & Rakic, P. (1973) Neuronal Migration with Special Reference to Developing Human Brain: a Review. *Brain Research* **62**, 1–35.
- [174] Muroyama, Y, Fujiwara, Y, Orkin, S. H, & Rowitch, D. H. (2005) Specification of astrocytes by bHLH protein SCL in a restricted region of the neural tube. *Nature* **438**, 360–363.
- [175] Rowitch, D. H & Kriegstein, A. R. (2010) Developmental genetics of vertebrate glial-cell specification. *Nature* **468**, 214–222.
- [176] Ginhoux, F, Greter, M, Leboeuf, M, et al. (2010) Fate mapping analysis reveals that adult microglia derive from primitive macrophages. *Science* **330**, 841–845.
- [177] Kierdorf, K, Erny, D, Goldmann, T, et al. (2013) Microglia emerge from erythromyeloid precursors via Pu.1-and Irf8-dependent pathways. *Nature Neuroscience* **16**, 273–280.
- [178] Bian, Z, Gong, Y, Huang, T, et al. (2020) Deciphering human macrophage development at single-cell resolution. *Nature* **582**, 571–576.

- [179] Profaci, C. P, Munji, R. N, Pulido, R. S, & Daneman, R. (2020) The blood–brain barrier in health and disease: Important unanswered questions. *Journal of Experimental Medicine* **217**, 1–16.
- [180] Werner, Y, Mass, E, Ashok Kumar, P, et al. (2020) Cxcr4 distinguishes HSC-derived monocytes from microglia and reveals monocyte immune responses to experimental stroke. *Nature Neuroscience* **23**, 351–362.
- [181] Crotti, A & Ransohoff, R. M. (2016) Microglial Physiology and Pathophysiology: Insights from Genome-wide Transcriptional Profiling.
- [182] Dai, X. M, Ryan, G. R, Hapel, A. J, et al. (2002) Targeted disruption of the mouse colony-stimulating factor 1 receptor gene results in osteopetrosis, mononuclear phagocyte deficiency, increased primitive progenitor cell frequencies, and reproductive defects. *Blood* **99**, 111–120.
- [183] Elmore, M, Najafi, A. R, Koike, M. A, et al. (2014) CSF1 receptor signaling is necessary for microglia viability, which unmask a cell that rapidly repopulates the microglia- depleted adult brain. *Neuron* **82**, 380–397.
- [184] Shi, Y, Cui, M, Ochs, K, et al. (2022) Long-term diazepam treatment enhances microglial spine engulfment and impairs cognitive performance via the mitochondrial 18 kDa translocator protein (TSPO). *Nature Neuroscience* **25**, 317–329.
- [185] Lin, H, Lee, E, Hestir, K, et al. (2008) Discovery of a Cytokine and Its Receptor by Functional Screening of the Extracellular Proteome. *Science* **320**, 807–811.
- [186] Ma, X, Lin, W. Y, Chen, Y, et al. (2012) Structural basis for the dual recognition of helical cytokines IL-34 and CSF-1 by CSF-1R. *Structure* **20**, 676–687.
- [187] Tay, T. L, Mai, D, Dautzenberg, J, et al. (2017) A new fate mapping system reveals context-dependent random or clonal expansion of microglia. *Nature Neuroscience* **20**, 793–803.
- [188] Askew, K, Li, K, Olmos-Alonso, A, et al. (2017) Coupled Proliferation and Apoptosis Maintain the Rapid Turnover of Microglia in the Adult Brain. *Cell Reports* **18**, 391–405.

- [189] Füger, P, Hefendehl, J. K, Veeraraghavalu, K, et al. (2017) Microglia turnover with aging and in an Alzheimer’s model via long-term in vivo single-cell imaging. *Nature Neuroscience* **20**, 1371–1376.
- [190] Réu, P, Khosravi, A, Bernard, S, et al. (2017) The Lifespan and Turnover of Microglia in the Human Brain. *Cell Reports* **20**, 779–784.
- [191] Matcovitch-Natan, O, Winter, D. R, Giladi, A, et al. (2016) Microglia development follows a stepwise program to regulate brain homeostasis. *Science* **353**.
- [192] Lawson, L. J, Perry, V. H, Dri, P, & Gordon, S. (1990) Heterogeneity in the distribution and morphology of microglia in the normal adult mouse brain. *Neuroscience* **39**, 151–170.
- [193] Marín-Teva, J. L, Dusart, I, Colin, C, et al. (2004) Microglia Promote the Death of Developing Purkinje Cells. *Neuron* **41**, 535–547.
- [194] Frost, J. L & Schafer, D. P. (2016) Microglia: Architects of the Developing Nervous System. *Trends in Cell Biology* **26**, 587–597.
- [195] Stevens, B, Allen, N. J, Vazquez, L. E, et al. (2007) The Classical Complement Cascade Mediates CNS Synapse Elimination. *Cell* **131**, 1164–1178.
- [196] Schafer, D. P & Stevens, B. (2010) Synapse elimination during development and disease: Immune molecules take centre stage.
- [197] Schafer, D. P, Lehrman, E. K, Kautzman, A. G, et al. (2012) Microglia Sculpt Postnatal Neural Circuits in an Activity and Complement-Dependent Manner. *Neuron* **74**, 691–705.
- [198] Stephan, A. H, Barres, B. A, & Stevens, B. (2012) The complement system: An unexpected role in synaptic pruning during development and disease. *Annual Review of Neuroscience* **35**, 369–389.
- [199] Hagemeyer, N, Hanft, K. M, Akriditou, M. A, et al. (2017) Microglia contribute to normal myelinogenesis and to oligodendrocyte progenitor maintenance during adulthood. *Acta Neuropathologica* **134**, 441–458.

- [200] Wlodarczyk, A, Holtman, I. R, Krueger, M, et al. (2017) A novel microglial subset plays a key role in myelinogenesis in developing brain. *The EMBO Journal* **36**, 3292–3308.
- [201] Erbllich, B, Zhu, L, Etgen, A. M, et al. (2011) Absence of colony stimulation factor-1 receptor results in loss of microglia, disrupted brain development and olfactory deficits. *PLoS ONE* **6**.
- [202] Gosselin, D, Link, V. M, Romanoski, C. E, et al. (2014) Environment drives selection and function of enhancers controlling tissue-specific macrophage identities. *Cell* **159**, 1327–1340.
- [203] Gautiar, E. L, Shay, T, Miller, J, et al. (2012) Gene-expression profiles and transcriptional regulatory pathways that underlie the identity and diversity of mouse tissue macrophages. *Nature Immunology* **13**, 1118–1128.
- [204] Beutner, C, Linnartz-Gerlach, B, Schmidt, S. V, et al. (2013) Unique transcriptome signature of mouse microglia. *Glia* **61**, 1429–1442.
- [205] Chiu, I. M, Morimoto, E. T. A, Goodarzi, H, et al. (2013) A neurodegeneration-specific gene expression signature and immune profile of acutely isolated microglia from an ALS mouse model. *Cell Reports* **4**, 385–401.
- [206] Zhang, Y, Chen, K, Sloan, S. A, et al. (2014) An RNA-sequencing transcriptome and splicing database of glia, neurons, and vascular cells of the cerebral cortex. *Journal of Neuroscience* **34**, 11929–11947.
- [207] Butovsky, O & Weiner, H. L. (2018) Microglial signatures and their role in health and disease. *Nature Reviews Neuroscience* **19**, 622–635.
- [208] Galatro, T. F, Holtman, I. R, Lerario, A. M, et al. (2017) Transcriptomic analysis of purified human cortical microglia reveals age-associated changes. *Nature Neuroscience* **20**, 1162–1171.
- [209] Olah, M, Patrick, E, Villani, A. C, et al. (2018) A transcriptomic atlas of aged human microglia. *Nature Communications* **9**.

- [210] Hickman, S. E, Kingery, N. D, Ohsumi, T. K, et al. (2013) The microglial sensome revealed by direct RNA sequencing. *Nature Neuroscience* **16**, 1896–1905.
- [211] Hanisch, U. K & Kettenmann, H. (2007) Microglia: Active sensor and versatile effector cells in the normal and pathologic brain. *Nature Neuroscience* **10**, 1387–1394.
- [212] Rogers, J, Mastroeni, D, Leonard, B, et al. (2007) Neuroinflammation in Alzheimer’s Disease and Parkinson’s Disease: Are Microglia Pathogenic in Either Disorder? *International Review of Neurobiology* **82**, 235–246.
- [213] Walker, D. G & Lue, L. F. (2015) Immune phenotypes of microglia in human neurodegenerative disease: Challenges to detecting microglial polarization in human brains. *Alzheimer’s Research and Therapy* **7**, 1–9.
- [214] Sasaki, Y, Ohsawa, K, Kanazawa, H, et al. (2001) Iba1 is an actin-cross-linking protein in macrophages/microglia. *Biochemical and Biophysical Research Communications* **286**, 292–297.
- [215] Ohsawa, K, Imai, Y, Sasaki, Y, & Kohsaka, S. (2004) Microglia/macrophage-specific protein Iba1 binds to fimbrin and enhances its actin-bundling activity. *Journal of Neurochemistry* **88**, 844–856.
- [216] Hopperton, K. E, Mohammad, D, Trépanier, M. O, et al. (2018) Markers of microglia in post-mortem brain samples from patients with Alzheimer’s disease: A systematic review.
- [217] Schlachetzki, J. C. M & Hüll, M. (2009) Microglial Activation in Alzheimer’s Disease. *Current Alzheimer Research* **6**, 554–563.
- [218] Hickman, S. E, Allison, E. K, & El Khoury, J. (2008) Microglial dysfunction and defective β -amyloid clearance pathways in aging alzheimer’s disease mice. *Journal of Neuroscience* **28**, 8354–8360.
- [219] Meyer-Luehmann, M, Spires-Jones, T. L, Prada, C, et al. (2008) Rapid appearance and local toxicity of amyloid- β plaques in a mouse model of Alzheimer’s disease. *Nature* **451**, 720–724.

- [220] Bolmont, T, Haiss, F, Eicke, D, et al. (2008) Dynamics of the microglial/amyloid interaction indicate a role in plaque maintenance. *Journal of Neuroscience* **28**, 4283–4292.
- [221] Lee, S, Varvel, N. H, Konerth, M. E, et al. (2010) CX3CR1 deficiency alters microglial activation and reduces beta-amyloid deposition in two Alzheimer’s disease mouse models. *American Journal of Pathology* **177**, 2549–2562.
- [222] Sarlus, H & Heneka, M. T. (2017) Microglia in Alzheimer’s disease.
- [223] Hellwig, S, Masuch, A, Nestel, S, et al. (2015) Forebrain microglia from wild-type but not adult 5xFAD mice prevent amyloid- β plaque formation in organotypic hippocampal slice cultures. *Scientific Reports* **5**, 1–9.
- [224] Monasor, L. S, Müller, S. A, Colombo, A. V, et al. (2020) Fibrillar $\alpha\beta$ triggers microglial proteome alterations and dysfunction in alzheimer mouse models. *eLife* **9**, 1–33.
- [225] Hong, S, Beja-Glasser, V. F, Nfonoyim, B. M, et al. (2016) Complement and microglia mediate early synapse loss in Alzheimer mouse model. *Science* **352**.
- [226] Spangenberg, E. E, Lee, R. J, Najafi, A. R, et al. (2016) Eliminating microglia in Alzheimer’s mice prevents neuronal loss without modulating amyloid- β pathology. *Brain* **139**, 1265–1281.
- [227] Spangenberg, E. E & Green, K. N. (2017) Inflammation in Alzheimer’s Disease: Lessons learned from microglia-depletion models. *Brain Behav Immun.* **61**, 1–11.
- [228] Zuroff, L, Daley, D, Black, K. L, & Koronyo-Hamaoui, M. (2017) *Clearance of cerebral A β in Alzheimer’s disease: reassessing the role of microglia and monocytes.* (Springer International Publishing) Vol. 74.
- [229] Deane, R, Yan, S. D, Subramanian, R. K, et al. (2003) RAGE mediates amyloid- β peptide transport across the blood-brain barrier and accumulation in brain. *Nature Medicine* **9**, 907–913.

- [230] Deane, R, Bell, R, Sagare, A, & Zlokovic, B. (2009) Clearance of Amyloid-Beta Peptide Across the Blood-Brain Barrier: Implication for Therapies in Alzheimers Disease. *CNS & Neurological Disorders - Drug Targets* **8**, 16–30.
- [231] Shibata, M, Ghiso, J, Zlokovic, B. V, et al. (2000) Clearance of Alzheimer 's amyloid- b 1-40 peptide from brain by LDL receptor – related protein-1 at the blood-brain barrier Find the latest version : Clearance of Alzheimer ' s amyloid- β 1-40 peptide from brain by LDL receptor – related protein-1 at the. *The Journal of Clinical Investigation* **106**, 1489–1499.
- [232] Wang, S, Wang, R, Chen, L, et al. (2010) Expression and functional profiling of neprilysin, insulin-degrading enzyme, and endothelin-converting enzyme in prospectively studied elderly and Alzheimer's brain. *Journal of Neurochemistry* **115**, 47–57.
- [233] Tamboli, I. Y, Barth, E, Christian, L, et al. (2010) Statins promote the degradation of extracellular amyloid β -peptide by microglia via stimulation of exosome-associated insulin-degrading enzyme (IDE) secretion. *Journal of Biological Chemistry* **285**, 37405–37414.
- [234] Posse De Chaves, E & Mohamed, A. (2011) A β internalization by neurons and glia. *International Journal of Alzheimer's Disease* **2011**, 15–17.
- [235] Mandrekar, S, Jiang, Q, Lee, C. Y, et al. (2009) Microglia mediate the clearance of soluble a β through fluid phase macropinocytosis. *Journal of Neuroscience* **29**, 4252–4262.
- [236] Knauer, M. F, Soreghan, B, Burdick, D, et al. (1992) Intracellular accumulation and resistance to degradation of the Alzheimer amyloid A4/ β protein. *Proceedings of the National Academy of Sciences of the United States of America* **89**, 7437–7441.
- [237] Bamberger, M. E, Harris, M. E, McDonald, D. R, et al. (2003) A cell surface receptor complex for fibrillar β -amyloid mediates microglial activation. *Journal of Neuroscience* **23**, 2665–2674.
- [238] Koenigsknecht-Talboo, J & Landreth, G. E. (2005) Microglial phagocytosis induced

by fibrillar β -amyloid and IgGs are differentially regulated by proinflammatory cytokines. *Journal of Neuroscience* **25**, 8240–8249.

- [239] Nixon, R. A. (2017) Amyloid precursor protein & endosomal-lysosomal dysfunction in Alzheimer's disease: Inseparable partners in a multifactorial disease. *FASEB Journal* **31**, 2729–2743.
- [240] Bertram, L, Lill, C. M, & Tanzi, R. E. (2010) The genetics of alzheimer disease: Back to the future. *Neuron* **68**, 270–281.
- [241] Majumdar, A, Cruz, D, Asamoah, N, et al. (2007) Activation of microglia acidifies lysosomes and leads to degradation of Alzheimer amyloid fibrils. *Molecular biology of the cell* **18**, 1490–1496.
- [242] Pomilio, C, Gorojod, R. M, Riudavets, M, et al. (2020) Microglial autophagy is impaired by prolonged exposure to β -amyloid peptides: evidence from experimental models and Alzheimer's disease patients. *GeroScience* **42**, 613–632.
- [243] Koellhoffer, E. C, McCullough, L. D, & Ritzel, R. M. (2017) Old maids: Aging and its impact on microglia function. *International Journal of Molecular Sciences* **18**, 1–25.
- [244] Floden, A. M & Combs, C. K. (2011) Microglia demonstrate age-dependent interaction with amyloid- β fibrils. *Journal of Alzheimer's Disease* **25**, 279–293.
- [245] Keren-Shaul, H, Spinrad, A, Weiner, A, et al. (2017) A Unique Microglia Type Associated with Restricting Development of Alzheimer's Disease. *Cell* **169**, 1276–1290.e17.
- [246] Krasemann, S, Madore, C, Cialic, R, et al. (2017) The TREM2-APOE Pathway Drives the Transcriptional Phenotype of Dysfunctional Microglia in Neurodegenerative Diseases. *Immunity* **47**, 566–581.e9.
- [247] Mathys, H, Adaikkan, C, Gao, F, et al. (2017) Temporal Tracking of Microglia Activation in Neurodegeneration at Single-Cell Resolution. *Cell Reports* **21**, 366–380.

- [248] Sala Frigerio, C, Wolfs, L, Fattorelli, N, et al. (2019) The Major Risk Factors for Alzheimer's Disease: Age, Sex, and Genes Modulate the Microglia Response to A β Plaques. *Cell Reports* **27**, 1293–1306.e6.
- [249] Mathys, H, Davila-Velderrain, J, Peng, Z, et al. (2019) Single-cell transcriptomic analysis of Alzheimer's disease. *Nature* **570**, 332–337.
- [250] Zhou, Y, Song, W. M, Andhey, P. S, et al. (2020) Human and mouse single-nucleus transcriptomics reveal TREM2-dependent and TREM2-independent cellular responses in Alzheimer's disease. *Nature Medicine* **26**, 131–142.
- [251] Masuda, T, Tsuda, M, Yoshinaga, R, et al. (2012) IRF8 Is a Critical Transcription Factor for Transforming Microglia into a Reactive Phenotype. *Cell Reports* **1**, 334–340.
- [252] Wang, Y, Cella, M, Mallinson, K, et al. (2015) TREM2 lipid sensing sustains the microglial response in an Alzheimer's Disease model. *Cell* **160**, 1061–1071.
- [253] Srinivasan, K, Friedman, B. A, Etxeberria, A, et al. (2020) Alzheimer's patient microglia exhibit enhanced aging and unique transcriptional activation. *Cell Reports* **31**.
- [254] Hall, A. M & Roberson, E. D. (2012) Mouse Models of Alzheimer's Disease. *Brain Res. Bull.* **88**, 3–12.
- [255] Huang, K. L, Marcora, E, Pimenova, A. A, et al. (2017) A common haplotype lowers PU.1 expression in myeloid cells and delays onset of Alzheimer's disease. *Nature Neuroscience* **20**, 1052–1061.
- [256] Sierra, A, Abiega, O, Shahraz, A, & Neumann, H. (2013) Janus-faced microglia: Beneficial and detrimental consequences of microglial phagocytosis. *Frontiers in Cellular Neuroscience* **7**, 1–22.
- [257] Steinberg, S, Stefansson, H, Jonsson, T, et al. (2015) Loss-of-function variants in ABCA7 confer risk of Alzheimer's disease. *Nature Genetics* **47**, 445–447.

- [258] Vardarajan, B, Zhang, Y, Lee, J, et al. (2015) Coding mutations in SORL1 and Alzheimer's Disease. *Annals of Neurology* pp. 2–31.
- [259] Xiang, X, Werner, G, Bohrmann, B, et al. (2016) TREM2 deficiency reduces the efficacy of immunotherapeutic amyloid clearance. *EMBO Molecular Medicine* **8**, 992–1004.
- [260] Lee, C. Y, Daggett, A, Gu, X, et al. (2018) Elevated TREM2 Gene Dosage Reprograms Microglia Responsivity and Ameliorates Pathological Phenotypes in Alzheimer's Disease Models. *Neuron* **97**, 1032–1048.e5.
- [261] Jiang, T, Tan, L, Zhu, X. C, et al. (2014) Upregulation of TREM2 ameliorates neuropathology and rescues spatial cognitive impairment in a transgenic mouse model of Alzheimer's disease. *Neuropsychopharmacology : official publication of the American College of Neuropsychopharmacology* **39**, 2949–2962.
- [262] Magno, L, Lessard, C. B, Martins, M, et al. (2019) Alzheimer's disease phospholipase C-gamma-2 (PLCG2) protective variant is a functional hypermorph. *Alzheimer's Research and Therapy* **11**, 1–11.
- [263] De Roeck, A, Van Broeckhoven, C, & Sleegers, K. (2019) The role of ABCA7 in Alzheimer's disease: evidence from genomics, transcriptomics and methylomics. *Acta Neuropathologica* **138**, 201–220.
- [264] Fu, Y, Hsiao, J. H. T, Paxinos, G, et al. (2016) ABCA7 Mediates Phagocytic Clearance of Amyloid- β in the Brain. *Journal of Alzheimer's Disease* **54**, 569–584.
- [265] Tebar, F, Bohlander, S. K, & Sorkin, A. (1999) Clathrin assembly lymphoid myeloid leukemia (CALM) protein: Localization in endocytic-coated pits, interactions with clathrin, and the impact of overexpression on clathrin-mediated traffic. *Molecular Biology of the Cell* **10**, 2687–2702.
- [266] Cormont, M, Metón, I, Mari, M, et al. (2003) CD2AP/CMS regulates endosome morphology and traffic to the degradative pathway through its interaction with Rab4 and c-Cbl. *Traffic* **4**, 97–112.

- [267] Pant, S, Sharma, M, Patel, K, et al. (2009) AMPH-1/Amphiphysin/Bin1 function with RME-1/Ehd in endocytic recycling. *Nat Cell Biol.* **11**, 1399–1401.
- [268] Seshadri, S, Fitzpatrick, A. L, Ikram, M. A, et al. (2010) Genome-wide analysis of genetic loci associated with Alzheimer disease. *JAMA - Journal of the American Medical Association* **303**, 1832–1840.
- [269] Ren, G, Vajjhala, P, Lee, J. S, et al. (2006) The BAR Domain Proteins: Molding Membranes in Fission, Fusion, and Phagy. *Microbiology and Molecular Biology Reviews* **70**, 37–120.
- [270] Taga, M, Petyuk, V. A, White, C, et al. (2020) BIN1 protein isoforms are differentially expressed in astrocytes, neurons, and microglia: neuronal and astrocyte BIN1 are implicated in tau pathology. *Molecular Neurodegeneration* **15**.
- [271] Peter, B. J, Kent, H. M, Mills, I. G, et al. (2004) BAR Domains as Sensors of Membrane Curvature: The Amphiphysin BAR Structure. *Science* **303**, 495–499.
- [272] Di Paolo, G & De Camilli, P. (2006) Phosphoinositides in cell regulation and membrane dynamics. *Nature* **443**, 651–657.
- [273] Ramjaun, A. R & McPherson, P. S. (1998) Multiple amphiphysin II splice variants display differential clathrin binding: Identification of two distinct clathrin-binding sites. *Journal of Neurochemistry* **70**, 2369–2376.
- [274] Prendergast, G. C, Muller, A. J, Ramalingam, A, & Chang, M. Y. (2009) BAR the door: Cancer suppression by amphiphysin-like genes. *Biochimica et Biophysica Acta - Reviews on Cancer* **1795**, 25–36.
- [275] Nicot, A. S, Toussaint, A, Tosch, V, et al. (2007) Mutations in amphiphysin 2 (BIN1) disrupt interaction with dynamin 2 and cause autosomal recessive centronuclear myopathy. *Nature Genetics* **39**, 1134–1139.
- [276] Sottejeau, Y, Bretteville, A, Cantrelle, F. X, et al. (2015) Tau phosphorylation regulates the interaction between BIN1's SH3 domain and Tau's proline-rich domain. *Acta neuropathologica communications* **3**, 58.

- [277] Butler, M. H, David, C, Ochoa, G. C, et al. (1997) Amphiphysin II (SH3p9; BIN1), a member of the amphiphysin/Rvs family, is concentrated in the cortical cytomatrix of axon initial segments and nodes of ranvier in brain and around T tubules in skeletal muscle. *Journal of Cell Biology* **137**, 1355–1367.
- [278] De Rossi, P, Buggia-Prévot, V, Clayton, B. L, et al. (2016) Predominant expression of Alzheimer’s disease-associated BIN1 in mature oligodendrocytes and localization to white matter tracts. *Molecular Neurodegeneration* **11**, 1–21.
- [279] Crotti, A, Sait, H. R, McAvoy, K. M, et al. (2019) BIN1 favors the spreading of Tau via extracellular vesicles. *Scientific Reports* **9**.
- [280] Li, Q, Cheng, Z, Zhou, L, et al. (2019) Developmental Heterogeneity of Microglia and Brain Myeloid Cells Revealed by Deep Single-Cell RNA Sequencing. *Neuron* **101**, 207–223.e10.
- [281] Elliott, K, Ge, K, Du, W, & Prendergast, G. C. (2000) The c-Myc-interacting adaptor protein Bin1 activates a caspase-independent cell death program. *Oncogene* **19**, 4669–4684.
- [282] Mee, Y. C, Boulden, J, Katz, J. B, et al. (2007) Bin1 ablation increases susceptibility to cancer during aging, particularly lung cancer. *Cancer Research* **67**, 7605–7612.
- [283] Cassimere, E. K, Pyndiah, S, & Sakamuro, D. (2009) The c-MYC-interacting proapoptotic tumor suppressor BIN1 is a transcriptional target for E2F1 in response to DNA damage. *Cell Death and Differentiation* **16**, 1641–1653.
- [284] Dräger, N. M, Nachman, E, Winterhoff, M, et al. (2017) Bin1 directly remodels actin dynamics through its BAR domain . *EMBO reports* **18**, 2051–2066.
- [285] Gao, P, Ye, L, Cheng, H, & Li, H. (2021) The Mechanistic Role of Bridging Integrator 1 (BIN1) in Alzheimer’s Disease.
- [286] Leprince, C, Le Scolan, E, Meunier, B, et al. (2003) Sorting nexin 4 and amphiphysin 2, a new partnership between endocytosis and intracellular trafficking. *Journal of Cell Science* **116**, 1937–1948.

- [287] Chapuis, J, Hansmannel, F, Gistelinc, M, et al. (2013) Increased expression of BIN1 mediates Alzheimer genetic risk by modulating tau pathology. *Molecular Psychiatry* **18**, 1225–1234.
- [288] Ubelmann, F, Burrinha, T, Salavessa, L, et al. (2017) Bin1 and CD2AP polarise the endocytic generation of beta-amyloid. *EMBO reports* **18**, 102–122.
- [289] Miyagawa, T, Ebinuma, I, Morohashi, Y, et al. (2016) BIN1 regulates BACE1 intracellular trafficking and amyloid- β production. *Human Molecular Genetics* **25**, 2948–2958.
- [290] Calafate, S, Flavin, W, Verstreken, P, & Moechars, D. (2016) Loss of Bin1 Promotes the Propagation of Tau Pathology. *Cell Reports* **17**, 931–940.
- [291] De Rossi, P, Nomura, T, Andrew, R. J, et al. (2020) Neuronal BIN1 Regulates Presynaptic Neurotransmitter Release and Memory Consolidation. *Cell Reports* **30**, 3520–3535.e7.
- [292] Schürmann, B, Bermingham, D. P, Kopeikina, K. J, et al. (2020) A novel role for the late-onset Alzheimer’s disease (LOAD)-associated protein Bin1 in regulating postsynaptic trafficking and glutamatergic signaling. *Molecular Psychiatry* **25**, 2000–2016.
- [293] Pratt, W. B, Gestwicki, J. E, Osawa, Y, & Lieberman, A. P. (2015) Targeting Proteostasis Through the Protein Quality Control Function of the Hsp90/Hsp70-based Chaperone Machinery for Treatment of Adult Onset Neurodegenerative Diseases. *Annual review of pharmacology and toxicology* **55**, 353–71.
- [294] Tang, D, Kang, R, Coyne, C, et al. (2012) PAMPs and DAMPs: signals that spur autophagy and immunity. *Immunological Reviews* **249**, 158–175.
- [295] Tan, M. S, Yu, J. T, & Tan, L. (2013) Bridging integrator 1 (BIN1): Form, function, and Alzheimer’s disease.
- [296] Konishi, H & Kiyama, H. (2018) Microglial TREM2/DAP12 signaling: A double-edged sword in neural diseases. *Frontiers in Cellular Neuroscience* **12**, 1–14.

- [297] Maes, M. E, Colombo, G, Schulz, R, & Siegert, S. (2019) Targeting microglia with lentivirus and AAV: Recent advances and remaining challenges. *Neuroscience Letters* **707**.
- [298] De Rossi, P, Andrew, R. J, Musial, T. F, et al. (2019) Aberrant accrual of BIN1 near Alzheimer's disease amyloid deposits in transgenic models. *Brain Pathology* **29**, 485–501.
- [299] Franzmeier, N, Rubinski, A, Neitzel, J, et al. (2019) The BIN1 rs744373 SNP is associated with increased tau-PET levels and impaired memory. *Nature Communications* **10**.
- [300] Holler, C. J, Davis, P. R, Beckett, T. L, et al. (2014) Bridging integrator 1 (BIN1) protein expression increases in the alzheimer's disease brain and correlates with neurofibrillary tangle pathology. *Journal of Alzheimer's Disease* **42**, 1221–1227.
- [301] Glennon, E. B, Whitehouse, I. J, Miners, J. S, et al. (2013) BIN1 Is Decreased in Sporadic but Not Familial Alzheimer's Disease or in Aging. *PLoS ONE* **8**, 1–11.
- [302] Hu, H, Tan, L, Bi, Y. L, et al. (2021) Association between methylation of BIN1 promoter in peripheral blood and preclinical Alzheimer's disease. *Translational Psychiatry* **11**.
- [303] Zhu, J, Liu, X, Yin, H, et al. (2021) Convergent lines of evidence support BIN1 as a risk gene of Alzheimer's disease. *Human Genomics* **15**.
- [304] Krabbe, G, Halle, A, Matyash, V, et al. (2013) Functional Impairment of Microglia Coincides with Beta-Amyloid Deposition in Mice with Alzheimer-Like Pathology. *PLoS ONE* **8**.
- [305] Kleinberger, G, Yamanishi, Y, Suárez-Calvet, M, et al. (2014) TREM2 mutations implicated in neurodegeneration impair cell surface transport and phagocytosis. *Science Translational Medicine* **6**, 23.
- [306] Rosario, A. M, Cruz, P. E, Ceballos-Diaz, C, et al. (2016) Microglia-specific targeting by novel capsid-modified AAV6 vectors. *Molecular Therapy - Methods and Clinical Development* **3**, 16026.

- [307] Butovsky, O, Jedrychowski, M. P, Moore, C. S, et al. (2014) Identification of a unique TGF- β -dependent molecular and functional signature in microglia. *Nature Neuroscience* **17**, 131–143.
- [308] Reiman, M, Laan, M, Rull, K, & Söber, S. (2017) Effects of RNA integrity on transcript quantification by total RNA sequencing of clinically collected human placental samples. *FASEB Journal* **31**, 3298–3308.
- [309] Labandeira-Garcia, J. L, Costa-Besada, M. A, Labandeira, C. M, et al. (2017) Insulin-like growth factor-1 and neuroinflammation.
- [310] Grubman, A, Choo, X. Y, Chew, G, et al. (2021) Transcriptional signature in microglia associated with A β plaque phagocytosis. *Nature Communications* **12**.
- [311] De Sousa Abreu, R, Penalva, L. O, Marcotte, E. M, & Vogel, C. (2009) Global signatures of protein and mRNA expression levels.
- [312] Vogel, C & Marcotte, E. M. (2012) Insights into the regulation of protein abundance from proteomic and transcriptomic analyses. *Nature Reviews Genetics* **13**, 227–232.
- [313] Maier, T, Güell, M, & Serrano, L. (2009) Correlation of mRNA and protein in complex biological samples.
- [314] Baker, S. K, Chen, Z. L, Norris, E. H, et al. (2018) Blood-derived plasminogen drives brain inflammation and plaque deposition in a mouse model of Alzheimer’s disease. *Proceedings of the National Academy of Sciences of the United States of America* **115**, E9687–E9696.
- [315] Rao, Y. L, Ganaraja, B, Murlimanju, B. V, et al. (2022) Hippocampus and its involvement in Alzheimer’s disease: a review. *3 Biotech* **12**, 1–10.
- [316] Hammond, B. P, Manek, R, Kerr, B. J, et al. (2021) Regulation of microglia population dynamics throughout development, health, and disease. *GLIA* **69**, 2771–2797.
- [317] He, Y, Yao, X, Taylor, N, et al. (2018) RNA sequencing analysis reveals quiescent microglia isolation methods from postnatal mouse brains and limitations of BV2 cells. *Journal of Neuroinflammation* **15**.

- [318] Franco-Bocanegra, McAuley, Nicoll, & Boche. (2019) Molecular Mechanisms of Microglial Motility: Changes in Ageing and Alzheimer's Disease. *Cells* **8**, 639.
- [319] Zhao, J, Bruck, S, Cemerski, S, et al. (2013) CD2AP Links Cortactin and Capping Protein at the Cell Periphery To Facilitate Formation of Lamellipodia. *Molecular and Cellular Biology* **33**, 38–47.
- [320] Barysch, S. V, Aggarwal, S, Jahn, R, & Rizzoli, S. O. (2009) Sorting in early endosomes reveals connections to docking- and fusion-associated factors. *Proceedings of the National Academy of Sciences of the United States of America* **106**, 9697–9702.
- [321] Nagano, M, Toshima, J. Y, Elisabeth Siekhaus, D, & Toshima, J. (2019) Rab5-mediated endosome formation is regulated at the trans-Golgi network. *Communications Biology* **2**, 1–12.
- [322] Bartlett, J. S, Samulski, R. J, & McCown, T. J. (1998) Selective and Rapid Uptake of Adeno-Associated Virus Type 2 in Brain. *Human Gene Therapy*.
- [323] Cucchiaroni, M, Ren, X. L, Perides, G, & Terwilliger, E. F. (2003) Selective gene expression in brain microglia mediated via adeno-associated virus type 2 and type 5 vectors. *Gene Therapy* **10**, 657–667.
- [324] Su, W, Kang, J, Sopher, B, et al. (2016) Recombinant adeno-associated viral (rAAV) vectors mediate efficient gene transduction in cultured neonatal and adult microglia. *Journal of Neurochemistry* **136**, 49–62.
- [325] Rangaraju, S, Dammer, E. B, Raza, S. A, et al. (2018) Quantitative proteomics of acutely-isolated mouse microglia identifies novel immune Alzheimer's disease-related proteins. *Molecular Neurodegeneration* **13**.
- [326] Horner, R, Gassner, J. G, Kluge, M, et al. (2019) Impact of Percoll purification on isolation of primary human hepatocytes. *Scientific Reports* **9**, 2–11.
- [327] Schroeder, A, Mueller, O, Stocker, S, et al. (2006) The RIN: An RNA integrity number for assigning integrity values to RNA measurements. *BMC Molecular Biology* **7**.

- [328] Kaiser, O, Aliuos, P, Wissel, K, et al. (2013) Dissociated neurons and glial cells derived from rat inferior colliculi after digestion with papain. *PLoS ONE* **8**.
- [329] Hu, C, Du, R, Xiao, Q, & Geng, M. (2022) Differences between cultured cortical neurons by trypsin and papain digestion. *Ibrain* **8**, 93–99.
- [330] Castillo, E, Leon, J, Mazzei, G, et al. (2017) Comparative profiling of cortical gene expression in Alzheimer’s disease patients and mouse models demonstrates a link between amyloidosis and neuroinflammation. *Scientific Reports* **7**.
- [331] Swartzlander, D. B, Propson, N. E, Roy, E. R, et al. (2018) Concurrent cell type-specific isolation and profiling of mouse brains in inflammation and Alzheimer’s disease. *JCI insight* **3**.
- [332] Jovanovic, M, Rooney, M. S, Mertins, P, et al. (2015) Dynamic profiling of the protein life cycle in response to pathogens HHS Public Access induction of novel cellular functions and remodeling of preexisting functions through the protein life cycle. *Science March* **6**, 1–16.
- [333] Imai, T, Hieshima, K, Haskell, C, et al. (1997) Identification and Molecular Characterization of Fractalkine Receptor CX 3 CR1, which Mediates Both Leukocyte Migration and Adhesion, Technical report.
- [334] Fuhrmann, M, Bittner, T, Jung, C. K, et al. (2010) Microglial Cx3cr1 knockout prevents neuron loss in a mouse model of Alzheimer’s disease. *Nature Neuroscience* **13**, 411–413.
- [335] Cho, S. H, Sun, B, Zhou, Y, et al. (2011) CX3CR1 protein signaling modulates microglial activation and protects against plaque-independent cognitive deficits in a mouse model of Alzheimer disease. *Journal of Biological Chemistry* **286**, 32713–32722.
- [336] Wolf, Y, Yona, S, Kim, K. W, & Jung, S. (2013) Microglia, seen from the CX3CR1 angle. *Frontiers in Cellular Neuroscience*.

- [337] Bennett, M. L, Bennett, F. C, Liddelov, S. A, et al. (2016) New tools for studying microglia in the mouse and human CNS. *Proceedings of the National Academy of Sciences of the United States of America* **113**, E1738–E1746.
- [338] Park, M. H, Lee, M, Nam, G, et al. (2019) N,N-Diacetyl-p-phenylenediamine restores microglial phagocytosis and improves cognitive defects in Alzheimer’s disease transgenic mice. *Proceedings of the National Academy of Sciences of the United States of America* **116**, 23426–23436.
- [339] Jay, T. R, Hirsch, A. M, Broihier, M. L, et al. (2017) Disease progression-dependent effects of TREM2 deficiency in a mouse model of Alzheimer’s disease. *Journal of Neuroscience* **37**, 637–647.
- [340] Mazaheri, F, Snaidero, N, Kleinberger, G, et al. (2017) TREM 2 deficiency impairs chemotaxis and microglial responses to neuronal injury . *EMBO reports* **18**, 1186–1198.
- [341] Götzl, J. K, Brendel, M, Werner, G, et al. (2019) Opposite microglial activation stages upon loss of PGRN or TREM 2 result in reduced cerebral glucose metabolism . *EMBO Molecular Medicine* **11**.
- [342] Wylot, B, Mieczkowski, J, Niedziolka, S, et al. (2019) Csf1 Deficiency Dysregulates Glial Responses to Demyelination and Disturbs CNS White Matter Remyelination. *Cells* **9**, 1–24.
- [343] Hu, X, Li, S, Doycheva, D. M, et al. (2020) Rh-CSF1 Attenuates Oxidative Stress and Neuronal Apoptosis via the CSF1R/PLCG2/PKA/UCP2 Signaling Pathway in a Rat Model of Neonatal HIE. *Oxidative Medicine and Cellular Longevity* **2020**, 1–18.
- [344] Boissonneault, V, Filali, M, Lessard, M, et al. (2009) Powerful beneficial effects of macrophage colony-stimulating factor on β -amyloid deposition and cognitive impairment in Alzheimers disease. *Brain* **132**, 1078–1092.
- [345] Smith, A. M, Gibbons, H. M, Oldfield, R. L, et al. (2013) M-CSF increases prolifera-

tion and phagocytosis while modulating receptor and transcription factor expression in adult human microglia. *Journal of Neuroinflammation* **10**, 1–15.

- [346] Akiyama, H, Nishimura, T, Kondo, H, et al. (1994) Expression of the receptor for macrophage colony stimulating factor by brain microglia and its upregulation in brains of patients with Alzheimer's disease and amyotrophic lateral sclerosis. *Brain Research* **639**, 171–174.
- [347] Gómez-Nicola, D, Fransen, N. L, Suzzi, S, & Hugh Perry, V. (2013) Regulation of microglial proliferation during chronic neurodegeneration. *Journal of Neuroscience* **33**, 2481–2493.
- [348] Olmos-Alonso, A, Schettters, S. T, Sri, S, et al. (2016) Pharmacological targeting of CSF1R inhibits microglial proliferation and prevents the progression of Alzheimer's-like pathology. *Brain* **139**, 891–907.
- [349] Chen, M. J, Ramesha, S, Weinstock, L. D, et al. (2021) Extracellular signal-regulated kinase regulates microglial immune responses in Alzheimer's disease. *Journal of Neuroscience Research* **99**, 1704–1721.
- [350] wen Han, Q, hang Shao, Q, tong Wang, X, et al. (2022) CB2 receptor activation inhibits the phagocytic function of microglia through activating ERK/AKT-Nurr1 signal pathways. *Acta Pharmacologica Sinica*.
- [351] Raposo, G & Stoorvogel, W. (2013) Extracellular vesicles: Exosomes, microvesicles, and friends.
- [352] Meldolesi, J. (2018) Exosomes and Ectosomes in Intercellular Communication. *Current Biology* **28**, R435–R444.
- [353] Hessvik, N. P & Llorente, A. (2018) Current knowledge on exosome biogenesis and release. *Cellular and Molecular Life Sciences* **75**, 193–208.
- [354] Paolicelli, R. C, Bergamini, G, & Rajendran, L. (2019) Cell-to-cell Communication by Extracellular Vesicles: Focus on Microglia. *Neuroscience* **405**, 148–157.

- [355] Verderio, C, Muzio, L, Turola, E, et al. (2012) Myeloid microvesicles are a marker and therapeutic target for neuroinflammation. *Annals of Neurology* **72**, 610–624.
- [356] Fernandes, A, Ribeiro, A. R, Monteiro, M, et al. (2018) Secretome from SH-SY5Y APPSwe cells trigger time-dependent CHME3 microglia activation phenotypes, ultimately leading to miR-21 exosome shuttling. *Biochimie* **155**, 67–82.
- [357] Guo, M, Hao, Y, Feng, Y, et al. (2021) Microglial Exosomes in Neurodegenerative Disease.
- [358] Guo, M, Wang, J, Zhao, Y, et al. (2020) Microglial exosomes facilitate a-synuclein transmission in Parkinson’s disease. *Brain* **143**, 1476–1497.
- [359] Karahan, H, Smith, D. C, Kim, B, et al. (2021) Deletion of Abi3 gene locus exacerbates neuropathological features of Alzheimer’s disease in a mouse model of A amyloidosis, Technical report.
- [360] Cherry, J. D, Meng, G, Daley, S, et al. (2020) CCL2 is associated with microglia and macrophage recruitment in chronic traumatic encephalopathy. *Journal of Neuroinflammation* **17**.
- [361] Scharzt, N. D & Tenner, A. J. (2020) The good, the bad, and the opportunities of the complement system in neurodegenerative disease.
- [362] Jin, J, Wang, Y, Ma, Q, et al. (2018) LAIR-1 activation inhibits inflammatory macrophage phenotype in vitro. *Cellular Immunology* **331**, 78–84.
- [363] Zöllner, T, Schneider, A, Kleimeyer, C, et al. (2018) Silencing of TGF β signalling in microglia results in impaired homeostasis. *Nature Communications* **9**.
- [364] Ley, K, Pramod, A. B, Croft, M, et al. (2016) How mouse macrophages sense what is going on.
- [365] Saito, T, Matsuba, Y, Mihira, N, et al. (2014) Single App knock-in mouse models of Alzheimer’s disease. *Nature Neuroscience* **17**, 661–663.

- [366] Rupp, N. J, Wegenast-Braun, B. M, Radde, R, et al. (2011) Early onset amyloid lesions lead to severe neuritic abnormalities and local, but not global neuron loss in APPPS1 transgenic mice. *Neurobiology of Aging* **32**, 2324.e1–2324.e6.
- [367] Bittner, T, Burgold, S, Dorostkar, M. M, et al. (2012) Amyloid plaque formation precedes dendritic spine loss. *Acta Neuropathologica* **124**, 797–807.
- [368] Koussounadis, A, Langdon, S. P, Um, I. H, et al. (2015) Relationship between differentially expressed mRNA and mRNA-protein correlations in a xenograft model system. *Scientific Reports* **5**.
- [369] Reed-Geaghan, E. G, Savage, J. C, Hise, A. G, & Landreth, G. E. (2009) CD14 and toll-like receptors 2 and 4 are required for fibrillar A β -stimulated microglial activation. *Journal of Neuroscience* **29**, 11982–11992.
- [370] Liu, S, Liu, Y, Hao, W, et al. (2012) TLR2 Is a Primary Receptor for Alzheimer's Amyloid β Peptide To Trigger Neuroinflammatory Activation. *The Journal of Immunology* **188**, 1098–1107.
- [371] Merlo, S, Spampinato, S. F, Beneventano, M, & Sortino, M. A. (2018) The contribution of microglia to early synaptic compensatory responses that precede β -amyloid-induced neuronal death. *Scientific Reports* **8**.
- [372] Porro, C, Pennella, A, Panaro, M. A, & Trotta, T. (2021) Functional role of non-muscle myosin ii in microglia: An updated review.
- [373] Gao, Y, Vidal-Itriago, A, Kalsbeek, M. J, et al. (2017) Lipoprotein Lipase Maintains Microglial Innate Immunity in Obesity. *Cell Reports* **20**, 3034–3042.
- [374] Loving, B. A, Tang, M, Neal, M. C, et al. (2021) Lipoprotein lipase regulates microglial lipid droplet accumulation. *Cells* **10**, 1–17.
- [375] Folick, A, Koliwad, S. K, & Valdearcos, M. (2021) Microglial Lipid Biology in the Hypothalamic Regulation of Metabolic Homeostasis.

- [376] Yeh, F. L, Wang, Y, Tom, I, et al. (2016) TREM2 Binds to Apolipoproteins, Including APOE and CLU/APOJ, and Thereby Facilitates Uptake of Amyloid-Beta by Microglia. *Neuron* **91**, 328–340.
- [377] Plastira, I, Bernhart, E, Joshi, L, et al. (2020) MAPK signaling determines lysophosphatidic acid (LPA)-induced inflammation in microglia. *Journal of Neuroinflammation* **17**.
- [378] Andoh, M & Koyama, R. (2021) Microglia regulate synaptic development and plasticity.
- [379] Van Acker, Z. P, Bretou, M, & Annaert, W. (2019) Endo-lysosomal dysregulations and late-onset Alzheimer’s disease: Impact of genetic risk factors.
- [380] Jurga, A. M, Paleczna, M, & Kuter, K. Z. (2020) Overview of General and Discriminating Markers of Differential Microglia Phenotypes. *Frontiers in Cellular Neuroscience* **14**.
- [381] Enquist, L. W & Card, J. P. (2003) Recent advances in the use of neurotropic viruses for circuit analysis.
- [382] Vannucci, L, Lai, M, Chiuppesi, F, et al. (2013) Viral vectors: a look back and ahead on gene transfer technology, Technical report.
- [383] Jiang, X.-s, Ni, Y.-q, Liu, T.-j, et al. (2012) CCR2 overexpression promotes the efficient recruitment of retinal microglia in vitro.
- [384] Åkerblom, M, Sachdeva, R, Quintino, L, et al. (2013) Visualization and genetic modification of resident brain microglia using lentiviral vectors regulated by microRNA-9. *Nature Communications* **4**.
- [385] Grace, P. M, Strand, K. A, Galer, E. L, et al. (2016) Morphine paradoxically prolongs neuropathic pain in rats by amplifying spinal NLRP3 inflammasome activation. *Proceedings of the National Academy of Sciences of the United States of America* **113**, E3441–E3450.

- [386] Brawek, B, Liang, Y, Savitska, D, et al. (2017) A new approach for ratiometric in vivo calcium imaging of microglia. *Scientific Reports* **7**.
- [387] Zhong, L, Li, B, Mah, C. S, et al. (2008) Next generation of adeno-associated virus 2 vectors: Point mutations in tyrosines lead to high-efficiency transduction at lower doses. *PNAS*.
- [388] Ussher, J. E & Taylor, J. A. (2010) Optimized transduction of human monocyte-derived dendritic cells by recombinant adeno-associated virus serotype 6. *Human Gene Therapy* **21**, 1675–1686.
- [389] Aslanidi, G. V, Rivers, A. E, Ortiz, L, et al. (2012) High-efficiency transduction of human monocyte-derived dendritic cells by capsid-modified recombinant AAV2 vectors. *Vaccine* **30**, 3908–3917.
- [390] Pandya, M, Britt, K, Hoffman, B, et al. (2015) Reprogramming immune response with capsid-optimized AAV6 vectors for immunotherapy of cancer. *Journal of Immunotherapy* **38**, 292–298.
- [391] Jiménez, A. J, Domínguez-Pinos, M. D, Guerra, M. M, et al. (2014) Structure and function of the ependymal barrier and diseases associated with ependyma disruption.
- [392] Brill, M. S, Kleele, T, Ruschkies, L, et al. (2016) Branch-Specific Microtubule Destabilization Mediates Axon Branch Loss during Neuromuscular Synapse Elimination. *Neuron* **92**, 845–856.
- [393] Wang, M, Misgeld, T, & Brill, M. S. (2022) Neural labeling and manipulation by neonatal intraventricular viral injection in mice. *STAR Protocols* **3**.
- [394] Kaul, M, Garden, G. A, & Lipton, S. (2001) Pathways to neuronal injury and apoptosis in HIV-associated dementia. *Nature*.
- [395] Frühbeis, C, Fröhlich, D, Kuo, W. P, & Krämer-Albers, E. M. (2013) Extracellular vesicles as mediators of neuron-glia communication.
- [396] Valdinocci, D, Radford, R. A, Siow, S. M, et al. (2017) Potential modes of intercellular α -synuclein transmission.

- [397] Saunders, A & Sabatini, B. L. (2015) Cre activated and inactivated recombinant adeno-associated viral vectors for neuronal anatomical tracing or activity manipulation. *Current Protocols in Neuroscience* **2015**, 1.24.1–1.24.15.
- [398] Yona, S, Kim, K. W, Wolf, Y, et al. (2013) Fate Mapping Reveals Origins and Dynamics of Monocytes and Tissue Macrophages under Homeostasis. *Immunity* **38**, 79–91.
- [399] Zhao, X. F, Alam, M. M, Liao, Y, et al. (2019) Targeting microglia using Cx3cr1-Cre lines: Revisiting the specificity. *eNeuro* **6**, 1–11.
- [400] Donocoff, R. S, Teteloshvili, N, Chung, H, et al. (2020) Optimization of tamoxifen-induced Cre activity and its effect on immune cell populations. *Scientific Reports* **10**.
- [401] Nie, X, Kitaoka, S, Tanaka, K, et al. (2018) The Innate Immune Receptors TLR2/4 Mediate Repeated Social Defeat Stress-Induced Social Avoidance through Prefrontal Microglial Activation. *Neuron* **99**, 464–479.e7.

Acknowledgements

First, I would like to express my sincere gratitude to my supervisor Prof. Dr. Jochen Herms for providing an excellent scientific infrastructure, which was of immeasurable value for the diverse methodological explorations of this fascinating topic. Our dynamic discussions throughout the course of my PhD and his support for my scientific career have helped me to develop scientifically and personally. I further owe him my involvement in other engaging topics, which gave me the opportunity to collaborate with several outstanding researchers and colleagues. Thank you for providing a great deal of freedom.

I would like to thank my mentor and friend Dr. Mario Dorostkar, who not only invested a substantial amount of time in my introduction to sequencing and big data analysis, but was also available around the clock if need be. Thank you so much for your vast knowledge, motivation and kindness.

Moreover, I would like to thank Prof. Dr. Stylianos Michalakis, who kindly agreed to represent this dissertation at the Faculty for Chemistry and Pharmacy and who was very helpful during the last crucial steps of my dissertation. I would also like to thank the entire thesis committee for their time and interest in this work.

Further, I would like to say a big thank you to all collaborators and colleagues for their teaching, fruitful discussions and companionship. Special thanks go to Dr. Sabina Tahirovic and her lab members Lina Dinkel and Dr. Laura Sébastian-Monazor, who generously shared their knowledge and have helped me in setting up a primary microglia culture system. Moreover, I would like to thank Dr. Lars Paeger and Dr. Paul Feyen for their enthusiasm and support of my project, many productive discussions and memorable moments in the lab. I feel honored to have been working with you and am looking forward to continue doing so. Another big thank you goes to Carolin Klaus, Svenja Rumpf, Nour Kassab, Prof. Dr. Gerhard Rammes, Georg Jocher, Dr. Felix Strübing, Dr. Stephan Müller, Dr. Xiao Feng, Mochen Cui and Dr. Yuan Shi for their cherished companionship and support during the last couple of years.

In addition, I would like to thank Ekrem Göcmenoglu, Claudia Ihbe and the entire DZNE

animal facility for their excellent help with all animal-related issues and Benno Fredmüller and Frank Meyer for their swift and amiable technical support.

I would like to express my very profound gratitude to my parents, for always believing in me and supporting me wherever possible. Thank you so much for your love and encouragement.

Finally, I am deeply grateful to Felix. Your kindness, understanding and support mean the world to me. Tá mo chroí istigh ionat.